Investigating the Epstein Barr virus-mediated perturbations and entry mechanism in brain cells: An insight into neuropathologies

Ph.D. Thesis

By

ANNU RANI

DEPARTMENT OF BIOSCIENCES AND BIOMEDICAL ENGINEERING

INDIAN INSTITUTE OF TECHNOLOGY INDORE

June 2024

Investigating the Epstein Barr virus-mediated perturbations and entry mechanism in brain cells: An insight into neuropathologies

A THESIS

Submitted in partial fulfilment of the requirements for the award of the degree

of

DOCTOR OF PHILOSOPHY

by

ANNU RANI

DEPARTMENT OF BIOSCIENCES AND BIOMEDICAL ENGINEERING

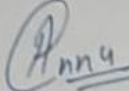# INDIAN INSTITUTE OF TECHNOLOGY INDORE

June 2024

INDIAN INSTITUTE OF TECHNOLOGY INDORE

I hereby certify that the work which is being presented in the thesis entitled **INVESTIGATING THE EPSTEIN BARR VIRUS-MEDIATED PERTURBATIONS AND ENTRY MECHANISM IN BRAIN CELLS: AN INSIGHT INTO NEUROPATHOLOGIES** in the partial fulfilment of the requirements for the award of the degree of **DOCTOR OF PHILOSOPHY** and submitted in the **DEPARTMENT OF BIOSCIENCES AND BIOMEDICAL ENGINEERING, INDIAN INSTITUTE OF TECHNOLOGY INDORE**, is an authentic record of my own work carried out during the time period from January 2020 to June 2024 under the supervision of Dr. Hem Chandra Jha, Associate Professor, Department of Biosciences and Biomedical Engineering.
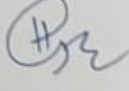
The matter presented in this thesis has not been submitted by me for the award of any other degree of this or any other institute.

Annu
20/11/2024
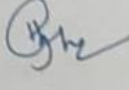**Signature of the student with date**

(Annu Rani)

This is to certify that the above statement made by the candidate is correct to the best of my knowledge.

20/11/2024

Signature of Thesis Supervisor with date

(Dr Hem Chandra Jha)

ANNU RANI has successfully given her Ph.D. Oral Examination held on 19 November 2024.

19/11/2024

Signature of Thesis Supervisor with date

(Dr Hem Chandra Jha)

ACKNOWLEDGEMENTS

शिक्षा का अर्थ बाल्टी भरना नहीं है बल्कि इसमें चरित्र निर्माण, मन की शक्ति बढ़ाना, बुद्धि का विस्तार करना आदि शामिल है, जिससे व्यक्ति अपने पैरों पर खड़ा हो सके।

-स्वामी विवेकानंद

Dedicated to all my Gurus, family and friends who have ignited my soul towards biology

SYNOPSIS

1.   Introduction

The *Herpesviridae* family entails more than 130 viruses that are known to infect mammals, birds, fish, reptiles, amphibians, and even molluscs. Herpesviridae subfamilies like alpha (α), beta (β), and gamma (γ) are known to infect humans, and they are categorised based on their replication strategies, host range and genetic organisation [1]. Herpesviruses are so ubiquitous that one or more herpesviruses infect almost all humans during their lifespan. Epstein Barr virus (EBV) is a member of the human γ-herpesvirus family, and it establishes its latency for a long period in B-cells, and their reactivation instigates and/or aggravates dreadful diseases from cancer to neurological modalities, i.e., Multiple Sclerosis (MS) and Alzheimer's disease (AD) [2].

The prevalence of EBV seropositivity in MS patients is approximately 99%. The history of infectious mononucleosis (IM) and CSF-confined EBV-specific oligoclonal bands (OCB) is significantly high in patients suffering from MS [3]. A cohort study with a mean follow-up of 7 years on 147 clinically isolated syndrome (CIS) patients and 50 controls demonstrated immune responses against EBV, human herpesvirus-6 (HHV-6), cytomegalovirus (CMV) and measles [4]. An elevated immune response toward EBV nuclear antigen 1 (EBNA1) was also observed. Thus, it suggests that the IgG titre of EBNA1 can use as a prognostic marker for the conversion and progression of the disease. The discrepant presence of EBV in MS lesions suggested that EBV-containing memory B-cells possibly lose the episomic EBV DNA during the replication process. However, it hangs on to forbidden epitopes recognition, it is likely to activate a molecular mimicry mechanism. The EBV-infected B-cells were actively found in demyelinating lesions of relapsing-remitting MS (RRMS) patients who died of lethal relapse [5].

EBV exhibited infection to brain cells such as SH-SY 5Y, NT-2 and human foetal cells [6]. Tropism of EBV is regulated by several envelope glycoproteins, which make a connection with the host cell receptors. For instance, glycoprotein 350/220, gp42, gHgL and gB of EBV establish an attachment with CD21, HLA-DR, Ephs, and other receptor molecules to hijack the B- and epithelial cell machinery [7]. For establishing the

infection in epithelial cells, EBV also uses several other receptors like integrin, neuropilin (NRP) and non-muscle myosin heavy chain (NMHC), possibly involving in viral transmission, replication and persistence. Previous reports suggested that EBV uses EphA2 as a receptor molecule to access epithelial cells, i.e., AGS, while Kaposi's Sarcoma-Associated virus (KSHV) is known to use EphA2 and EphA4. The ELEFN region of KSHV gH was involved in the interaction with EphA2, whereas, the interacting region of EBV gH is elusive. Further, the gHgL of KSHV and EBV form a complex with the EphA2 ligand-binding domain (LBD). Primarily by using gL, both KSHV and EBV gHgL bind to the peripheral regions of LBD [8]. In addition to γ-herpesviruses, several other viruses like Nipah virus, Cedar virus, Hepatitis C virus and Rhesus macaque rhadinovirus (RRV) also access the host cells via Eph receptors. Once the virus attaches to the receptor and undergoes a conformational change, it gets translocated into the lipid raft region of the plasma membrane. The lipid raft region is well-known to reinforce the entry of viruses such as human immunodeficiency virus (HIV), Ebola virus and herpesviruses [9]. KSHV is known to attach with the receptor and translocate in the lipid raft region for successful entry into the cell. The indispensable role of dynamin protein in pinching the endocytic vesicle from the plasma membrane is long known to be exploited by viruses for internalisation, e.g., Herpes-simplex virus-1 (HSV-1). The endocytic pathway further progresses into the formation of endosomal vesicles (early and late endosomes).

Besides, EBV glycoprotein M (gM) is a membrane protein conserved throughout the family of Herpesviridae. In HSV-1, gM is involved in localising herpesvirus envelope proteins to sites of secondary envelopment. Upon depletion of gM expression, there is a substantial inhibition of gHgL-mediated internalisation in the infected cells was observed. Though the abrogation of gM does not affect the expression of gH and gL, yet the assembly of virions suggested significantly reduced and eventually correlated with the defects of the gM-negative virus in entry and cell-to-cell spread. Therefore, it suggested the critical role of gM in the virus internalisation [10]. We have looked into the gM peptide-mediated modulations in the neurological compartment. Furthermore, EBV proteins like gp350 have a crucial role in viral tropism, which was further targeted therapeutically. Altogether, the current work implicitly indicates that EBV follows the endocytic pathway to enter brain cells, the role of membrane cholesterol and EBV/gM-mediated modulations in the neuronal milieu.

2. Objective of the research

- Objective 1: Exploring the plausible entry mechanism of Epstein-Barr virus in the brain astrocytes.

- Objective 2: Deciphering the role of membrane cholesterol in the EBV entry in astrocytes.

- Objective 3: Understanding the relationship of EBV and its glycoprotein M peptide with the neurological ailments like Alzheimer's disease and Multiple Sclerosis at *in-vitro* and *in-vivo* levels.

- Objective 4: Evaluating the possible EBV anti-glycoprotein 350 phytocompounds: an insight through, *in-silico*, *in-vitro* and *in-vivo* approach.

3. Structure of Chapters

The following chapters cover the work performed to study the objectives:

- Chapter 1: Introduction of the thesis work.
- Chapter 2: Dissecting the Epstein-Barr virus entry pathway into astrocytes: unfolding the involvement of endosome trafficking.
- Chapter 3: Understanding the role of membrane cholesterol upon Epstein Barr virus infection in astroglial cells.
- Chapter 4: Unravelling the Connection of Epstein-Barr Virus and its Glycoprotein $M_{146-157}$ Peptide with Neurological Ailments at *in-vitro* and *in-vivo* level.
- Chapter 5: Demethoxycurcumin and Rosmarinic acid are plausible inhibitors against glycoprotein 350 of Epstein Barr virus in the neuronal milieu.
- Chapter 6: Conclusion and future prospects.

4. Summary of the chapters and Conclusion

Chapter 1 provides a necessary introduction to relevant concepts, which will help to understand the work in subsequent chapters. Precisely, this chapter discussed about EBV and its connection with neurological manifestation, i.e., MS and virus entry assisting proteins like gHgL, gM and gp350. In **chapter 2**, we have looked into the

possible pathway EBV follows to access the astrocytes. For the virus entry, receptors are considered a critical instrumental moiety for the infection. Hereby, upon screening, we have found amendments in the essential receptors-like Ephrin receptor-A4, -A10 (EPHA4, EPHA10) and non-muscle myosin heavy chain-IIB (NMHC-IIB) in a time-dependent infection of EBV. Once the virus binds to the receptor, it translocates into the lipid-raft region. Membrane cholesterol depletion indicated a decline in the EBV infection in cells like LN-229 and U-87 MG. Inhibition of dynamin with dynasore exhibited mitigation in EBV-GFP and EBV nuclear antigen 1 (EBNA1) in both cell lines. Furthermore, EBV exhibited co-localisation in the early and late endosomes. A significantly higher presence of EBV was found in late endosomes by using markers like Rab7 and LAMP1 at 1 hr and 2 hr of infection. The current work explicitly indicates that EBV follows the endocytic pathway to enter brain cells, although further validation by knocking down these proteins is needed. It will further enable us to pinpoint the potential therapeutic target.
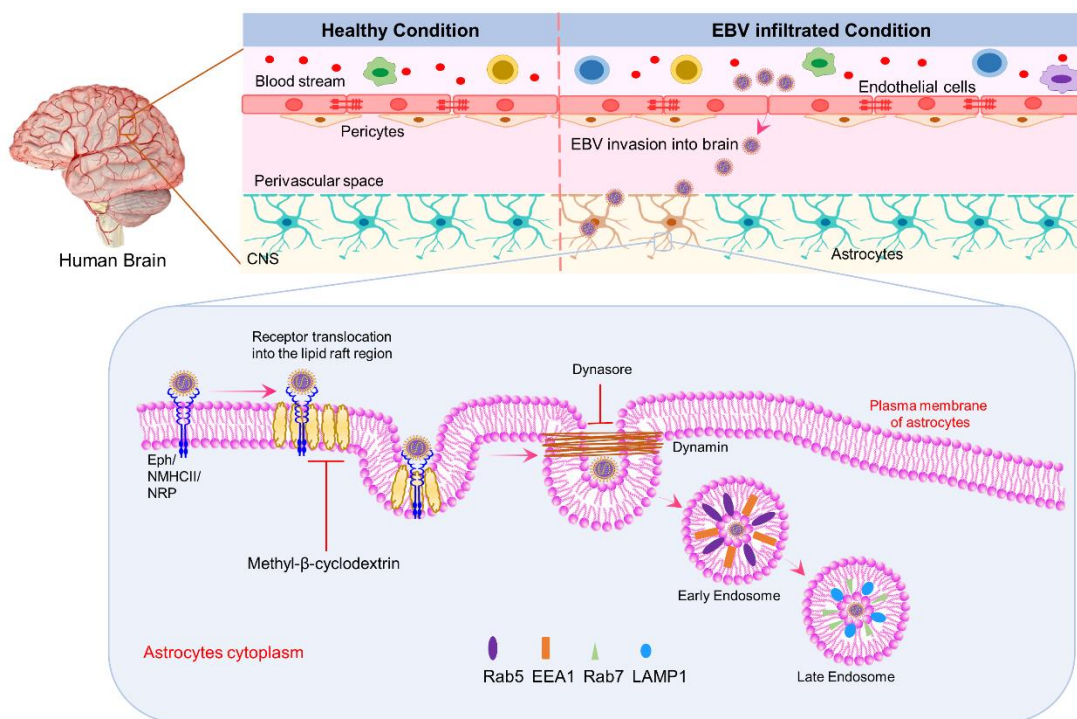
Figure 1: Delineation of EBV entry pathway in the astrocytes.

The **Chapter 3** further extend towards the entry of the virus in neuronal cells, which is assisted by several host factors, including membrane cholesterol. In order to understand its role in EBV infection and pathogenesis into astroglia cells, we have used its

inhibitor, methyl-β-cyclodextrin (MβCD). The membrane cholesterol-depleted cells were infected with EBV, and its latent genes expression were assessed. Further, EBV-mediated downstream signalling molecules, namely STAT3, RIP, NF-kB and TNF-α levels, were checked at protein level along with spatial (periphery and nucleus) and temporal changes in biomolecular fingerprints with Raman microspectroscopy (RS). Upon treatment with MβCD, lmp1 and lmp2a suggested significant downregulation compared to EBV infection. Downstream molecules, like STAT3 and RIP exhibited a decrease in protein levels temporally upon exposure to MβCD while NF-kB levels were found to be increased. Further, the intensity of the Raman spectra showed an increase in triglycerides and fatty acids in the cytoplasm of EBV-infected LN-229 cells compared to MβCD+EBV. Likewise, the Raman peak width of cholesterol, lipids and fatty acids were found to be reduced in EBV-infected samples indicating elevation in the cholesterol-specific moieties. In contrast, an opposite pattern was observed in the nucleus. Moreover, the ingenuity pathway analysis revealed protein molecules such as VLDLR, MBP and APP that are associated with altered profiles of cholesterol, fatty acids and triglycerides with infection-related CNS disorders. Taken together, our results underline the critical role of membrane cholesterol over EBV entry/pathogenesis in astroglia cells, which further trigger/exacerbate virus-associated neuropathologies. These results are likely to aid in the prognosis of neurological diseases like MS.
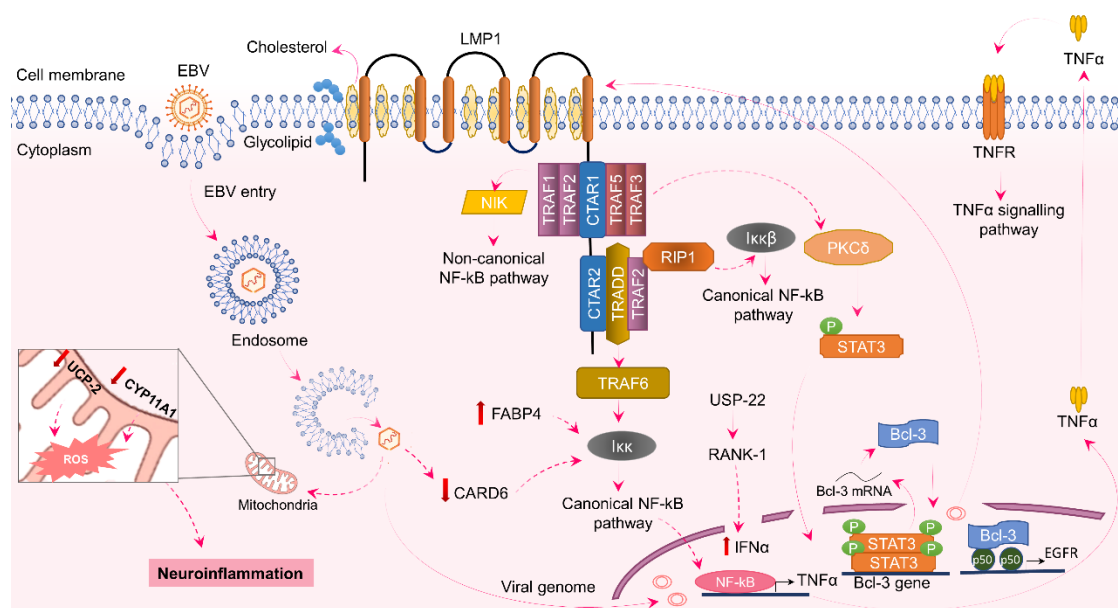
Figure 2: A schematic representation of EBV downstream signalling cascade in astroglial cells.

Consistent with this, **Chapter 4** entails the information about EBV-gM peptide ($_{146}$SYKHVFLSAFVY$_{157}$) exhibits amyloid aggregate-like properties. In the current study, we have investigated the effect of EBV and gM$_{146-157}$ on neural cells (*in-vitro* and *in-vivo*) immunology and eventually in disease-associated genes. Upon incubation with gM$_{146-157}$, a significant elevation was observed in the Aβ$_{42}$ peptide aggregation. Subsequently, the infection of EBV and gM$_{146-157}$ at *in-vitro* (e.g., neuronal cells) indicated upregulation in the inflammatory molecules like IL-1β, IL-6, TNF-α and TGF-β that suggested neuroinflammation. Likewise, at the *in-vivo* level, amendments to the mice's behaviour, neuronal cell disorganization and enhanced inflammatory markers like TNF-α and IL-6 were observed. Amelioration in the Ca^{2+} ions suggested Ca^{2+}-mediated excitotoxicity. A decrease in the mitochondrial potential again affirmed the EBV/gM$_{146-157}$ stimulated neuroinflammatory environment. Furthermore, the level of disease hallmarks like APP, MBP, and ApoE4 also exhibited EBV and gM$_{146-157}$-associated deterioration. Overall, this study delineates a direct connection of EBV and its peptide gM$_{146-157}$ with neurological illnesses such as AD and MS.
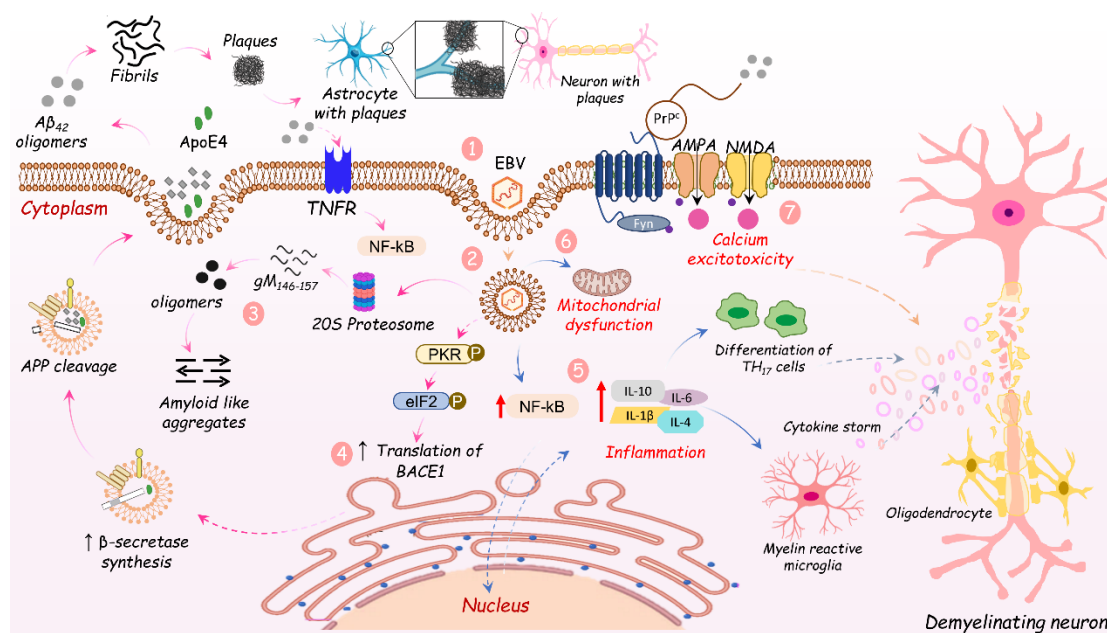
Figure 3: Illustration of a possible downstream pathway involved in the EBV infection and its cleaved peptides in the neuronal cells.

EBV proteins like EBNA1, LMP1, BZLF1 and gp350 have shown continuous presence in the cerebrospinal fluid of patients suffering from neurological disorders. Earlier reports showed that EBV establishes its infection in brain cells, yet limited information

is available on its entry mechanisms. EBV proteins like gp350 have a vital role in the viral tropism. Thereby, in the **Chapter 5**, the extra virion region of gp350 was targeted *in-silico* with phytocompounds. Further, based on the binding affinity, phytocompounds were subjected to molecular dynamics simulation for 100 ns. Compounds namely, demthoxycurumin (DMC) and rosmarinic acid (RA), were considered for further validation *in-vitro* on the EBV-exposed neuronal cells, i.e., IMR-32. Our study indicated a decline of gp350 in DMC+EBV and RA+EBV samples compared to EBV-infected samples. EBV-exposed IMR-32 cells have shown an increase in transcript level of neuro-inflammatory markers like *il-1β, il-6, il-10, il-13* and *tnf-α* while DMC+EBV and RA+EBV exhibited a decrease in these markers. Likewise, the levels of TNF-α, NF-kB and STAT3, which play crucial roles in the inflammatory cascades, and they have shown time-dependent mitigation. Therefore, DMC and RA showed appreciable anti-gp350 effects, and therefore, can be used as therapeutic agents. Eventually, **Chapter 6** summarises the conclusion and future prospects of overall work from all the chapters.

5.   References

1. Sehrawat S, Kumar D, Rouse BT (2018) Herpesviruses: Harmonious Pathogens but Relevant Cofactors in Other Diseases? Front Cell Infect Microbiol 8:177. https://doi.org/10.3389/fcimb.2018.00177

2. Zhang N, Zuo Y, Jiang L, Peng Y, Huang X, Zuo L (2022) Epstein-Barr Virus and Neurological Diseases. Front Mol Biosci 8:816098. https://doi.org/10.3389/fmolb.2021.816098

3. Haahr S, Höllsberg P (2006) Multiple sclerosis is linked to Epstein-Barr virus infection. Reviews in Medical Virology 16:297–310. https://doi.org/10.1002/rmv.503

4. Lünemann JD, Tintoré M, Messmer B, Strowig T, Rovira A, Perkal H, Caballero E, Münz C, Montalban X, Comabella M (2010) Elevated Epstein-Barr virus-encoded nuclear antigen-1 immune responses predict conversion to multiple sclerosis. Ann Neurol 67:159–169. https://doi.org/10.1002/ana.21886

5. Guan Y, Jakimovski D, Ramanathan M, Weinstock-Guttman B, Zivadinov R (2019) The role of Epstein-Barr virus in multiple sclerosis: from molecular pathophysiology to in vivo imaging. Neural Regen Res 14:373–386. https://doi.org/10.4103/1673-5374.245462

6. Jha HC, Mehta D, Lu J, El-Naccache D, Shukla SK, Kovacsics C, Kolson D, Robertson ES (2015) Gammaherpesvirus Infection of Human Neuronal Cells. mBio 6:e01844-15. https://doi.org/10.1128/mBio.01844-15

7. Bu G-L, Xie C, Kang Y-F, Zeng M-S, Sun C (2022) How EBV Infects: The Tropism and Underlying Molecular Mechanism for Viral Infection. Viruses 14:2372. https://doi.org/10.3390/v14112372

8. Totonchy J, Osborn JM, Chadburn A, Nabiee R, Argueta L, Mikita G, Cesarman E (2018) KSHV induces immunoglobulin rearrangements in mature B lymphocytes. PLoS Pathog 14:e1006967. https://doi.org/10.1371/journal.ppat.1006967

9. Jin C, Che B, Guo Z, Li C, Liu Y, Wu W, Wang S, Li D, Cui Z, Liang M (2020) Single virus tracking of Ebola virus entry through lipid rafts in living host cells. Biosaf Health 2:25–31. https://doi.org/10.1016/j.bsheal.2019.12.009

10. Ren Y, Bell S, Zenner HL, Lau S-YK, Crump CM (2012) Glycoprotein M is important for the efficient incorporation of glycoprotein H–L into herpes simplex virus type 1 particles. Journal of General Virology 93:319–329. https://doi.org/10.1099/vir.0.035444-0

LIST OF PUBLICATIONS

A. Publications from PhD thesis work

- **Rani, A**.; Jha H.C. Dissecting the Epstein-Barr virus entry pathway into astrocytes: unfolding the involvement of late endosome. Future Virology. 2024, 19:381-391. https://doi.org/10.1080/17460794.2024.2407729.

- **Rani, A**.; Tanwar, M.; Verma, T.P[#].; Patra, P[#].; Trivedi, P.; Kumar, R.; Jha, H.C. Understanding the role of membrane cholesterol upon Epstein-Barr virus infection in astroglial cells. ***Front. Immunol.*** 2023, 14:1192032, https://doi.org/10.3389/fimmu.

- Patra, P[#].; **Rani, A**[#].; Sharma, N.; Mukherjee, C.; Jha, H. C. Unraveling the Connection of Epstein–Barr Virus and Its Glycoprotein M 146–157 Peptide with Neurological Ailments. ***ACS Chem. Neurosci***. 2023, *14* (13), 2450–2460. https://doi.org/10.1021/acschemneuro.3c00231. ([#]Equal contribution).

- **Rani, A**.; Patra, P.; Verma, T.P.; Singh, A.; Jain, AK.; Jaiswal, N.; Narang, S.; Mittal, N.; Parmar, HS.; Jha, H.C. Deciphering the association of Epstein-Barr virus and its glycoprotein M peptide with neurological ailments in mice. ***ACS Chem. Neurosci***. 2024, 15, 6, 1254–1264. https://doi.org/10.1021/acschemneuro.4c00012.

- **Rani, A**.; Jakhmola, S.; Karnati, S.; Parmar, H. S.; Chandra Jha, H. Potential Entry Receptors for Human γ-Herpesvirus into Epithelial Cells: A Plausible Therapeutic Target for Viral Infections. ***Tumour Virus Research*** 2021**,** *12*, 200227. https://doi.org/10.1016/j.tvr.2021.200227.

- **Rani, A**.; Kumar, P.; Bagde, PH.; Kaithwas, R.; Bhandari, V.; Giri, R.; Jha, H.C. Demethoxycurcumin and Rosmarinic acid are plausible inhibitors against glycoprotein 350 of Epstein-Barr virus in the neuronal milieu (Manuscript under revision in iScience). Manuscript ID: 844bbba69da859ae.

B. Patents:

- Jha, H.C.; Tiwari, D.; **Rani, A**. Potential involvement of viral peptide to instigate amyloid-like aggregate formation. Granted (Patent Id: 202121032715 and filed in July 20, 2021).

- Jha, H.C.; **Rani, A**.; Bagde, P.H. Demethoxycurcumin and Rosmarinic acid are plausible inhibitors against glycoprotein 350 of Epstein Barr virus in the neuronal milieu. (In process)

C. Other publications during Ph.D. work:

1. **Rani, A**.; Ergün, S.; Karnati, S.; Jha, H.C. Understanding the Links Between Neurotropic Viruses, BBB Permeability and MS Pathogenesis. J. Neurovirol. (2024). https://doi.org/10.1007/s13365-023-01190-8.

2. **Rani, A**.; Saini, V.; Patra, P.; Prashar, T.; Pandey, R. K.; Mishra, A.; Jha, H. C. Epigallocatechin Gallate: A Multifaceted Molecule for Neurological Disorders and Neurotropic Viral Infections. ACS Chem. Neurosci. 2023, 14 (17), 2968–2980. https://doi.org/10.1021/acschemneuro.3c00368.

3. Tiwari, D#.; **Rani, A**#.; Jha, H.C. Homocysteine and Folic acid metabolism. Springer link, 2022; pp 3–36. DOI: 10.1007/978-981-16-6867-8_1. (#Equal contribution) (Book Chapter)

4. Indari, O.; **Rani, A**.; Baral, B.; Ergün, S.; Bala, K.; Karnati, S.; Jha, H. C. Modulation of Peroxisomal Compartment by Epstein-Barr Virus. Microbial Pathogenesis 2023, 174, 105946. https://doi.org/10.1016/j.micpath.2022.105946.

5. Varshney, N.; **Rani, A**.; Kashyap, D.; Tiwari, D.; Jha, H. C. Aurora Kinase: An Emerging Potential Target in Therapeutics. In Protein Kinase Inhibitors; Elsevier, 2022; pp 261–322. https://doi.org/10.1016/B978-0-323-91287-7.00028-4. (Book Chapter)

6. Saini, V.; **Rani, A**.; Kumar, A.; Jha, K.; Karnati, S.; Jha, H. C. Altered Synaptic Plasticity: Plausible Mechanisms Associated with Viral Infections. Future Virology 2023, 18 (11), 733–752. https://doi.org/10.2217/fvl-2023-0105.

7. Jakhmola, S.; Indari, O.; Kashyap, D.; Varshney, N.; **Rani, A**.; Sonkar, C.; Baral, B.; Chatterjee, S.; Das, A.; Kumar, R.; Jha, H. C. Recent Updates on COVID-19: A Holistic Review. Heliyon 2020, 6 (12), e05706. https://doi.org/10.1016/j.heliyon.2020.e05706.

8. Jakhmola, S.; Jonniya, N. A.; Sk, M. F.; **Rani, A**.; Kar, P.; Jha, H. C. Identification of Potential Inhibitors against Epstein–Barr Virus Nuclear Antigen 1 (EBNA1): An Insight from Docking and Molecular Dynamic Simulations. ACS Chem. Neurosci. 2021, 12 (16), 3060–3072. https://doi.org/10.1021/acschemneuro.1c00350.

9. **Rani, A**.; Saini, V.; Njini N.G.; Dixit, A.K.; Meena, A.; Jha, H.C. Interpreting the role of Epigallocatechin-3-gallate in Epstein-Barr virus mediated neuronal diseases. (Communicated to Results in Chemistry) Manuscript ID: RECHEM-D-24-00677.

10. **Rani, A**.; Saini, V.; Kaithwas, R.; Jha, H.C. Multiple sclerosis: An insight into the peripheral nervous system. (Communicated to Journal of Neurology) Manuscript ID: JOON-D-24-01702.

11. Kaithwas, R.; Saini, V.; Varshney, N.; **Rani, A**.; H.S. Parmar, H.C. Jha. The Gut-Thyroid Interplay: Understanding Microbial Influence on Gastric Cancer. (Communicated to Journal of the Endocrine Society) Manuscript ID: js.2024-00153

12. Njini, N.; Kandpal, M.; **Rani, A**.; Kumar, Sachin.; Jha, H.C. African medicinal plants for neurological disorder: Therapeutic connotations and plausible mechanism of action. (Communicated to Journal of Herbs, Spices & Medicinal Plants) Manuscript ID: WHSM-2024-0245.

13. Bagde, H.P.; Kandpal, M.; **Rani, A**.; Kumar, S.; Mishra, M.; Jha, H.C. Proteasomal Dysfunction in Cancer: Mechanistic Pathways and Targeted Therapies (In revision from Journal of Cellular Biochemistry) Manuscript ID: JCB-24-0792.R1.

TABLE OF CONTENTS

LIST OF FIGURES

Chapter 1:

Chapter 2:

Chapter 3:

Chapter 4:

Chapter 5:

Chapter 6:

LIST OF TABLES

NOMENCLATURE

Abbreviations used for amino acids, peptides, derivatives, substituents, reagents, etc. are largely in accordance with the recommendations of the IUPAC-IUB commission on Biochemical Nomenclature, 1974, Pure and Applied Chemistry, 40, 315-331. All amino acids are in L-configuration.

kDa   kilodalton

mg   milligram

ml   millilitre

µM   micromolar

nM   nanomolar

nS   nanosecond

ps   picosecond

µl   microlitre

µS   microsecond

ºC   Degree centigrade

Å   angstrom

α   alpha

β   beta

γ   gamma

κ   kappa

K   kelvin

ABBREVIATIONS

ACA- Acute Cerebellar Ataxia

AD- Alzheimer's Disease

ADEM- Acute Disseminated Encephalomyelitis

ADMET- Absorption, distribution, metabolism, excretion, and toxicity

ADT- AutoDock tool

ALS- Amyotrophic lateral sclerosis

APE1- Apurinic/apyrimidinic endonuclease 1

Apo- Apoliporotein

APP- Amyloid precursor protein

Aβ- Amyloid-β

BAC- Bacterial artificial chromosome

BACE-1- Beta site APP cleaving enzyme-1

BDNF- Brain derived neurotrophic factor

BL- Burkitt's lymphoma

CCI- Chronic constriction injury

CHIKV- Chikungunya virus

CMV- Cytomegalovirus

CNTF- Ciliary neurotrophic factor

CNS- Central nervous system

CR2- Complement receptor 2

CSF- Cerebrospinal fluid

CTD- C-terminal domain

DC-SIGN- Dendritic cell-specific intercellular adhesion molecule-3-grabbing non-integrin

DMC- Demthoxycurcumin

DMSO- Dimethyl sulfoxide

EBNAs- EBV nuclear antigens

EBV- Epstein-Barr virus

EGCG- Epigallocatechin gallate

Eph- Erythropoietin-producing human hepatocellular receptors

FTY- Fingolimod

GAPDH- Glyceraldehyde 3-phosphate dehydrogenase

GBS- Guillain-Barre syndrome

gM- glycoprotein-M

gp350- glycoprotein-350

HIV- Human immunodeficiency virus

HHVs- Human Herpesviruses

HLA-DR- Human leukocyte antigen-DR isotype

HSV- Herpes simplex virus

IL- Interleukin

IM- Infectious mononucleosis

JNK- Jun N-terminal kinase dependent

JEV- Japanese Encephalitis virus

KSHV- Kaposi sarcoma-associated herpesvirus

LCV- Lymphocryptovirus

LDLR- Low-density lipoprotein receptor

LMPs- Latent membrane proteins

LRP1- Low Density Lipoprotein Receptor-Related Protein 1

MD- Molecular dynamics

MAPK- Mitogen-activated protein kinase

MMP- Mitochondrial membrane potential

MS- Multiple sclerosis

NF-kB- Nuclear factor kappa-light-chain-enhancer of activated B cells

NGF- Nerve growth factor

NMHC-IIA- Non-muscle myosin heavy chain IIA

NPECs- Nasopharyngeal epithelial cells

NRP- Neuropilin

OPLS- Optimized Potential for Liquid Simulations

PD- Parkinson's Disease

PFA- Paraformaldehyde

PIK3/PKB- Phosphatidylinositol 3-kinase/Protein kinase B

RA- Rosmarinic acid

Rg, Radius of gyration

RMSD- Root means square deviation

RMSF- Root means square fluctuations

ROS- Reactive oxygen species

RS- Raman spectroscopy

STAT3- Signal transducer and activator of transcription 3

Th S- Thioflavin-S

TIMP2- Tissue inhibitor of metalloproteinases 2;

TNF-α- Tumor necrosis factor-alpha;

TRADD- TNFR1-associated death domain protein;

VEGF- Vascular endothelial growth factor

VZV- Varicella-zoster virus

Chapter 1: Introduction

1.1 Epstein-Barr virus

The *Herpesviridae* family encompasses more than 130 viruses that are known to infect mammals, birds, fish, reptiles, amphibians, and even molluscs [1]. Its subfamilies include alpha (α), beta (β), gamma (γ), are known to infect humans and they are categorised based on their replication strategies, which involves host range and genetic organisation [1]. The α-herpesviruses include herpes simplex virus (HSV) 1, -2 and varicella-zoster virus (VZV); β-herpesviruses contain cytomegalovirus (CMV), human herpesvirus (HHV)-6 and -7 while γ-herpesviruses include Epstein Barr Virus (EBV) and HHV-8 [2]. Herpesviruses are so ubiquitous that one or more herpesviruses infect almost all humans during their lifespan. EBV, a dsDNA virus, was first identified in a case of Burkitt lymphoma in 1964 in Africa (Figure 1.1).
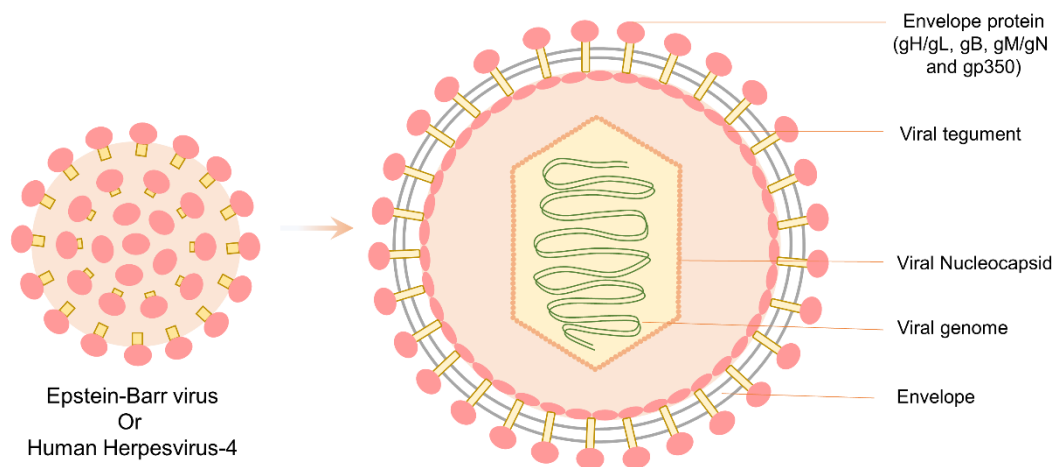
Figure 1.1: Structural framework of Epstein-Barr virus.
EBV contains double-stranded DNA genome enclosed in icosahedral nucleocapsid which is surrounded by tegument protein. Nucleocapsid is further wrapped by envelope and envelope proteins.

Although patients are usually asymptomatic, EBV causes lifelong persistent infection in more than 90% of adults worldwide [2]. EBV is associated with lymphomas and cancers of epithelial cells and EBV replicates with proliferating B-cells or replicates via lytic virion production. Latency of the virus exists in three distinct processes like viral persistence, limited virus expression, which changes the cell growth and

proliferation, and retained potential for reactivation to lytic replication (Figure 1.2) [3]. EBV expresses more than 100 different proteins. In the latent stage, the virus expresses protein, namely EBV-encoded nuclear antigens (EBNA1, -2, -LP [leader protein], -3A, -3B, and -3C), latent membrane proteins (LMP1, -2a -2b), small noncoding RNAs (EBER1 and -2), Bam-HI A rightward transcripts (BARTs) and Bam-HI H left-ward reading frame (BHLF), which are produced during latent infection to stimulate host cell proliferation (Figure 1.2) [4]. EBNA1 plays a significant role in viral persistence and replication, i.e., tyrosine 518 (Y518) forms a crosslink with DNA and facilitates the replication termination at the EBV origin of plasmid replication (OriP). EBNA2 is essential for the immortalization of B-lymphocyte and it induced the expression of LMP1, -2a and -2b. LMP1 prevents EBV-infected B-cells' apoptosis, induces epithelial-mesenchymal transitions (EMT) and its associated cell adhesion, motility and invasion features. LMP2a activates B-cells by the Ras pathway [5]. EBNA3A and EBNA3C support a long-lived reservoir of EBV-memory B-cells, whereas EBNA3B supports by interacting with the T-cells and regulating the germinal centre. EBERs gene shows resistance to apoptosis in B-cells [5].

These genes are expressed differentially in latency stages of type III, type II, type I and type 0. EBV-induced establishment of lymphoblastoid cell line (LCL) shows type III latency, in which most latent genes are expressed (EBER1/2 RNA, EBNALP, EBNA2, EBNA3A/3B/3C, EBNA1, LMP2A/2B, LMP1 protein, BART RNA) (Figure 1.2) [6]. In Hodgkin's lymphoma and nasopharyngeal carcinoma demonstrate type II latency (EBER1/2 RNA, EBNA1, LMP2A/B, LMP1 (type IIa) or EBNA2 (type IIb), BART RNA) and Burkitt's lymphoma shows type I latency (EBER1/2 RNA, EBNA1, LMP2A/2B, BART RNA) [6]. In latency III, the EBV-associated post-transplant lymphoproliferative disease (PTLD) is mainly regulated by genes like EBNA2, EBNALP, EBNA3A and EBNA3C, and these eventually upregulate the expression of cMyc expression and cell proliferation [6]. Latency II in HL and NPC, LMP1 and LMP2 expression contributes to cell survival by activating the nuclear factor-κB (NF-κB) and phosphatidyl inositol 3 kinase (PI3K) pathways.

In-vitro transformation of primary B-cells to LCLs, the expression of EBNA1 and LMP2A play a crucial role and EBNALP, EBNA2, EBNA3A, EBNA3C, LMP1 are

also individually essential [7]. During immunocompromised conditions, the virus gets reactivated and goes for lytic replication by inducing the expression of immediate early genes, which in turn activates early genes and ultimately, late lytic genes. Induction of certain chemicals like butyric acid and 12-O-tetradecanoylphorbol-13-acetate initiate the expression of the first group of lytic genes such as BZLF1, BRLF1 and BMLF1, which play key roles in the transition from latent to lytic cycle of infection [8]. In turn, these genes activate the expression of early genes like BALF5, BALF2, BORF2, NARF1, BGLF5, BXLF1, BHRF1, BMRF1 and BSMLF1, that are involved with the virus replication (Figure 1.2) [9]. Further, the late lytic genes encode for the viral structural protein and DNA replication including BLLF1, BALF4, BXLF2 and BCRF1 [5].
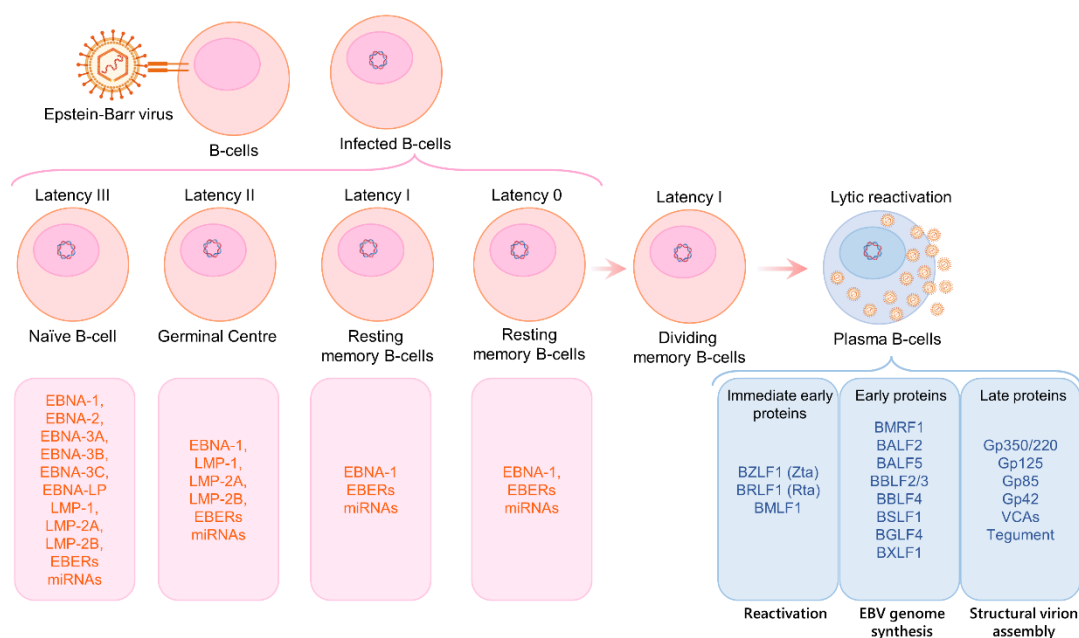
Figure 1.2: Representation of EBV latent and lytic cycle expressing genes.
EBV infects and maintain in latency III in naïve B-cells and latency II (germinal centre), latency I and 0 (resting memory B-cells). Virus expresses differential pattern of genes in these latencies. Upon opportunity, this virus goes for lytic reactivation which is initiated by immediate early gene followed by early proteins and eventually late lytic proteins.

1.2 Delineation of neurological ailments

1.2.1 Multiple Sclerosis

Multiple Sclerosis (MS) is a central nervous system (CNS) disorder and it has an autoimmune nature [10]. Several autoreactive lymphocytes cross the blood-brain

barrier (BBB) and enter into the brain and trigger the local inflammation that results in demyelination, gliotic scarring and axonal loss (Figure 1.3) [10]. Young individuals between 20-40 years of age are mainly affected and a high frequency of MS is seen in women, who are affected twice as often as men [11]. Variant of HLA genes of major histocompatibility complex (MHC) was also found to be associated with the MS (Figure 1.3) [11]. This disease is likely to be affected by B-cells through various mechanisms like ectopic lymphoid follicles within the CNS, cytokine production, antigen presentation and antibody production [12]. It usually follows the relapsing-remitting disease course is followed by a progressive phase. Pathophysiological hallmarks include inflammatory lesions, axonal damage, eventually, the neuronal dysfunction, which results in plaques/lesions formation in the brain's white matter (Figure 1.3) [13]. These lesions are associated with sensory loss, visual impairment, muscles weakness, ataxia and impaired balance. MS plaques are found in the white matter around the ventricles, optic nerves and tracts, corpus callosum, cerebellar peduncles, long tracts and subpial region of the spinal cord and brainstem [11]. White matter transfers neural signals to the body after gathering from the grey matter. MS majorly involves two steps: i) formation of lesions in CNS due to damage in the myelin sheath and ii) debilitation of neuronal tissues due to severe inflammation [14].

MS patients generally show focal inflammatory plaques consists demyelinated axons a declined number of oligodendrocytes, and parenchymal infiltration of lymphocytes and macrophages [15]. The progressive course of MS is profoundly affected by grey and white matter atrophy, microglial activation, inflammation, axonal and myelin injury. Demyelination, and eventually, degeneration of neurons is associated with various forms of MS, and involves adaptive and innate immunity. Besides, myelin sheath or myelin proteins [myelin basic protein (MBP), myelin oligodendrocyte glycoprotein (MOG), and proteolipid protein (PLP)], are prone to the activated microglia and macrophages, which secrete several cytotoxic cytokines, excitotoxins, reactive oxygen and nitric oxide species (Figure 1.3) [16]. Demyelination harbours changes like antibody and complement-associated perturbations, degeneration of distal oligodendrocyte processes, loss of astrocyte polarity and disturbances of the structural organization of perivascular glia limitans [17]. MS is majorly contributed by T-cells having a preponderance of CD8+ cells compared to other T-, B- and plasma cells. Inflammatory lesion consists mainly of CD8+, CD4+ T-cells and activated glial

cells. CD8+ T-cells interact with target cells through MHC-I, which is stringently regulated in neurons and hereby, MHC-I molecules get activated in the presence of a significant signal of IFN-γ or TNF-α (Figure 1.3) [18].
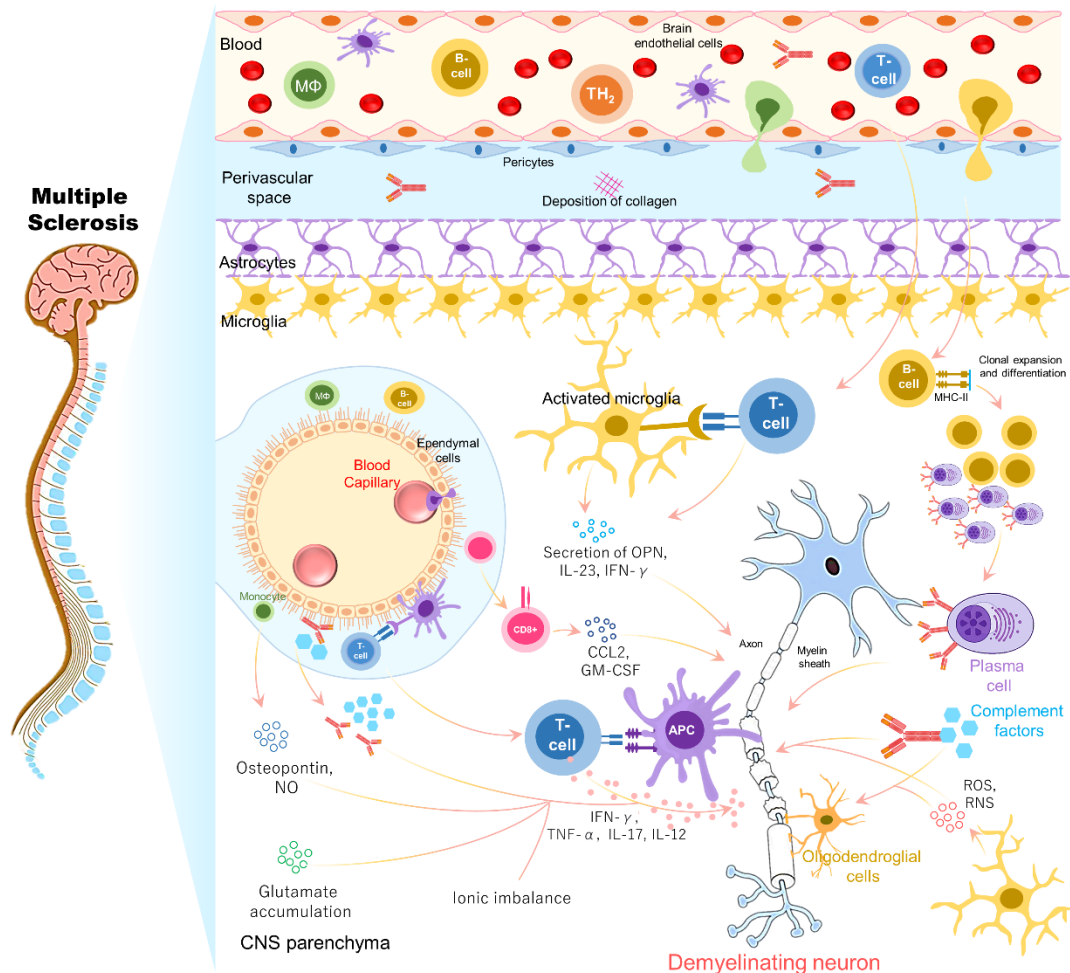
Figure 1.3: Delineating the pathophysiology of Multiple Sclerosis.
Majorly contributed by immune or autoimmune responses. Immune cells cross the blood-brain barrier and reach the brain parenchyma, which they secrete inflammatory moieties like IL-23, IFN-γ, CCL-2, GM-CSF, TNF-α, IL-17, IL-12, NO, ROS and RNS. Glial cells like microglia and astrocytes get reactivated. Immune molecules like complement factors, antibodies, osteopontin, glutamate accumulation and ionic imbalance aid in MS pathology. These immune responses eventually trigger the demyelination of neurons and apoptosis of oligodendrocyte precursor cells.

Active demyelinating plaques are speculated into four different pathological patterns. Macrophages and T-cells present predominantly and surrounded by veins and venules found in patterns I and II, while the presence of immunoglobulin precipitation and activated complement is distinguished in pattern II [19]. In patterns I and II, the expression of myelin proteins (MBP, PLP, MOG and MAG) was found to be reduced

by some degree and the loss of oligodendrocytes variably. Remyelination process is also extensive in the pattern I and II lesions. The infiltration of macrophages, T-cells, activated microglia, loss of MAG and severed oligodendrocyte loss and evidence of oligodendrocyte apoptosis are mainly observed in the pattern III lesions [19]. While pattern IV lesions demonstrate the inflammation mediated by macrophages and T-cells, the presence of peri-plaque in the white matter and the loss of myelin proteins at the active edge of the plaque. Patterns III and IV exhibit minimal remyelination [19]. Several shadow plaques are also seen in the concomitance of active demyelinating lesions and retain viable oligodendrocytes in the I and II pattern lesions [19].

1.2.2 Alzheimer's diseases

Alzheimer's disease (AD) is a multifactorial neurodegenerative disorder characterised by progressive cognitive and motor function decline, and it is primarily affecting aged population [20]. Pathological hallmark of the disease includes the aggregation of amyloid-beta peptide outside cells and hyperphosphorylated Tau forms intracellular neurofibrillary tangles which result in neuroinflammation, gliosis and neurodegeneration (Figure 1.4) [21]. It has been found that numerous viruses are involved in several pathways varying distribution in brain regions and especially in the older brains, it induces chronic inflammation and ultimately neurodegeneration [20]. This progressive and irreversible damage in neurons leads to cognitive impairment. A total of 60-70% of cases of AD predominantly cause senile dementia globally [20]. Incidents of dementia associated with AD are predicted to be increased up to 300% from 2020 to 2040 in South-East Asian countries, including India [22]. Along with plaques, the damage in AD is induced by oxidative stress, which is another crucial facet of neurodegeneration (Figure 1.4) [23]. Progression of AD pathology leads to apathy, depression, impaired communication, disorientation, poor judgement, behavioural changes, difficulty in walking and swallowing [23]. Factors like age, sex and genetics also determines the disease symptoms. Several genome-wide association studies (GWAS) on AD suggested the concurrence of single nucleotide polymorphisms (SNPs), which predispose individuals to the disease [24]. Aβ is derived by sequential cleavage of amyloid precursor protein (APP) via enzyme beta-secretase and gamma-secretase [25]. Aggregation of Aβ thus forms toxic oligomers

that are harmful to the neurons. Senile plaques of AD are made of variety of 36-43 residue-long amyloid peptides that undergo fibrilization to form Aβ sheets that are resistant to degradation (Figure 1.4) [26]. Tau is derived through alternative splicing of the microtubule-associated protein tau (MAPT) gene and results in the soluble protein isoforms and form neurofibrillary tangles in the neurons (NFTs) (Figure 1.4) [26].
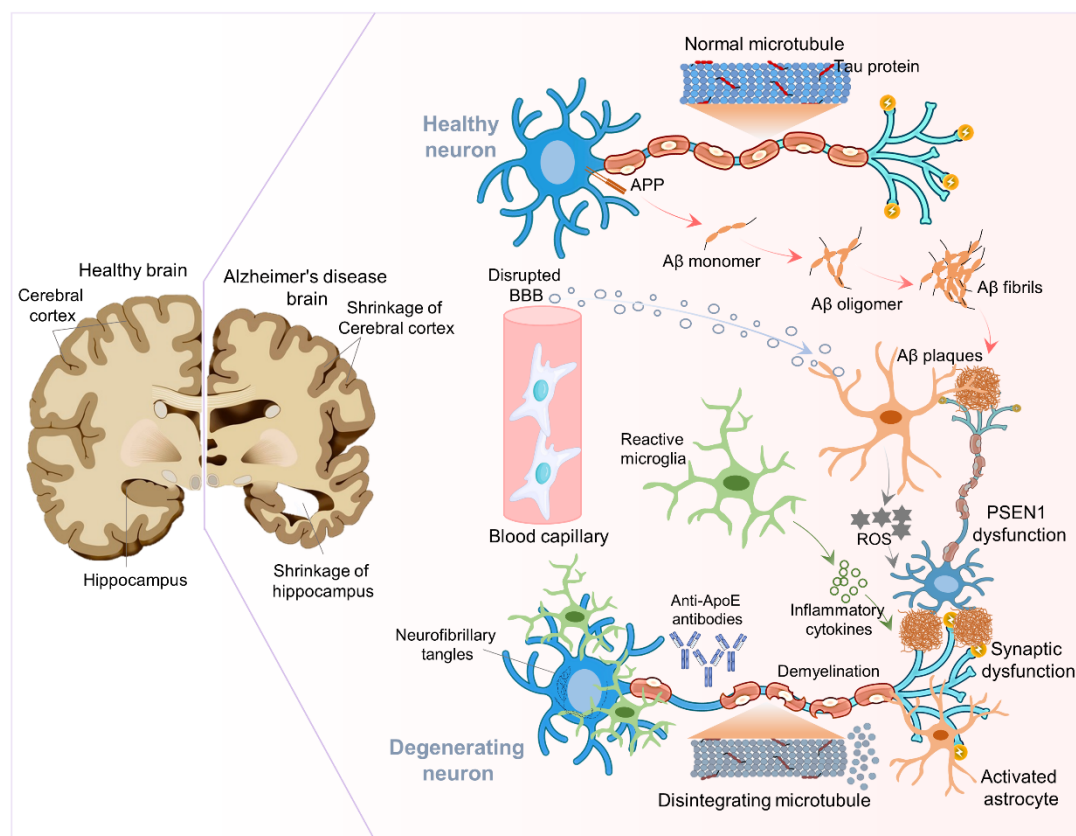
Figure 1.4: Pathophysiology of Alzheimer's disease.
The brain cortex and hippocampal region of brain get shrank. The amyloid-beta form fibrils outside the neurons and create hindrance in the neuronal communication. Microtubule also gets disintegrated which affect the Tau protein and eventually commence the tauopathies. Immune responses and activation of glial cells further aid in the disease pathology.

NFTs comprise the paired helical fragments (PHFa) of the Tau fibrils ~20 nm in diameter. These plaques spread throughout the brain as the disease progresses. In AD stage I-II, tangles showed presence in the trans-entorhinal region and in the III-IV stage, these tangles unfold into the limbic system, and eventually, in stage V-VI, the pathology is seen in the neocortex [27]. Intriguingly, several other neurodegenerative diseases also come under the umbrella of tauopathies, like Parkinson's disease, progressive supranuclear palsy, frontotemporal dementia, and corticobasal

degeneration. Numerous functional interactions between Aβ and Tau have revealed damage to the neural circuits and a decline in cognition [26].

AD triggers due to familial Mendelian inheritance as well as sporadic. The early onset of AD (EOAD) happens due to mutations in the genes like APP, PSEN1 and PSNE2 (Figure 1.4) [28]. AD also involves perturbations in the morphology/number/transport of mitochondria, declined cytochrome oxidase activity and deficiency of metabolic proteins. These impairments in the mitochondria lead to oxidative stress at the synapse. In EOAD, Aβ induces mitochondrial deficits, increases the aging rate and increase susceptiblity towards AD [28]. The APP transgenic mice exhibited elevation of Aβ in the synaptic mitochondria, resulting in the ROS production and accumulation of plaques by affecting the activity of β-secretase. Synapse loss and atrophy in the neurons throughout the cerebral cortex and medial temporal lobe have been observed in AD patients. Disease commences from the hippocampus and entorhinal regions, then spreads throughout the frontotemporal lobes and eventually reaches the striatum, thalamus and cerebellum. The pyramidal cells of the hippocampal cornu ammonis (CA1) region are prone to morphological changes and cell death, results in memory loss [29].

1.3 Entanglement of Epstein-Barr with neurological disorders

1.3.1 EBV-mediated molecular mimicry and association with Multiple Sclerosis

Infection of EBV induces immune disorders, and it promotes the development of neurological ailments. EBV infection was detected in B- and plasma cells inside the brain which is nearly 100% of the cases examined for multiple sclerosis (MS), whereas it is not the case in other inflammation-mediated brain diseases [30]. Therefore, the exact mechanism of EBV in the brain is again a profoundly fascinating question. Different modes of EBV pathogenesis that have been speculated: i) EBV may directly infiltrate the nervous system (NS). Most children with EBV viral encephalitis did not have any infection symptoms outside the brain like tonsillitis and enlarged lymph nodes. This suggested a primary neurological infection of EBV. ii) EBV potentially triggered immune-mediated symptoms in the NS. EBV may share a common antigen (molecular mimicry) with the myelin glycoprotein of oligodendrocytes (Figure 1.5) [31]. Molecular mimicry induces the immune system

to generate autoimmune T-lymphocytes as well as anti-neuronal antibodies against the autoantigens (Figure 1.5) [32]. iii) EBV reactivation from latency could trigger pathogenic features of neuronal disorders, especially in immunosuppressed patients.
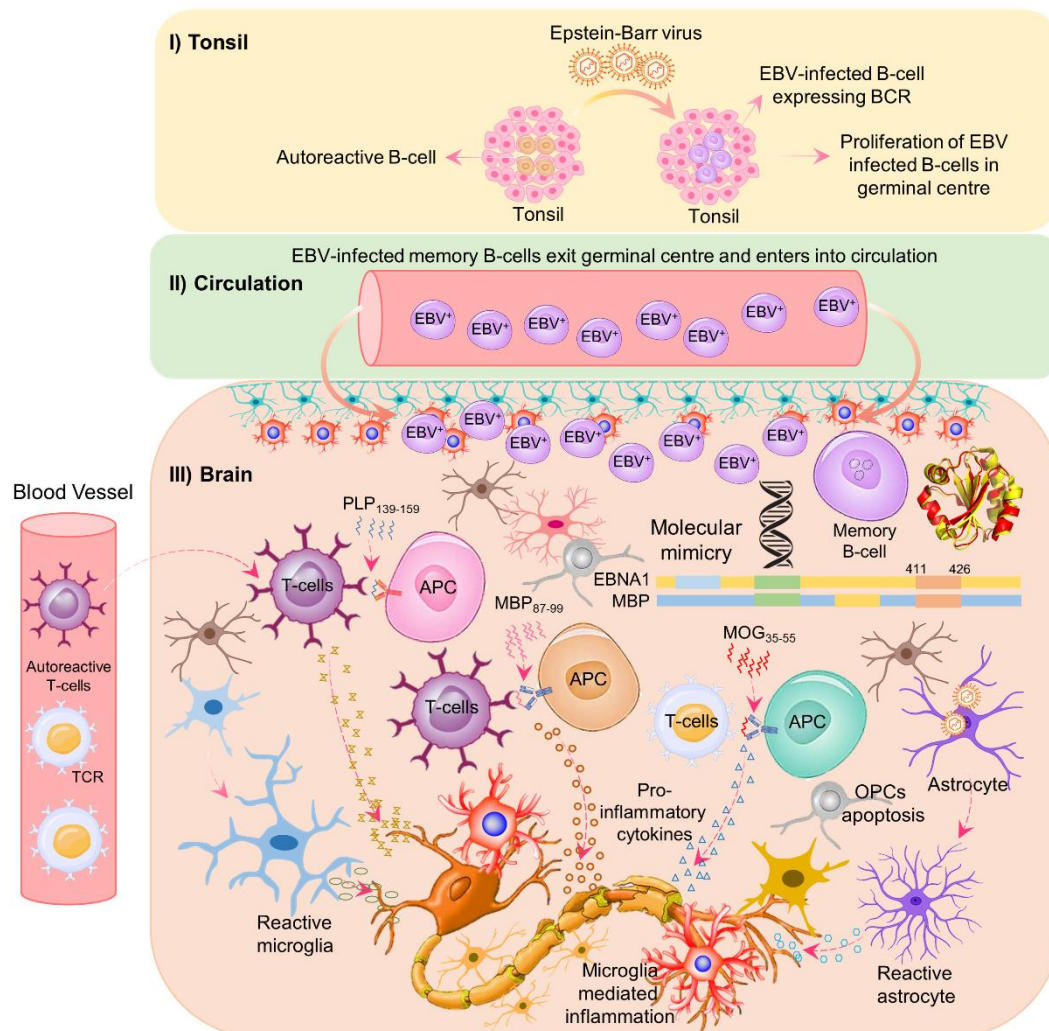
Figure 1.5: Underpinning the molecular mimicry mechanism by EBV.
I) EBV infects the nasopharyngeal epithelial cells where is infects the B-cells. II) These memory B-cells come into the circulation and travel to the brain by the trojan horse mechanism. III) In the CNS parenchyma, EBV gets reactivated release into the CNS. Several EBV proteins exhibit molecular mimicry with myelin protein, i.e., $EBNA1_{411-426}$ with MBP. Other myelin proteins like MOG_{35-55}, MBP_{87-99}, and $PLP_{139-159}$ potentially generate autoimmune responses. Autoimmune responses in the brain activate cells like astrocytes and microglia and results in the massive neuroinflammation.

EBV induce changes in the tight junctions (TJ) proteins of endothelial cells, basal lamina, cytoskeleton, growth factors, cytokines/chemokines, matrix metalloproteinases (MMPs), various lipid mediators, ROS and cell adhesion

molecules (CAMs) (Figure 1.5) [33]. A cohort study with a mean follow-up of 7 years on 147 clinically isolated syndromes (CIS) patients and 50 controls demonstrated immune responses against EBV, HHV-6, CMV and measles [34]. The aforementioned study also revealed an elevated immune reaction toward EBNA1. Discrepant presence of EBV in MS lesions suggested that EBV-containing memory B-cells possibly lose the episomic EBV DNA during the replication [34]. However, it hangs on to forbidden epitopes recognition, it is likely to activate a molecular mimicry mechanism. MBPs bind to EBNA1-specific antibodies and also with specific epitopes 411-426 (Figure 1.5) [35]. The monoclonal antibodies against MBP transact with LMP1 to subdue the T-cell activation (CD4+) and increase the antibody concentration against CTARs in MS pathogenesis [36]. Likewise, the viral protein exosome released from oligodendrocytes exhibited reduced MBP and induced demyelination. In B-cells, LMP2A and -2B prime TLR9 are linked with the progression of experimental autoimmune encephalomyelitis (EAE) by activating immune responses and inflammation by releasing factors like IFNγ [37].

There are shreds of evidence suggesting an association of EBNA2 with neurological ailments, e.g., MS. EBNA2 can accelerate the expression of various host genes, signals recruitment of transcription activations factors such as immunoglobulin kappa J region (RBPJ) and the vitamin D receptor (VDR) [38]. An *in-vitro* study by Jha *et al*. has manifested that EBV effectively infects neuroblastoma (i.e., SH-SY5Y and Ntera2) as well as primary fetal neuronal cells [38]. Another study from our group has shown EBV infection to U-87 MG cells and suggested EBV aids neuroinflammatory reactions by increasing proinflammatory cytokines (IL-6 and TNF-α) and also through peripheral blood mononuclear cells (PBMCs) infiltration [39]. Presentation of recombinant human MOG (rhMOG) by EBV-infected B-cells to CD8^{+} T-cells was observed [40]. The higher expression of CD40 on B-cells from the relapsing patients of MS suggests increased antigen presentation by B-cells (Figure 1.6) [40]. Additionally, the EBV-infected B-cells were actively found in demyelinating lesions of relapsing-remitting multiple sclerosis (RRMS) patients who died of lethal relapse [41]. An increased titre of anti-EBV antibodies instigates the development of more contrast-enhancing lesions in magnetic resonance imagining (MRI) and higher disability scores [41]. Authors have also reported an opposite association between IgM against viral capsid antigen (VCA) and inflammatory activities [41]. Moreover, the presence of EBV DNA in the CSF of MS patients was also linked with elevated

contrast-enhancing lesions. Postmortem analysis of white matter tissues of MS patients exhibited upregulation of inflammatory cytokine, i.e., IFN-α along with RNA positivity of EBV proteins was detected [41]. In animal models, EBV-containing B-cells regulate the migration of lymphocytes via MS-related markers, namely EBV-induced gene 2 (EBI2) and an orphan G-protein coupled receptor. EBI2 activation by oxysterols (7-alpha-25-dihydroxycholesterol) regulates myelin development and effectively inhibits the secretion of proinflammatory cytokines, disrupting BBB and microglial activation [42].

An increase in the EBNA1-primed T-cells (CD4+) was found in MS patients; these T-cells further secrete the IFN-γ and cross-react with myelin antigens. MS postmortem brain samples revealed T-cell infiltration and CD8+ T-cell-mediated cytotoxic activity (Figure 1.6) [43]. T-cells (CD8+CD28−CD57+) play a predominant role in EBV-mediated immune responses, namely augmentation in the expression of PD-1 and elevation in the release of IFN-γ (Figure 1.6) [44]. The EBV+ B-cells were found to accumulate in the patients with RRMS. EBV encoded proteins like EBNA1, EBNA2, EBNA3B, LMP1 and LMP2A derived from EBV-infected B-cells involved in developing MS via regulating the B- and T-cells. Alleles like EBNA3B1.2, EBNA3B2.1, and LMP1.1 are positively correlated with the risk towards MS, while the downregulated expression of alleles LMP1.5, LMP2A4.2, EBNA1.3, EBNA2.1 and EBNA3B2.2 showed protective effect against the MS pathogenesis [31]. Hintzen *et al.* study established that an elevated serum EBNA1 IgG antibodies are associated with SNP risk alleles in gene-gene interactions namely, rs3135388 (HLA-DRB1*1501), rs2744148 (SOX8), rs11154801 (MYB), rs1843938 (CARD11), and rs7200786 (CLEC16A/CIITA) [45]. Human leukocyte antigen (HLA)-DR haplotype allele DRB1*1501 impact the risk of developing MS. GWAS studies unveiled more than 200 susceptibility genes and HLA-DRB1*1501 allele act in a collegial manner with EBV-mediated immune responses and ultimately increase the vulnerability towards MS several folds [46]. Notably, anti-EBNA1 IgG at the C-terminus of this fragment (385-420) were positively correlated with the HLA-DRB1*1501. Myelin protein epitopes (PLP$_{139-151}$, MOG$_{35-55}$ and MBP$_{87-99}$) are being used to generate model systems for MS such as EAE to understand the disease mechanism and therapeutics (Figure 1.5) [47]. Viruses like Theiler's murine encephalomyelitis virus (TMEV) is also commonly used to generate EAE.
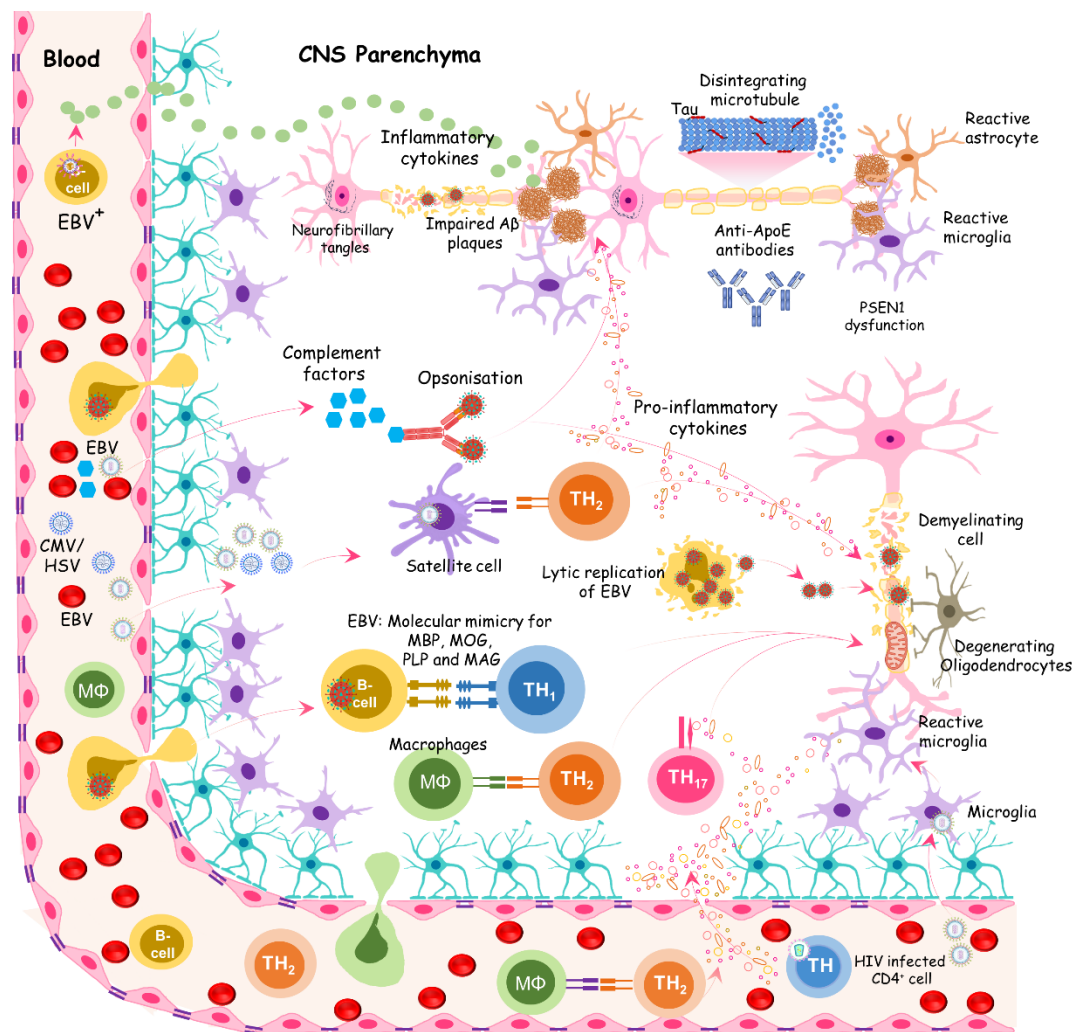
Figure 1.6: Plausible illustration of communication of EBV with Multiple Sclerosis and Alzheimer's disease.
Herpesviruses like EBV, VZV, HSV-1, HSV-2 and CMV get access to the CNS through the circulatory system. Viruses induce the immune cells to release cytokines. Viruses like EBV maintain latency in the B-cells, conventionally mimic at the molecular level and generate autoimmune responses. CD4^{+}-infected T-cells infected with HIV potentially cross the endothelial barrier, reach the peripheral neuronal site, and trigger a massive cytokine storm. Along with cytokine storm, the host cellular organelles, i.e., mitochondria, also participate in the demyelination process of neuronal cells. Complement factors and antibodies travel to the brain and follow the opsonisation process. In addition, these immune responses or viruses also potentially commence the accumulation of Aβ42 aggregates. Microtubule disintegration eventually contributes to the abnormal Tau physiology and results in its accumulation.

1.3.2 Association of EBV with Alzheimer's disease

Several histological findings confirmed the presence of herpesvirus infection in the NFT as well as in the hippocampus. Latent EBV infection in AD patients results in cognitive decline upon EBV reactivation/replication, serologic EBV positivity and

EBV-IgG in plasma have been observed [31]. Anti-EBV IgG antibody concentration indicated a significant association with mild cognitive impairment (aMCI) and eventual link with AD (Figure 1.6) [31]. Thereby, this EBV antibody concentration can be used as a biomarker to decipher the risk of aMCI. Neuroinflammation induced by EBV-infected peripheral blood mononuclear cells and brain monocytes/macrophages exhibits loss of neurons in the white matter. Elevated TNF-α leads to hyperphosphorylation of Tau protein and amyloid plaques (Figure 1.6) [31]. The lymphoblastoid cell line, where EBV immortalizes B-cells, indicated elevated expression of TNF-α and induced amyloid β-protein aggregation and hyperphosphorylation of Tau protein and fostered the AD pathogenesis [48]. The CD8+ TEMRA cells interaction with the EBNA3A and BZLF1 stimulates the release of proinflammatory cytokines, namely IFNγ, TNF-α, and cytotoxic factors (NKG7, GZMA, and B2M), which are associated with cognitive decline and AD pathogenesis. EBV-encoded BNLF-2a blocks the transporter-associate with antigen processing (TAP), which eventually downregulates the MHC I and II expression and accelerates the accumulation of polypeptide environment in the neuronal cells (Figure 1.6) [31]. EBV+ AD patients brain tissues were ApoE4 carriers and they had high level of EBV+ leukocytes [49]. In addition, aberrant cell cycle re-entry of neurons is also associated with AD pathogenesis. EBV-LMP1 is known to influence the activation of the Ras-MAPK pathway and aid in the development of neurological diseases (Figure 1.6) [50]. The likelihood of an infectious etiology of AD with viruses, bacteria and parasites. Herpesviruses such as EBV, HSV-1, and HHV-6 have indicated association with neurological ailments, even though the clear mechanistic detail in currently elusive [51]. Recently, a new perspective detected the presence of EBV-specific T-cell receptors in the CSF of AD patients, which elevated the antigen-specific clonal expansion of CD8+ T-cells in AD. GWAS study indicated the link of AD with herpesvirus infection, i.e., VZV, HSV-1 and EBV [52].

1.3.3 Association of EBV with other neurological disorders

In addition to AD and MS, Parkinson's disease (PD) is another neurodegenerative disorder triggered by a combination of genetic and environmental factors. The primary pathology of PD is degeneration of dopaminergic neurons in the substantia nigra region and abnormal aggregation of proteins such as Lewy bodies in the brain [53].

The aging brain is vulnerable to pathogenic infection. Antibodies against EBV have been observed in the CSF and serum samples of patients with PD. The latent infection of EBV triggers the release of autoantibodies that cross-react with α-synuclein (α-syn) and upregulate its level [31]. Notably, LMP1 and α-syn protein share the primary amino acid sequence PXDPDN, where DPDN sequence is cross-reactive target of α-syn. The genetically prone individuals, DDNGPQDPDN repeat region of LMP1 initiate the immune response to the α-syn epitope EDMPPVDPDN [31]. It further releases systemic inflammatory markers like interleukin-1β (IL-1β), interleukin-6 (IL-6), TNF-α, and C-reactive protein (CRP), which are linked with the development of PD [31].

The direct infection of the virus also leads to encephalitis and meningitis. The critical clinical outcome of encephalitis includes brain parenchymal damage and intracranial hypertension. The virus-induced meningitis involves the diffusion of inflammatory moieties through the pia mater and arachnoid layer [33]. Infiltration of cytotoxic CD8+ lymphocytes induced by the virus entails antigen-antibody complexes and triggers immune damage. EBV-mediated encephalitis is profoundly aided by transformed B-cells and secrete anti-neuronal and anti-EBV antibodies [54]. Anti-EBV proteins cross-react with neuronal antigens. The elevated level of PD-L1 induced by activated CD4+ T-cells. EBV expresses several viral proteins (e.g., EBNA1, LMP1, LMP2A) and exhibits immune evasion function, which results in the development of EBV encephalitis [54]. Reactivation of latently infected B-cells occurs in two different ways in the CNS: activation of abnormal lymphoid follicles and transplantation of EBV-infected memory B-cells into the CNS [55]. An individual with suppressed immunity entails the EBV-infected B-lymphocytes and have increased EBV antibody titre. The reactivation of the virus in the blood circulation and virus particles eventually cross the blood-cerebrospinal fluid barrier and enter into CNS parenchyma. EBV lytic replication gene BZLF1 presence has been confirmed in the CSF of certain immunocompetent patients [31]. Increased levels of factors like BDNF, NGF has observed in patients in EBV-mediated meningitis, and suggesting the neuroinflammation [31].

EBV also exhibited profound association with acute disseminated encephalomyelitis (ADEM). This virus can directly induce encephalopathy or indirectly trigger the

autoimmune ADEM [56]. EBV-linked ADEM results in the multifocal demyelination of venous white matter and the presence of EBV-IgM in CSF along with EBV DNA in the serum [31]. The cross-reactivity of EBNA1 with myelin glycoproteins also contributes to the development of ADEM [31]. Also, the immunosuppressed transplant patients with ADEM indicated the local reactivation of EBV, which triggers the inflammatory diseases or aggravates the existing disease [31]. Besides, EBV infection disclosed consortium with acute cerebellar ataxia. These patients showed seropositivity for EBV IgM, IgG and the presence of OCBs of viral capsid antigen antibodies in the CSF [57]. Infection of EBV affects the cerebral hemispheres that triggers hydrocephalus and elevate the intracranial pressure. Expression of BZLF1 has also been detected in cerebellar ataxia patients [58]. However, the mechanistic details have yet to unravel.

1.4 Epstein-Barr virus entry mechanism into brain cells

Virus infection into the host cells involves a complex multi-step process, the first step includes the virus attachment to different host cells using distinct sets of viral glycoproteins [59]. Upon attachment, the processes of viral fusion and entry get initiated. For instance, EBV infection of epithelial cells mainly relies upon the interaction of gHgL with host surface integrin molecules ($\alpha v \beta 5$, $\alpha v \beta 6$, and $\alpha v \beta 8$), neuropilin (NRP1), non-muscle myosin heavy chain-IIA (NMHC-IIA) and the recently reported erythropoietin-producing human hepatocellular (Eph) receptors (Figure 1.7) [60]. Kaposi's Sarcoma herpesvirus (KSHV) is also known to utilise Eph and ephrins as attachment or entry receptors [61]. Binding of the viral proteins to the host receptors trigger conformational changes, leading to membrane fusion. Eph is involved in multiple life processes and several diseases, and at the same time, it is closely related to viral infections.

Under normal physiological conditions, these receptors regulate neuron-glia communication, early brain development, maintaining cell-cell junctions and myelination [62]. EphA2 was identified as a specific host entry receptor for EBV. The EBV gHgL is known to make a complex with ligand-binding domain (LBD) region of Eph receptor to gain entry into the epithelial cells (Figure 1.7) [63], [64]. EBV gHgL binds to the peripheral region of LBD primarily by using gL. An RNAi and knockout analysis of EphA2 showed reduced EBV epithelial cell fusion and infection

by 90% and 80%, respectively [63]. A similar study also revealed that EphA2 gene knockout in HEK293T cells reduced EBV infection up to 85%. Also, the overexpression of EphA2 increased EBV infection in epithelial cells [64]. Moreover, the intracellular kinase domain of EphA2 was reported to be dispensable for EBV infection. The gL mutant (N69L/S71V) study of EBV showed a higher binding affinity for EphA2 compared to the wild type [65]. It was evaluated that this glycosylation site (N69/S71) possibly offered steric hindrance in the wild type interaction scenario.
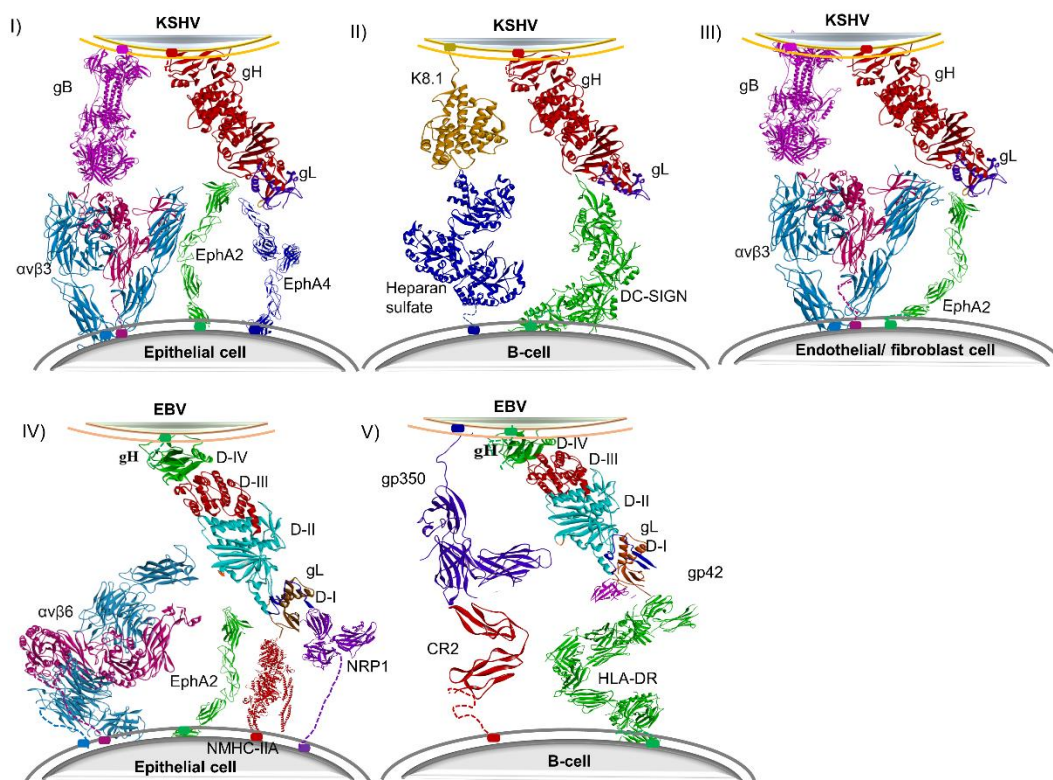
Figure 1.7: Human γ-herpesviruses attachment to different cells
I) KSHV gHgL and gB (modelled structures) make an attachment with epithelial cell via integrin (αVβ3; Pdb Id: 1JV2) and EphA2 (Pdb Id: 2X10) and -A4 (Pdb Id: 4BK4). II) KSHV gHgL and K8.1 (Pdb Id: 5ZB1) make an attachment with heparan sulfate (Pdb Id: 1VKJ) and DC-SIGN (Pdb Id: 6GHV) receptor in B-cell. III) KSHV (gHgL and gB) attach with endothelial and fibroblast cells via integrins and EphA2. IV) EBV gHgL (Pdb Id: 3PHF) attaches to epithelial cell receptors EphA2, integrins (αVβ6; Pdb Id: 4UM8), NRP1 (Pdb Id: 2QQM) and NMHC-IIA (Pdb Id: 4PD3). V) EBV (gp350; Pdb Id: 2H6O, gHgL; Pdb Id: 3PHF and gp42; Pdb Id: 5T1D) attachment to B-cell receptors CR2 (Pdb Id: 1LY2) and HLA-DR (Pdb Id: 2WBJ).

Yet another γ-herpesvirus, i.e., KSHV uses EphA2 to infect the endothelial cells and indicated its interaction with gHgL protein complex (Figure 1.7) [63]. Mutations in gH ELEFN motif (Glu-Leu-Glu-Phe-Asn50-54) results in decreased interaction with EphA2 [65]. Contrarily, EBV gHgL is deprived of this domain, so, it is likely that

EBV gHgL utilizes some other domain for the fusion activity. In contrast, for establishing the attachment with B-cell, KSHV glycoprotein K8.1 and gHgL uses receptors like HS and DC-SIGN (Figure 1.8) [66]. The primary attachments of the virus trigger the downstream cascading factors in the host cells and eventually results in macropinocytosis or clathrin-dependent endocytosis (CME) in epithelial cells [66]. Once KSHV makes an attachment to Eph (EphA2 and -A4); c-Cbl E3 ubiquitin ligase participates in KSHV entry through polyubiquitination of EphA2 at K63 which is necessary for effective internalization (Figure 1.8) [64], [68], [69]. EphA2 knockdown and mutations in the tyrosine kinase domain (TKD) or sterile alpha motif (SAM) domains significantly reduces the signal inductions, virus internalization and gene expression (Figure 1.8) [70]. The essential role c-Cbl was also checked in KSHV infection by knocking down the c-Cbl (Figure 1.8). The c-Cbl play an essential role in clathrin-mediated endocytosis. The c-Cbl knockdown abolished the polyubiquitination of EphA2 and eventually the association with clathrin protein [70]. The PI3K also regulates herpesviruses phagocytosis coupled pathways which could be an important mechanism for virus entry into host cells. Apart from EphA2 and -A4, KSHV is also known to use EPHA7 for its attachment to the receptor [71]. EBV infection along with a bacterium (*H. pylori*) showed enhanced levels of EphB6 in gastric epithelial cell lines which eventually contribute to cancer progression [72]. A mitigated expression of the Eph receptor (EphA2, -B4) was observed in HCMV infection to fibroblast cells [73]. Likewise, NMHC-IIA act as a receptor for entry of viruses like EBV and KSHV into the epithelial cells. EBV gH/gL interacts with the C-terminal 1665–1960 amino acids region of NMHC-IIA [74]. Inhibition of NMHC-IIA ATPase activity or c-Cbl silencing suggested a decline in the entry and infection efficiency of KSHV virions [74]. Moreover, NRP1 serves as the entry factor for EBV and makes an attachment with gB. Deletion mutant of the CendR motif (23-427) of gB showed a reduction in NRP1 interaction. Other deletions of gB in regions like 23-88, and 428-431 abolished the interaction between NRP1 and gB [75]. In addition, gB-specific antibodies like 3A3 and 3A5 indicated EBV infection neutralization in both B- and epithelial cells. These mAbs protected against EBV viremia and EBV-mediated lymphoproliferative disorders (LPD) in humanized mice [76].
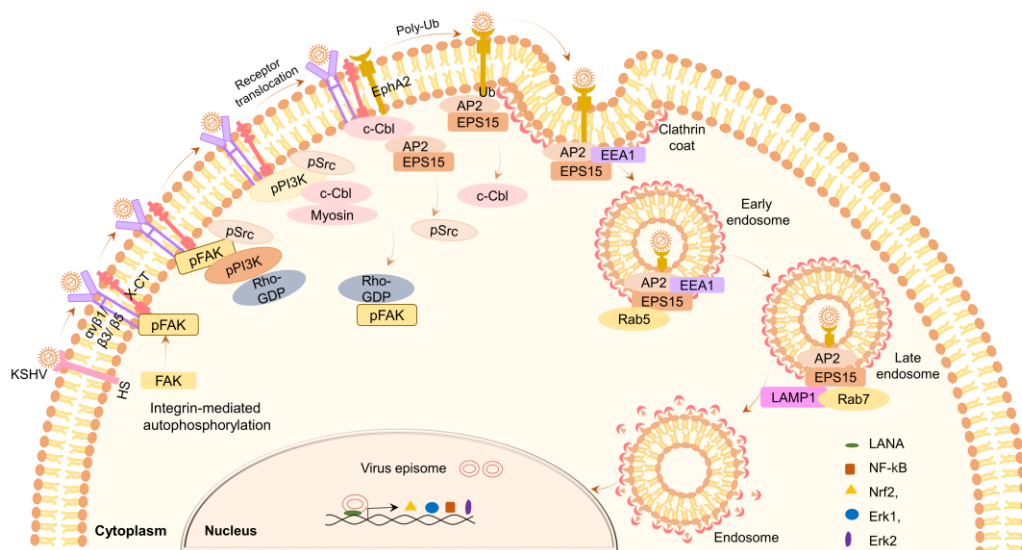
Figure 1.8: Possible mechanism of KSHV/EBV entry into the epithelial cell.
Virus infection is initiated by binding to the cell surface proteoglycans HS. Temporal association of HS subsequently followed by interaction with integrins (αvβ1, αvβ3, αvβ5) and X-CT molecules in the non-lipid raft (NLR) parts of the membranes. EBV/KSHV's interactions with integrins and trigger autophosphorylation of FAK at tyrosine 397, which creates a binding site for the SH2 domain-containing Src family kinases and subsequently leads to the activation of PI3-K and Rho-GTPases and further is recruited c-Cbl. c-Cbl mediates a rapid selective translocation of KSHV into the lipid rafts (LR) along with the integrin (except αvβ5) and xCT receptors to the Eph molecule. c-Cbl ubiquitinate the Eph receptor and recruit AP2 and Eps15, and triggers the assembly of clathrin-coated pits. Clathrin-mediated endocytosis and form vesicle with the help of dynamin protein. Complete clathrin-coated vesicle forms release of virus particle from the endosome. Virus replicates into the nucleus and modulate genes expression of NF-κB, Nrf2, Erk1 and Erk2.

1.5 Objectives of the thesis

EBV is known to be involved with neurological diseases like MS and AD. The prevalence of EBV seropositivity in MS patients is approximately 99%. The history of infectious mononucleosis (IM) and CSF-confined EBV-specific oligoclonal bands (OCB) is significantly high in patients suffering from MS. EBV exhibited infection to brain cells such as SH-SY5Y, NT-2 and human fetal cells. Tropism of EBV is regulated by several envelope glycoproteins, which make a connection with the host cell receptors. For instance, glycoprotein 350/220, gp42, gHgL and gB of EBV establish an attachment with CD21, HLA-DR, Ephs, and other receptor molecules to hijack the B- and epithelial cell machinery, which possibly involves viral transmission, replication and persistence. Previous reports suggested that EBV uses EphA2 as a receptor molecule to access epithelial cells, i.e., AGS, while KSHV is known to use

EphA2 and EphA4. These viruses also use NMHC-IIA and NRP1 receptors for attachment. Once the virus attaches to the receptor, it undergoes a conformational change and translocate into the lipid raft region of the plasma membrane for successful entry into the cell. EBV-LMP1 is also known to localise in the membrane cholesterol-rich region and amend the downstream signalling pathways. The indispensable role of dynamin protein in pinching the endocytic vesicle from the plasma membrane is long known to be exploited by viruses for internalisation, e.g., HSV-1. The endocytic pathway further progresses into the formation of endosomal vesicles (early and late). Besides, EBV glycoprotein M (gM) is a membrane protein conserved throughout the family of *Herpesviridae*. In HSV-1, gM is involved in localising herpesvirus envelope proteins to sites of secondary envelopment. Upon depletion of gM expression, there is a substantial inhibition of gHgL internalisation in the infected cells. Therefore, it suggested the critical role of gM in the virus internalisation. Furthermore, EBV proteins like gp350 have a crucial role in viral tropism and inhibition of this protein possibly leads to blocking the entry of EBV. Altogether, the current work aims to evaluate that EBV follows the endocytic pathway to enter brain cells, the role of membrane cholesterol and EBV/gM-mediated modulations in the neuronal milieu.

Objective 1: Exploring the plausible entry mechanism of Epstein-Barr virus in the brain astrocytes.

Objective 2: Deciphering the role of membrane cholesterol in the EBV entry in astrocytes.

Objective 3: Understanding the relationship of EBV and its glycoprotein M peptide with the neurological ailments at *in-vitro* and *in-vivo* levels.

Objective 4: Evaluating the possible EBV anti-glycoprotein 350 phytocompounds: an insight through, *in-silico*, *in-vitro* and *in-vivo* study.

1.6 Organisation and Scope of the Thesis

The thesis work performed to address the above-mentioned objectives has been organised into six chapters. Chapter 1 provides a necessary introduction to relevant concepts, which will help to understand the work in subsequent chapters. This chapter specifically discussed about EBV and its connection with neurological diseases, i.e.,

MS, AD and virus entry assisting proteins like gHgL, gM, gp350. We have looked into the possible pathway EBV follows to access the astrocytes in chapter 2. For the virus entry, receptors are considered as a critical molecule for the infection. Hereby, upon screening, we have found amendments in the essential receptors. Once the virus binds to the receptor, it translocates into the lipid-raft region and subsequently dynamin protein plays key role in the vesicle excision inside the cell. Furthermore, EBV exhibited colocalisation in the early and late endosomes. The chapter 3 further extend towards understanding the role of membrane cholesterol and the downstream signalling. In order to understand its role in EBV infection and pathogenesis into astroglia, we have used its inhibitor, methyl-β-cyclodextrin (MβCD). EBV-LMP1 protein localises in the cholesterol region of the plasma membrane, and by using inhibitor, we have assessed the downstream signalling pathway. Consistent with this, we checked perturbation in the biomolecular signatures spatially (periphery and nucleus) and temporally by using Raman spectroscopy (RS). The outcome of this work navigated towards several proteins associated with neurological modalities.

Pertinently, chapter 4 entails the information about EBV-gM peptide ($_{146}$SYKHVFLSAFVY$_{157}$) exhibits amyloid aggregate-like properties. We investigated the effect of EBV and gM$_{146-157}$ on neural cells (*in-vitro* and *in-vivo*) immunology and eventually in neurological disease-associated genes (i.e., AD and MS). Yet, another EBV protein, gp350, has a key role in the viral tropism. Thereby, in Chapter 5, the extra virion region of gp350 was targeted *in-silico* with phytocompounds. Further, based on the binding affinity, phytocompounds were subjected to molecular dynamics simulation. Compounds, namely demthoxycurumin (DMC) and rosmarinic acid (RA) were considered for further validation *in-vitro* and *in-vivo*. Eventually, Chapter 6 summarises the conclusion and future prospects of the overall work mentioned in the above-chapters.

1.7 References

1. Luczkowiak J, Álvarez M, Sebastián-Martín A, Menéndez-Arias L (2019) DNA-Dependent DNA Polymerases as Drug Targets in Herpesviruses and Poxviruses. In: Viral Polymerases. Elsevier, pp 95–134

2.   Sehrawat S, Kumar D, Rouse BT (2018) Herpesviruses: Harmonious Pathogens but Relevant Cofactors in Other Diseases? Front Cell Infect Microbiol 8:177. https://doi.org/10.3389/fcimb.2018.00177

3.   Shechter O, Sausen DG, Gallo ES, Dahari H, Borenstein R (2022) Epstein-Barr Virus (EBV) Epithelial Associated Malignancies: Exploring Pathologies and Current Treatments. Int J Mol Sci 23:14389. https://doi.org/10.3390/ijms232214389

4.   NovaliA Z, Van Rossen TM (2016) Agents and Approaches for Lytic Induction Therapy of Epstein-Barr Virus Associated Malignancies. Med chem (Los Angeles) 6:. https://doi.org/10.4172/2161-0444.1000384

5.   Liu Y, Hu Z, Zhang Y, Wang C (2021) Long non-coding RNAs in Epstein–Barr virus-related cancer. Cancer Cell Int 21:278. https://doi.org/10.1186/s12935-021-01986-w

6.   Kang M-S, Kieff E (2015) Epstein-Barr virus latent genes. Exp Mol Med 47:e131. https://doi.org/10.1038/emm.2014.84

7.   Saha A, Robertson ES (2019) Mechanisms of B-Cell Oncogenesis Induced by Epstein-Barr Virus. J Virol 93:e00238-19. https://doi.org/10.1128/JVI.00238-19

8.   Gao X, Ikuta K, Tajima M, Sairenji T (2001) 12-O-Tetradecanoylphorbol-13-acetate Induces Epstein–Barr Virus Reactivation via NF-κB and AP-1 as Regulated by Protein Kinase C and Mitogen-Activated Protein Kinase. Virology 286:91–99. https://doi.org/10.1006/viro.2001.0965

9.   Sugimoto A, Yamashita Y, Kanda T, Murata T, Tsurumi T (2019) Epstein-Barr virus genome packaging factors accumulate in BMRF1-cores within viral replication compartments. PLoS One 14:e0222519. https://doi.org/10.1371/journal.pone.0222519

10.   Barkhane Z, Elmadi J, Satish Kumar L, Pugalenthi LS, Ahmad M, Reddy S (2022) Multiple Sclerosis and Autoimmunity: A Veiled Relationship. Cureus 14:e24294. https://doi.org/10.7759/cureus.24294

11. Huang W-J, Chen W-W, Zhang X (2017) Multiple sclerosis: Pathology, diagnosis and treatments. Exp Ther Med 13:3163–3166. https://doi.org/10.3892/etm.2017.4410

12. Negron A, Stüve O, Forsthuber TG (2020) Ectopic Lymphoid Follicles in Multiple Sclerosis: Centers for Disease Control? Front Neurol 11:607766. https://doi.org/10.3389/fneur.2020.607766

13. Pukoli D, Vécsei L (2023) Smouldering Lesion in MS: Microglia, Lymphocytes and Pathobiochemical Mechanisms. Int J Mol Sci 24:12631. https://doi.org/10.3390/ijms241612631

14. Tillema J-M, Pirko I (2013) Neuroradiological evaluation of demyelinating disease. Ther Adv Neurol Disord 6:249–268. https://doi.org/10.1177/1756285613478870

15. Popescu BFG, Pirko I, Lucchinetti CF (2013) Pathology of multiple sclerosis: where do we stand? Continuum (Minneap Minn) 19:901–921. https://doi.org/10.1212/01.CON.0000433291.23091.65

16. Höftberger R, Lassmann H (2017) Inflammatory demyelinating diseases of the central nervous system. Handb Clin Neurol 145:263–283. https://doi.org/10.1016/B978-0-12-802395-2.00019-5

17. Sharma R, Fischer M-T, Bauer J, Felts PA, Smith KJ, Misu T, Fujihara K, Bradl M, Lassmann H (2010) Inflammation induced by innate immunity in the central nervous system leads to primary astrocyte dysfunction followed by demyelination. Acta Neuropathol 120:223–236. https://doi.org/10.1007/s00401-010-0704-z

18. Machado-Santos J, Saji E, Tröscher AR, Paunovic M, Liblau R, Gabriely G, Bien CG, Bauer J, Lassmann H (2018) The compartmentalized inflammatory response in the multiple sclerosis brain is composed of tissue-resident CD8+ T lymphocytes and B cells. Brain 141:2066–2082. https://doi.org/10.1093/brain/awy151

19. Breij ECW, Brink BP, Veerhuis R, Van Den Berg C, Vloet R, Yan R, Dijkstra CD, Van Der Valk P, Bö L (2008) Homogeneity of active demyelinating lesions in established multiple sclerosis. Annals of Neurology 63:16–25. https://doi.org/10.1002/ana.21311

20. DeTure MA, Dickson DW (2019) The neuropathological diagnosis of Alzheimer's disease. Mol Neurodegeneration 14:32. https://doi.org/10.1186/s13024-019-0333-5

21. Rajmohan R, Reddy PH (2017) Amyloid-Beta and Phosphorylated Tau Accumulations Cause Abnormalities at Synapses of Alzheimer's disease Neurons. J Alzheimers Dis 57:975–999. https://doi.org/10.3233/JAD-160612

22. Ferri CP, Prince M, Brayne C, Brodaty H, Fratiglioni L, Ganguli M, Hall K, Hasegawa K, Hendrie H, Huang Y, Jorm A, Mathers C, Menezes PR, Rimmer E, Scazufca M, Alzheimer's Disease International (2005) Global prevalence of dementia: a Delphi consensus study. Lancet 366:2112–2117. https://doi.org/10.1016/S0140-6736(05)67889-0

23. Scarian E, Viola C, Dragoni F, Di Gerlando R, Rizzo B, Diamanti L, Gagliardi S, Bordoni M, Pansarasa O (2024) New Insights into Oxidative Stress and Inflammatory Response in Neurodegenerative Diseases. IJMS 25:2698. https://doi.org/10.3390/ijms25052698

24. Nazarian A, Yashin AI, Kulminski AM (2019) Genome-wide analysis of genetic predisposition to Alzheimer's disease and related sex disparities. Alz Res Therapy 11:5. https://doi.org/10.1186/s13195-018-0458-8

25. Zhang C, Browne A, Divito JR, Stevenson JA, Romano D, Dong Y, Xie Z, Tanzi RE (2010) Amyloid-β production via cleavage of amyloid-β protein precursor is modulated by cell density. J Alzheimers Dis 22:683–984. https://doi.org/10.3233/JAD-2010-100816

26. Abedin F, Kandel N, Tatulian SA (2021) Effects of Aβ-derived peptide fragments on fibrillogenesis of Aβ. Sci Rep 11:19262. https://doi.org/10.1038/s41598-021-98644-y

27. Rudrabhatla P, Jaffe H, Pant HC (2011) Direct evidence of phosphorylated neuronal intermediate filament proteins in neurofibrillary tangles (NFTs): phosphoproteomics of Alzheimer's NFTs. FASEB J 25:3896–3905. https://doi.org/10.1096/fj.11-181297

28. Lanoiselée H-M, Nicolas G, Wallon D, Rovelet-Lecrux A, Lacour M, Rousseau S, Richard A-C, Pasquier F, Rollin-Sillaire A, Martinaud O, Quillard-Muraine M, de la Sayette V, Boutoleau-Bretonniere C, Etcharry-Bouyx F, Chauviré V, Sarazin M, le Ber I, Epelbaum S, Jonveaux T, Rouaud O, Ceccaldi M, Félician O, Godefroy O, Formaglio M, Croisile B, Auriacombe S, Chamard L, Vincent J-L, Sauvée M, Marelli-Tosi C, Gabelle A, Ozsancak C, Pariente J, Paquet C, Hannequin D, Campion D, collaborators of the CNR-MAJ project (2017) APP, PSEN1, and PSEN2 mutations in early-onset Alzheimer disease: A genetic screening study of familial and sporadic cases. PLoS Med 14:e1002270. https://doi.org/10.1371/journal.pmed.1002270

29. Moodley KK, Chan D (2014) The Hippocampus in Neurodegenerative Disease. In: Szabo K, Hennerici MG (eds) Frontiers of Neurology and Neuroscience. S. Karger AG, pp 95–108

30. Serafini B, Rosicarelli B, Franciotta D, Magliozzi R, Reynolds R, Cinque P, Andreoni L, Trivedi P, Salvetti M, Faggioni A, Aloisi F (2007) Dysregulated Epstein-Barr virus infection in the multiple sclerosis brain. The Journal of Experimental Medicine 204:2899–2912. https://doi.org/10.1084/jem.20071030

31. Zhang N, Zuo Y, Jiang L, Peng Y, Huang X, Zuo L (2022) Epstein-Barr Virus and Neurological Diseases. Front Mol Biosci 8:816098. https://doi.org/10.3389/fmolb.2021.816098

32. Maoz-Segal R, Andrade P (2015) Molecular Mimicry and Autoimmunity. In: Infection and Autoimmunity. Elsevier, pp 27–44

33. Dando SJ, Mackay-Sim A, Norton R, Currie BJ, St. John JA, Ekberg JAK, Batzloff M, Ulett GC, Beacham IR (2014) Pathogens Penetrating the Central Nervous System: Infection Pathways and the Cellular and Molecular

Mechanisms of Invasion. Clin Microbiol Rev 27:691–726. https://doi.org/10.1128/CMR.00118-13

34. Lünemann JD, Tintoré M, Messmer B, Strowig T, Rovira Á, Perkal H, Caballero E, Münz C, Montalban X, Comabella M (2010) Elevated Epstein–Barr virus-encoded nuclear antigen-1 immune responses predict conversion to multiple sclerosis. Annals of Neurology 67:159–169. https://doi.org/10.1002/ana.21886

35. Jog NR, McClain MT, Heinlen LD, Gross T, Towner R, Guthridge JM, Axtell RC, Pardo G, Harley JB, James JA (2020) Epstein Barr virus nuclear antigen 1 (EBNA-1) peptides recognized by adult multiple sclerosis patient sera induce neurologic symptoms in a murine model. J Autoimmun 106:102332. https://doi.org/10.1016/j.jaut.2019.102332

36. Hedegaard CJ, Chen N, Sellebjerg F, Sørensen PS, Leslie RGQ, Bendtzen K, Nielsen CH (2009) Autoantibodies to myelin basic protein (MBP) in healthy individuals and in patients with multiple sclerosis: a role in regulating cytokine responses to MBP. Immunology 128:e451-461. https://doi.org/10.1111/j.1365-2567.2008.02999.x

37. Chakravorty S, Afzali B, Kazemian M (2022) EBV-associated diseases: Current therapeutics and emerging technologies. Front Immunol 13:1059133. https://doi.org/10.3389/fimmu.2022.1059133

38. Ricigliano VAG, Handel AE, Sandve GK, Annibali V, Ristori G, Mechelli R, Cader MZ, Salvetti M (2015) EBNA2 Binds to Genomic Intervals Associated with Multiple Sclerosis and Overlaps with Vitamin D Receptor Occupancy. PLoS ONE 10:e0119605. https://doi.org/10.1371/journal.pone.0119605

39. Jakhmola S, Jha HC (2021) Glial cell response to Epstein-Barr Virus infection: A plausible contribution to virus-associated inflammatory reactions in the brain. Virology 559:182–195. https://doi.org/10.1016/j.virol.2021.04.005

40. 'T Hart BA, Jagessar SA, Haanstra K, Verschoor E, Laman JD, Kap YS (2013) The Primate EAE Model Points at EBV-Infected B Cells as a Preferential

Therapy Target in Multiple Sclerosis. Front Immunol 4:. https://doi.org/10.3389/fimmu.2013.00145

41. Guan Y, Jakimovski D, Ramanathan M, Weinstock-Guttman B, Zivadinov R (2019) The role of Epstein-Barr virus in multiple sclerosis: from molecular pathophysiology to in vivo imaging. Neural Regen Res 14:373–386. https://doi.org/10.4103/1673-5374.245462

42. Kerr JR (2019) Epstein-Barr Virus Induced Gene-2 Upregulation Identifies a Particular Subtype of Chronic Fatigue Syndrome/Myalgic Encephalomyelitis. Front Pediatr 7:59. https://doi.org/10.3389/fped.2019.00059

43. Soldan SS, Lieberman PM (2023) Epstein–Barr virus and multiple sclerosis. Nat Rev Microbiol 21:51–64. https://doi.org/10.1038/s41579-022-00770-5

44. Ruiz-Pablos M (2022) CD4+ Cytotoxic T Cells Involved in the Development of EBV-Associated Diseases. Pathogens 11:831. https://doi.org/10.3390/pathogens11080831

45. Kreft KL, Van Nierop GP, Scherbeijn SMJ, Janssen M, Verjans GMGM, Hintzen RQ (2017) Elevated EBNA-1 IgG in MS is associated with genetic MS risk variants. Neurol Neuroimmunol Neuroinflamm 4:e406. https://doi.org/10.1212/NXI.0000000000000406

46. Delfan N, Galehdari H, Shafiei M, Ghanbari-Mardasi F, Latifi T, Majdinasab N, Seifi T (2018) Association of human leukocyte antigen-DRB haplotype in multiple sclerosis population of Khuzestan, Iran. Iran J Neurol 17:154–160

47. Sundström P, Nyström M, Ruuth K, Lundgren E (2009) Antibodies to specific EBNA-1 domains and HLA DRB1∗1501 interact as risk factors for multiple sclerosis. Journal of Neuroimmunology 215:102–107. https://doi.org/10.1016/j.jneuroim.2009.08.004

48. Skovronsky DM, Zhang B, Kung M-P, Kung HF, Trojanowski JQ, Lee VM-Y (2000) *In vivo* detection of amyloid plaques in a mouse model of Alzheimer's disease. Proc Natl Acad Sci USA 97:7609–7614. https://doi.org/10.1073/pnas.97.13.7609

49. Emrani S, Arain HA, DeMarshall C, Nuriel T (2020) APOE4 is associated with cognitive and pathological heterogeneity in patients with Alzheimer's disease: a systematic review. Alzheimers Res Ther 12:141. https://doi.org/10.1186/s13195-020-00712-4

50. Tiwari D, Mittal N, Jha HC (2022) Unraveling the links between neurodegeneration and Epstein-Barr virus-mediated cell cycle dysregulation. Curr Res Neurobiol 3:100046. https://doi.org/10.1016/j.crneur.2022.100046

51. Hogestyn JM, Mock DJ, Mayer-Proschel M (2018) Contributions of neurotropic human herpesviruses herpes simplex virus 1 and human herpesvirus 6 to neurodegenerative disease pathology. Neural Regen Res 13:211–221. https://doi.org/10.4103/1673-5374.226380

52. Huang S-Y, Yang Y-X, Kuo K, Li H-Q, Shen X-N, Chen S-D, Cui M, Tan L, Dong Q, Yu J-T (2021) Herpesvirus infections and Alzheimer's disease: a Mendelian randomization study. Alzheimers Res Ther 13:158. https://doi.org/10.1186/s13195-021-00905-5

53. Dong-Chen X, Yong C, Yang X, Chen-Yu S, Li-Hua P (2023) Signaling pathways in Parkinson's disease: molecular mechanisms and therapeutic interventions. Sig Transduct Target Ther 8:73. https://doi.org/10.1038/s41392-023-01353-3

54. Sausen DG, Poirier MC, Spiers LM, Smith EN (2023) Mechanisms of T cell evasion by Epstein-Barr virus and implications for tumor survival. Front Immunol 14:1289313. https://doi.org/10.3389/fimmu.2023.1289313

55. Márquez AC, Horwitz MS (2015) The Role of Latently Infected B Cells in CNS Autoimmunity. Front Immunol 6:. https://doi.org/10.3389/fimmu.2015.00544

56. Kim S, Ahn S-J, Chu K (2021) Epstein-Barr virus-associated acute disseminated encephalomyelitis successfully treated with rituximab: a case report. Encephalitis 1:85–88. https://doi.org/10.47936/encephalitis.2021.00066

57. Barnes SL, Brew BJ (2019) Acute cerebellar ataxia after Epstein-Barr virus infection. Neurol Clin Pract 9:505–506. https://doi.org/10.1212/CPJ.0000000000000659

58. Menet A, Speth C, Larcher C, Prodinger WM, Schwendinger MG, Chan P, Jäger M, Schwarzmann F, Recheis H, Fontaine M, Dierich MP (1999) Epstein-Barr virus infection of human astrocyte cell lines. J Virol 73:7722–7733. https://doi.org/10.1128/JVI.73.9.7722-7733.1999

59. Villanueva RA, Rouillé Y, Dubuisson J (2005) Interactions between virus proteins and host cell membranes during the viral life cycle. Int Rev Cytol 245:171–244. https://doi.org/10.1016/S0074-7696(05)45006-8

60. Bu G-L, Xie C, Kang Y-F, Zeng M-S, Sun C (2022) How EBV Infects: The Tropism and Underlying Molecular Mechanism for Viral Infection. Viruses 14:2372. https://doi.org/10.3390/v14112372

61. Dollery SJ (2019) Towards Understanding KSHV Fusion and Entry. Viruses 11:1073. https://doi.org/10.3390/v11111073

62. Rahman MM, Islam MR, Yamin M, Islam MM, Sarker MT, Meem AFK, Akter A, Emran TB, Cavalu S, Sharma R (2022) Emerging Role of Neuron-Glia in Neurological Disorders: At a Glance. Oxid Med Cell Longev 2022:3201644. https://doi.org/10.1155/2022/3201644

63. Wang J, Zheng X, Peng Q, Zhang X, Qin Z (2020) Eph receptors: the bridge linking host and virus. Cell Mol Life Sci 77:2355–2365. https://doi.org/10.1007/s00018-019-03409-6

64. Su C, Wu L, Chai Y, Qi J, Tan S, Gao GF, Song H, Yan J (2020) Molecular basis of EphA2 recognition by gHgL from gammaherpesviruses. Nat Commun 11:5964. https://doi.org/10.1038/s41467-020-19617-9

65. Chakraborty S, Veettil MV, Bottero V, Chandran B (2012) Kaposi's sarcoma-associated herpesvirus interacts with EphrinA2 receptor to amplify signaling essential for productive infection. Proc Natl Acad Sci USA 109:. https://doi.org/10.1073/pnas.1119592109

66. Chen J, Schaller S, Jardetzky TS, Longnecker R (2020) Epstein-Barr Virus gH/gL and Kaposi's Sarcoma-Associated Herpesvirus gH/gL Bind to Different

Sites on EphA2 To Trigger Fusion. J Virol 94:e01454-20. https://doi.org/10.1128/JVI.01454-20

67. Veettil M, Bandyopadhyay C, Dutta D, Chandran B (2014) Interaction of KSHV with Host Cell Surface Receptors and Cell Entry. Viruses 6:4024–4046. https://doi.org/10.3390/v6104024

68. Chen J, Zhang X, Schaller S, Jardetzky TS, Longnecker R (2019) Ephrin Receptor A4 is a New Kaposi's Sarcoma-Associated Herpesvirus Virus Entry Receptor. mBio 10:e02892-18. https://doi.org/10.1128/mBio.02892-18

69. Chen J, Longnecker R (2019) Epithelial cell infection by Epstein–Barr virus. FEMS Microbiology Reviews 43:674–683. https://doi.org/10.1093/femsre/fuz023

70. Dutta D, Chakraborty S, Bandyopadhyay C, Valiya Veettil M, Ansari MA, Singh VV, Chandran B (2013) EphrinA2 regulates clathrin mediated KSHV endocytosis in fibroblast cells by coordinating integrin-associated signaling and c-Cbl directed polyubiquitination. PLoS Pathog 9:e1003510. https://doi.org/10.1371/journal.ppat.1003510

71. Großkopf AK, Schlagowski S, Hörnich BF, Fricke T, Desrosiers RC, Hahn AS (2019) EphA7 Functions as Receptor on BJAB Cells for Cell-to-Cell Transmission of the Kaposi's Sarcoma-Associated Herpesvirus and for Cell-Free Infection by the Related Rhesus Monkey Rhadinovirus. J Virol 93:e00064-19. https://doi.org/10.1128/JVI.00064-19

72. Rani A, Jakhmola S, Karnati S, Parmar HS, Chandra Jha H (2021) Potential entry receptors for human γ-herpesvirus into epithelial cells: A plausible therapeutic target for viral infections. Tumour Virus Res 12:200227. https://doi.org/10.1016/j.tvr.2021.200227

73. TerBush AA, Hafkamp F, Lee HJ, Coscoy L (2018) A Kaposi's Sarcoma-Associated Herpesvirus Infection Mechanism Is Independent of Integrins α3β1, αVβ3, and αVβ5. J Virol 92:e00803-18. https://doi.org/10.1128/JVI.00803-18

74. Tan L, Yuan X, Liu Y, Cai X, Guo S, Wang A (2019) Non-muscle Myosin II: Role in Microbial Infection and Its Potential as a Therapeutic Target. Front Microbiol 10:401. https://doi.org/10.3389/fmicb.2019.00401

75. Wang H-B, Zhang H, Zhang J-P, Li Y, Zhao B, Feng G-K, Du Y, Xiong D, Zhong Q, Liu W-L, Du H, Li M-Z, Huang W-L, Tsao SW, Hutt-Fletcher L, Zeng Y-X, Kieff E, Zeng M-S (2015) Neuropilin 1 is an entry factor that promotes EBV infection of nasopharyngeal epithelial cells. Nat Commun 6:6240. https://doi.org/10.1038/ncomms7240

76. Zhang X, Hong J, Zhong L, Wu Q, Zhang S, Zhu Q, Chen H, Wei D, Li R, Zhang W, Zhang X, Wang G, Zhou X, Chen J, Kang Y, Zha Z, Duan X, Huang Y, Sun C, Kong X, Zhou Y, Chen Y, Ye X, Feng Q, Li S, Xiang T, Gao S, Zeng M-S, Zheng Q, Chen Y, Zeng Y-X, Xia N, Xu M (2022) Protective anti-gB neutralizing antibodies targeting two vulnerable sites for EBV-cell membrane fusion. Proc Natl Acad Sci USA 119:e2202371119. https://doi.org/10.1073/pnas.2202371119

Chapter 2: Dissecting the Epstein-Barr virus entry pathway into astrocytes: Unfolding the involvement of endosomal trafficking

2.1 Graphical Abstract
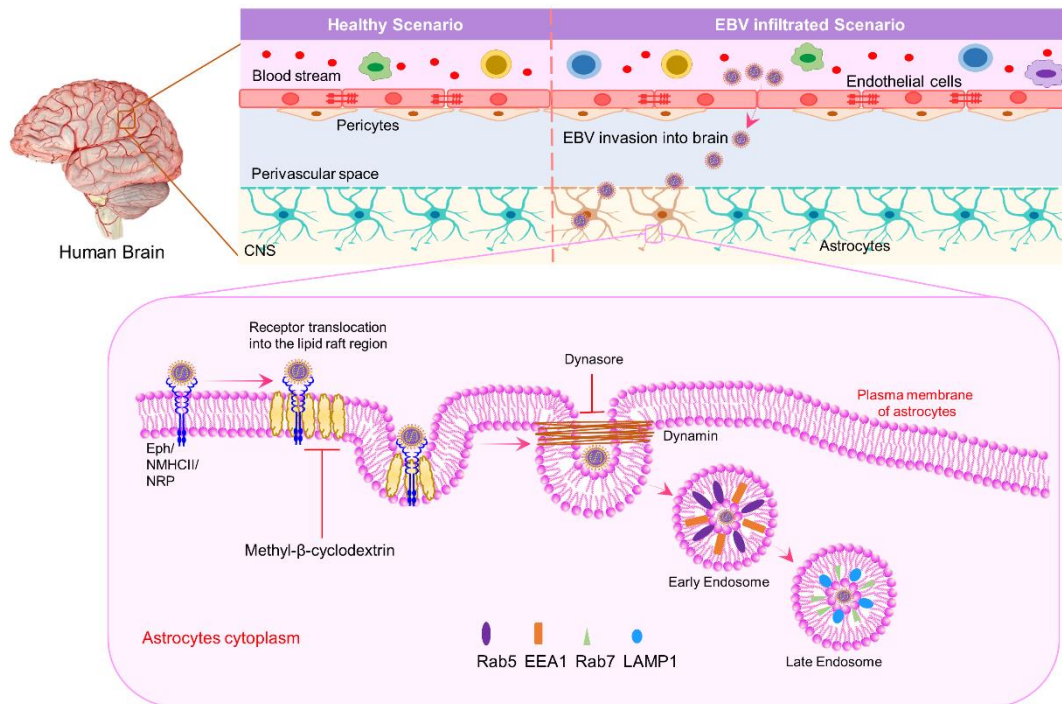
2.2 Abstract

Epstein-Barr virus (EBV) shares an abiding relation with numerous diseases like cancers and neurological ailments, i.e., Multiple Sclerosis. Previous reports have suggested the successful infection of EBV in various brain cells. Yet, the mechanism or the host molecules facilitating its entry into the brain cells is still elusive. In the current study, we have looked into possible EBV entry pathway to access the astrocytes. For the virus entry, host cell receptors play critical role. Hereby, upon screening, we have observed profound amendments in the essential receptors-like ephrin receptor-A4, -A10 (EPHA4, EPHA10) and non-muscle myosin heavy chain-IIB (NMHC-IIB) in a time-dependent infection of EBV. Once the virus binds to the receptor, it translocates into the lipid-raft region. Depletion of this lipid raft region indicated a decline in the EBV infection in cells like LN-229 and U-87 MG. Inhibition of dynamin with dynasore exhibited mitigation in EBV-GFP and EBV nuclear antigen 1 (EBNA1) in both the cell lines. Furthermore, EBV exhibited colocalisation in the

endosomes and lysosome. A significantly higher presence of EBV was found in late endosomes and lysosome by using markers like Rab7 and LAMP1 at 1hr and 2hr of infection. The current work assessed the entry mechanism of EBV in the brain astrocytes using receptor-mediated endocytosis. The virus follows the endocytic pathway to enter brain cells, although further validation by knocking down of attachment proteins is needed. It will further enable us to pinpoint the potential therapeutic target.

Keywords: Epstein-Barr virus, internalisation, EPH, NMHC-II, lipid raft, dynamin, late endosome

2.3 Introduction

The ubiquitously present herpesviruses like Epstein-Barr virus (EBV) maintain their tropism in B- and epithelial cells resulting in a disease condition ranging from cancer to neurodegenerative disorders. Reports from our group have demonstrated the direct infection of EBV [1]. Virus infection is primarily aided by a multi-step process of virus entry where it attaches to different host receptors using several glycoproteins followed by the fusion process. EBV infection in epithelial cells relies on the interaction of its glycoprotein complex (gH/gL) with host cell receptors, namely integrins (αvβ5, αvβ6, and αvβ8), ephrins (EPH), neuropilins (NRP1), and non-muscle myosin heavy chain-IIA (NMHC-IIA) [2]. These receptors are involved with multiple other cellular and disease cascades. Once the virus attaches to the receptor and undergoes a conformational change, it gets translocated into the lipid raft region of the plasma membrane. The lipid raft region is well-known to reinforce the entry of viruses such as human immunodeficiency virus (HIV), Ebola virus and herpesviruses [3]. The indispensable role of dynamin protein in pinching the endocytic vesicle from the plasma membrane is long known to be exploited by viruses for internalisation, e.g., HSV-1 [4]. The endocytic pathway further progresses into the formation of endosomal vesicles (early and late). Viruses like HSV-2, Hepatitis B-virus, rabies virus (RABV), and dengue virus (DENV) exhibited their presence with markers like Rab5 and Rab7 [5].

In the current work, we have used techniques which enable us to track, visualise, and localise the virus at different stages of entry into astrocyte cell lines, i.e., LN-229 and U-87 MG. We have screened the plausible epithelial cell receptor-like *ephA1, -A2, -*

A3, -A4, A5, -A6, -A7, -A8, -A10, -B1, -B2, -B3, -B4, -B6, nrp1, nrp2, myh-9, myh-10 and *myh-14* at the transcript level upon temporal infection of EBV. Lipid raft region and dynamin protein importance were elucidated using an inhibitor methyl-beta-cyclodextrin (MβCD) and dynasore, respectively. Subsequently, EBV co-localisation was traced in the endosomes and lysosome, which suggested the apparant infection of EBV in the astrocytes. Furthermore, it will help to target the proteins and design therapeutic approaches for virus-mediated neurological ailments.

2.4 Results

2.4.1 Temporal examining the perturbation of possible epithelial receptors for Epstein Barr virus entry into astrocyte

The titre of EBV infection on LN-229 and U-87 MG was determined using EBV-*gfp* and *ebna1*, as mentioned previously [6], [7] (Figure 2.1 I-IV). In the all-mentioned experiments, 2.5 MOI of EBV was used.
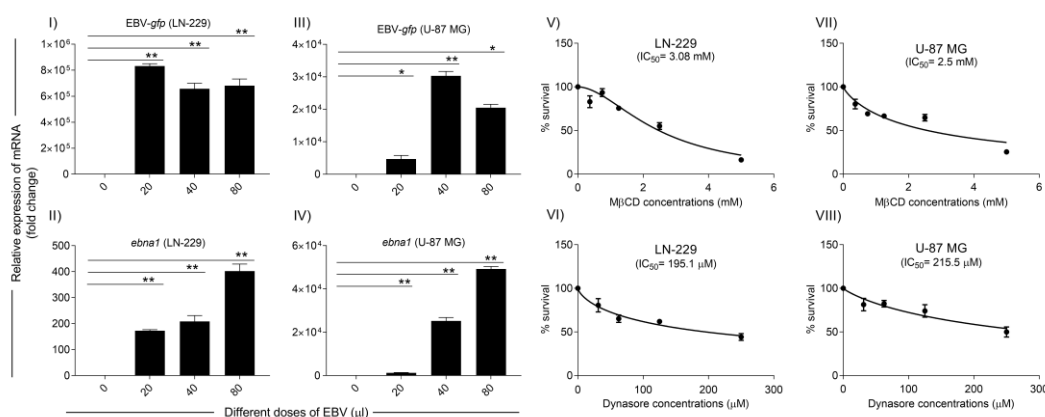
Figure 2.1: Epstein-Barr virus titre determination on LN-229 and U-87 MG cells through qRT-PCR at different doses.
I-II) Differential expression of EBV-GFP and EBNA1 level exhibits differential expression upon EBV infection to LN-229 cells. III-IV) Successful EBV infection to U-87 MG cells at different doses given to U-87 MG cells. V-VIII) Delineation of IC50 values of MβCD and dynasore on LN-229 and U-87 MG cells.

The primitive step in the virus entry is attachment with the receptor. We have observed differential expression in both the cell-line LN-229 and U-87 MG. In the LN-229 cells, *ephA3, -A4, -A6, -A8, -A10, -B1, -B4, myh-9* (NMHC-IIA), *myh-10* (NMHC-IIB) and *myh-14* (NMHC-IIC) exhibited an increase in the expression at 2, 6, 12, 24 and 72 hrs of time-points (p<0.05, p<0.01, p<0.0001) (Figure 2.2I). The *ephA2, -B6, nrp1, nrp2*

and *myh-9* have shown elevation till 24 hrs (p<0.05 and p<0.01) (Figure 2.2I). Further, *ephB3* showed a decline in the mRNA expression upon EBV infection (p<0.01) (Figure 2.2I).
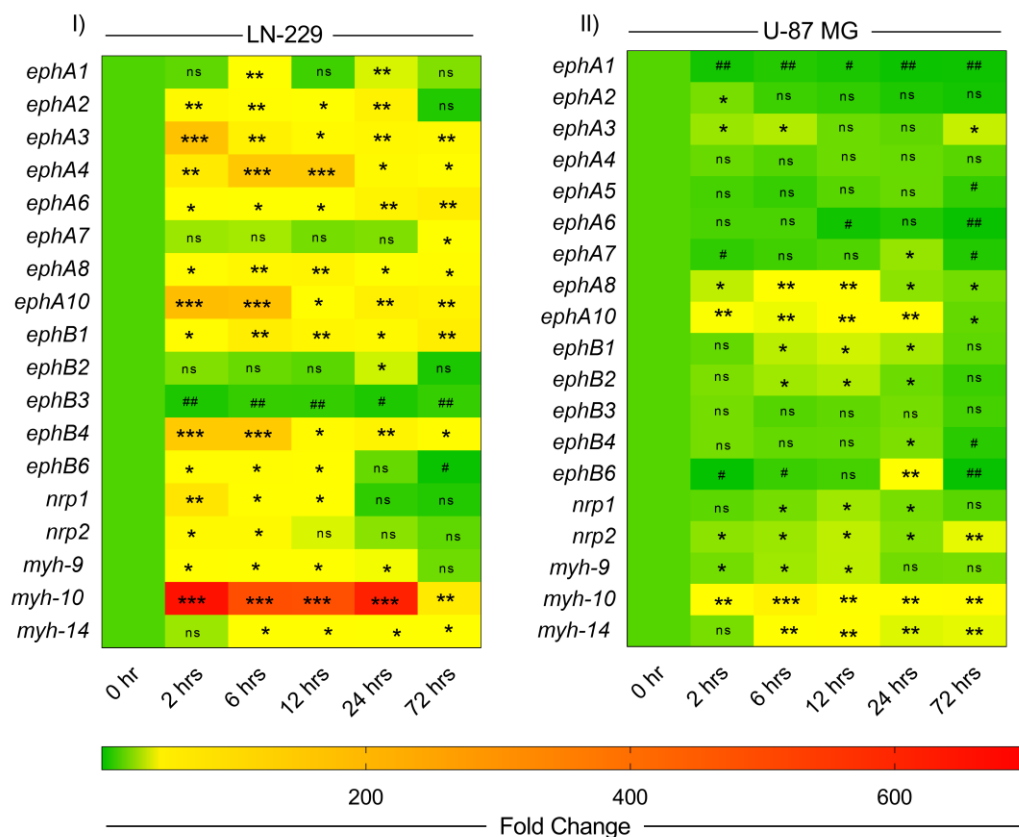
Figure 2.2: Investigation of possible perturbations in the epithelial cell receptors upon EBV infection to LN-229 and U-87 MG cells.
I) In LN-229 cells EPHA3, -A4, -A6, -A10, -B1, -B4 showed consistently from 2 hr to 72 hrs. NMHC-IIB and -IIC showed constant elevation in a time-dependent manner. II) In the U-87 MG cells, EPHA8, -A10, NRP2, NMHC-IIB and -IIC showed constant augmentation in the upon EBV infection. The *p*-values of <0.05, <0.01 and <0.0001 are considered statistically significant and are represented with *, ** and *** respectively. The increase and decrease are represented by * and # respectively.

In the U-87 MG cells, *ephA8, -A10, myh-10* and *myh-14* manifested upregulation after EBV infection (p<0.05, p<0.01 and p<0.0001) (Figure 2.2II). The *ephA3*, *nrp2* and *myh-9* showed an increase at the initial time points. The *ephA1* exhibited a significant decline in a time-dependent manner (p<0.01) (Figure 2.2II). Receptors like *ephA4, -A5, -B3* and *-B4* exhibited no statistically significant changes (Figure 2.2II).

2.4.2 Apprehending the role of membrane cholesterol in EBV entry

Upon attachment with the receptor, virus get translocated in the lipid-raft region of the plasma membrane, which is rich with the sphingolipids and membrane cholesterol. The depletion of membrane cholesterol in LN-229 and U-87 MG cells in a time-dependent manner exhibited a decline in EBV infection.
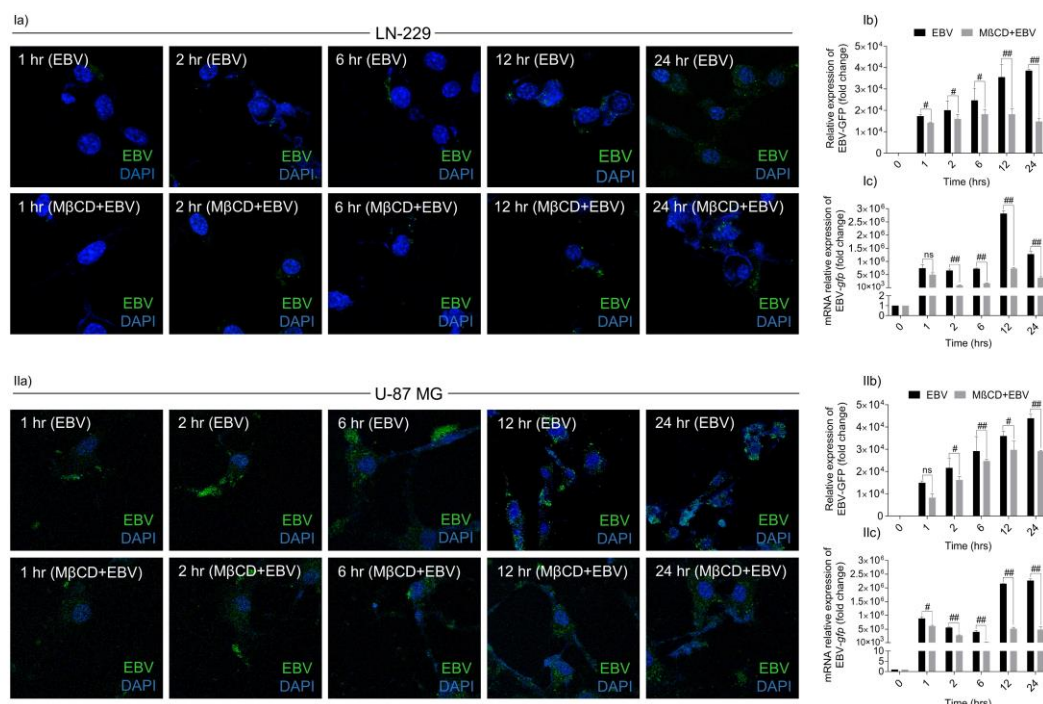
Figure 2.3: Underpinning the role of astrocyte membrane cholesterol in EBV entry.
Ia) Immunofluorescence images of EBV infection to LN-229 cells alongside with inhibitor MβCD+EBV at 1, 2, 6, 12 and 24 hrs. Ib) Quantification of immunofluorescence EBV infected LN-229 cells and MβCD+EBV samples. Mitigation in the EBV infection was observed at 2, 6, 12 and 24 hrs. Ic) Decline in the EBV infection observed at the mRNA level from 2 to 24 hrs. IIa) Immunofluorescence images of EBV infection to U-87 MG cells alongside with inhibitor MβCD+EBV at 1, 2, 6, 12 and 24 hrs. IIb) Quantification of immunofluorescence of U-87 MG cells infected EBV infected on U-87 MG cells as well as MβCD+EBV samples. IIc) Decrease in EBV infection in the U-87 MG cells upon exposure to MβCD at 1, 2, 6, 12 and 24 hrs. Given plots; *x*-axis, time-dependent EBV infection; *y*-axis, fold change with respect to EBV infected samples. The *p*-values of <0.05, <0.01 and <0.0001 are considered statistically significant and are represented with *, ** and *** respectively. The increase and decrease are represented by * and # respectively.

Upon membrane cholesterol depletion by using MβCD in the LN-229 cells and U-87 MG cells, we observed a decrease in the EBV infection at 1, 2, 6, 12 and 24 hrs (p<0.05 and p<0.01) (Figure 2.3Ia, Ib, IIa-IIb). Akin to this, the mRNA level of EBV-*gfp* showed mitigation in the expression at 2, 6, 12, and 24 hrs (p<0.01) (Figure 2.3Ic, IIc).

Likewise, EBV-*gfp* showed downregulation at the transcript level 1, 2, 6, 12, and 24 hrs (p<0.01) in U-87 MG cells (Figure 2.3IIc).

2.4.3 Role of dynamin protein in EBV receptor-mediated endocytosis

In herpesviruses infection, the dynamin protein is known to play a role in the constriction of the vesicle and its excision into the cell cytoplasm. Out of total three mammals expressing dynamin protein (dynamin 1, -2 and -3); where all three expresses in the brain cells. At this moment, we have inhibited dynamin protein using an inhibitor, dynasore. Upon inhibition of dynamin protein in the LN-229 cells, we have observed diminish in the transcript level of EBV-GFP at 2, 6, 12 and 24 hrs (p<0.05) and *ebna1* at 6, 12, 24 hrs p<0.01, p<0.01 and p<0.01, respectively (Figure 2.4I, III). [8]. Similarly, in the U-87 MG cells, the mRNA level of EBV-*gfp* exhibited a decline at 1, 2, 6, 12 and 24 hrs (p<0.05 and p<0.01) (Figure 2.4II). The *ebna1* also exhibited downregulation in the dynamin-inhibited cells at all the time points (p<0.05) (Figure 2.4IV).
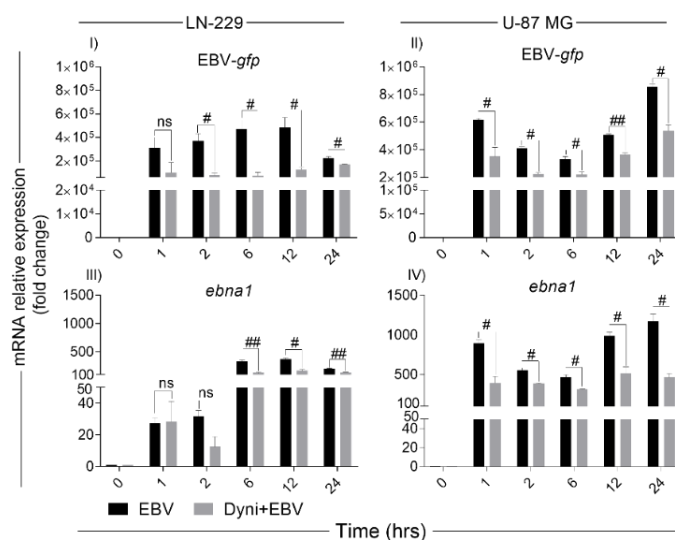
Figure 2.4: Decline in the EBV infection upon inhibiting the dynamin protein in a time-dependent manner.
I) Decline in the EBV-*gfp* transcript was observed in LN-229 cells before and after inhibiting the dynamin using inhibitor dynasore. II) Mitigation in the EBV infection upon inhibiting the dynasore at 6, 12 and 24 hrs in LN-229 cells. III-IV) Decrease in the EBV infection was observed after dynamin inhibition using EBV-*gfp* and *ebna1* at 1, 2, 6, 12 and 24 hrs. Given plots; x-axis, time-dependent EBV infection; y-axis, fold change with respect to EBV infected samples. The p-values of <0.05, <0.01 and

<0.0001 are considered statistically significant and are represented with *, ** and ***
respectively. The increase and decrease are represented by * and # respectively.

2.4.4 Co-localisation of EBV in the endosomes

The infection of numerous viruses in the cells is facilitated by different pathways,
including receptor-mediated endocytosis or micropinocytosis. During endocytosis,
the virus, i.e., KSHV, has been detected in endosomal vesicles [9]. We have also
observed the EBV presence in the endosomes (early and late) and lysosomes by using
markers such as Rab5, EEA1, Rab7 and LAMP1. Early endosome markers were
evaluated from 10 min to 120 min and late endosome markers was checked from 30
min to 120 mins. In LN-229 cells, Rab5 and EEA1 exhibited ~30-40% of co-
localisation with EBV-GFP at 20 min of EBV infection (Figure 2.5Ia-Ic). EBV-GFP
showed more colocalisation with late endosomal proteins like Rab7 (~80%) and
LAMP1 (~65%) mainly at 60 min (Figure 2.5Ia-Ic). Similarly, in U-87 MG cells, early
endosome markers such as Rab5 (~60%) and EEA1 (~50%) indicated co-presence
with EBV-GFP after 20 min of infection (Figure 2.5IIIa-IIIc).
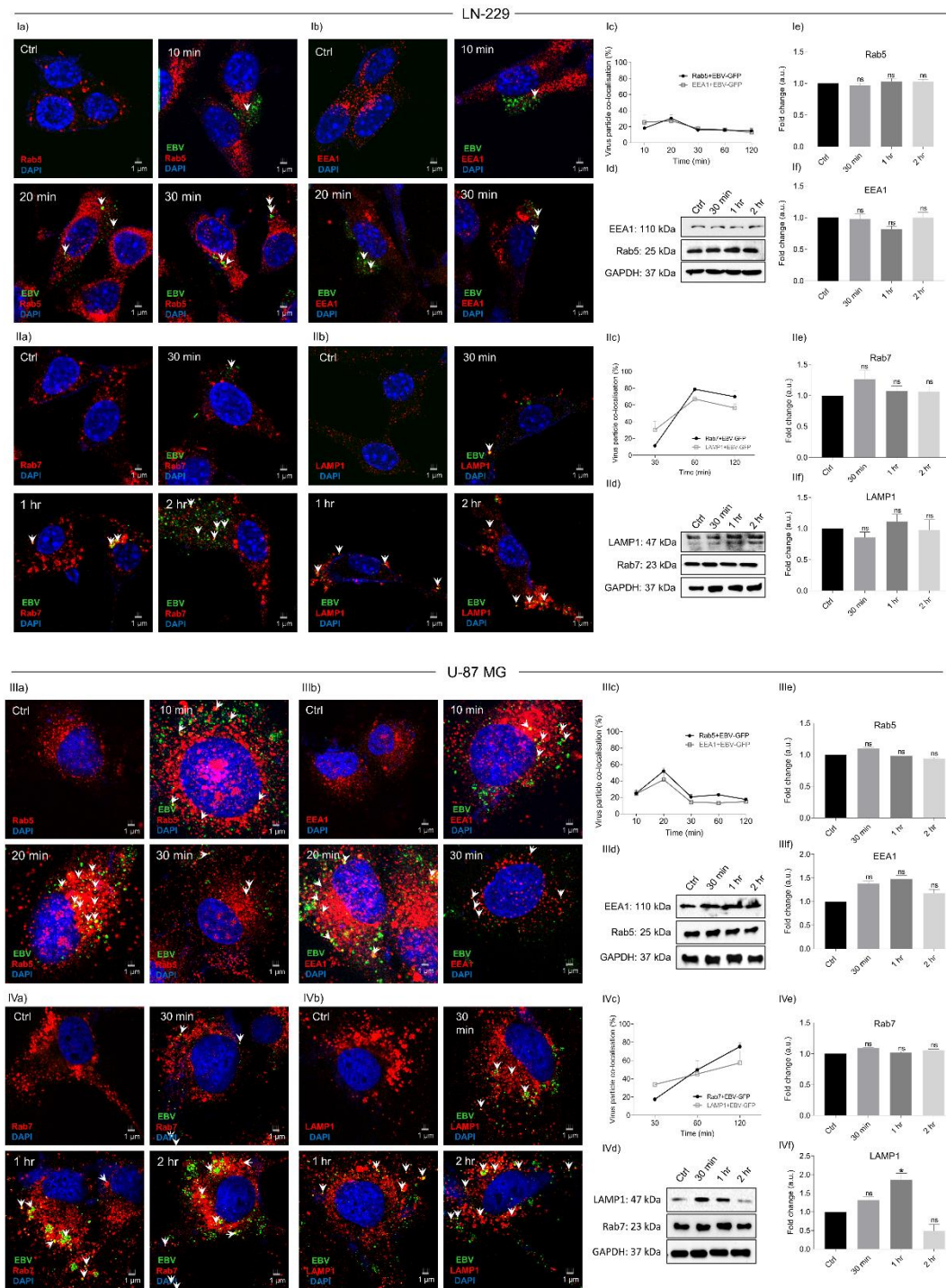
Figure 2.5: Marking the presence of EBV in the endosomes of LN-229 and U-87 MG cells.
Ia-Ib) Representation of LN-229 cells immunofluorescence of EBV colocalisation in the early endosome markers like Rab5 and EEA1 at 10 min, 20 min and 30 min. Ic) Quantification of % EBV-GFP colocalisation for early endosomal markers at 10, 20-, 30-, 60- and 120-min. Id-If) Western blot for Rab5 and EEA1 and its quantification. IIa-IIb) Depiction of immunofluorescence in LN-229 cells in the late endosome. IIc) Quantification of % EBV-GFP colocalisation for late endosomal markers 30, 60 and 120 min. IId-IIf) Western blot for Rab7 and LAMP1 and its quantification. IIIa-IIIb) Representation of U-87 MG cells immunofluorescence of EBV colocalisation in the

early endosome markers like Rab5 and EEA1 at 10 min, 20 min and 30 min. IIIc) Quantification of % EBV-GFP colocalisation for early endosomal markers at 10, 20, 30, 60 and 120 min. IIId-IIIf) Western blot for Rab5 and EEA1 and its quantification. IVa-IVb) Immunofluorescence of Rab7 and LAMP1 in U-87 MG cells. IVc) Quantification of % EBV-GFP colocalization for late endosomal markers 30, 60 and 120 min. IVd-IVf) Western blot for Rab7 and LAMP1 and its quantification. Given plots; x-axis, time-dependent EBV infection; y-axis, % colocalisation/fold change with respect to EBV infected samples. The p-values of <0.05, are considered statistically significant and are represented with *.

EBV exhibited significantly higher co-localisation in late endosomes and lysosomes ~80% and ~70 % using markers Rab7 and LAMP1 at 60 min after infection, respectively (Figure 2.5IVa-IVc). However, we have not observed any changes in the early, late endosomal and lysosomal total protein level by western blotting in both the cell-lines upon EBV infection (Figure 2.5Id-If, IId-IIf, IIId-IIIf and IVd-IVf).

2.5 Discussion

EBV is reported to be present in infected brain cells such as SH-SY5Y, NT-2, and human fetal cells. The infection of EBV and KSHV in epithelial cells is facilitated by EPHA2 and KSHV is also known to use EphA4 [10], [11], [12]. Our study has also shown consistent changes in the expression of EphA4 (LN-229 cells). Previously, the infection of HCMV in the fibroblast cells have shown mitigation in the expression of EphA2 and -B4 [13]. A siRNA-based study revealed the function of EphA2 as a cofactor in Hepatitis C Virus (HCV) entry [14]. This initial virus attachment to the host cell further facilitates endocytosis by manipulating the signalling pathways. Likewise, Rhesus macaque rhadinovirus (RRV) uses ten different EPHs to establish a successful infection [15]. Paramyxoviridae family viruses such as Nipah viruses (NiV), Hendra virus (HeV), Mojiang virus (MojV), Cedar virus (CeV) and African henipavirus take advantage of EPH and ephrin molecules for the attachment and entry receptor [16].

Further, NMHC-IIA act as a receptor for entry of viruses like EBV and KSHV into the epithelial cells. EBV gH/gL interacts with the C-terminal 1665–1960 amino acids region of NMHC-IIA. NMHC-IIA indicated extensive colocalisation and membrane redistribution upon virus infection [17]. Knockdown of NMHC-IIA in nasopharyngeal epithelial cells (NPECs) showed declined entry efficiency of EBV. Our study also showed significant amendments in the NMHC-IIB upon EBV infection in both the cell lines. In the KSHV infection, NMHC-IIA interacts directly with a multidomain

protein c-Cbl, which is crucial for the virus's bleb-associated micropinocytosis. The inhibition of NMHC-IIA ATPase activity or c-Cbl silencing suggested a decline in the entry and infection efficiency of KSHV virions [18]. Intriguingly, the micropinocytosis of KSHV is being tuned by proteins like EPHA2 and calcium and integrin binding protein-1 (CIB1). CIB1 promotes the activity of EPHA2 and assist its interaction with NMHC-IIA with the alpha-actinin 4 and facilitates the mechanical support for micropinocytosis [18]. Similarly, HSV-1, major tegument protein VP22 participate in the interaction with NM-IIA. Upon blocking of NM-IIA ATPase activity indicated mitigation in the yield of extracellular HSV-1 production. For the entry mechanism of HSV-1, the NM-IIA and NM-IIB participate as cellular receptors or factors that interact with glycoprotein B on the cell surface. The ectopic expression of NM-IIA in HL 60 cells showed susceptibility towards HSV-1 infection [17]. Knockdown of nectin-1 and NMHC-IIB indicated mitigation in the HSV-1 entry into trigeminal ganglion (TG). It is further observed that nectin-1 interacts with the gD receptor and NMHC-IIB with gB receptors for facilitating the HSV-1 entry and holds promise as a therapeutic target for HSV-1 latency and herpes simplex keratitis (HSK) recurrence [19]. Nonetheless, HSV-1 entry is lubricated by NMHC-IIA by interacting with gB in the COS-1 cells [20]. MYH9 (NMHC-IIB) have also shared links with the infection of severe acute respiratory syndrome coronavirus-2 (SARS-CoV-2) in the human lung's cells [21]. MYH9 indicated colocalisation with SARS-CoV-2 at the membrane, which interacts with S2 and S1 subunits and enhances the SARS-CoV-2 entry in an ACE-2 dependent manner [22]. In addition, we have observed amendments in the NRP1 and -2 genes only at the initial time of EBV infection. Earlier, NRP1 served as the entry factor for EBV and makes an attachment with gB. A deletion mutant of the CendR motif (23-427) of gB showed reduced NRP1 interaction. Further, other deletions of gB in regions like 23-88, and 428-431 abolished the interaction between NRP1 and gB [23]. Akin to this, NRP1 binds to the cleaved substrates of furin and expresses in abundance in the respiratory and olfactory epithelial, which hints towards its potential as a receptor for SARS-CoV-2 infection [24].

After attachment with the receptor and virus translocate in the lipid raft region for successful entry into the cell. These regions play significant role in infection of several pathogens. Lipid raft region plays a crucial role in KSHV infection to endothelial cells along with the expression of numerous gene expression (ORF73 and ORF50) and

KSHV-mediated signalling cascades like PI3-K, RhoA-GTPase and Dia-2 [25]. Treatment of MβCD removes the membrane cholesterol from the MDBK cells and mitigates the infection of CpHV.1 [26]. Likewise, we have also observed a decline in EBV internalisation upon membrane cholesterol depletion using MβCD in LN-229 and U-87 MG cells. Mitigated entry of HSV was also observed in the Vero cells treated with MβCD/nystatin in a dose-dependent manner [27]. Glycoprotein Q of HHV-6 makes an attachment with the CD46, which gets relocated in the lipid raft region and helps in the successful infection of the virus. Treatment of MβCD to HSB-2 indicates a decline in HHV-6 infection [28].

Earlier, by using inhibitor dynasore in the early phase of infection of murine cytomegalovirus (MCMV), it abolishes the establishment of the pre-assembly compartment and results in inhibition of virus maturation and egress [29]. The knockdown of dynamin 2 protein in the keratocytes after adenovirus infection resulted in the cumulation of acetylated tubulin, positioning of microtubule organizing centres (MTOCs) near the nuclei, elevated virus in the cytosol, declined proinflammatory cytokine and augmented binding of the virus to the nucleoporin, Nup358. It suggested the repressing role of dynamin 2 on adenoviral trafficking and influences host responses to infection. The current study has also observed mitigation in the EBV internalisation upon exposure to dynamin inhibitor. The entry of HSV-1 into mouse fibroblast showed dependency on the dynamin protein while upon depletion of dynamin (by dynasore and double-knockout of dynamin 1 and -2), the virus still getting internalised, suggesting the alternative pathway that accomplishes the virus entry [4]. In addition, KSHV infection in human foreskin fibroblast (HFF) cells indicated the crucial role of markers like Rab5, EEA1 Rab7 and LAMP1 via subcellular fractionation [30]. HSV-2 showed entry in human vaginal epithelial cells, i.e., VK2 cells, through the endosomal-lysosomal pathway, where the virus replication showed a pivotal correlation with the LAMP3. Knockdown of LAMP3 indicated diminished virus entry and the overexpression of LAMP3 was found to be heavily colocalised with HSV-2 [31]. Our study also showed the colocalisation with endosomes (early and late) and lysosome suggesting the presence of EBV in the endosomal trafficking. In the primary fibroblast, a significant fraction of virions exhibited endocytosis, indicating presence in the early endocytic marker proteins [32]. In addition to herpesviruses, Rab5 exhibited a crucial molecule for internalisation of

DENV and West Nile viruses in the HeLa cells [33]. RABV has been traced in the endosomes (early and late) of the hippocampal neurons [34]. These results indicated the significantly higher presence of EBV in the late endosome, which suggests their therapeutic potential.

Taken together, the current work discussed the plausible entry receptors of EBV into brain astrocytes. The crucial role of the lipid raft region and dynamin protein suggests that EBV undergoes an endocytic pathway in the neuronal cells. The significantly augmented presence of EBV with endosomal markers further affirms the entry of EBV via the endocytic pathway. Further, deciphering the preferred path of EBV entry and replication in the brain cells helps design the prophylactic intervention strategies to mitigate the EBV infection.

2.6 Methods

2.6.1 Cells

The human astroglia cell LN-229 and U-87 MG cells were procured from the Professor Kumaravel Somasundaram's Lab, Department of Microbiology & Cell Biology, Indian Institute of Science Bangalore, and National Centre for Cell Science, Pune, India, respectively. For virus purification, HEK 293T cells were used, which contain stably transfected bacterial artificial chromosome (BAC) green fluorescent protein (GFP)-EBV [35]. The cells were cultured in Dulbecco's modified Eagle's medium (DMEM; Thermo Scientific, USA) supplemented with 10% fetal bovine serum (FBS; Thermo Scientific, USA), 50 U/ml, 100 μg/ml and 2 mM of penicillin, streptomycin and L-Glutamine respectively. The growing cell environment was humidified with 5% CO_2 at 37 °C.

2.6.2 Purification of virus particles

The BAC-GFP-EBV has stably transfected HEK 293T cells [35] and were grown in complete DMEM with puromycin selection. EBV particles were obtained by using the following protocol, as illustrated previously [7].

2.6.3 Cell viability or MTT assay

For (3-(4,5-Dimethylthiazol-2-yl)-2,5-Diphenyltetrazolium Bromide) (MTT) assay. A total of 10×10^3 LN-229 and U-87 MG cells were seeded in a 96-well culture plate in complete DMEM supplemented with 10% of FBS and maintained for 24 hrs at 37 °C with 5% CO_2. MβCD and dynasore were dissolved in double distilled water. Upon treatment with MβCD and dynasore, the morphological changes in the cells were monitored using bright-field microscopy. After 24 hrs of treatment, media was removed and 100 μL of fresh media containing 0.5 mg/mL MTT was added to each well and incubated for 3 hrs at 37 °C. The MTT reagent was removed, 100 μL of DMSO was added to dissolve formazan crystals by shaking for 2 hrs, and absorbance was measured at 570 and 590 nm. For experimentation purposes, MβCD used was ~1mM, and 70 μM concentrations were used (Figure 2.1V-VIII).

2.6.4 Quantitative real time-polymerase chain reaction

EBV infections and receptor gene profiles were analysed using qRT-PCR. A total of 2.5×10^4 cells were seeded in a 6-well plate, followed by EBV exposure for different time points. Total RNA extraction, complementary DNA preparation and qRT-PCR were carried out as described earlier [36]. Gene-specific primers were designed from Primer-BLAST and are listed in Table S1. Glyceraldehyde 3-phosphate dehydrogenase (GAPDH) was used as a housekeeping gene and experiment was performed in two biological one technical repeats.

2.6.5 Immunofluorescence

Immunofluorescence assay was used for demonstrating EBV infections using GFP (1:1000; 4B10, from Cell Signalling Technology (CST), Danvers, MA, USA), Rab5 (1:200; C8B1, CST), EEA1 (1:200; C45B10, CST), Rab7 (1:200; D95F2, CST) and LAMP1 (1:200; D2D11, CST) antibodies. 2.5×10^4 cells were seeded in a 6-well plate onto the coverslips and exposed to EBV for different time points, and immunostaining was performed as explained previously [6]. Cells were observed under a confocal microscope and observed under CLSM (FluoView 1000, Olympus America Inc., USA). Analysis and quantification of the image were done as mentioned previously. The fluorescence intensity was calculated and plotted compared to the uninfected control of the respective groups.

2.6.6 Western blot

LN-229 and U-87 MG cells infected with EBV samples were harvested, washed with PBS and lysed in radioimmunoprecipitation assay buffer (RIPA) as described earlier [6]. Antibodies against Rab5, EEA1, Rab7, LAMP1 and GAPDH (1 μg/ml; AM4300; applied biosystems) were used as per the protocol [6]. For the western blot, GAPDH was used as a housekeeping gene. Image analysis and quantification of blots were performed using Image J software (National Institutes of Health, Bethesda, MA, USA).

2.6.7 Statistical analysis

The t-test (Two samples) was carried out to compare values of compound-treated samples with EBV infection samples. The t-statistic was significant at the 0.05 critical alpha level, $p < 0.05$ at the 95% confidence interval. The *p*-values of <0.05, <0.01 and <0.0001 are considered statistically significant and are represented with *, ** and ***, respectively. The increase and decrease are represented by * and #, respectively.

2.7 References

1. Jha HC, Mehta D, Lu J, El-Naccache D, Shukla SK, Kovacsics C, Kolson D, Robertson ES (2015) Gammaherpesvirus Infection of Human Neuronal Cells. mBio 6:e01844-15. https://doi.org/10.1128/mBio.01844-15

2. Rani A, Jakhmola S, Karnati S, Parmar HS, Chandra Jha H (2021) Potential entry receptors for human γ-herpesvirus into epithelial cells: A plausible therapeutic target for viral infections. Tumour Virus Research 12:200227. https://doi.org/10.1016/j.tvr.2021.200227

3. Lopez LA, Yang SJ, Exline CM, Rengarajan S, Haworth KG, Cannon PM (2012) Anti-Tetherin Activities of HIV-1 Vpu and Ebola Virus Glycoprotein Do Not Involve Removal of Tetherin from Lipid Rafts. J Virol 86:5467–5480. https://doi.org/10.1128/JVI.06280-11

4. Möckel M, Rahn E, De La Cruz N, Wirtz L, Van Lent JWM, Pijlman GP, Knebel-Mörsdorf D (2019) Herpes Simplex Virus 1 Can Enter Dynamin 1 and 2 Double-Knockout Fibroblasts. J Virol 93:e00704-19. https://doi.org/10.1128/JVI.00704-19

5. Mardi N, Haiaty S, Rahbarghazi R, Mobarak H, Milani M, Zarebkohan A, Nouri M (2023) Exosomal transmission of viruses, a two-edged biological sword. Cell Commun Signal 21:19. https://doi.org/10.1186/s12964-022-01037-5

6. Rani A, Tanwar M, Verma TP, Patra P, Trivedi P, Kumar R, Jha HC (2023) Understanding the role of membrane cholesterol upon Epstein Barr virus infection in astroglial cells. Front Immunol 14:1192032. https://doi.org/10.3389/fimmu.2023.1192032

7. Jakhmola S, Jha HC (2021) Glial cell response to Epstein-Barr Virus infection: A plausible contribution to virus-associated inflammatory reactions in the brain. Virology 559:182–195. https://doi.org/10.1016/j.virol.2021.04.005

8. Lee JS, Ismail AM, Lee JY, Zhou X, Materne EC, Chodosh J, Rajaiya J (2019) Impact of dynamin 2 on adenovirus nuclear entry. Virology 529:43–56. https://doi.org/10.1016/j.virol.2019.01.008

9. Akula SM, Naranatt PP, Walia N-S, Wang F-Z, Fegley B, Chandran B (2003) Kaposi's sarcoma-associated herpesvirus (human herpesvirus 8) infection of human fibroblast cells occurs through endocytosis. J Virol 77:7978–7990. https://doi.org/10.1128/jvi.77.14.7978-7990.2003

10. Chen J, Sathiyamoorthy K, Zhang X, Schaller S, Perez White BE, Jardetzky TS, Longnecker R (2018) Ephrin receptor A2 is a functional entry receptor for Epstein–Barr virus. Nat Microbiol 3:172–180. https://doi.org/10.1038/s41564-017-0081-7

11. Zhang H, Li Y, Wang H-B, Zhang A, Chen M-L, Fang Z-X, Dong X-D, Li S-B, Du Y, Xiong D, He J-Y, Li M-Z, Liu Y-M, Zhou A-J, Zhong Q, Zeng Y-X, Kieff E, Zhang Z, Gewurz BE, Zhao B, Zeng M-S (2018) Author Correction: Ephrin receptor A2 is an epithelial cell receptor for Epstein–Barr virus entry. Nat Microbiol 3:1075–1075. https://doi.org/10.1038/s41564-018-0155-1

12. Chen J, Zhang X, Schaller S, Jardetzky TS, Longnecker R (2019) Ephrin Receptor A4 is a New Kaposi's Sarcoma-Associated Herpesvirus Virus Entry Receptor. mBio 10:e02892-18. https://doi.org/10.1128/mBio.02892-18

13. Dong X-D, Li Y, Li Y, Sun C, Liu S-X, Duan H, Cui R, Zhong Q, Mou Y-G, Wen L, Yang B, Zeng M-S, Luo M-H, Zhang H (2023) EphA2 is a functional entry receptor for HCMV infection of glioblastoma cells. PLoS Pathog 19:e1011304. https://doi.org/10.1371/journal.ppat.1011304

14. Lupberger J, Zeisel MB, Xiao F, Thumann C, Fofana I, Zona L, Davis C, Mee CJ, Turek M, Gorke S, Royer C, Fischer B, Zahid MN, Lavillette D, Fresquet J, Cosset F-L, Rothenberg SM, Pietschmann T, Patel AH, Pessaux P, Doffoël M, Raffelsberger W, Poch O, McKeating JA, Brino L, Baumert TF (2011) EGFR and EphA2 are host factors for hepatitis C virus entry and possible targets for antiviral therapy. Nat Med 17:589–595. https://doi.org/10.1038/nm.2341

15. Hahn AS, Desrosiers RC (2013) Rhesus monkey rhadinovirus uses eph family receptors for entry into B cells and endothelial cells but not fibroblasts. PLoS Pathog 9:e1003360. https://doi.org/10.1371/journal.ppat.1003360

16. De Boer ECW, Van Gils JM, Van Gils MJ (2020) Ephrin-Eph signaling usage by a variety of viruses. Pharmacological Research 159:105038. https://doi.org/10.1016/j.phrs.2020.105038

17. Tan L, Yuan X, Liu Y, Cai X, Guo S, Wang A (2019) Non-muscle Myosin II: Role in Microbial Infection and Its Potential as a Therapeutic Target. Front Microbiol 10:401. https://doi.org/10.3389/fmicb.2019.00401

18. Valiya Veettil M, Sadagopan S, Kerur N, Chakraborty S, Chandran B (2010) Interaction of c-Cbl with myosin IIA regulates Bleb associated macropinocytosis of Kaposi's sarcoma-associated herpesvirus. PLoS Pathog 6:e1001238. https://doi.org/10.1371/journal.ppat.1001238

19. Wang C, Liang Q, Sun D, He Y, Jiang J, Guo R, Malla T, Hamrah P, Liu X, Huang Z, Hu K (2022) Nectin-1 and Non-muscle Myosin Heavy Chain-IIB: Major Mediators of Herpes Simplex Virus-1 Entry Into Corneal Nerves. Front Microbiol 13:830699. https://doi.org/10.3389/fmicb.2022.830699

20. Arii J, Hirohata Y, Kato A, Kawaguchi Y (2015) Nonmuscle Myosin Heavy Chain IIB Mediates Herpes Simplex Virus 1 Entry. J Virol 89:1879–1888. https://doi.org/10.1128/JVI.03079-14

21. Liu Q, Cheng C, Huang J, Yan W, Wen Y, Liu Z, Zhou B, Guo S, Fang W (2024) MYH9: A key protein involved in tumor progression and virus-related diseases. Biomedicine & Pharmacotherapy 171:116118. https://doi.org/10.1016/j.biopha.2023.116118

22. Chen J, Fan J, Chen Z, Zhang M, Peng H, Liu J, Ding L, Liu M, Zhao C, Zhao P, Zhang S, Zhang X, Xu J (2021) Nonmuscle myosin heavy chain IIA facilitates SARS-CoV-2 infection in human pulmonary cells. Proc Natl Acad Sci USA 118:e2111011118. https://doi.org/10.1073/pnas.2111011118

23. Wang H-B, Zhang H, Zhang J-P, Li Y, Zhao B, Feng G-K, Du Y, Xiong D, Zhong Q, Liu W-L, Du H, Li M-Z, Huang W-L, Tsao SW, Hutt-Fletcher L, Zeng Y-X, Kieff E, Zeng M-S (2015) Neuropilin 1 is an entry factor that promotes EBV infection of nasopharyngeal epithelial cells. Nat Commun 6:6240. https://doi.org/10.1038/ncomms7240

24. Cantuti-Castelvetri L, Ojha R, Pedro LD, Djannatian M, Franz J, Kuivanen S, van der Meer F, Kallio K, Kaya T, Anastasina M, Smura T, Levanov L, Szirovicza L, Tobi A, Kallio-Kokko H, Österlund P, Joensuu M, Meunier FA, Butcher SJ, Winkler MS, Mollenhauer B, Helenius A, Gokce O, Teesalu T, Hepojoki J, Vapalahti O, Stadelmann C, Balistreri G, Simons M (2020) Neuropilin-1 facilitates SARS-CoV-2 cell entry and infectivity. Science 370:856–860. https://doi.org/10.1126/science.abd2985

25. Raghu H, Sharma-Walia N, Veettil MV, Sadagopan S, Caballero A, Sivakumar R, Varga L, Bottero V, Chandran B (2007) Lipid Rafts of Primary Endothelial Cells Are Essential for Kaposi's Sarcoma-Associated Herpesvirus/Human Herpesvirus 8-Induced Phosphatidylinositol 3-Kinase and RhoA-GTPases Critical for Microtubule Dynamics and Nuclear Delivery of Viral DNA but Dispensable for Binding and Entry. J Virol 81:7941–7959. https://doi.org/10.1128/JVI.02848-06

26. Pratelli A, Colao V (2016) Critical role of the lipid rafts in caprine herpesvirus type 1 infection in vitro. Virus Research 211:186–193. https://doi.org/10.1016/j.virusres.2015.10.013

27. Bender FC, Whitbeck JC, Ponce De Leon M, Lou H, Eisenberg RJ, Cohen GH (2003) Specific Association of Glycoprotein B with Lipid Rafts during Herpes Simplex Virus Entry. J Virol 77:9542–9552. https://doi.org/10.1128/JVI.77.17.9542-9552.2003

28. Tang H, Kawabata A, Takemoto M, Yamanishi K, Mori Y (2008) Human herpesvirus-6 infection induces the reorganization of membrane microdomains in target cells, which are required for virus entry. Virology 378:265–271. https://doi.org/10.1016/j.virol.2008.05.028

29. Štimac I, Jug Vučko N, Blagojević Zagorac G, Marcelić M, Mahmutefendić Lučin H, Lučin P (2021) Dynamin Inhibitors Prevent the Establishment of the Cytomegalovirus Assembly Compartment in the Early Phase of Infection. Life 11:876. https://doi.org/10.3390/life11090876

30. Walker LR, Hussein HAM, Akula SM (2016) Subcellular fractionation method to study endosomal trafficking of Kaposi's sarcoma-associated herpesvirus. Cell Biosci 6:1. https://doi.org/10.1186/s13578-015-0066-2

31. Nazli A, Chow R, Zahoor MA, Workenhe ST, Dhawan T, Verschoor C, Kaushic C (2022) LAMP3/CD63 Expression in Early and Late Endosomes in Human Vaginal Epithelial Cells Is Associated with Enhancement of HSV-2 Infection. J Virol 96:e0155322. https://doi.org/10.1128/jvi.01553-22

32. Hetzenecker S, Helenius A, Krzyzaniak MA (2016) HCMV Induces Macropinocytosis for Host Cell Entry in Fibroblasts. Traffic 17:351–368. https://doi.org/10.1111/tra.12355

33. Krishnan MN, Sukumaran B, Pal U, Agaisse H, Murray JL, Hodge TW, Fikrig E (2007) Rab 5 Is Required for the Cellular Entry of Dengue and West Nile Viruses. J Virol 81:4881–4885. https://doi.org/10.1128/JVI.02210-06

34. Piccinotti S, Whelan SPJ (2016) Rabies Internalizes into Primary Peripheral Neurons via Clathrin Coated Pits and Requires Fusion at the Cell Body. PLoS Pathog 12:e1005753. https://doi.org/10.1371/journal.ppat.1005753

35. Halder S, Murakami M, Verma SC, Kumar P, Yi F, Robertson ES (2009) Early Events Associated with Infection of Epstein-Barr Virus Infection of Primary B-Cells. PLoS ONE 4:e7214. https://doi.org/10.1371/journal.pone.0007214

36. Patra P, Rani A, Sharma N, Mukherjee C, Jha HC (2023) Unraveling the Connection of Epstein–Barr Virus and Its Glycoprotein M $_{146-157}$ Peptide with Neurological Ailments. ACS Chem Neurosci 14:2450–2460. https://doi.org/10.1021/acschemneuro.3c00231

Chapter 3: Understanding the role of membrane cholesterol upon Epstein Barr virus infection in astroglial cells

3.1 Graphical Abstract
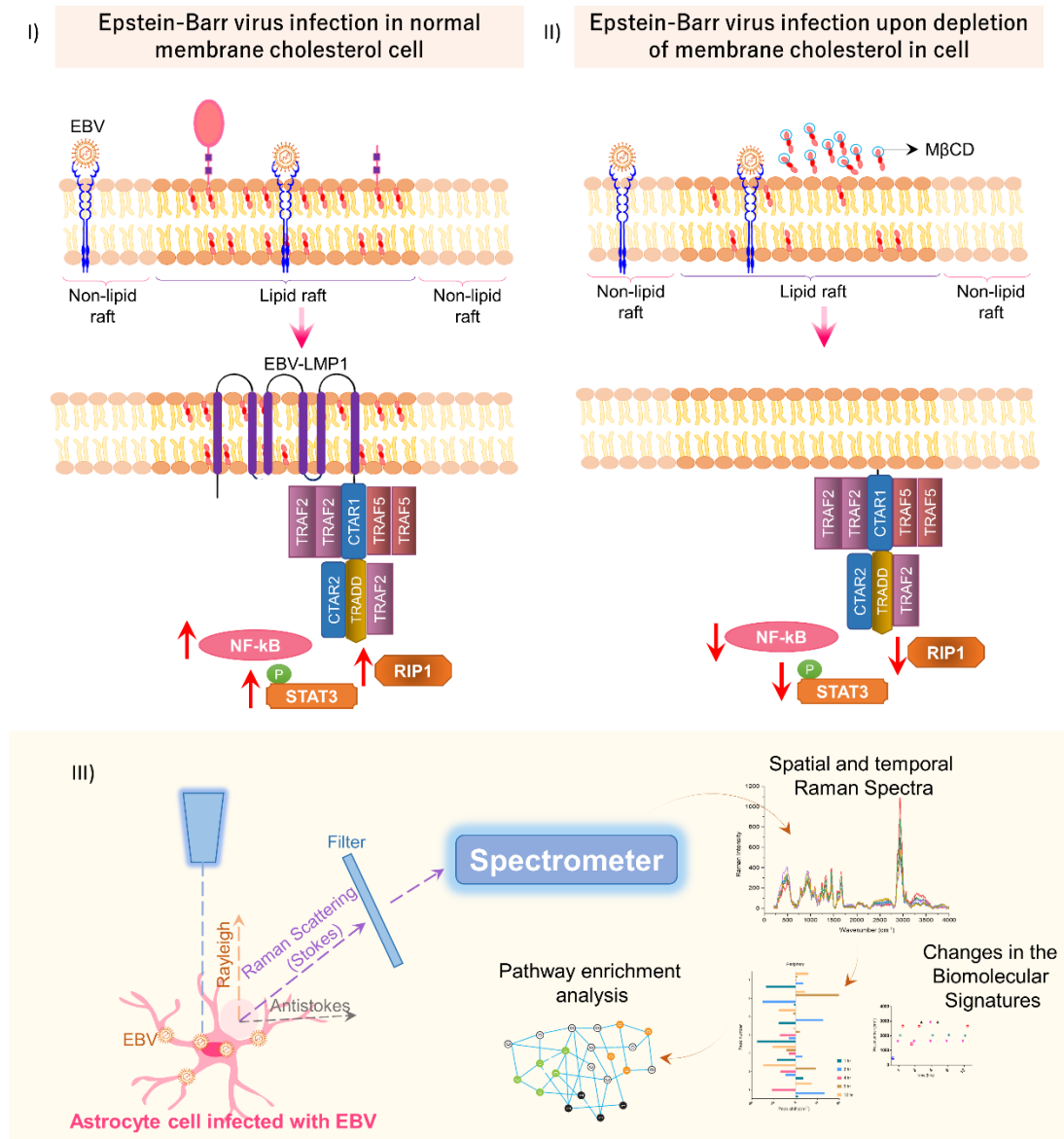
3.2 Abstract

EBV infection has long been postulated to trigger/exacerbate multiple sclerosis (MS) and anti-EBV antibodies showed a consistent presence in MS patients. Previous reports from our group have shown that EBV infects different brain cells. Entry of the virus in neuronal cells is assisted by several host factors, including membrane cholesterol. In order to understand its role in EBV infection and pathogenesis into

astroglia cells, here we have used its inhibitor, methyl-β-cyclodextrin (MβCD). The membrane cholesterol-depleted cells were infected with EBV and its latent genes expression were assessed. Further, EBV-mediated downstream signalling molecules, namely STAT3, RIP, NF-kB and TNF-α levels were checked at protein level along with spatial (periphery and nucleus) and temporal changes in biomolecular fingerprints with Raman spectroscopy (RS). Upon treatment with MβCD, lmp1, lmp2a and lmp2b suggested significant downregulation compared to EBV infection. Downstream molecules, like STAT3 and RIP, exhibited a decrease in protein levels temporally upon exposure to MβCD while NF-kB levels were found to be increased. Further, the intensity of the Raman spectra exhibited an increase in triglycerides and fatty acids in the cytoplasm of EBV-infected LN-229 cells compared to MβCD+EBV. Likewise, the Raman peak width of cholesterol, lipid and fatty acids were found to be reduced in EBV-infected samples, indicates elevation in the cholesterol specific moieties. In contrast, an opposite pattern was observed in the nucleus. Moreover, the ingenuity pathway analysis revealed protein molecules such as VLDLR, MBP and APP that are associated with altered profiles of cholesterol, fatty acids and triglycerides with infection-related CNS disorders. Taken together, our results underline the important role of membrane cholesterol over EBV entry/pathogenesis in astroglia cells, which further trigger/aggravate virus-associated neuropathologies. These results will eventually aid in the prognosis of neurological diseases like MS.

3.3 Introduction

EBV is associated with various cancers and several neurological diseases like viral encephalitis, CNS-lymphoma, cerebral ataxia, meningitis, Multiple sclerosis (MS), Alzheimer's disease (AD) and Parkinson's disease (PD) [1], [2]. Patients with a history of infectious mononucleosis are reported to be more vulnerable to MS [3]. The cross-reactivity of antibodies was reported, such as amino acids 411–440 of the viral protein EBV nuclear antigen 1 (EBNA1) with the human chloride-channel protein, anoctamin 2, α-crystallin B chain and glial cell adhesion protein [4]. Notably, EBNA1 residues 411–426 suggested cross-reactivity with myelin basic protein (MBP), which is directly associated with MS [5], [6]. Several anti-EBV drugs have been used as therapeutics for MS [7], [8]. Therefore, these findings directing towards the presence of EBV as a vital factor in MS. Viruses and their associated factors acquire control over the brain cells and modulates neural niche. Membrane cholesterol facilitates the

entry and assembly of various pathogens in the cells, including viruses like EBV. Reports suggested that the entry of EBV and another gamma herpesvirus, KSHV, into epithelial cells is enabled by sphingolipids and cholesterol of the plasma membrane [9]. These lipid assemblies are known to contain receptors that are tempered by pathogens for entry and/or egress [10], [11]. Soon after infection, these pathogens tend to alter the process of lipid metabolism and contribute to neuropathologies [12], [13].

Membrane cholesterol-binding molecules like MβCD and nystatin have been shown to reduce EBV infection in previous *in-vitro* studies [14], [15]. On treatment with MβCD, the EBV latent membrane protein 2A (LMP2A), a crucial factor for viral latency and pathogenesis, has shown an increase in its exosome secretion [16]. Besides, another virally encoded transmembrane protein, LMP1 also localises in the cholesterol assemblies. It further activates a ligand-independent cascade through its two signalling domains, namely C-terminal-activating regions 1 and 2 (CTAR1 and CTAR2), mimicking CD40 signalling [17]. Subsequently, it activates the canonical nuclear factor kappa B (NF-kB), phosphoinositide-3-kinase-protein kinase B (PI3K-AKT) and epidermal growth factor receptor extracellular-regulated kinase-mitogen-activated protein kinase (ERK-MAPK) pathways [18], [19]. The above-mentioned changes in the membrane cholesterol region-mediated signalling help the virus's association and assembly [20]. In addition, receptor-interacting protein (RIP) kinase interacts with TNF receptor-associated factor 2 (TRAF2), which is essential for the activation of NF-kB in a tumour necrosis factor-alpha (TNF-α) dependent manner [21]. Viral infection results in the activation of various kinases leading to the phosphorylation of signal transducer and transcription 3 (STAT3), which ultimately migrates into the nucleus and regulates the expression of cytokines/chemokines [22]. Furthermore, a plethora of tools has been used to unravel the altered biomolecular profile of host cells after infection with viruses and bacteria [23], [24]. Raman spectroscopy (RS) is one such paramount non-destructive tool for quantitative and qualitative analysis of biomolecular fingerprints in cells, biofluids (i.e., serum) and tissues [11], [25]. RS provides detailed information about the chemical structure, crystallinity and molecular interactions by interacting with chemical bonds in a given material [26].

Raman signals specific to biomolecules such as cholesterol, lipids, glucose, phenylalanine and phosphoinositide can be obtained from several pathogen-infected and uninfected samples [8]. Significantly, alteration in the above-mentioned molecules is closely related to numerous neurological ailments [27], [28]. As observed in the recent SARS-CoV-2 pandemic, viral infections and their outbreak are the results of rapid evolution. For limiting the virus-mediated spread, a holistic awareness of virus-mediated cell manipulations needs a better understanding [29]. Although numerous reports suggested the link of EBV with MS, no reports have highlighted the crucial role of membrane cholesterol. Therefore, the current study has taken on the challenge of elucidating the importance of membrane cholesterol upon EBV infection in astrocytes. Here, we showed for the first time the importance of membrane cholesterol in EBV-mediated downstream cascade, which has critical implications in causing neuroinflammation and associated disease pathologies. Transcript profile for EBV latent genes was investigated. In order to explore the downstream signalling pathway affected by EBV, we have analysed the protein level of STAT3, RIP kinase, NF-kB and TNF-α. Lastly, RS was performed to explore the biomolecular profile of astroglia cells exposed to EBV in the presence and absence of the cholesterol inhibitor in a spatial and temporal-manner.

3.4 Results

3.4.1 Investigation of EBV latent genes after depleting the membrane cholesterol

Previously, EBV exhibited infection to neuronal and several glial cells [30], [31]. EBV titre was determined using qRT-PCR of EBV-green fluorescent protein (EBV-*gfp*) and EBV nuclear antigen 1 (*ebna1*) after infecting LN-229 cells at different concentrations (Figure 3.1I-II). Therefore, 2.5 MOI was used to infect the cells as described previously [31]. For MβCD treatment of LN-229 cells, the IC_{50} value of MβCD was 3.008 mM. For further experiments, 1 mM concentration was used since more than 90% of cells were alive and subsequently infected with EBV (Figure 3.1III).
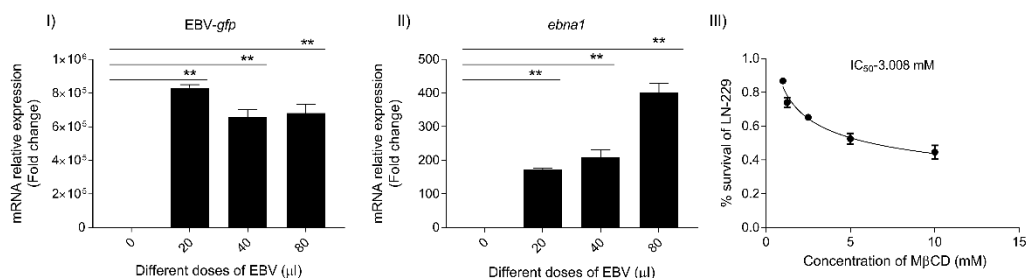
Figure 3.1: EBV titre and MβCD dose determination on LN-229 cells.
From this graph the 25 μl of diluted EBV corresponds to 2.5 MOI. Cell cytotoxicity assay of LN-229 cells upon MβCD treatment. Inhibitory concentration 50 (IC_{50}) was 3.008 mM.

LN-229 cells were exposed to EBV alone and in the presence of MβCD for 1, 2, 4, 6 and 12 hrs and the mRNA levels of EBV latent genes were examined. Since the latent viral genes are critical for establishing a successful infection and/or maintaining latency, the mRNA levels of EBV-*gfp*, virus latent genes *ebna1, -2, -3a, -3b, -3c, -lp, lmp1, -2a* and *-2b* were checked. EBV-*gfp* showed a significant decrease in the presence of MβCD in comparison to EBV alone at 1, 2, 4, 6 and 12 hrs ($p<0.05$, $p<0.01$, $p<0.001$, $p<0.01$ and $p<0.05$ respectively) (Figure 3.2I). Likewise, the *ebna1* transcript level diminished significantly ($p<0.01$) in MβCD+EBV samples (Figure 3.2II). In contrast, *ebna3a, -3b*, and *-3c* and exhibited a significant decrease only in the initial hours (1, 2 and 4 hrs) post EBV infection, while *ebnalp* indicated decline only at 12 hrs ($p<0.01$) (Figure 3.2III-VI). Interestingly, the *lmp1* mRNA was significantly downregulated in MβCD+EBV samples compared to EBV infection alone at all time points 1, 2, 4, 6 and 12 hrs ($p<0.01$, $p<0.05$, $p<0.01$, $p<0.01$ and $p<0.05$ respectively) (Figure 3.2VII). A similar pattern was observed for *lmp2a* and -*2b* transcripts (Figure 3.2VIII-IX).
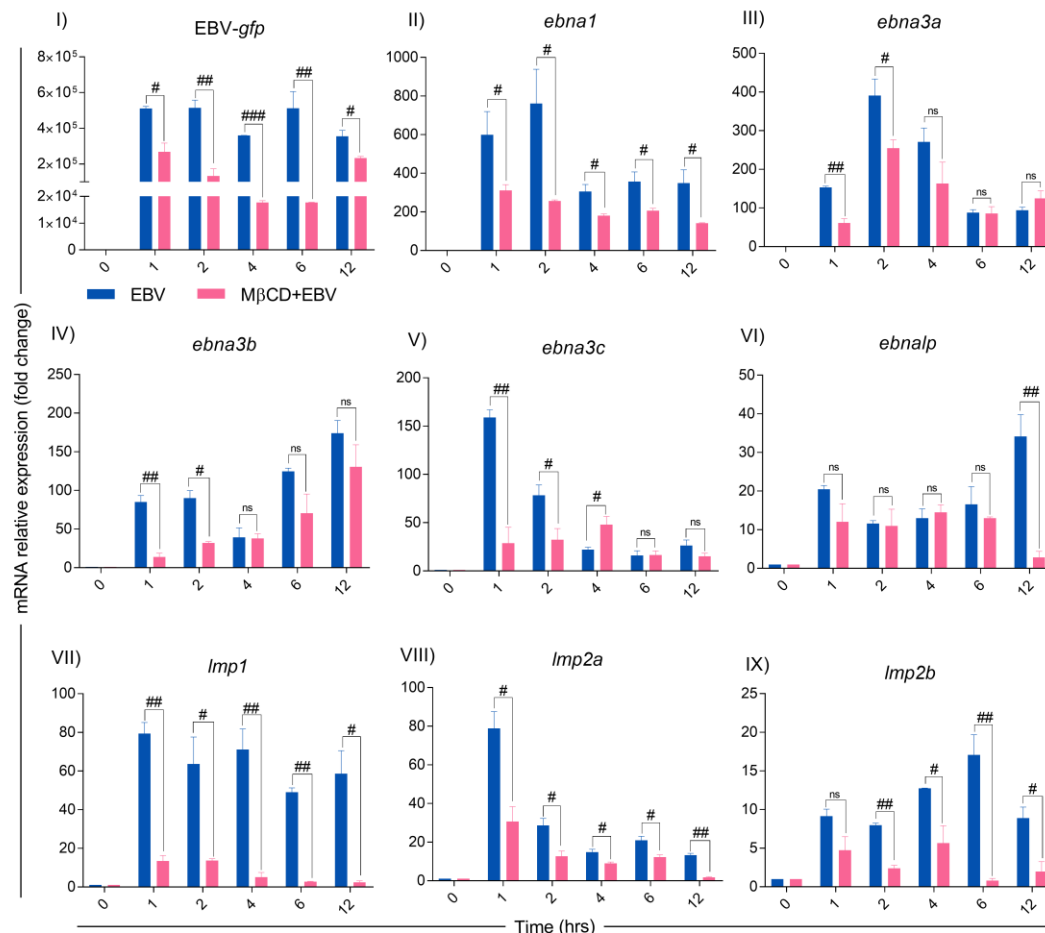
Figure 3.2: MβCD treatment curtails the expression of EBV latent genes in astroglia cells at different time points.

I) Reduced transcription of EBV-*gfp*, II) *ebna1*, III) *ebna3a*, IV) *ebna3b*, V) *ebna3c* and VI) *ebnalp* manifested reduced transcription at different time points. Significant down-regulation of IV) *lmp1*, VIII) *lmp2a* and IX) *lmp2b* expression in MβCD+EBV samples compared to EBV alone temporally. Given plots; *x*-axis, time-dependent EBV infection; *y*-axis, fold change with respect to EBV infected samples. The *p*-values of <0.05, <0.01 and <0.0001 are considered statistically significant and are represented with *, ** and *** respectively. The increase and decrease are represented by * and # respectively.

3.4.2 EBV-mediated downstream signalling after membrane cholesterol disruption

The EBV-encoded latent genes affect several critical downstream signalling pathways, we investigated protein levels of STAT3, RIP, NF-kB and TNF-α in LN-229 cells treated with MβCD+EBV and EBV alone at 0, 1, 2, 4, 6 and 12 hrs by immunoblotting.
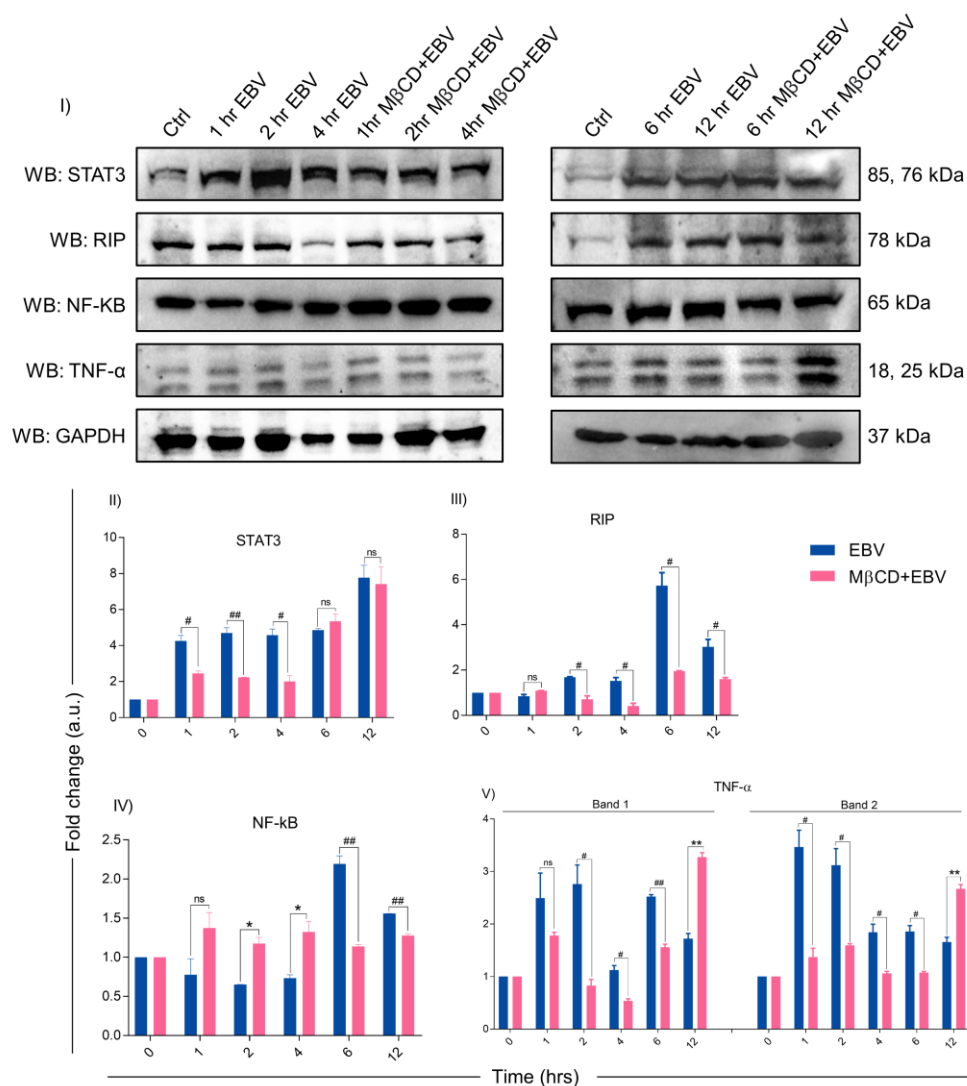
Figure 3.3: Representation of changes in EBV-mediated downstream signalling pathway proteins after MβCD treatment.

I) Western blot representation of STAT3, RIP, NF-kB and TNF-α. II-V) Quantification of western blots. II) STAT3 expression was reduced in MβCD treated samples at various time points i.e., 1, 2 and 4 hrs (p<0.05, p<0.01 and p<0.05 respectively). III) RIP was also found to be decreased in MβCD+EBV compared to EBV-infected samples at 2, 4, 6 and 12 hrs (p<0.05). IV) NF-kB was found to be increased after pre-treatment of MβCD at 2, 4 hrs and at 6, 12 hrs indicated decline. V) TNF-α levels showed an initial decline upon exposure to MβCD at 2, 4 and 6 (p<0.05, p<0.05 and p<0.01) and at 12 hrs an increase in its expression was observed (p<0.01). Given plots; *x*-axis, time-dependent EBV infection; *y*-axis, fold change with respect to EBV infected samples. The *p*-values of <0.05, <0.01 and <0.0001 are considered statistically significant and are represented with *, ** and *** respectively. The increase and decrease are represented by * and # respectively.

The results show that STAT3 exhibited a decline in MβCD+EBV samples at 1, 2 and 4 hrs compared to EBV-infected samples (p<0.05, p<0.01, p<0.05 respectively) (Figure 3.3I-II). A similar pattern was observed for RIP kinase expression at 2, 4, 6

and 12 hrs (p<0.05) (Figure 3.3 I, III). In contrast, the elevation in NF-kB was observed in MβCD+EBV samples compared to EBV alone at 2 and 4 hrs and at 6 and 12 hrs, it exhibited decline (p<0.01) (Figure 3.3 I, IV). The expression of TNF-α was found to be decreased (both bands, p<0.05) in MβCD+EBV up until 6 hrs and the pattern was the opposite at 12 hrs of time point (Figure 3.3 I, V).

3.4.3 Analysis of altered biomolecular fingerprint in EBV-infected astroglia cells after depleting the membrane cholesterol

3.4.3.1 Raman spectral analysis

To define the biomolecular fingerprints of EBV infection in astroglia cells and the role of cholesterol in it, we have used the Raman spectral analysis.
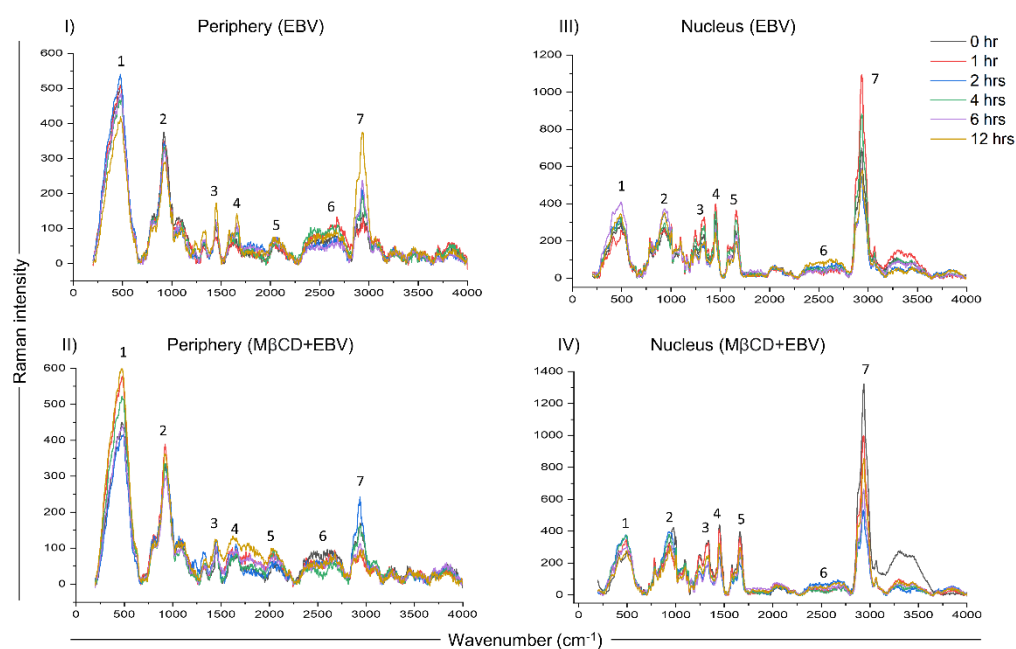
Figure 3.4: Raman spectra in EBV and MβCD+EBV exposed LN-229 astroglial cells.
I) Raman spectra of the periphery for only EBV exposed sample, II) Periphery spectra for MβCD+EBV cells, III) Spectra for nucleus after EBV infection and IV) Spectra for nucleus for MβCD+EBV samples. The data were plotted as average spectra of 9 different points of three different cells.

We observed various Raman spectra in LN-229 cells exposed to EBV and MβCD+EBV samples at two different cellular locations, namely, the nucleus and periphery (transmembrane and cytoplasmic conjunction region of the cells). The raw

data points of the spectra were plotted (wavenumber vs intensity) at 0, 1, 2, 4, 6, and 12 hrs (Figure 3.4I-IV).

A total of seven major Raman peaks were observed at the periphery in the wavenumber ranges periphery 473-490, 917-933, 1439-1452, 1615-1675, 2035-2060, 2599-2684, and 2838-2940 cm^{-1} (Figure 3.5I). In the periphery, the level of biomolecules like DNA and polysaccharides showed an increase in the MβCD+EBV samples at initial time points and eventually, a decline was observed compared to only EBV-exposed samples (Figure 3.5I). The level of cholesterol, fatty acids, phospholipids and triglycerides exhibited elevation in both EBV and MβCD+EBV samples initially and later there was an abundant increase in the EBV-exposed samples (Figure 3.5I). Contrarily, nucleic acids, tyrosine, tryptophan, C-N stretch and methionine exhibited similar kinds of changes in both type of samples (Figure 3.5I). Likewise, there were seven prominent peaks observed in the nucleus named 476-496, 929-976, 1091-1099, 1334-1338, 1446-1452, 1657-1664 and 2931-2937 cm^{-1} (Figure 3.5II). Fatty acid, cholesterol, lipids and nucleic acids indicated a decrease in only EBV-infected samples compared to MβCD+EBV in the later time points (Figure 3.5II). While the carbohydrates, glycogen were higher in EBV-exposed samples, suggesting an increase in the carbohydrate metabolism (Figure 3.5II).
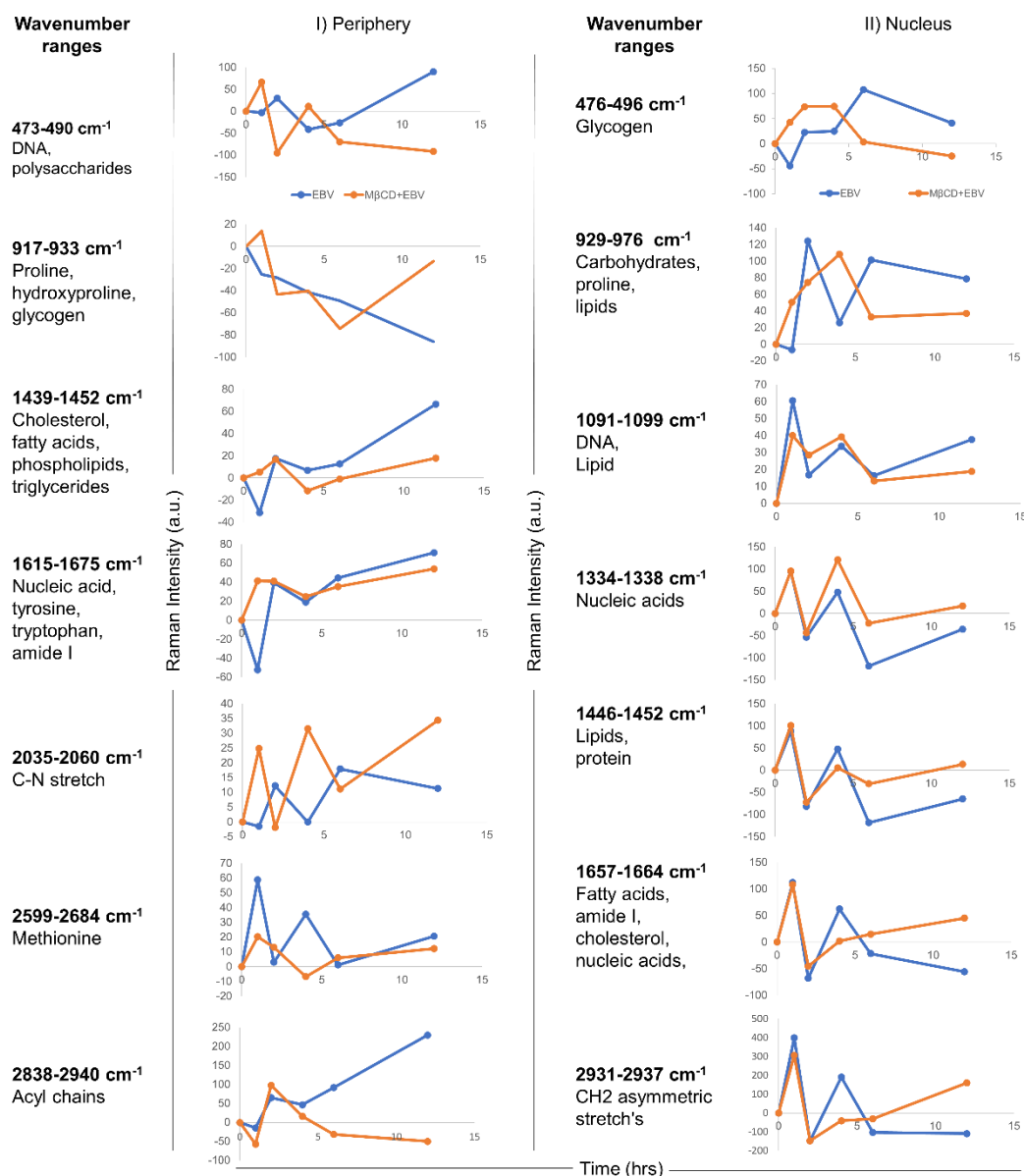
Figure 3.5: Temporal comparison of biomolecular signatures in EBV and MβCD+EBV exposed LN-229 cells.
I) Periphery, at 0, 1, 2, 4, 6 and 12 hrs. The wavenumber ranges represent specific cellular components- 476-496 cm-1 (glycogen), 929-976 cm-1 (carbohydrates and proline lipids), 1091-1099 cm-1 (DNA and lipid), 1334-1338 cm-1 (nucleic acids), 1446-1452 cm-1 (lipids and protein), 1657-1664 cm-1 (fatty acids, amide I, cholesterol and nucleic acids) and 2931-2937 cm-1 (CH2 asymmetric stretch's). II) Nucleus, a total of seven wavenumber ranges were observed which correspond to specific biomolecules. Specifically, these peak ranges from 473-490 cm-1 (DNA and polysaccharides), 917-933 cm-1 (proline, hydroxyproline and glycogen), 1439-1452 cm-1 (cholesterol, fatty acids and phospholipids), 1615-1675 cm-1 (nucleic acid, tyrosine, tryptophane and amide I), 2035-2060 cm-1 (C-N stretch), 2599-2684 cm-1 (Methionine) and 2838-2934 cm-1 (Acyl chains). The data were plotted as average spectra of 9 different points of three different cells.

3.4.3.2 Raman intensity analysis of EBV-exposed LN-229 cells and its comparison with MβCD+EBV exposed counterparts

To investigate the spectral information corresponding to the biomolecular status, the signature spectra of unique biomolecules were listed [32], [33], [34]. All the peak intensities were normalised with uninfected controls. The positive and negative variation, i.e., up and downregulation of intensity from the basal level of uninfected cells were further corroborated with the anabolic and catabolic activity of the molecules (Figure 3.6). In the periphery, biomolecule like DNA, polysaccharides, glycogen, proline, hydroxyproline and valine exhibited significant decline in MβCD+EBV samples at 1 hr of time point ($p < 0.05$) (Figure 3.6Ia). Similarly, at 2 hrs CH_2 asymmetric stretch and lipids showed a decrease ($p < 0.05$) (Figure 3.6Ib). Further at 4 hrs lipids, triglycerides, C-N stretch and CH_2 asymmetric stretch exhibited decline in MβCD+EBV samples compared to EBV infection ($p < 0.05$) (Figure 3.6Ic). DNA and glycogen manifested significant downregulation after disruption of cholesterol at 6 and 12 hrs of time points ($p < 0.05$, $p < 0.01$ respectively) (Figure 3.6Id and Ie). In contrast, molecules like amide I, fatty acids and OH-NH-CH group indicated increase in MβCD+EBV samples at 4 and 6 hrs of time points respectively ($p < 0.01$) (Figure 3.6Ic and IId). In the nucleus, proline and cholesterol exhibited significant diminish at 1 ($p < 0.01$), 4 ($p < 0.05$), 6 ($p < 0.05$) and 12 hrs ($p < 0.05$) while protein showed significant upregulation in MβCD+EBV samples ($p < 0.05$) (Figure 3.6IIa-IIe). Likewise, glycogen indicated significant decrease at 1 and 12 hrs of MβCD+EBV samples compared to EBV infection ($p < 0.01$ and $p < 0.05$ respectively) (Figure 3.6IIa and IIe).
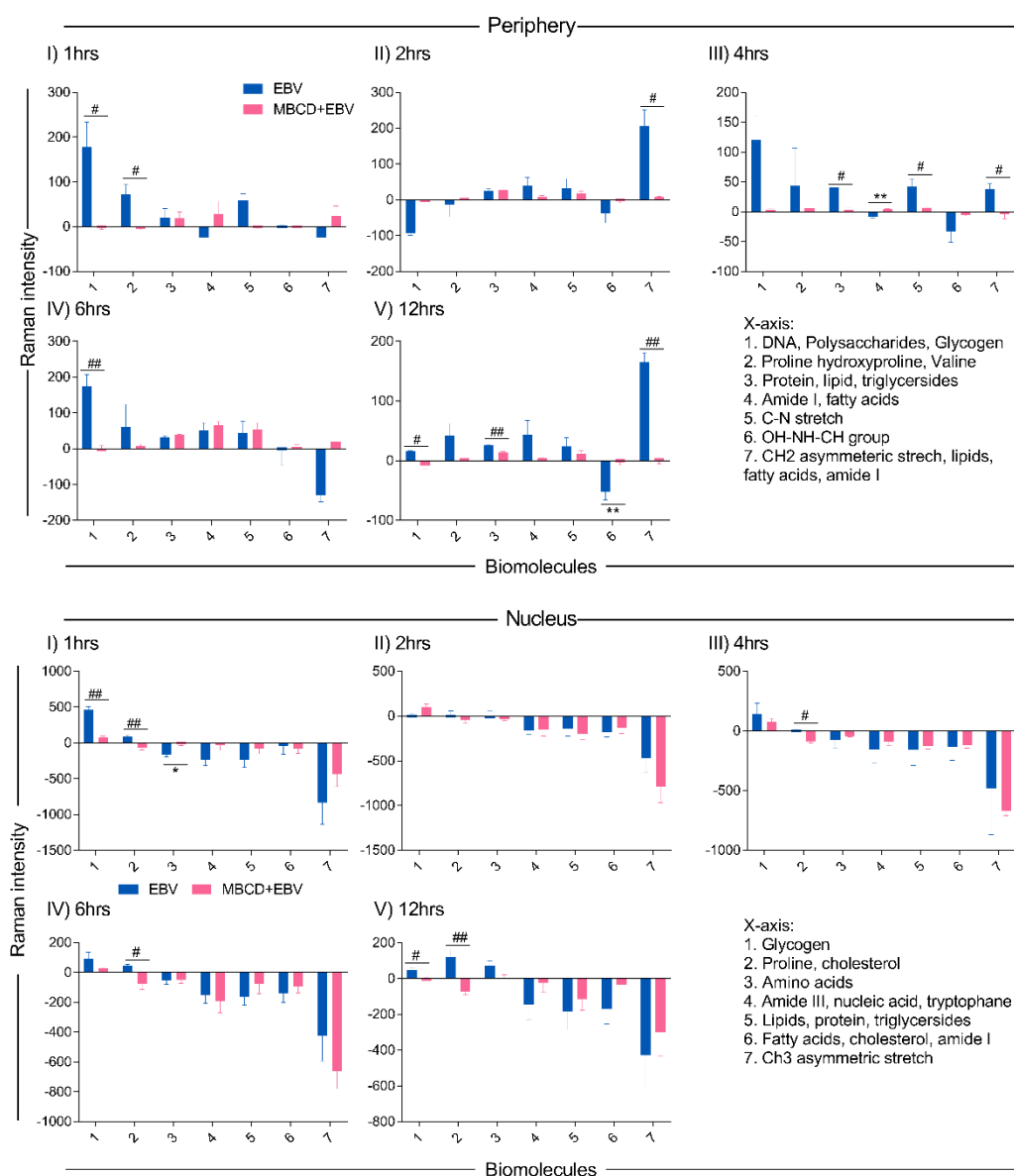
Figure 3.6: Illustration of changes in the biomolecular profile of LN-229 astroglia cells (periphery and nucleus) upon exposure to EBV and MβCD+EBV.
I) Altered biomolecules in the periphery a) Augmented biomolecules in EBV-infected samples, b) Increased molecules in LN-229 cells upon MβCD+EBV, c) Declined biomolecules in EBV-infected samples, d) Downregulated molecule in MβCD+EBV samples. II) List of amended biomolecular signatures at the nucleus a) Elevated biomolecules in EBV-infected samples, b) Upregulated molecules in MβCD+EBV, c) Downregulated molecules in EBV samples, d) Reduced biomolecule profile in MβCD+EBV samples. The data were plotted as average spectra of nine points of three different cells. The *p*-values of <0.05, <0.01 and <0.0001 are considered statistically significant and are represented with *, ** and *** respectively. The increase and decrease are represented by * and # respectively.

3.4.3.3 Analysis of biomolecular amendments using spectral width after depleting membrane cholesterol in astroglia cells

To investigate, biomolecular amendments after inhibition of cholesterol in EBV-infected astroglia cells and MβCD+EBV samples, we employed spectral width measurements of Raman peaks. At both cellular locations, i.e., periphery and nucleus, the full-width half maxima (FWHM) were calculated and normalized with uninfected control. FWHM represents the peak width of different biomolecules [35]. A steeper peak width is related to the presence of unique biomolecules and a broader peak represents the presence of a derivative of that unique biomolecule [35]. The FWHM was compared for samples with EBV alone and MβCD+EBV treatments. At the periphery, the MβCD+EBV samples showed a significant elevation ($p < 0.01$) in the proline, and hydroxyproline levels compared to EBV alone at 12 hrs of time point (Figure 3.7Ib). Intriguingly, cholesterol, lipid and fatty acids exhibited a significant decline in the MβCD+EBV-exposed samples at 1 and 12 hrs ($p < 0.01$) compared to MβCD+EBV samples (Figure 3.7Ic). While nucleic acid, OH-NH-CH group and CH_2 asymmetric stretch significant increase at all times in the MβCD+EBV samples ($p < 0.01$) (Figure 3.7Id, If and Ig). The C-N stretch depicted major augmentation in EBV samples at 6 and 12 hrs ($p < 0.01$) (Figure 3.7Ie).

In nucleus, the FWHM related to proline and cholesterol was significantly up in MβCD+EBV ($p < 0.01$) at 4 and 6 hrs of time point (Figure 3.7IIb). Molecules like glycogen, amino acids, protein, lipids and CH_2 asymmetric stretch exhibited a decline in the initial time points (Figure 3.7IIa, IIc and IIe). FWHM of nucleic acid showed an increase in MβCD+EBV samples at 1 and 12 hrs compared to EBV infection ($p < 0.01$) (Figure 3.7IId).
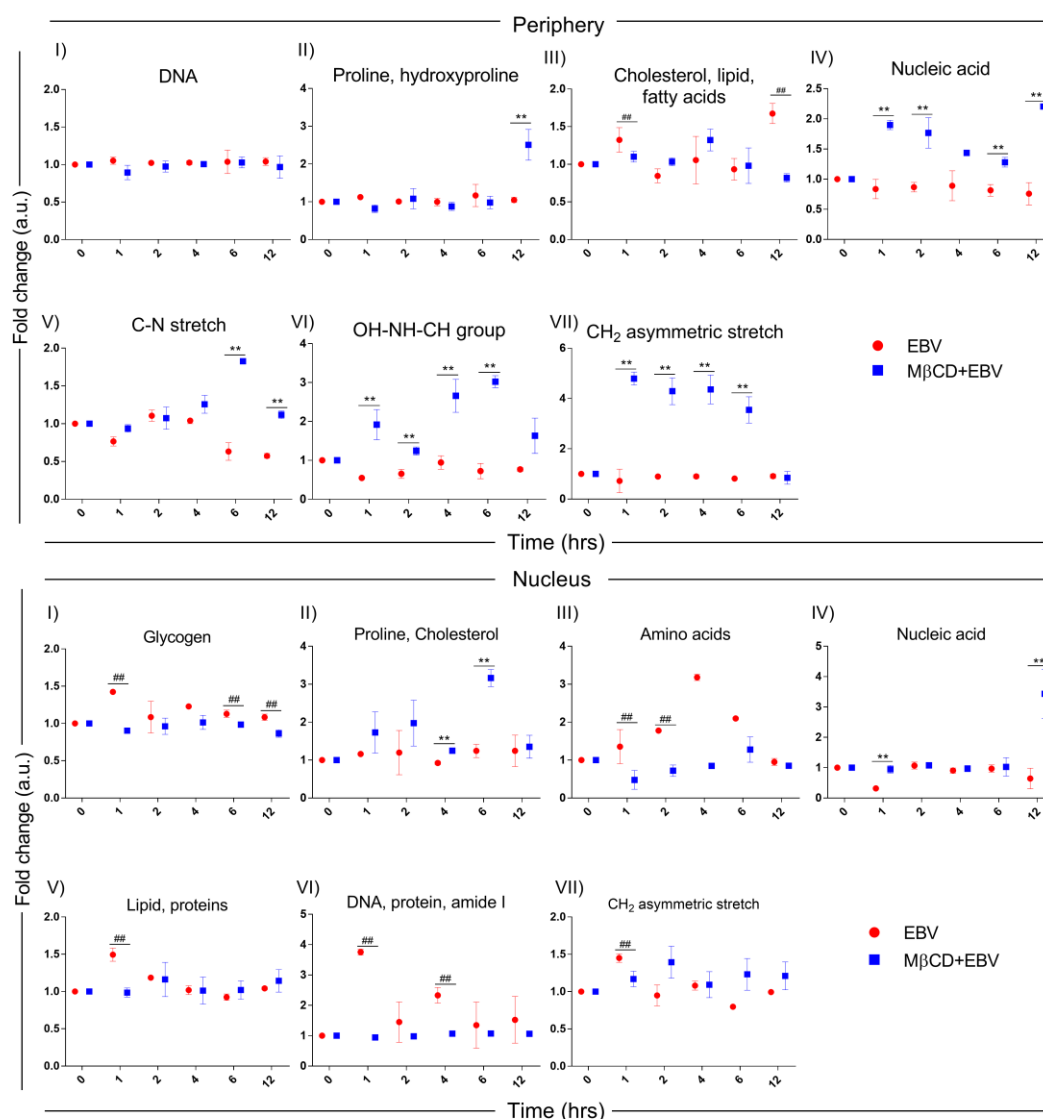
Figure 3.7: Representation of full-width half maxima of astroglia cells exposed to EBV and MβCD+EBV at periphery and nucleus.
I) FWHM of different biomolecules observed in the periphery. a) Glycogen, b) Proline and cholesterol, c) Amino acids, d) Nucleic acids, e) Lipid and proteins, f) DNA, protein and amide I, g) CH2 asymmetric stretch. II) FWHM of biomolecular alterations at the nucleus. a) DNA b) Proline and hydroxyproline, c) Cholesterol, lipid and fatty acids, d) Nucleic acid, e) C-N stretch, f) OH-NH-CH group, f) CH2 asymmetric stretch. The data was represented as Mean ± SEM of nine points of three different cells. The *p*-values of <0.05, <0.01 and <0.0001 are considered statistically significant and are represented with *, ** and *** respectively. The increase and decrease are represented by * and # respectively.

3.4.3.4 LN-229 peripheral Raman peak Shift in MβCD+EBV samples compared to EBV infection

It is known that external stimuli including pathogens tend to trigger shifts in Raman peaks. Each peak corresponds to a specific molecular bond vibration [36]. Shifts in these peaks at lower (blue shift) and higher (red shift) wavenumbers are due to the chemical bond length of molecules [37]. The larger bond length causes a shift to a lower wavenumber and vice-versa [38].
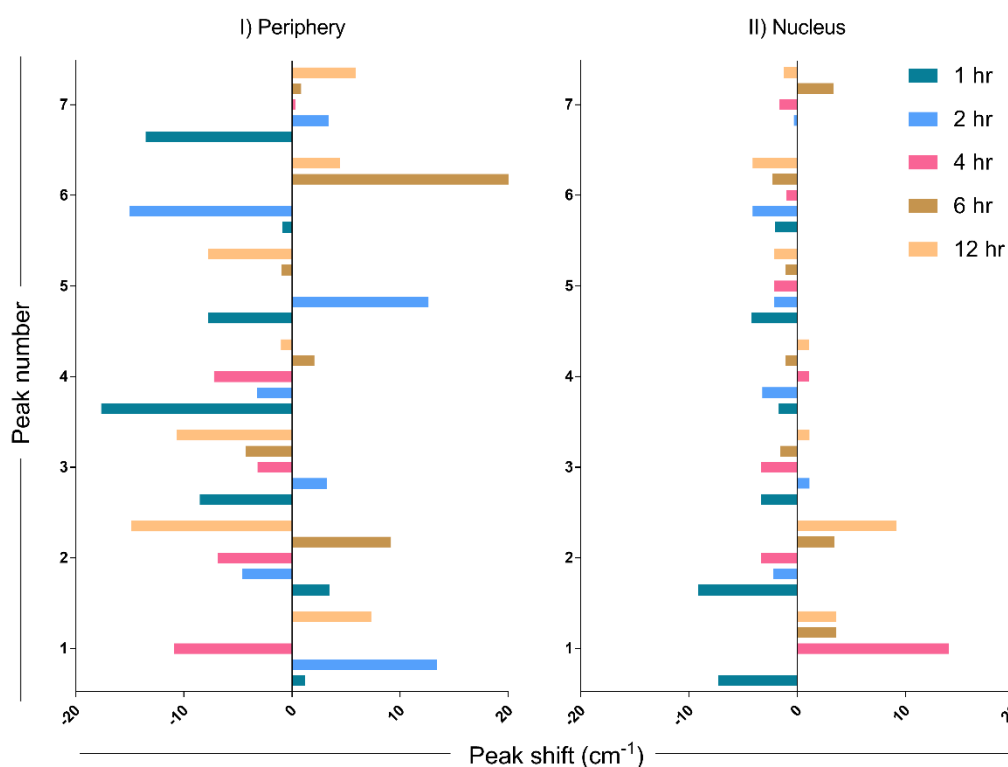
Figure 3.8: Interpretation of peak shift in Raman spectra from EBV to MβCD+EBV samples in the periphery and nucleus.
I) Peak shifts in the nucleus, II) Peak shifts in the periphery. The data were plotted as average spectra of nine points of three different cells.

Major peak shifts were observed in LN-229 cells at the periphery compared to the nucleus (Figure 3.8I & Table 3.1). The peak shift data was observed by subtracting the wavenumber maxima of EBV samples from MβCD+EBV and ±5 cm^{-1} peak shift was considered for further biomolecular signature observation (Table 3.1). The first peak shift was observed in the periphery at 2, 4 and 12 hrs (Figure 3.8I). At 2 and 4 hrs, the Raman shift corresponds to the same molecule, namely carbohydrate. In comparison, the shift at 12 hrs suggests conversion of polysaccharides into DNA

(Figure 3.8I). At 12 hrs, the second peak indicated a major change from carbohydrates to RNA (Figure 3.8I).

Table 3.1: Enlistment of wavenumber maxima for nucleus and periphery.
Peak shift (Δcm^{-1}) is indicating the difference in the peak maxima of MβCD+EBV and EBV samples.

		Nucleus					Periphery				
Time (hrs)		1	2	4	6	12	1	2	4	6	12
Peak 1	EBV	496.41	487.89	476.40	491.54	491.54	475.72	476.93	486.67	483.03	473.28
	MβCD+EBV	489.11	487.89	490.38	495.12	495.12	476.93	490.33	475.78	483.03	480.59
	Peak shift (Δcm^{-1})	-7.30	0.00	13.98	3.58	3.58	1.21	13.40	-10.8	0.00	7.31
Peak 2	EBV	941.57	931.20	935.86	933.58	933.58	917.56	921.00	927.86	924.43	931.29
	MβCD+EBV	932.40	929.00	932.49	937.01	942.72	921.00	916.42	921.00	933.58	916.42
	Peak shift (Δcm^{-1})	-9.17	-2.20	-3.37	3.43	9.14	3.44	-4.58	-6.86	9.15	-14.8
Peak 3	EBV	1097.30	1091.72	1099.53	1097.30	1096.18	1452.25	1443.73	1446.93	1447.99	1450.12
	MβCD+EBV	1093.95	1092.83	1096.18	1095.70	1097.30	1443.73	1446.93	1443.73	1443.73	1439.47
	Peak shift (Δcm^{-1})	-3.35	1.11	-3.35	-1.60	1.12	-8.52	3.20	-3.20	-4.26	-10.6
Peak 4	EBV	1337.37	1337.37	1337.37	1336.29	1337.37	1632.82	1655.70	1667.94	1658.66	1658.66
	MβCD+EBV	1335.65	1334.14	1338.45	1335.21	1338.45	1615.19	1652.47	1660.73	1660.73	1657.63
	Peak shift (Δcm^{-1})	-1.72	-3.23	1.08	-1.08	1.08	-17.6	-3.23	-7.21	2.07	-1.03
Peak 5	EBV	1452.25	1449.06	1452.25	1451.19	1450.12	2043.27	2051.04	2043.27	2060.75	2045.22
	MβCD+EBV	1447.99	1446.93	1450.12	1450.12	1447.99	2035.49	2063.66	2043.27	2059.78	2037.44
	Peak shift (Δcm^{-1})	-4.26	-2.13	-2.13	-1.07	-2.13	-7.78	12.62	0.00	-0.97	-7.78
Peak 6	EBV	1661.76	1657.63	1660.73	1662.00	1664.85	2674.66	2678.19	2630.34	2684.36	2669.36
	MβCD+EBV	1659.70	1653.50	1659.70	1659.70	1660.73	2673.77	2663.17	2630.34	2780.83	2673.77
	Peak shift (Δcm^{-1})	-2.06	-4.13	-1.03	-2.30	-4.12	-0.89	-15.0	0.00	96.4	4.41
Peak 7	EBV	2934.74	2936.50	2937.28	2931.36	2937.70	2943.19	2932.21	2937.80	2934.74	2935.59
	MβCD+EBV	2934.74	2936.19	2935.59	2934.74	2936.43	2929.67	2935.59	2938.12	2935.59	2941.50

Peak shift **(Δcm^{-1})**	0.00	- 0.31	- 1.69	3.38	-1.27	- 13.5	3.38	0.32	0.85	5.91

Importantly, the third peak at 1hr showed a change from protein band to triglycerides and lipids. Notably, the fourth peak showed major transpose at 1 and 4 hrs, whereas at 1 hr it exhibited a swap of amide I into tyrosine and tryptophan (Figure 3.8I). While, at 4 hrs protein got changed with amide I. No major changes were observed in peak number six and seven (Figure 3.8I). No considerable peak shifts were observed in the nucleus except at 1 and 2 hrs which showed shifts into the same biomolecule such as glycogen to glycogen and polysaccharides to glycogen (Figure 3.8II).

3.4.3.5 Ingenuity pathway analysis of altered biomolecular signature in LN-229 cells

IPA tools were used to identify the possible biomolecule-associated pathways and gene networks that correspond to infectious diseases, inflammatory responses and neurological disorders in the CNS and neuronal cell lines. The comprehensive molecular network, ingenuity pathway knowledge base (IPKB) identified canonical/non-canonical pathways and gene networks associated with specific biomolecule-related neuropathologies. Prominently altered molecules obtained after EBV infection in cholesterol-depleted and intact astroglial cells include cholesterol, triglycerides, lipids, glycogen and aromatic amino acids. Likewise, the biomolecules subjected to IPA input were cholesterol, triacylglycerol, L-tryptophane, L-tyrosine, L-proline, hydroxyproline, lipids, glycogen and proteins like RIP, STAT, TNF and NF-kB (Figure 3.9). Intriguingly, cholesterol trafficking is acclaimed to be altered in several neurological disorders [39].

Briefly, the IPA connectome unravelled new proteins associated with altered cholesterol and lipid such as Neimann-Pick C2 (NPC2), perilipin 2 (PLIN2), histamine receptor H1 (HRH1) and very low-density lipoprotein receptor (VLDLR) and patatin-like phospholipase domain containing 1 (PNPLA1). Similarly, mitochondrial uncoupling protein 2 (UCP-2) declines ATP production and expression in the brain and reduces oxidative stress (Figure 3.9). Altered L-tyrosine, triglycerides and glycogen showed association with enzymes like dopamine beta-hydroxylase (DBH) which play a role in the conversion of dopamine into nor-epinephrine (Figure 3.9). While butyrylcholinesterase (BChE) plays an important role in the production of

pseudocholinesterase (Figure 3.9). Amendments in the lipid profile are connected with potassium calcium-activated channels subfamily M regulatory bet subunit 1 (KCNMB1) and adrenomedullin (ADM) proteins which are widely expressed in the brain. Triglycerides, lipids and cholesterol showed an interrelation with the cholesterol side-chain cleavage enzyme (CYP11A1) (Figure 3.9). Glycogen and cholesterol changes draw a link with fatty acid binding protein 3 (FABP3) (Figure 3.9). The networking pathway of glycogen and lipid revealed the relation with sphingomyelin phosphodiesterase 1 (SMPD1), acyl-CoA dehydrogenase very long chain (ACADVL) (Figure 3.9).
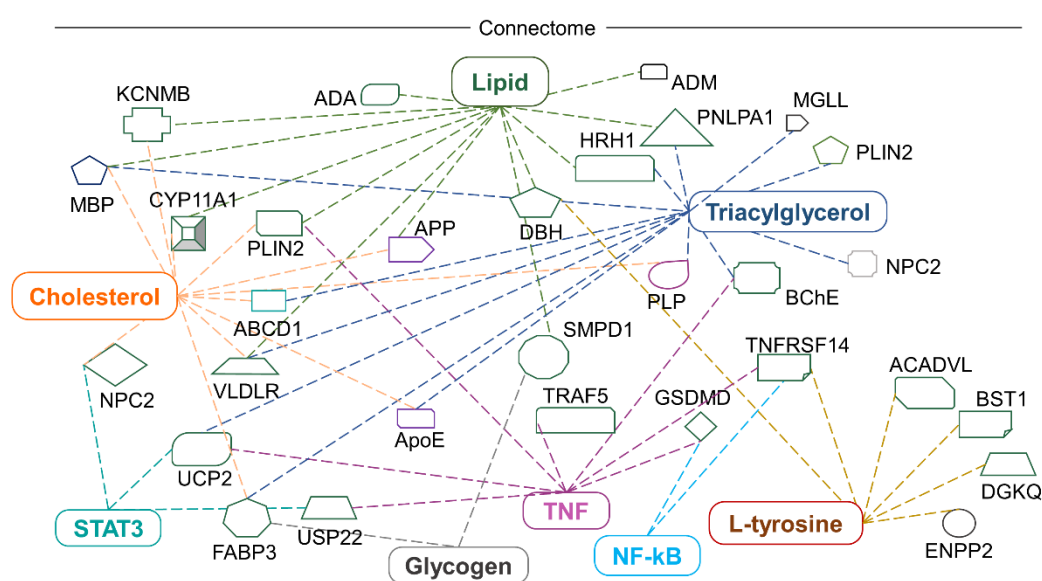
Figure 3.9: Biomolecular connectome of astroglia cells by IPA.
The connectome shows the factors involved in infectious, neurological and inflammatory diseases and responses as revealed by the IPA knowledge database. A majority of the biomolecules observed in the astroglia cells after EBV infection in the intact and disrupted membrane cholesterol linked to various individual or familiar molecular entities are also present in the network.

3.5 Discussion

Given the interesting association of EBV with neurological diseases has been corroborated by an increasing number of studies, yet the mechanistic details are still ambiguous [4], [7], [40]. Previous reports suggested that in case of EBV entry, cholesterol plays an important role in membrane fusion, receptor localisation in membrane microdomains and/or early viral signalling events or fusion of the EBV envelope with the cellular membrane might require a cholesterol-rich environment

[41]. Moreover, cholesterol and lipid moieties are found in abundance within the brain. Largest pool of free cholesterol in the myelin sheath is a crucial component taking part in electrochemical conduction along the axons. Therefore, disruption in cholesterol homeostasis becomes detrimental, as seen in MS at its various stages. The present investigation sought to understand the role of membrane cholesterol in EBV-mediated pathogenesis. By using MβCD, we noted a decline in the expression of EBV-*gfp* and *ebna1* which suggest a delay in EBV infection. A similar result was observed earlier after depleting the cholesterol in order to understand EBV entry into Daudi B-cell [14]. Also, cholesterol depletion in LCL cells exhibited a blockage in the LMP2A endocytosis resulting in its accumulation on plasma membrane [14], [16]. Notably, our results also showed downregulation of *lmp1* and *lmp2a* upon disruption of membrane cholesterol, underpinning its important role in reducing EBV entry/viral gene expression into astroglia cells. Interestingly, an *in-vivo* study suggested that MBP-specific antibodies exhibited cross-reactivity with EBV-LMP1 and insisted its role in MS pathology [42]. Besides, the effect on downstream signalling molecules affected by EBV infection in cholesterol-depleted astroglia cells was examined by analysing STAT3, RIP, NF-kB and TNF-α expression at protein level. EBV infection triggers the activation of STAT3 and RIP proteins and contributes to neuroinflammation and cell death [43]. In our study, inhibition of cholesterol led to reduced expression of the above proteins in astroglia cells except for NF-kB. A study by Vorst et al. suggested, the depletion of membrane cholesterol leads to increased expression of NF-kB [44]. Notably, EBV-LMP1 has been found to constitutively activate NF-kB through numerous mechanisms and instigates the cytokine storm in case of autoimmune disease like MS (Fig. S4). Several MS therapeutics drugs like fingolimod have been implicated as an influencer of NF-kB signalling [45]. EBNA1-specific CD4$^+$ T-cell clones cross-react with peptide mixture derived from CNS autoantigens. These autoantigens are capable of producing IL-2, IFN-γ and TNF-α cytokines and imparts in MS pathology [46]. This is in line with data by others, which showed that disrupted membrane cholesterol in Raji B-cells blocked the cytotoxicity of transmembrane TNF [47]. The IPA network suggested a direct link of RIP and TNF with caspase recruitment protein with FGF-like domain 1 (CARD6) and TNF Receptor Associated Factor 5 (TRAF5). In order to explore the detail biomolecular changes in the current infection model, RS was used for checking the systemic biomolecular signature.

Precisely, the cholesterol and related moieties showed major changes in EBV-infected samples at the cell periphery while this pattern was reversed at the initial time points of nucleus. MβCD removes cholesterol molecules from the cell membrane, thus MβCD+EBV samples showed a low presence of cholesterol and related molecules in the periphery. While in the nucleus of MβCD+EBV samples, cholesterol, triglycerides and lipids continued to show their prominent presence. The accumulation of cholesteryl ester in the brain is scrutinized to be linked with demyelination during MS and other CNS demyelinating diseases [48]. It suggests that the differential cellular changes in the nucleus and periphery are due to maintenance of cellular homeostasis. In the cellular periphery, EBV infection showed an increase in Raman intensity of triglycerides and fatty acids which were not observed after membrane cholesterol turmoiling. The aforementioned alterations are due to EBV-mediated changes in the cells and suggesting a reduction in viral entry and consequent pathogenesis such as MS.

The energy shifts of RS can be used to obtain information regarding the molecular composition of the sample with very high accuracy [49]. In the current samples, the periphery of the cells showed more shifts compared to the nucleus at initial time points. A shift at the periphery indicated a change from protein to triglycerides and lipids. These molecules have a pleiotropic role in viral infection [50], [51], [52]. The shift in these molecules also suggested an increase in their number which may help in maintaining the membrane fluidity. Previously, severe hypertriglyceridemia concentrations >300 mg/dL was been reported during infectious mononucleosis [53]. Patients with infectious mononucleosis showed a higher incidence of MS than to patients without infectious mononucleosis [54]. Albeit, the ingenuity connectome showed that lipids and cholesterol were found to be prominently linked with receptors like HRH1/VLDLR and altered function of these receptors has a significant role in infection-related neuroinflammation. Likewise, compared to healthy subjects, in the MS patients had elevated sub-fractions of VLDL and HDL lipoprotein [55]. Furthermore, Raman shifts analysis indicated two major transposes including polysaccharides to DNA and carbohydrates to RNA. These data are pointing towards an increase in replication and transcription. We observed an elevation in the triglycerides and fatty acids upon exposure to EBV at the periphery whereas it was absent in the cholesterol-depleted LN-229 cells. Alterations in the lipid profile seem to be a hallmark of this pathology which can contribute to the dysregulation of lipid

homeostasis and metabolism in MS [56]. The clinical lipidomic profile is potent as a tool to aid in MS diagnosis and therapeutics by allowing a detailed lipidome profiling of the patients suffering with disease [57]. The connectome of triglycerides highlighted a consortium with UCP-2 and CYP11A1. Our data further show how usage of MβCD can decrease EBV gene expression and eventually reduce activation of CYP11A1, UCP-2 and related neuropathologies. The latter converts cholesterol into pregnenolone and serves as a substrate for vitamin D2/D3. Vitamin D deficiency is also a diverse risk factor for MS. Notably, 1,25(OH)2D3 and vitamin D receptor were shown to interact with EBNA1 and contribute to MS. EBNA2 and VDR have common DNA binding sites associated with MS [58].

Previous studies have suggested that the amide I signature represents sphingomyelin which is widely present in the plasma membrane [59], [60]. Likewise, we observed peak width of amide I showed an increase in the EBV-infected cells in the periphery at the initial time points. Additionally, elevated Raman spectra for the Phe-Tyr ratio have been used to measure phenylalanine hydroxylase activity that is indirectly related to immune activation and inflammatory process through tetrahydrobiopterin (BH4) [61]. The MβCD treated samples showed an elevation in tyrosine and tryptophane which indicates that EBV potentially alters these amino acids immediately after the infection to circumvent immune responses. Altogether, our results highlight the important role of membrane cholesterol in EBV entry/pathogenesis in astroglia cells which might further trigger or exacerbate virus-associated neuropathologies.

3.6 Conclusion

Briefly, to the best of our knowledge, the present study shows for the first time how membrane cholesterol plays a critical role in EBV infection of astroglia cells. We also discerned molecular pathways affected by cholesterol depletion. Using the sophisticated RS technology, we have identified the molecular fingerprint of EBV and its interaction with astrocytes. In view of the recent and growing evidence of EBV's involvement in MS and other neuropathologies, our data set the stage for a better understanding for the prognosis marker of neurological disease i.e., MS.

3.7 Material and methodology

3.7.1 Cell culture

The human glioblastoma cell LN-229 was acquired from Professor Kumaravel Somasundaram's Lab, Department of Microbiology & Cell Biology, Indian Institute of Science Bangalore, India. For virus purification, HEK 293T cells were used which contain stably transfected bacterial artificial chromosome (BAC) green fluorescent protein (GFP)-EBV [62]. The cells were cultured in Dulbecco's modified Eagle's medium (DMEM; Himedia Laboratories Pvt. Limited, India) supplemented with 10% fetal bovine serum (FBS; Himedia Laboratories Pvt. Limited, India), 50 U/ml, 100 μg/ml and 2 mM of penicillin, streptomycin and L-Glutamine respectively. The growing cell environment was humidified with 5% CO_2 at 37 °C. Methyl-β-cyclodextrin (MβCD) was obtained from Sigma-Aldrich Corp., St. Louis. MβCD was dissolved in milli-Q water and made the stock of 1mM.

3.7.2 Virus Isolation and Purification

The BAC-GFP-EBV was stably transfected into HEK 293T cells [63], [64] and were grown in complete DMEM with puromycin selection. EBV particles were obtained by using the protocol illustrated previously [31].

3.7.3 Cell cytotoxicity through MTT assay

For 3-(4,5-Dimethylthiazol-2-yl)-2,5-Diphenyltetrazolium Bromide (MTT) assay 10,000 LN-229 cells were seeded in each well of 96-well culture plate in complete DMEM supplemented with 10% of FBS and maintained for 24 hrs at 37 °C with 5% CO_2. MβCD was dissolved in milli-Q water and the final stock of 1 mM was prepared. Upon treatment with MβCD, the morphological changes in the cells were monitored using bright-field microscopy. After 24 hrs of treatment, medium was removed and 100 μL of fresh medium containing 0.5 mg/mL MTT was added to each well and incubated for 3 hrs at 37 °C. MTT was removed and 100 μL of DMSO was added to dissolve formazan crystals by shaking for 2 hrs.

3.7.4 qRT-PCR

The EBV latent gene profile was analysed using qRT-PCR (Table S1). A total of 0.25 million cells were seeded in a 6-well plate and pre-treated with MβCD for 1 hr followed by EBV infection for 1, 2, 4, 6 and 12 hrs along with corresponding negative control. Total RNA extraction, complementary DNA preparation and qRT-PCR were

carried out as described earlier [31]. Gene-specific primers were designed from Primer-BLAST and are listed in Table S1. The qPCR was performed on two biological and two technical replicates with glyceraldehyde 3-phosphate dehydrogenase (GAPDH) as a housekeeping gene.

3.7.5 Western Blotting

After exposure to MβCD and EBV for various time points, the LN-229 cells were harvested, washed with PBS and lysed in radioimmunoprecipitation assay buffer (RIPA) as described earlier [65]. Antibodies against NF-kB (1:1000; D14E12 from Cell Signalling Technology (CST), Danvers, MA, USA), TNF-α (1:1000; D1G2 from CST), RIP (1:1000; D94C12 from CST), STAT3 (1;1000, 124H6 from CST) and GAPDH (1 μg/ml; AM4300; applied biosystems) were used for staining of the blots. GAPDH) was used as a housekeeping gene. Images of the blots were captured using the gel documentation system from BIO-RAD (ChemiDoc XRS+ System with Image Lab Software). Further, these images were analysed and quantified using Image J software (National Institutes of Health, Bethesda, MA, USA).

3.7.6 EBV infection and sample preparation for Raman microspectroscopy

LN-229 cells were grown to 40–60% confluency over coverslips in the six-well plate. Cells were gently washed with PBS and supplied with fresh media. The cells were then exposed to EBV. In MβCD-treatment, the cells were incubated with MβCD for 1 hr prior to the exposure to EBV. The uninfected control cells were harvested at 0 hr and fixed with 4% paraformaldehyde for 20 min at room temperature, washed with $1\times$ PBS and stored at 4 °C after drying. The other sets were separately harvested at 1, 2, 4, 6 and 12 hrs followed by fixing with PFA as mentioned before. The coverslips carrying fixed cells were arranged onto the glass slides such that cells face the upper side before visualisation under the microscope. Raman spectra was recorded from three different cells at three different points for each sample at nucleus and periphery (transmembrane and cytoplasmic conjunction region of the cells).

3.7.7 Raman microspectroscopy and Spectral Analysis

Raman microspectroscopy of the prepared samples was carried out using a LabRAM HR Evolution (Horiba-Jobin Yvon) spectrometer attached to an optical compound

microscope. The excitation source was the He–Ne laser (λexc = 633 nm, ~10 mW). The minimum possible laser power adjusted using a neutral-density filter was employed for the Raman measurement for subsiding the laser-induced biological sample damage. Spectral capturing of cells was done as mentioned previously [11]. Further, the obtained spectra were analysed using OriginPro 2021. For the deconvolution of the Raman data, all the spectra were smoothed by 20 pts using the Savitzky–Golay filter in the signal processing to remove the irregularities and noise. The data was analysed by checking the changes in the Raman peak intensity, peak width and peak shift upon EBV and MβCD+EBV-infection. For intensity-based analysis, the average spectra were considered for further analysis [10], [11]. Peak width was checked using FWHM and the peak shifts were examined by comparing the wavenumber maxima difference of MβCD+EBV with EBV samples [35]. Raman spectra shift was also calculated for MβCD+EBV samples after subtracting the wavenumber maxima with EBV-infected samples (Table 3.1).

3.7.8 Biomolecular Connectome Analysis

The ingenuity pathway analysis (QIAGEN) was performed for biomolecules acquired from the consecutive biomolecular change analysis in order to develop a connectome. The connectome was then percolated only for infectious diseases, inflammatory responses, and neurological disorders in the CNS and neuronal cell lines.

3.7.9 Statistical analysis

The t-test (Two-samples) was carried out to compare values of compound-treated samples with EBV infection samples. The t-statistic was significant at the 0.05 critical alpha level, $P < 0.05$ at the 95% confidence interval.

3.8 References

1. Iizasa H, Nanbo A, Nishikawa J, Jinushi M, Yoshiyama H (2012) Epstein-Barr Virus (EBV)-associated Gastric Carcinoma. Viruses 4:3420–3439. https://doi.org/10.3390/v4123420

2. Zhang N, Zuo Y, Jiang L, Peng Y, Huang X, Zuo L (2022) Epstein-Barr Virus and Neurological Diseases. Front Mol Biosci 8:816098. https://doi.org/10.3389/fmolb.2021.816098

3. Nielsen TR, Rostgaard K, Nielsen NM, Koch-Henriksen N, Haahr S, Sørensen PS, Hjalgrim H (2007) Multiple Sclerosis After Infectious Mononucleosis. Arch Neurol 64:72. https://doi.org/10.1001/archneur.64.1.72

4. Soldan SS, Lieberman PM (2023) Epstein–Barr virus and multiple sclerosis. Nat Rev Microbiol 21:51–64. https://doi.org/10.1038/s41579-022-00770-5

5. Robinson WH, Steinman L (2022) Epstein-Barr virus and multiple sclerosis. Science 375:264–265. https://doi.org/10.1126/science.abm7930

6. Houen G, Trier NH (2021) Epstein-Barr Virus and Systemic Autoimmune Diseases. Front Immunol 11:587380. https://doi.org/10.3389/fimmu.2020.587380

7. Bjornevik K, Cortese M, Healy BC, Kuhle J, Mina MJ, Leng Y, Elledge SJ, Niebuhr DW, Scher AI, Munger KL, Ascherio A (2022) Longitudinal analysis reveals high prevalence of Epstein-Barr virus associated with multiple sclerosis. Science 375:296–301. https://doi.org/10.1126/science.abj8222

8. Borges R de CF, Navarro RS, Giana HE, Tavares FG, Fernandes AB, Silveira Junior L (2015) Detecting alterations of glucose and lipid components in human serum by near-infrared Raman spectroscopy. Res Biomed Eng 31:160–168. https://doi.org/10.1590/2446-4740.0593

9. Raghu H, Sharma-Walia N, Veettil MV, Sadagopan S, Caballero A, Sivakumar R, Varga L, Bottero V, Chandran B (2007) Lipid Rafts of Primary Endothelial Cells Are Essential for Kaposi's Sarcoma-Associated Herpesvirus/Human Herpesvirus 8-Induced Phosphatidylinositol 3-Kinase and RhoA-GTPases Critical for Microtubule Dynamics and Nuclear Delivery of Viral DNA but Dispensable for Binding and Entry. J Virol 81:7941–7959. https://doi.org/10.1128/JVI.02848-06

10. Tiwari D, Jakhmola S, Pathak DK, Kumar R, Jha HC (2020) Temporal *In Vitro* Raman Spectroscopy for Monitoring Replication Kinetics of Epstein–Barr Virus Infection in Glial Cells. ACS Omega 5:29547–29560. https://doi.org/10.1021/acsomega.0c04525

11. Indari O, Jakhmola S, Pathak DK, Tanwar M, Kandpal M, Mishra A, Kumar R, Jha HC (2022) Comparative Account of Biomolecular Changes Post Epstein Barr Virus Infection of the Neuronal and Glial Cells Using Raman Microspectroscopy. ACS Chem Neurosci 13:1627–1637. https://doi.org/10.1021/acschemneuro.2c00081

12. Wang LW, Wang Z, Ersing I, Nobre L, Guo R, Jiang S, Trudeau S, Zhao B, Weekes MP, Gewurz BE (2019) Epstein-Barr virus subverts mevalonate and fatty acid pathways to promote infected B-cell proliferation and survival. PLoS Pathog 15:e1008030. https://doi.org/10.1371/journal.ppat.1008030

13. Apostolou F, Gazi IF, Lagos K, Tellis CC, Tselepis AD, Liberopoulos EN, Elisaf M (2010) Acute infection with Epstein–Barr virus is associated with atherogenic lipid changes. Atherosclerosis 212:607–613. https://doi.org/10.1016/j.atherosclerosis.2010.06.006

14. Katzman RB, Longnecker R (2003) Cholesterol-dependent infection of Burkitt's lymphoma cell lines by Epstein–Barr virus. Journal of General Virology 84:2987–2992. https://doi.org/10.1099/vir.0.19252-0

15. Raghu H, Sodadasu PK, Malla RR, Gondi CS, Estes N, Rao JS (2010) Localization of uPAR and MMP-9 in lipid rafts is critical for migration, invasion and angiogenesis in human breast cancer cells. BMC Cancer 10:647. https://doi.org/10.1186/1471-2407-10-647

16. Ikeda M, Longnecker R (2007) Cholesterol is critical for Epstein-Barr virus latent membrane protein 2A trafficking and protein stability. Virology 360:461–468. https://doi.org/10.1016/j.virol.2006.10.046

17. Kaykas A (2001) CD40 and LMP-1 both signal from lipid rafts but LMP-1 assembles a distinct, more efficient signaling complex. The EMBO Journal 20:2641–2654. https://doi.org/10.1093/emboj/20.11.2641

18. Ersing I, Bernhardt K, Gewurz B (2013) NF-κB and IRF7 Pathway Activation by Epstein-Barr Virus Latent Membrane Protein 1. Viruses 5:1587–1606. https://doi.org/10.3390/v5061587

19. Hulse M, Johnson SM, Boyle S, Caruso LB, Tempera I (2021) Epstein-Barr Virus-Encoded Latent Membrane Protein 1 and B-Cell Growth Transformation Induce Lipogenesis through Fatty Acid Synthase. J Virol 95:e01857-20. https://doi.org/10.1128/JVI.01857-20

20. Sviridov D, Bukrinsky M (2014) Interaction of pathogens with host cholesterol metabolism: Current Opinion in Lipidology 25:333–338. https://doi.org/10.1097/MOL.0000000000000106

21. Devin A, Cook A, Lin Y, Rodriguez Y, Kelliher M, Liu Z (2000) The Distinct Roles of TRAF2 and RIP in IKK Activation by TNF-R1. Immunity 12:419–429. https://doi.org/10.1016/S1074-7613(00)80194-6

22. Yu H, Pardoll D, Jove R (2009) STATs in cancer inflammation and immunity: a leading role for STAT3. Nat Rev Cancer 9:798–809. https://doi.org/10.1038/nrc2734

23. Burbelo PD, Iadarola MJ, Chaturvedi A (2019) Emerging technologies for the detection of viral infections. Future Virology 14:39–49. https://doi.org/10.2217/fvl-2018-0145

24. Sertbas M, Ulgen KO (2020) Genome-Scale Metabolic Modeling for Unraveling Molecular Mechanisms of High Threat Pathogens. Front Cell Dev Biol 8:566702. https://doi.org/10.3389/fcell.2020.566702

25. Butler HJ, Ashton L, Bird B, Cinque G, Curtis K, Dorney J, Esmonde-White K, Fullwood NJ, Gardner B, Martin-Hirsch PL, Walsh MJ, McAinsh MR, Stone N, Martin FL (2016) Using Raman spectroscopy to characterize biological materials. Nat Protoc 11:664–687. https://doi.org/10.1038/nprot.2016.036

26. Saletnik A, Saletnik B, Puchalski C (2021) Overview of Popular Techniques of Raman Spectroscopy and Their Potential in the Study of Plant Tissues. Molecules 26:1537. https://doi.org/10.3390/molecules26061537

27. Kadyrov M, Whiley L, Brown B, Erickson KI, Holmes E (2022) Associations of the Lipidome with Ageing, Cognitive Decline and Exercise Behaviours. Metabolites 12:822. https://doi.org/10.3390/metabo12090822

28. Pietz J (1998) Neurological aspects of adult phenylketonuria: Current Opinion in Neurology 11:679–688. https://doi.org/10.1097/00019052-199812000-00012

29. Lambert PJ, Whitman AG, Dyson OF, Akula SM (2006) Raman spectroscopy: the gateway into tomorrow's virology. Virol J 3:51. https://doi.org/10.1186/1743-422X-3-51

30. Jha HC, Mehta D, Lu J, El-Naccache D, Shukla SK, Kovacsics C, Kolson D, Robertson ES (2015) Gammaherpesvirus Infection of Human Neuronal Cells. mBio 6:e01844-15. https://doi.org/10.1128/mBio.01844-15

31. Jakhmola S, Jha HC (2021) Glial cell response to Epstein-Barr Virus infection: A plausible contribution to virus-associated inflammatory reactions in the brain. Virology 559:182–195. https://doi.org/10.1016/j.virol.2021.04.005

32. Talari ACS, Movasaghi Z, Rehman S, Rehman I ur (2015) Raman Spectroscopy of Biological Tissues. Applied Spectroscopy Reviews 50:46–111. https://doi.org/10.1080/05704928.2014.923902

33. De Gelder J, De Gussem K, Vandenabeele P, Moens L (2007) Reference database of Raman spectra of biological molecules. J Raman Spectrosc 38:1133–1147. https://doi.org/10.1002/jrs.1734

34. Niaura G (2000) Raman Spectroscopy in Analysis of Biomolecules. In: Meyers RA (ed) Encyclopedia of Analytical Chemistry. John Wiley & Sons, Ltd, Chichester, UK, p a0212

35. Kaushik R, Rani C, Neeshu K, Tanwar M, Pathak DK, Chaudhary A, Siraj F, Jha HC, Kumar R (2022) Brain Tumour Detection and Grading Using Raman Scattering: Analogy from Semiconductors for Solving Biological Problem. Advances in Materials and Processing Technologies 8:703–714. https://doi.org/10.1080/2374068X.2020.1829959

36. Pershin SM (2005) Raman Spectroscopy of the OH Group Vibrations in Structural Complexes of Liquid Water. Opt Spectrosc 98:543. https://doi.org/10.1134/1.1914890

37. Pan LK, Sun CQ, Li CM (2004) Elucidating Si−Si Dimmer Vibration from the Size-Dependent Raman Shift of Nanosolid Si. J Phys Chem B 108:3404–3406. https://doi.org/10.1021/jp037891s

38. Plé J, Dabert M, Lecoq H, Hellé S, Ploux L, Balan L (2023) Antimicrobial and mechanical properties of functionalized textile by nanoarchitectured photoinduced Ag@polymer coating. Beilstein J Nanotechnol 14:95–109. https://doi.org/10.3762/bjnano.14.11

39. Orth M, Bellosta S (2012) Cholesterol: Its Regulation and Role in Central Nervous System Disorders. Cholesterol 2012:1–19. https://doi.org/10.1155/2012/292598

40. Serafini B, Rosicarelli B, Franciotta D, Magliozzi R, Reynolds R, Cinque P, Andreoni L, Trivedi P, Salvetti M, Faggioni A, Aloisi F (2007) Dysregulated Epstein-Barr virus infection in the multiple sclerosis brain. Journal of Experimental Medicine 204:2899–2912. https://doi.org/10.1084/jem.20071030

41. Chandra A, Xu YM (2016) Cholesterol: A necessary evil from a multiple sclerosis perspective. Clin Exp Neuroimmunol 7:145–157. https://doi.org/10.1111/cen3.12289

42. Lomakin Y, Arapidi GP, Chernov A, Ziganshin R, Tcyganov E, Lyadova I, Butenko IO, Osetrova M, Ponomarenko N, Telegin G, Govorun VM, Gabibov A, Belogurov A (2017) Exposure to the Epstein–Barr Viral Antigen Latent Membrane Protein 1 Induces Myelin-Reactive Antibodies In Vivo. Front Immunol 8:777. https://doi.org/10.3389/fimmu.2017.00777

43. Jangra S, Yuen K-S, Botelho MG, Jin D-Y (2019) Epstein–Barr Virus and Innate Immunity: Friends or Foes? Microorganisms 7:183. https://doi.org/10.3390/microorganisms7060183

44. van der Vorst EPC, Theodorou K, Wu Y, Hoeksema MA, Goossens P, Bursill CA, Aliyev T, Huitema LFA, Tas SW, Wolfs IMJ, Kuijpers MJE, Gijbels MJ, Schalkwijk CG, Koonen DPY, Abdollahi-Roodsaz S, McDaniels K, Wang C-C, Leitges M, Lawrence T, Plat J, Van Eck M, Rye K-A, Touqui L, de Winther MPJ,

Biessen EAL, Donners MMPC (2017) High-Density Lipoproteins Exert Pro-inflammatory Effects on Macrophages via Passive Cholesterol Depletion and PKC-NF-κB/STAT1-IRF1 Signaling. Cell Metabolism 25:197–207. https://doi.org/10.1016/j.cmet.2016.10.013

45. Leibowitz SM, Yan J (2016) NF-κB Pathways in the Pathogenesis of Multiple Sclerosis and the Therapeutic Implications. Front Mol Neurosci 9:. https://doi.org/10.3389/fnmol.2016.00084

46. Läderach F, Münz C (2022) Altered Immune Response to the Epstein–Barr Virus as a Prerequisite for Multiple Sclerosis. Cells 11:2757. https://doi.org/10.3390/cells11172757

47. Zhang S, Liu T, Liang H, Zhang H, Yan D, Wang N, Jiang X, Feng W, Wang J, Li P, Li Z (2009) Lipid rafts uncouple surface expression of transmembrane TNF-α from its cytotoxicity associated with ICAM-1 clustering in Raji cells. Molecular Immunology 46:1551–1560. https://doi.org/10.1016/j.molimm.2009.01.001

48. Wender M, Filipek-Wender H, Stanisławska J (1974) Cholesteryl esters of the brain in demyelinating diseases. Clinica Chimica Acta 54:269–275. https://doi.org/10.1016/0009-8981(74)90245-9

49. Farber C, Li J, Hager E, Chemelewski R, Mullet J, Rogachev AYu, Kurouski D (2019) Complementarity of Raman and Infrared Spectroscopy for Structural Characterization of Plant Epicuticular Waxes. ACS Omega 4:3700–3707. https://doi.org/10.1021/acsomega.8b03675

50. Heaton NS, Randall G (2011) Multifaceted roles for lipids in viral infection. Trends in Microbiology 19:368–375. https://doi.org/10.1016/j.tim.2011.03.007

51. Stavropoulou E, Pircalabioru GG, Bezirtzoglou E (2018) The Role of Cytochromes P450 in Infection. Front Immunol 9:89. https://doi.org/10.3389/fimmu.2018.00089

52. Ketter E, Randall G (2019) Virus Impact on Lipids and Membranes. Annu Rev Virol 6:319–340. https://doi.org/10.1146/annurev-virology-092818-015748

53. Páez-Guillán E-M, Campos-Franco J, Alende R, Garitaonaindía Y, González-Quintela A (2021) Transient hypertriglyceridemia: a common finding during Epstein-Barr virus-induced infectious mononucleosis. Lipids Health Dis 20:177. https://doi.org/10.1186/s12944-021-01603-9

54. Loosen SH, Doege C, Meuth SG, Luedde T, Kostev K, Roderburg C (2022) Infectious mononucleosis is associated with an increased incidence of multiple sclerosis: Results from a cohort study of 32,116 outpatients in Germany. Front Immunol 13:937583. https://doi.org/10.3389/fimmu.2022.937583

55. Gafson AR, Thorne T, McKechnie CIJ, Jimenez B, Nicholas R, Matthews PM (2018) Lipoprotein markers associated with disability from multiple sclerosis. Sci Rep 8:17026. https://doi.org/10.1038/s41598-018-35232-7

56. Podbielska M, O'Keeffe J, Pokryszko-Dragan A (2021) New Insights into Multiple Sclerosis Mechanisms: Lipids on the Track to Control Inflammation and Neurodegeneration. IJMS 22:7319. https://doi.org/10.3390/ijms22147319

57. Ferreira HB, Neves B, Guerra IM, Moreira A, Melo T, Paiva A, Domingues MR (2020) An overview of lipidomic analysis in different human matrices of multiple sclerosis. Multiple Sclerosis and Related Disorders 44:102189. https://doi.org/10.1016/j.msard.2020.102189

58. Miclea A, Bagnoud M, Chan A, Hoepner R (2020) A Brief Review of the Effects of Vitamin D on Multiple Sclerosis. Front Immunol 11:781. https://doi.org/10.3389/fimmu.2020.00781

59. Shirota K, Yagi K, Inaba T, Li P-C, Murata M, Sugita Y, Kobayashi T (2016) Detection of Sphingomyelin Clusters by Raman Spectroscopy. Biophysical Journal 111:999–1007. https://doi.org/10.1016/j.bpj.2016.07.035

60. Simons K, Toomre D (2000) Lipid rafts and signal transduction. Nat Rev Mol Cell Biol 1:31–39. https://doi.org/10.1038/35036052

61. John RV, Devasia T, N. M, Lukose J, Chidangil S (2022) Micro-Raman spectroscopy study of blood samples from myocardial infarction patients. Lasers Med Sci 37:3451–3460. https://doi.org/10.1007/s10103-022-03604-1

62. PLOS ONE Editors (2021) Expression of Concern: Early Events Associated with Infection of Epstein-Barr Virus Infection of Primary B-Cells. PLoS One 16:e0256674. https://doi.org/10.1371/journal.pone.0256674

63. Yuen K-S, Chan C-P, Kok K-H, Jin D-Y (2017) Mutagenesis and Genome Engineering of Epstein–Barr Virus in Cultured Human Cells by CRISPR/Cas9. In: Reeves A (ed) In Vitro Mutagenesis. Springer New York, New York, NY, pp 23–31

64. Halder S, Murakami M, Verma SC, Kumar P, Yi F, Robertson ES (2009) Early Events Associated with Infection of Epstein-Barr Virus Infection of Primary B-Cells. PLoS ONE 4:e7214. https://doi.org/10.1371/journal.pone.0007214

65. Kashyap D, Baral B, Jakhmola S, Singh AK, Jha HC (2021) Helicobacter pylori and Epstein-Barr Virus Coinfection Stimulates Aggressiveness in Gastric Cancer through the Regulation of Gankyrin. mSphere 6:e00751-21. https://doi.org/10.1128/mSphere.00751-21

Chapter 4: Deciphering the association of Epstein-Barr virus and its glycoprotein M$_{146-157}$ peptide with neurological ailments at *in-vitro* and *in-vivo* level

4.1 Graphical abstract
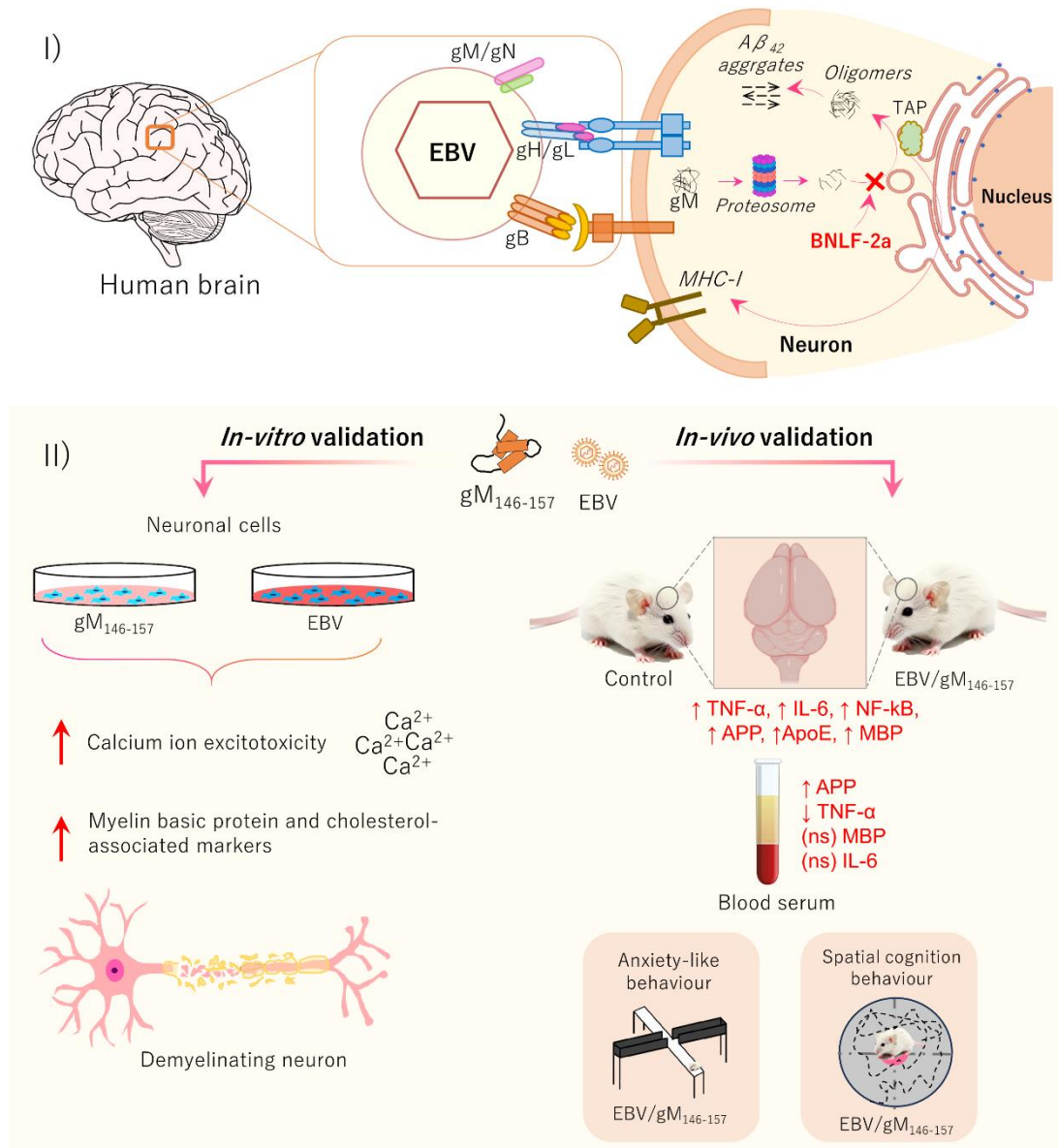
4.2 Abstract

The reactivation of ubiquitously present Epstein-Barr virus (EBV) is known to be involved in numerous diseases, including neurological ailments. A previous study from our group revealed that the EBV-glycoprotein M (gM) peptide ($_{146}$SYKHVFLSAFVY$_{157}$) exhibits amyloid aggregate-like properties. In the current

study, we have investigated the effect of EBV and $gM_{146-157}$ on neural cells (*in-vitro* and *in-vivo*) and mediated immunological modulations and disease markers. Then, EBV and $gM_{146-157}$-mediated amendments on the brain cells, mice serum and brain samples were demonstrated through neuroinflammatory and pro-neurodegenerative markers by using qRT-PCR, western blotting, ELISA, calcium ion excitotoxicity, etc. Subsequently, the infection of EBV and $gM_{146-157}$ at *in-vitro* manifested upregulation in the inflammatory molecules like IL-1β, IL-6, TNF-α and TGF-β that suggested neuroinflammation. Likewise, at the *in-vivo* level, amendments to the mice's behaviour, neuronal cell disorganisation and enhanced inflammatory markers like TNF-α and IL-6 were observed. Amelioration in the Ca^{2+} ions suggested Ca^{2+}-mediated excitotoxicity. A decrease in the mitochondrial potential again affirmed the EBV/$gM_{146-157}$ stimulated neuroinflammatory environment. Furthermore, the level of disease hallmarks like APP, MBP, and ApoE4 also exhibited EBV and $gM_{146-157}$-associated deterioration. Taken together, this study delineates a direct connection of EBV and its peptide $gM_{146-157}$ with neurological illnesses such as Alzheimer's disease and Multiple Sclerosis.

Keywords: EBV, gM, Alzheimer's disease, Multiple Sclerosis, APP, MBPs

4.3 Introduction

Epstein-Barr virus (EBV) ubiquitously infects about 90-95% of the human population in their adolescent phase and remains asymptomatic [1]. EBV has been persistently found in the CSF samples of patients suffering from neurological disorders like multiple sclerosis (MS) and Alzheimer's disease (AD). Reactivation of the virus in adults leads to various anomalies like infectious mononucleosis (IM). Notably, studies showed that IM, a prototype of EBV infection, exhibited more vulnerability towards brain disorders, e.g. AD and MS [2], [3]. An *in-vitro* investigation illustrated direct infection of EBV in neuronal cells like Ntra2, SH-SY5Y and the primary neurons [4]. EBV infection in glial cells (U-87 MG) triggers inflammatory cascades, which possibly corroborate with various neurological abnormalities [5]. A recent report put forward a 12 amino acid peptide ($_{146}$SYKHVFLSAFVY$_{157}$) of glycoprotein M (gM) to have comparable properties to the amyloid-β 42 ($Aβ_{42}$) [6]. EBV-gM is a transmembrane protein forms a complex with gN. It has a role in directing capsids to the site of envelopment by recruiting capsid-associating tegument protein [7]. The

gMgN complex is also involved in the efficient incorporation of gHgL protein in the virion membrane, which in turn helps in herpes simplex virus (HSV) entry, fusion as well as in viral replication [8], [9].

A higher presence of anti-Aβ auto-antibodies secreted by EBV-transformed B-cell lines observed in patients with AD [10]. EBV-derived proteins, precisely EBNA1 and BZLF1, have shown an association with neurological diseases [11], [12]. Apart from the production of Aβ peptides, their clearance is indispensable for interneuron communication [13]. Clearance of these plaques takes place in a receptor-mediated manner facilitated by Apolipoprotein E (ApoE), with ApoE4 being the least capable [14]. Intriguingly, ApoE3 C-terminus have shown interaction with EBV proteins, namely EBNA1 and BZLF1 and are postulated to be interfering with the clearance of Aβ$_{42}$ [15]. Although, the detailed mechanism involved in the pathogenesis of EBV-mediated AD needs more profound understanding. Additionally, the cross-reactivity of several neuronal proteins with exogenous antigens is one of the plausible mechanisms for MS development. The myelin basic protein (MBP) autoreactive T-cells also showed cross-reactivity against the EBV protein EBNA1 [16]. Albeit of MBP, these cells exhibited cross-reactivity towards other host proteins such as anoctamin 2, α-crystallin B chain and glial cell adhesion molecule (GlialCAM) [17]. Cross-reactivity of antibodies towards GlialCAM and EBNA1 have shown their presence in the CSF of MS patients [18]. Antibody reactivity against the EBNA1 domain (aa385–420) is found to be a strong risk factor for MS [19]. Vaccination of recombinant gp350 to EBV-seronegative adolescents showed prevention of EBV-induced acute infectious mononucleosis (AIM) [20]. As AIM promotes the risk of MS, the above-mentioned therapy is proposed to reduce the prevalence of the disease [21]. Therefore, several anti-EBV drugs are gaining attention as a therapeutic for MS. Several MS oral drugs also exhibited anti-EBNA1 activity [22].

Alike EBV, other viruses, i.e., human herpesvirus (HHV-6), HHV-1, Varicella zoster virus (VZV), human endogenous retroviruses (HERVs) and bacteria's (e.g. *Chlamydia pneumonia, Staphylococcus aureus*) have a clinical association with MS [23], [24]. Glycoprotein 116 antigen (gp116) of HHV-6 was also noticed in the astrocytes and its major DNA binding protein gene (MDBP), p41 and p101 found in MS lesions. HSV-1 DNA have been found in acute MS patients whereas not found in stable MS patients.

HSV-1 glycoprotein B exhibited epitope similarity with MS17-CRBF (MS17 cross-reacting brain factor) [25]. Nonetheless, VZV DNA revealed frequent presence in 31.6% of MS patients and 43.5% in RRMS patients as compared to other neurological diseases [26]. HSV-1, VZV and HHV-6A/B were found in the reactivation of human endogenous retroviruses (HERVs) [27]. HERVs like HERV-H, HEKV-K and HERV-W have consistently been associated with MS. In addition, gastrointestinal or genitourinary bacterial infections, i.e., *Staphylococcus aureus*, *Helicobacter pylori* and *Chlamydia pneumoniae*, express superantigens and plausibly participate in exacerbation of brain disorders [24].

Besides, EBV infects numerous *in-vivo* models like immunosuppressed mice (NOG, NSG and BRG), humanised mice, tamarin, common marmoset, owl monkeys and rabbits [28]. Certain monkey species and other animals fall under the criteria of endangered species; therefore, mice models are widely used for understanding EBV biology. The acute mouse models of EBV through the conditional expression of LMP1 and LMP2A have been used in EBV-related studies [29]. Pathologically, EBV-associated chronic diseases such as B-cell lymphoma studies unveiled human-mice chimeric models as well as genetically engineered mice [30]. EBV also shares properties with Murine gammaherpesvirus-68 (MHV-68), i.e., eliciting mononucleosis-like syndrome and maintaining tenacious infection in memory B-cells [31]. A report by Efstathiou et al. outlined that MHV-68 shares homology with EBV genes like BXLF1, BNRF1, BORF2, BVRF1, BVRF2, BXRF1, BcLFl, BALF5, BALF2, which suggests EBV likeliness to infect mice [32]. Likewise, the immunosuppressed mice model is also used in other viral infections, such as influenza B by using dexamethasone and cyclophosphamide [33]. Also, dengue virus titre was found to be elevated upon immunosuppression in mice [34].

Further, the development of neurodegenerative pathologies involves inflammatory responses, and Ca^{2+}-mediated neuronal excitotoxicity [35], [36], [37]. EBV is well known to trigger the formation of inflammasomes and to regulate the secretion of inflammatory entities like IL-1β, IL-8 and apoptotic markers (caspase-1) [38]. Increased oxidative and inflammatory stress results in mitochondrial dysfunction/lipid peroxidation and generates a product 4-hydroxynonenal, which eventually amplifies

the γ-secretase activity [39]. ROS induced by mitochondrial dysfunction and the elevated Ca^{2+} contributes to the accumulation of pTau aggregates [40].

Although, there are numerous reports have shown a connection between EBV with multiple neurological diseases, yet till now there is no *in-vitro* or animal studies have shown a direct connection. Hence, we have demonstrated this connection for the first time on neuronal cells, which can further be evaluated on pre-clinical models. The present study gives insight into the potential involvement of EBV and its derived peptide $gM_{146-157}$ in instigating/exacerbating neurological disorders. Here, we have studied the inflammatory responses triggered by the exposure of EBV and $gM_{146-157}$ to IMR-32 cells *in-vitro* and on mice. Total Ca^{2+} ion level was assessed to examine the excitotoxicity mediated by EBV and $gM_{146-157}$. The cholesterol metabolic genes were then analysed to bridge an association with diseases like MS, where demyelination is a hallmark. In consistent with this, mice were exposed to $EBV/gM_{146-157}$ and cognitive decline was observed using Morris-water maze (MWM) behavioral assays. Pertinently, the hippocampal region's cellular organization and degeneration were evaluated. Neuronal disease-associated proteins like APP, ApoE and MBP were investigated, and they can subsequently be endorsed with AD and MS in neuronal cells and in mice brain cortex and serum samples.

4.4 Results

4.4.1 Epstein-Barr virus tropism to IMR-32 cells

An *in-vitro* investigation from our group demonstrated the direct infection of EBV in neuronal cells like Ntra2, SH-SY5Y and the primary neurons and further EBV infection in glial cells (U-87 MG) triggers inflammatory cascades which possibly corroborate with various neurological abnormalities [4], [5]. Hereby, the IMR-32 cells were infected with EBV for 12, 24 and 48 hrs in order to estimate the EBV titre (Figure 4.1I-III). For further experimentation, the multiplicity of infection (MOI) 5 was used (Figure 4.1I-III). Besides, as reported previously, the IC_{50} value of $gM_{146-157}$ was 37.03 μM and 12 μM concentration was used in the experimentation where >90% of cells were alive [6].
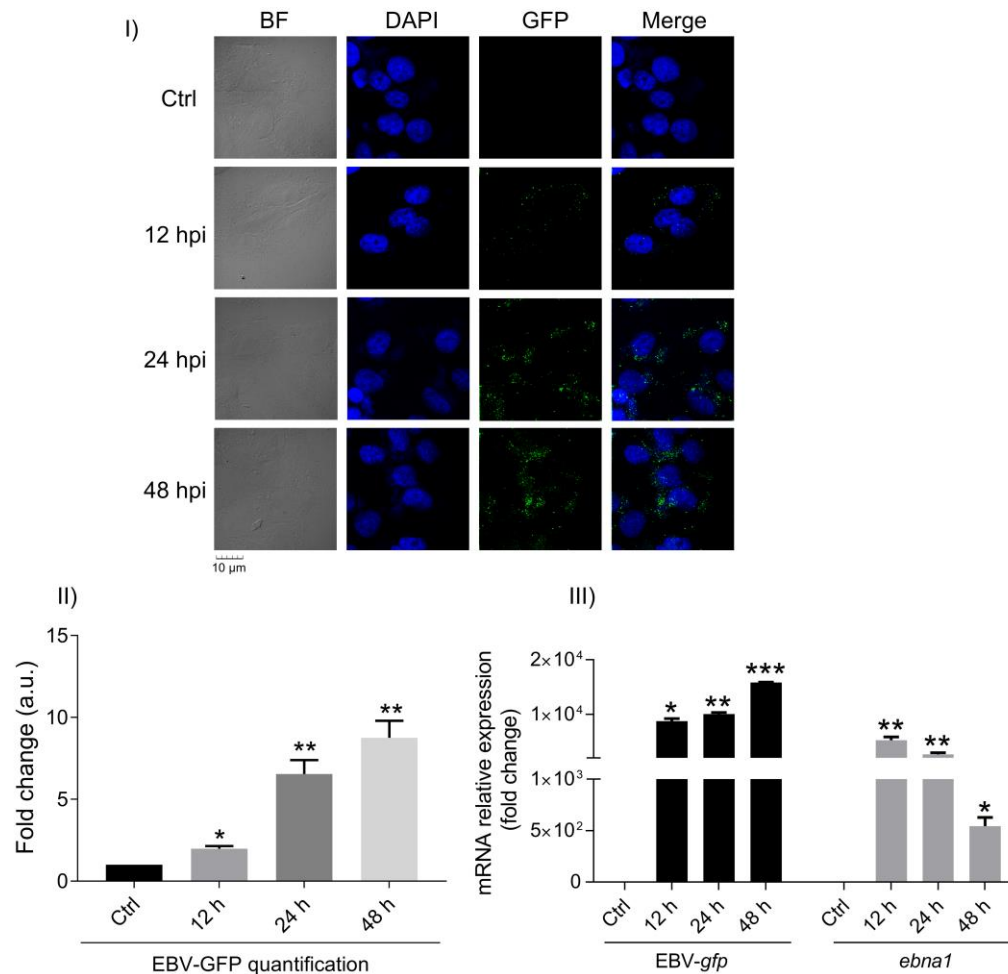
Figure 4.1: EBV titre determination on IMR-32 cells through qRT-PCR at different time-points.

IIIa). Immunofluorescence (IF) of EBV-gfp representing its infection into IMR-32 cells. In the immunofluorescence images the scale bar was 10 μm. This experiment was performed in three biological repeats. IIIb). Quantitative representation of IF EBV-GFP at 12 ($p<0.05$), 24 ($p<0.05$) and 48 h ($p<0.01$). IIIc) Representation of EBV infection associated genes at mRNA level in a time-dependent manner infection. MOI 5 was calculated and used for all the experiments discussed in the manuscript. Given plots; x-axis, time-dependent EBV infection; y-axis, fold change in EBV infection w.r.t uninfected samples. The p-values of <0.05, <0.01 and <0.0001 are considered statistically significant (one-way ANOVA and posthoc) and are represented with *, ** and *** respectively.

4.4.2 EBV and $gM_{146-157}$-mediated increase in the total Ca^{2+} ions

The Ca^{2+} ion homeostasis is the key factor for interneuron communication of CNS and its dysregulation is reported to be entangled with AD and MS [36]. The surge of calcium ions triggers excitotoxicity and potentially leads to neuronal death [25]. Besides, according to the calcium hypothesis of AD, amyloid metabolism possibly

influences neuronal apoptosis and synaptic plasticity by manipulating the Ca^{2+} signalling [41]. We have thus evaluated the changes in intracellular Ca^{2+} ions by using a ratio metric dye Fura-2/AM and found a significant increase in the Ca^{2+} ion concentration. The fluorescence excitation ratio at 340 (Ca^{2+} bound Fura-2/AM) and 380 nm (Ca^{2+} unbound Fura-2/AM) was calculated at 12, 24 and 48 hrs. A significant increase in the ratio was detected upon EBV infection at all considered time points (p<0.01) and a similar observation was found for $gM_{146-157}$ exposed cells (Figure 4.2I).
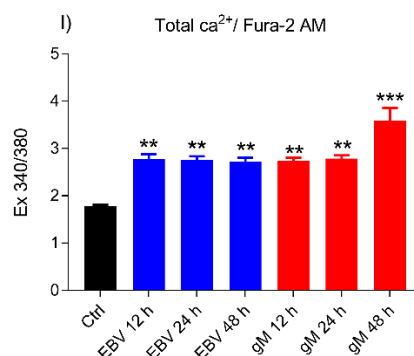
Figure 4.2: Assessment of total cellular calcium ions by Fura-2/AM in the neuronal cells exposed to EBV and gM$_{146-157}$.
The 340/380 excitation ratio of Fura-2/AM showed a significant increase at all time points of EBV infection (p<0.01). The gM-treated samples also showed statistical elevation at 12 (p<0.05), 24 (p<0.01) and 48 h (p<0.0001). Given plots; x-axis, time-dependent EBV and $gM_{146-157}$ exposure; y-axis, fold change in EBV/$gM_{146-157}$ with respect to unexposed samples. The p-values of <0.05, <0.01 and <0.0001 are considered statistically significant (one-way ANOVA and posthoc) and are represented with *, ** and *** respectively. This experiment was performed in three biological repeats.

4.4.3 Amendments in the level of myelin basic protein and cholesterol-metabolism-associated genes in IMR-32 cells after subjecting to EBV and gM$_{146-157}$

The association of EBV with MS has long been a topic of debate. Several EBV proteins have shown molecular homology with host molecules such as MBP and trigger several autoimmune responses [42]. It is suspected that memory B-cells play a paramount role in MS pathogenesis, possibly because of EBV latency and antigen-presenting features which activate auto-aggressive T-cells against the myelin proteins [43]. The current study suggested a significant elevation of MBP at 12 (p<0.01), 24

(p<0.0001) and 48 hrs (p<0.01) upon exposure with EBV and gM$_{146-157}$ as compared to the uninfected control (Figure 4.3AI-AII).
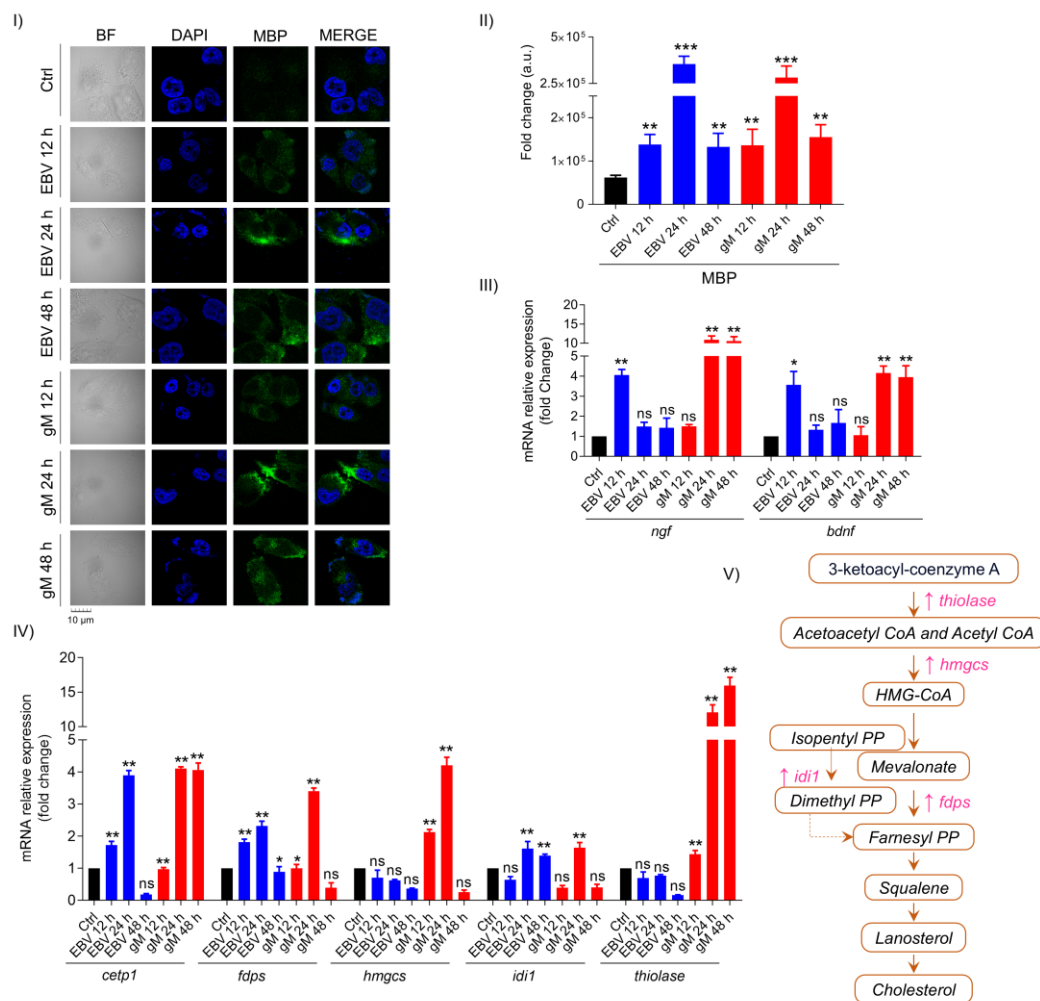
Figure 4.3: Entanglement of EBV and its gM146-157 peptide with multiple sclerosis.
AI) Illustration of MBP immunofluorescence at different time points. AII) MBP upon quantification depicted elevation at 12 (p<0.01), 24 (p<0.0001) and 48 hrs (p<0.01). This experiment was performed in three biological replicates. BI) qRT-PCR of cholesterol metabolism-related genes namely CETP1, FDPS, HMGCS, IDI1 and thiolase. BII) Representation of transcript level of NGF and BDNF neurotrophic factors. Given plots; *x*-axis, time-dependent EBV and gM$_{146-157}$ exposure; *y*-axis, fold change in EBV/gM$_{146-157}$ with respect to unexposed samples. The *p*-values of <0.05, <0.01 and <0.0001 are considered statistically significant (one-way ANOVA and posthoc) and are represented with *, ** and *** respectively.

Demyelination of neurons is a hallmark of MS and myelin sheath consists of ~70% of lipid-associated species [44], [45]. Genes linked with cholesterol synthesis were reported to be significantly increased at the transcript level of patients suffering from MS [46]. We went forward to assess certain cholesterol-metabolic genes at the

transcript level, namely *cetp1 fdps, hmgcs, idi1* and *thiolase*. A significant upregulation in the transcript level of *cetp1* was found upon exposure to EBV (12, 24 h) as well as $gM_{146-157}$ (12, 24, 48 h) (p<0.01). Genes like *fdps* and *idi1* also showed an increase at 24 h (p<0.01) upon both exposures (Figure 4.3CI-CII). EBV infection d to a decline in the transcript level of *hmgcs* and *thiolase* (p<0.01) at all time points while exposure to $gM_{146-157}$ increased the expression of both the genes (p<0.01) (Figure 4.3CI-CII).

Additionally, the alterations in the expression of neurotrophic factors can lead the way to neuronal death and contribute to numerous neurological anomalies and senescence [47]. Therefore, we have investigated the changes in neurotrophic factors, i.e., *ngf* and *bdnf* at the mRNA level. Both genes revealed a significant increase (p<0.01) at 12 h of post-EBV infection. Upon exposure to $gM_{146-157}$, both *ngf* and *bdnf* have shown an increase at 24 and 48 h (p<0.01) (Figure 4.3BI).

4.4.4 Spatial cognition and memory analysis by Morris-water Maze assay

To evaluate the spatial learning and memory, mice were tested in the MWM at the age of 2 months. Mice were divided into four groups, namely G1, G2, G3, and G4. Group 1 mice represent immunosuppressive control; G2 mice were exposed to only IMR-32 cells, whereas G3 and G4 comprised mice exposed to EBV and $gM_{146-157}$, respectively. To test for spatial reference memory, mice were trained in a water-filled maze. Before being immunosuppressed, all mice were trained in the water maze, where all the groups of mice took almost similar time to reach the platform placed in the middle (Figure 4.4I). A similar pattern was observed at day zero of EBV and $gM_{146-157}$ exposure, where no significant difference was discerned across all groups (Figure 4.4II). Notably, during the exposure of EBV/$gM_{146-157}$, we observed a statistical increase in G3 and G4, as compared to the control G1 on D5, D10 and D15 (p<0.01) (Figure 4.4III).
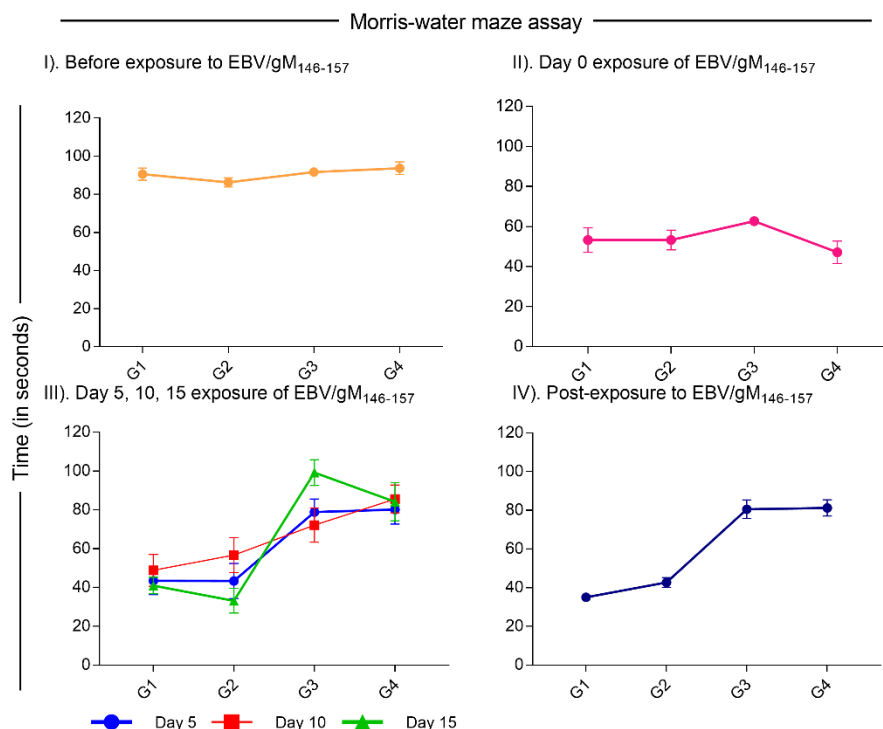
Figure 4.4: Morris-water maze assay at different time-points.
I) Before exposure to EBV/gM$_{146-157}$ where there was no significant difference observed. II) At day zero no statistical difference was observed in all four groups. III) At D5 exposure of EBV/gM$_{146-157}$, G3 and G4 showed significant difference $p<0.01$ compared to G1. At D10 of exposure G4 showed significant difference $p<0.01$. At D15 exposure of EBV/gM$_{146-157}$, G3 and G4 showed significant difference $p<0.01$ compared to G1. IV) Post-exposure of EBV/gM$_{146-157}$, G3 and G4 showed significant difference $p<0.0001$ compared to G1.

4.4.5 Evaluation of structural amendments in the hippocampal arch of mice

Mice hippocampus is formed of Cornu ammonis (CA) which is further divided into CA1, CA2, CA3 and dentate gyrus regions. In G1 and G2, CA1 and CA2 areas comprise of small pyramidal cells. CA3 zones of hippocampi likely show large pyramidal cells, whereas the dentate gyrus region is composed of granular cells (Figure 4.5I). Areas in between compact zones of cells encompass the molecular layer, which consists of neuronal processes (axons and dendrites), glial cells, and scattered nerve cells. The arrangement of cells in the CA1, CA2 and CA3 zones of G1 and G2 were normal with thick bundles of pyramidal cells. Further, the CA3 zones of G1 and G2, neurons were markedly organized with minimum appearance of apoptosis. (Figure 4.5I). While in the experimental group (G3), cells with dark and condensed nuclei were detected, and a minimal layer of cells was observed in CA1 and CA2

regions (Figure 4.5I). Total shrinkage of zonal arc was found in this group. Likewise, samples belonging to G4, project a disorganized layer of larger pyramidal cells in CA3 regions with a noticeable increase in apoptotic cells marked with an arrow in Figure 4.5I. Contrarily, CA1 and CA2 regions showed normal arrangements like G1 (Figure 4.5I).

The dentate gyrus regions from G1 and G2 showed normal thickness with abundant mass of granular cells. While G3 and G4 suggested disorganization, degeneration/loss of cells (Figure 4.5I). Subsequently, cells from the olfactory region of G1 mice showed pyramidal morphology with no signs of apoptosis and a darkened condensed nucleus. Neuronal cells from G2 were organized with very few projections of apoptotic and condensed nuclear cells (Figure 4.5I). In contrast, G3 and G4 exhibited a rise in the appearance of apoptotic cells and disorganized neurons were observed as compared to the control mice (Figure 4.5I).
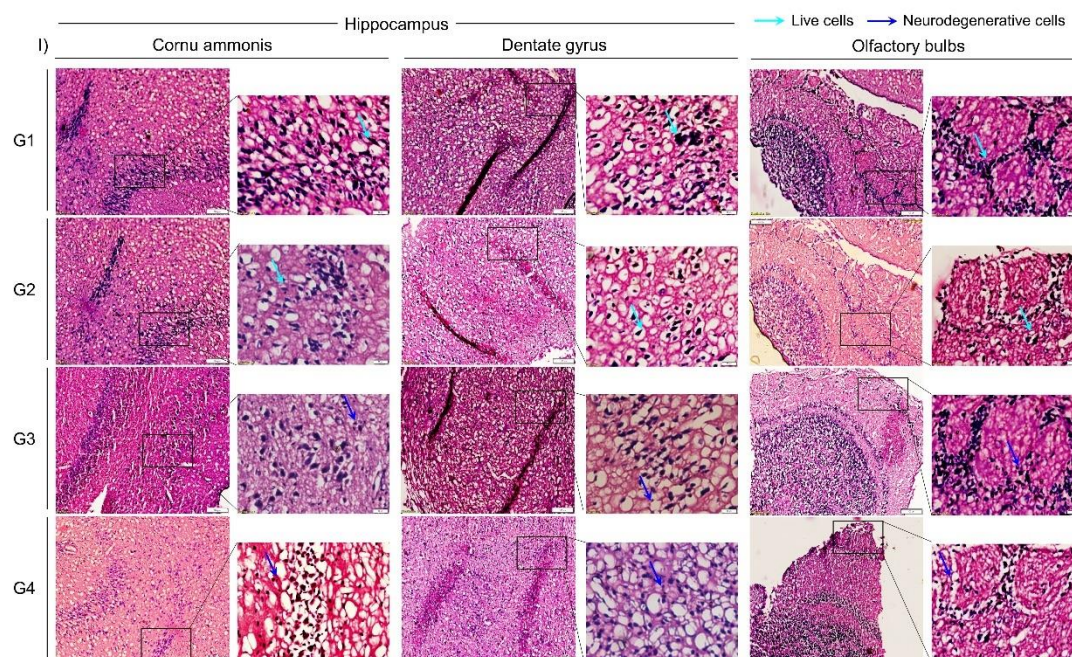
Figure 4.5: Histopathological changes on the mice brain tissue samples upon exposure to EBV and gM$_{146-157}$ via Hematoxylin and Eosin staining.
I) Panel underlies hippocampal region of mice in all four groups. G3 and G4 showed increase in the cell shrinkage and distorted arrangement compared to G1 and G2. II) Representation of dentate gyrus region of brain and apoptotic projections were observed in the G3 and G4. III) Neuronal cells from olfactory bulb region represents change in the appearance as well as decrease observable cell count in G3 and G4 compared to G1 and G2.

4.4.6 EBV infection in brain

EBV shared several properties with the Murine gammaherpesvirus-68 (MHV-68), like eliciting mononucleosis-like syndrome and maintaining chronic infection in memory B-cell [31]. Notably, MHV-68 shares homology with EBV genes like BXLF1, BNRF1, BORF2, BVRF1, BVRF2, BXRF1, BcLFl, BALF5, BALF2, which suggests EBV potency to infect mice [32]. Hereby, the EBV exposure was evaluated using EBV nuclear antigen 1 (EBNA1) and EBV-GFP on mice brain tissue samples; EBNA1 exhibited an increase in the G3 (EBV-infected mice) as compared to G1 (control mice) (P<0.0001) (Fig 4.6I-II).
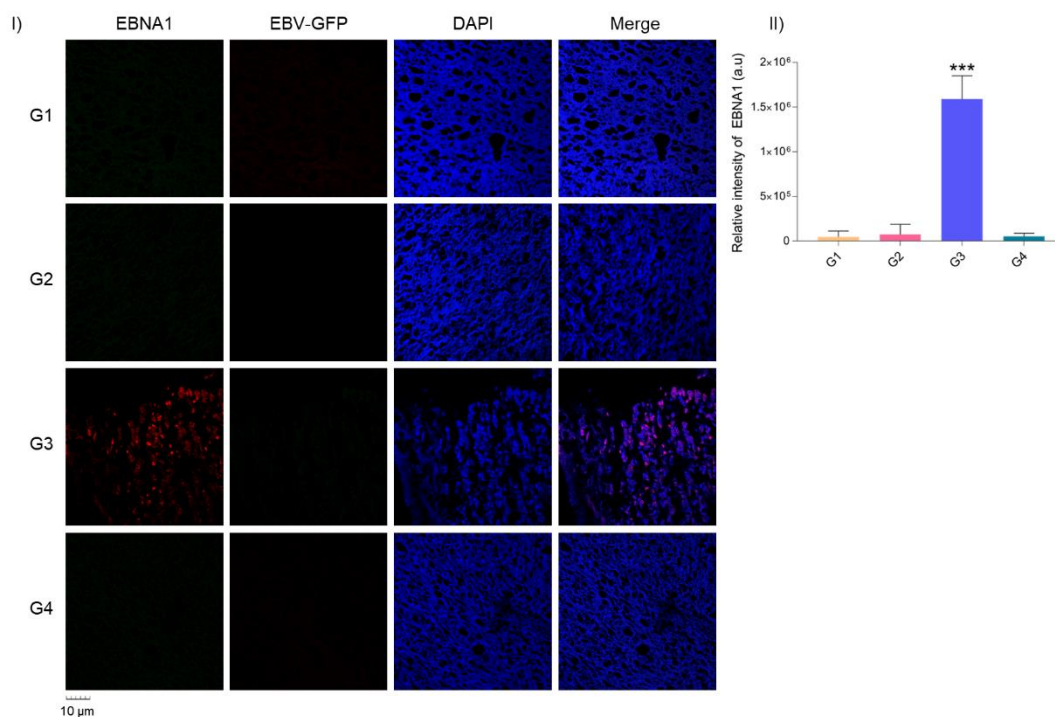
Figure 4.6: Immunohistochemistry of Epstein-Barr virus nuclear antigen 1 and EBV-GFP on mice brain tissue samples.
I). Panel representing EBNA1 and EBV-GFP in the cortical region of mice brain II) Quantification of EBNA1 and G3 showed significant increase (p<0.0001).

4.4.7 Perturbations in the inflammation-associated changes in EBV and gM$_{146-157}$ challenged mice

Exposures of numerous pathogens to brain cells trigger inflammatory responses. A chronic immune system activation triggers inflammation in the brain, eventually predisposing to neurological pathologies [48]. Therefore, we have assessed the levels of TNF-α and IL-6 cytokines in mice's brain tissue and serum by using ELISA. In

brain tissue samples, TNF-α exhibited an increase in G2 (p<0.01), G3 (p<0.0001) and G4 (p<0.01) mice, as compared to G1 (Figure 4.7Ia). However, serum TNF-α levels decreased in all studied groups (Figure 4.7Ib).
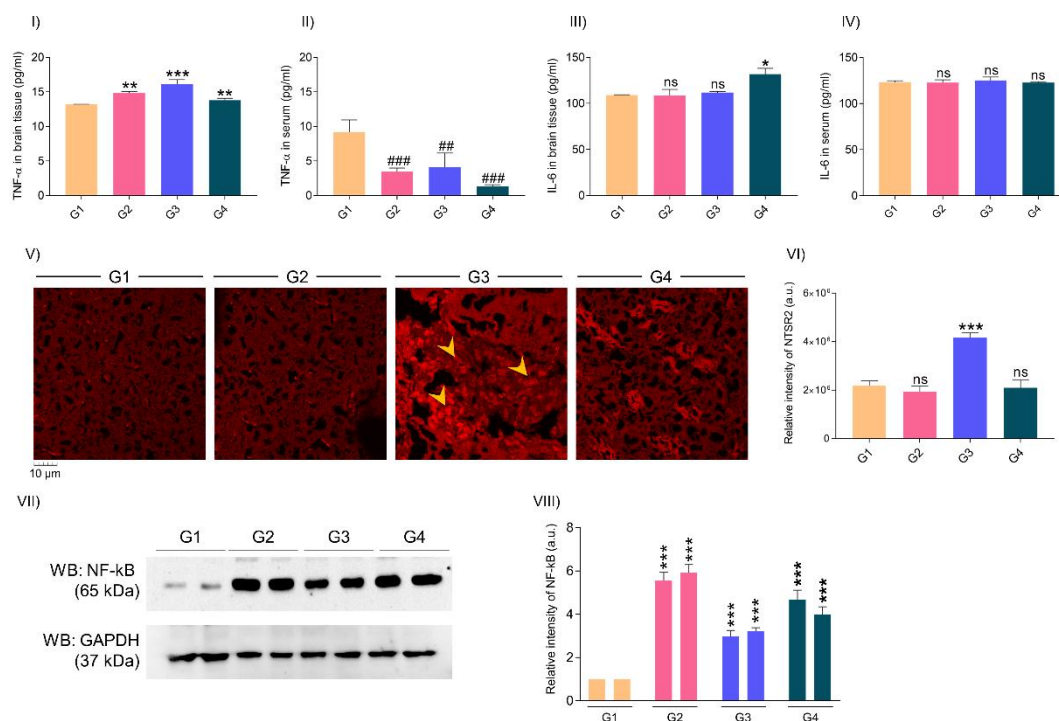
Figure 4.7: Changes in the inflammatory moieties of mice brain.
Ia-Ib) ELISA of TNF-α in brain-tissue and serum sample of mice. In brain tissue samples, TNF-α (pg/ml) showed an increase in G2 (p<0.01), G3 (p<0.0001) and G4 (p<0.01) compared to G1. While in the TNF-α serum, a decrease was observed. Ic-Id) ELISA of IL-6 (pg/ml) in brain-tissue and serum samples of mice. IIa) IHC of calretinin and NTR2. IIb) Quantification of IHC of calretinin and NTR2 (p<0.0001). IIIa) Western blotting of NF-kB (65 kDa) and housekeeping gene GAPDH (37 kDa). IIIb) Quantification of NF-kB showed an increase in G2, G3 and G4 (p<0.0001) compared to G1. Given plots; *x*-axis, different groups; *y*-axis, protein concentration or fold change in EBV/gM$_{146-157}$ concerning unexposed samples. The *p*-values of <0.05, <0.01 and <0.0001 are considered statistically significant (one-way ANOVA and posthoc) and are represented with */#, **/## and ***/### upregulation/downregulation, respectively.

IL-6 showed changes only in the G4 (p<0.05) of brain tissue samples compared to G1, whereas no changes were observed in the serum samples (Figure 4.7Ic). Moreover, a neuroinflammatory transcription factor NF-kB was assessed. NF-kB has shown elevation in all three groups G2 (p<0.0001), G3 (p<0.0001) and G4 (p<0.0001), as compared to G1 (Figure 4.7IIIa-b). Neuropeptides and their precursor proteins can be detected as granules or clumped reaction products in the perikaryal cytoplasm of neurons in which they are expressed (Figure 4.7IIa-IIb). Likewise, a noticeable

increase was found in the NTSR2 (Figure 4.7IIa-b). Neurons were defined as positive if the neuropeptide- or precursor-immunoreactivity was detected in the soma in more than one consecutive confocal optical section (Figure 4.7IIa-b).

4.4.8 Assessment of Alzheimer's disease markers in mice brain tissue and serum samples upon exposure to EBV/ gM$_{146-157}$

Pathophysiology of AD is mainly served by APP due to its sequential proteolytic cleavage that generates amyloid-β peptides (Aβ).
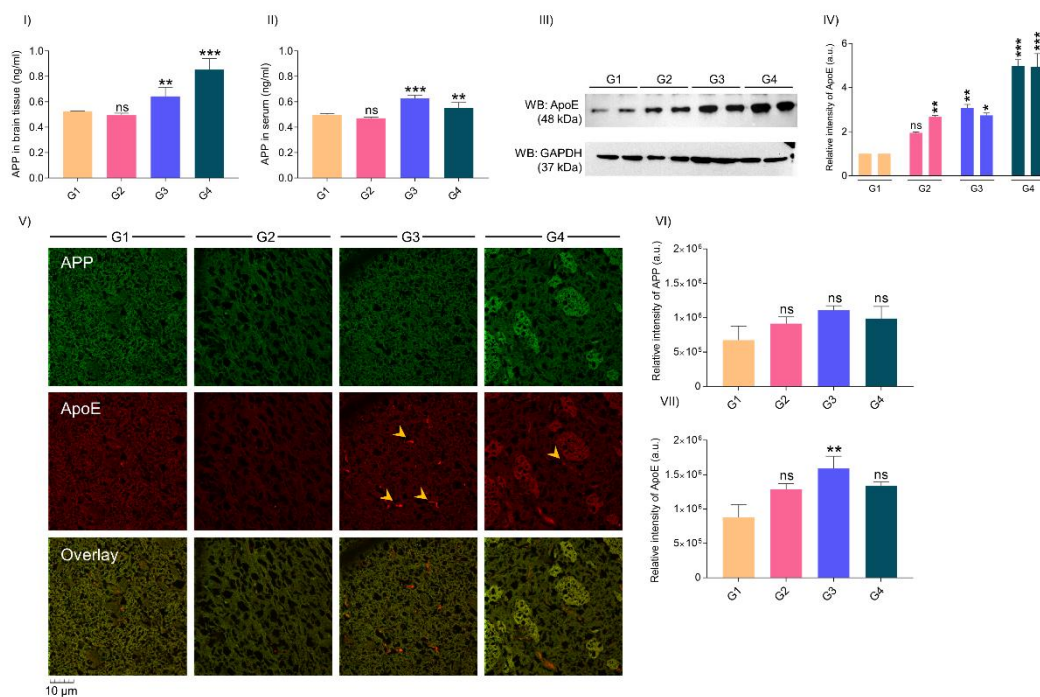
Figure 4.8: Amendments in the AD disease markers after challenging with EBV gM$_{146-157}$.
Ia-b) APP (ng/ml) was estimated in brain tissue and serum samples. G3 (p<0.01) and G4 (p<0.0001) showed increase in brain tissue sample of mice and similar observation was found in the serum samples. IIa) IHC of APP and ApoE. IIb-c) IHC quantification of APP in G3 (p<0.05), G4 (p<0.0001) whereas ApoE showed an increase in G2 (p<0.05), G3 and G4 (p<0.0001). IIIa) Western blotting of ApoE (48 kDa) and housekeeping gene GAPDH (37 kDa). IIIb) Quantification of ApoE4 of western blot, G3 and G4 showed a major increase (p<0.01 and p<0.0001). Given plots: *x*-axis, different groups; *y*-axis, protein concentration or fold change in EBV/gM$_{146-157}$ with respect to unexposed samples. The *p*-values of <0.05, <0.01 and <0.0001 are considered statistically significant (one-way ANOVA and posthoc) and are represented with */#, **/## and ***/### upregulation/downregulation, respectively.

The continuous clearance of these peptides is driven by ApoE proteins, where E4 is the least potent (E2>E3>E4). Therefore, we assessed the level of APP in the mice brain tissue and serum samples. We observed a significant increase in the

concentration (ng/ml) of APP in brain tissue samples of G3 (p<0.01) and G4 (p<0.0001) as compared to G1 (Figure 4.8Ia). Notably, it also showed an elevation in the serum samples of G3 (p<0.0001) and G4 (p<0.01) (Figure 4.8Ib). At the same time, we have observed no changes in the APP via IHC (Figure 4.8IIa-b). ApoE level was evaluated using IHC and western blotting. ApoE has shown a rise in the experimental group G3 (p<0.01) as compared to the control group (G1) (Figure 4.8IIa, IIc). It exhibited a similar pattern in western blotting (Figure 4.8IIIa-b).

4.4.9 Evaluation of Multiple sclerosis markers post-exposure to EBV/ $gM_{146-157}$

In the central nervous system, MBP is one of the abundantly expressed proteins responsible for the adhesion of cytosolic surfaces of multilayered compact myelin.
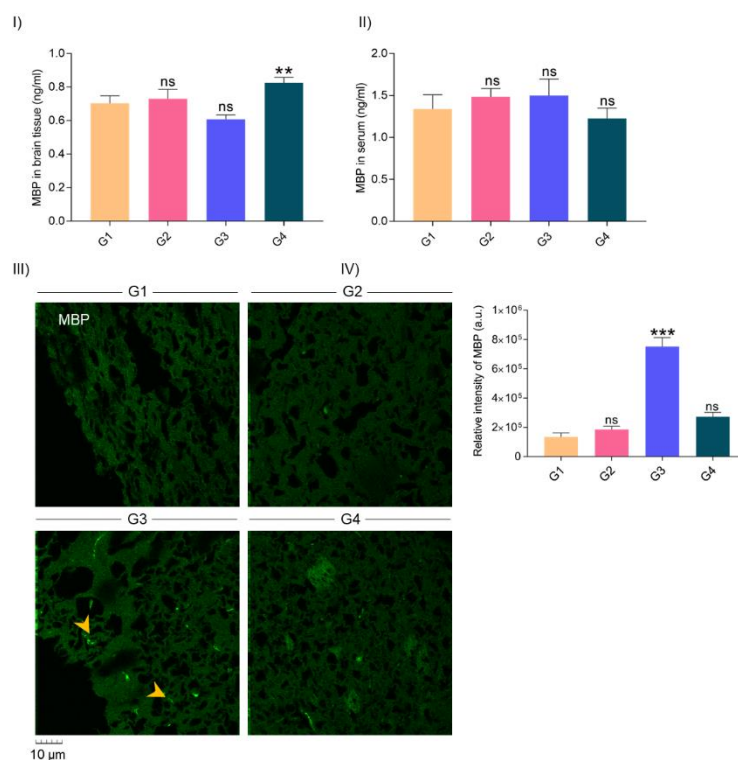
Figure 4.9: Alterations in the MS disease markers in the mice.
Ia-b) ELISA of MBP (ng/ml) in mice brain tissue and serum samples. MBP has shown elevation in the G4 (p<0.01) compared to G1 and no significant changes were observed in serum. IIa) IHC of MBP. IIb) IHC quantification of MBP, increase observed in the G2 (p<0.05), G3 (p<0.01) and G4 (p<0.01). Given plots *x*-axis, different groups; *y*-axis, protein concentration or fold change in EBV/gM$_{146-157}$ with respect to unexposed samples. The *p*-values of <0.05, <0.01 and <0.0001 are considered statistically significant (one-way ANOVA and posthoc) and are represented with */#, **/## and ***/### upregulation/downregulation, respectively.

It binds with numerous polyanionic proteins, namely actin, tubulin, clathrin, calmodulin and negatively charged lipids [49]. Pathogens like EBV exhibit molecular mimicry for this protein, resulting in numerous disease pathologies [50]. MBP indicated an augmentation in the mice brain cortical tissue samples in the G4 ($p<0.01$) on ELISA, whereas no significant changes were observed in the serum samples (Figure 4.9Ia-b). Similarly, IHC revealed an increase in the G3 ($p<0.01$) as compared to G1 (Figure 4.9IIa-b).

4.5 Discussion

Numerous studies have shown a connection among EBV with neurological diseases. A previous study carried out by our group indicated the self-aggregation property of EBV-gM$_{146-157}$ [6]. In continuation to this, current work revealed the changes in IMR-32 cells and mice brain after challenging EBV and gM$_{146-157}$. EBV exhibited successful infection to neuronal cells, which complemented the previously reported studies that showed the viral infection to neuronal cells. Upon infection to EBV and gM we observed elevation in the total Ca^{2+} ions. Calcium ion excitotoxicity was observed in the MS and AD. In the neuronal cells, the increased Ca^{2+} ions in the cells result in augmentation of Aβ oligomers and release of APP intracellular domain (AICD). The release of AICD potentially modulates the calcium signalling system by altering the expression of the Rayanodone receptor (RYR) [41]. Aβ oligomers possibly get associated with cellular prion protein (PrP^c) and intensify the intracellular concentration of calcium ions via receptor-mediated channels, e.g. N-methyl-D-aspartate (NMDA) [41]. In the case of MS, the excitotoxicity is triggered by receptors like amino-3-hydroxy-5-methyl-4-isoxazolepropionic acid (AMPA) and kainic acid (KA). Moreover, an elevated level of glutamate in MS triggers the increase of intracellular Ca^{2+} levels inside the cell [36]. Our study showed an elevation in MBP upon infection of EBV and gM peptide. Similarly, the level of MBP in CSF of MS patients was found to be frequently increased and remains increased until 5 to 6 weeks after the onset of symptoms [51]. The myelin basic protein (MBP)-specific antibodies from MS patients showed cross-reactivity with EBV latent membrane protein 1 (LMP1) *in-vitro* and *in-vivo* [52]. Also, the homology of EBV proteins (LMP2B and gp350/220) with several myelin sheath proteins, i.e., MOG, MBP, PLP1 and MAG clearly indicated molecular mimicking and its peculiar association with MS [53]. Myelin sheath is made up of ~70% cholesterol and ~30% protein, upon exposure to

be EBV/gM exhibits changes and suggests their possible impact on myelin sheath. Precisely, *cetp1* showed a consistent increase after subjecting to EBV and $gM_{146-157}$. CETP is associated with lipid homeostasis by transferring cholesterol esters from HDL to LDL/VDL [54]. Likewise, the RNA sequencing analyses on MS tissue samples showed elevated expression of FDPS and HMGCS, which play a pivotal role in cholesterol metabolism. Epidemiological research has shown that vascular comorbidities, including hypercholesterolemia, contribute to a more rapid MS disease progression [55]. Accumulation of NGF at brain lesions and inflammation indicates that inflammatory stimuli contribute to enhanced NGF production in MS. Inflammatory molecules like IL-1, IL-6 and TNF-α are potent inducers of NGF [56]. NGF further induces the synthesis of BDNF. Both NGF and BDNF have a crucial role in axonal regeneration, survival, protection and myelination [57].

Subsequently, our findings on mice suggested diminished learning/memory and cognitive recognition in mice exposed to EBV and $gM_{146-157}$. A previous report highlighted that the weanling mice learned the navigational task and developed a spatial map that possibly enabled them to remember the platform location in the MWM task [58]. Likewise, Influenza-induced cognitive deficits were also observed when infected mice showed impaired ability to efficiently navigate to the platform [59]. Likewise, previous report highlighted that the weanling mice learned the navigational task and developed a spatial map, which possibly enables them to remember the platform location in the MWM task [60]. Influenza-induced cognitive deficits were also observed when infected mice showed impaired ability to efficiently navigate to the platform [59]. Upon exposure to EBV/gM, multiple pyknotic cells have been observed in the hippocampal region. Akin to this, a time-dependent infection of HSV on mice exhibited pyknosis, eosinophilic cytoplasm, and karyorrhexis (necrosis) and with increasing infection incubation, swelling of myelin sheath was observed in trigeminal nerve root [61]. Intriguingly, HSV-1 and VZV have shown their presence in the olfactory bulbs of human post-mortem samples, thus, it is suggesting possible EBV-mediated effects in olfactory neurons [62].

In consistent with our *in-vitro* system, the exposure of EBV/$gM_{146-157}$ to mice instigated the expression of inflammatory moieties, namely IL-6 and TNF-α. Similarly, mice infected with Japanese Encephalitis virus (JEV) have shown an increased chemokines and cytokines like IL-6, TNF-α, and TGF-β. The elevated level

of IL-6 and TNF-α can potentially induce irreversible changes in the CNS, such as neuronal damage [63]. Neuroinflammation in the mice infected with the influenza virus triggered changes in the hippocampal structural plasticity, eventually underlying cognitive dysfunction [64]. Increased level of NF-kB further endorsed with the elevated level of inflammation in the groups exposed to EBV/ gM$_{146-157}$. Notably, upon exposure to pathogens, NF-kB gets activated canonically (p65-p50) and non-canonically (RelB-p52) and further aggravates the inflammation in the CNS [65]. Moreover, we have determined the proportion of neuropeptide-expressing cells using neurotensin immunoreactive antibody staining. NTS, a neurotransmitter and neuromodulator in the CNS, has been shown to be involved in epilepsy. NTSR2 is expressed in the hippocampal astrocytes and its expression increases along with astrocyte reactivity. Previously, NTSR2 has been implicated in astroglia and gliovascular inflammation, which could be a potent therapeutic target [66]. Thus, this data highlighted the changes in the level of NTSR2 that can further be corroborated with the increased inflammatory moieties.

The neocortex and hippocampal region of mice brains showed progressive accumulation of AD biomarkers (Aβ, hyperphosphorylated Tau) upon recurrent HSV1 infection, which eventually correlated with cognitive deficits [67]. Further, in the case of AD, latent viral infections and ApoE4 are vital emerging risk factors. Exposure of EBV/gM induced changes in the APP, ApoE and MBP-like proteins. Earlier, the virus and ApoE protein competed for the same binding molecule, heparan sulfate proteoglycan, before entering the cell through specific receptors. Thus, the weaker binding of ApoE4 makes it a weaker competitor relative to the other ApoE4 isoforms. The level of latent HSV1 DNA in the brain was higher in mice expressing the human ApoE4 than in mice carrying the ApoE3 allele [68]. Pathogens like EBV exhibits molecular mimicry for this protein resulting in numerous disease pathologies [50]. Previously, EBV has shown a prominent association with MS, i.e. the mean titre of EBNA in the MS group was 21.32, significantly higher than the healthy controls (15.37) [69]. HHV-6 protein U24 residue 4-10 is an autoantigen candidate for MS with MBP residues 96-102. Authors have shown that >50% of T-cells recognizing MBP (93-105) cross-react with and could be activated by a synthetic peptide corresponding to residues 1 to 13 of HHV-6 U24 in MS patients [70]. Notably, the reduced level of Aβ and soluble APP (sAPP) fragments are reported in inflammatory diseases, e.g. MS,

but the clear mechanism is yet to be understood [71]. Intriguingly, the co-existence of AD and MS was reported in a case series of 4 patients by confirming through autopsy samples [72].
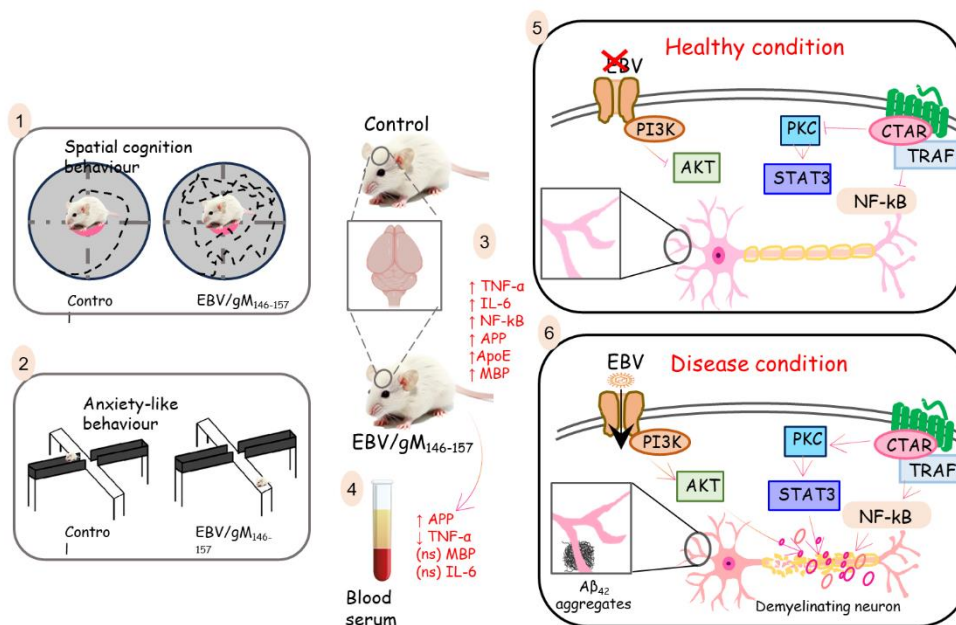
Figure 4.10: Underpinning amendments in behaviors, inflammatory and disease markers upon exposure to EBV and gM$_{146-157}$.
1) An increase in time to reach the platform in the Morris-water maze after exposure to EBV/gM$_{146-157}$ suggested cognitive decline. 2) Experimental group exhibited anxiety-like behaviour by showing entry on the open arm of the elevated maze. 3) The cortical region of mice exposed to EBV/gM$_{146-157}$ manifested elevation in inflammatory markers (TNF-α, IL-6 and NF-kB) and disease markers (APP, ApoE4 and MBP) compared to a control group of mice. 4) The level of APP and TNF-α was also found to be altered in the blood serum of the experimental group. 5-6) Possible pathways in normal and disease conditions of neurons. In disease conditions, EBV triggers numerous changes in the cells including activation of AKT, STAT3 and NF-kB and aids in neuroinflammation. In long-term exposure, it can lead to AD and MS disease-like pathology.

This concurrency of diseases also poses a difficulty in their detection. A study by Londono et al. proposed that using the amyloid/Tau/neurodegeneration (A/T/N) classification scheme for Alzheimer's disease biomarkers can help to distinguish the coexistent neurodegenerative dementia subtypes with primary progressive MS [73]. Furthermore, a deeper understanding is needed to determine the clinical, demographic and risk factors associated with comorbid MS and AD [72]. Moreover, numerous pathogens, including bacteria and viruses facilitates EBV reactivation and its mediated pathologies. A study from our group has suggested that the EBV-*Plasmodium*

falciparum co-infection significantly elevates the RBC adhesion to human brain microvascular cells (HBECs), which is a hallmark of cerebral malaria [74]. Therefore, our study also discerned an increased level of MBP in the mice groups exposed to EBV/ $gM_{146-157}$. Overall, the current study provides insights into EBV's association with neuropathologies (Fig. 4.10).

4.6 Conclusion

EBV has been gaining continuous attention for its mysterious involvement with numerous neurological diseases. Till now, no study has shown its direct association with diseases like AD and MS. Hereby, we investigated the direct connection of EBV and $gM_{146-157}$ with neurological manifestation on a cell-line and mice-based models. The EBV-$gM_{146-157}$ aggregates showed potential seeding ability for $A\beta_{42}$. Further, in the *in-vitro* system, inflammatory species exhibited an elevation and suggested neuroinflammation. Likewise, upregulation in the inflammatory moieties, i.e., TNF-α and IL-6, were observed in the brain tissue samples upon exposure to EBV/$gM_{146-157}$. Exposure to EBV/$gM_{146-157}$ also exhibited a decline in spatial memory formation and an increase in anxiety-like symptoms in mice. An increase in total Ca^{2+} ions suggested excitotoxicity in neurons, which complemented the inflammatory results. Further, the current study also suggested attenuation in the membrane potential of mitochondria post-exposure to EBV and $gM_{146-157}$, which act as an adjuvant in neuroinflammation. Hippocampal neurons of mice brains showed significant disorganization as well as cell shrinkage, which suggested apoptotic changes. Eventually, the neurological disease markers like APP, ApoE and MBP suggested an increase in a time-dependent manner. EBV and $gM_{146-157}$ have exhibited elevation in the disease makers like APP, MBP and risk factor ApoE at *in-vivo* level. Moreover, cholesterol metabolism-related genes manifested significant nuances which had a key association with MS. Taken together, this study provides a direct link of EBV with neurological diseases in the *in-vivo* model system and further raises the need to investigate the detailed mechanism, so, that we can find numerous potent therapeutic targets.

4.7 Material and Methods

4.7.1 Cells

The human neuroblastoma cell line (IMR-32) was procured from the National Centre

for Cell Science, Pune, India. For virus purification, HEK 293T cells were used which contain stably transfected bacterial artificial chromosome (BAC) green fluorescent protein (GFP)-EBV [75]. The cells were cultured in Dulbecco's modified Eagle's medium (DMEM; Himedia Laboratories Pvt. Limited, India) supplemented with 10% fetal bovine serum (FBS; Himedia Laboratories Pvt. Limited, India), 50 U/ml, 100 µg/ml and 2 mM of penicillin, streptomycin and L-Glutamine respectively. The growing cell environment was humidified with 5% CO_2 at 37 °C.

4.7.2 Animals

Adult Swiss albino female mice weighing ~30 gms, age approximately 2 months were housed in polypropylene cages and acclimated for a week before experimentation in a 14 h light: 10 h dark in an environment with a temperature of 23 ± 2 °C and humidity under control, with free access to laboratory feed and drinking water. Animals were maintained as per the guidelines of the Institutional Animal Ethics Committee (IAEC), the Committee for the Purpose of Control and Supervision of Experiments on Animals (CPCSEA), and the Ministry of Environment and Forests, Government of India, New Delhi. The experimental protocol was approved by the IAEC of the School of Biotechnology, Devi Ahilya Vishwavidyalaya, Indore (Registration no. 779).

Precisely, a total of five groups (each having 6 mice) were made namely immunosuppressed control, IMR-32 cells exposed, EBV infected IMR-32 and $gM_{146-157}$ exposed IMR-32 subjected with one neat control group (negative control). For immunosuppression, mice were subjected to peritoneal cyclosporin (working concentration; 10 mg/kg) on alternate days for 10 days and then xenograft of IMR-32 prior-exposed with EBV or $gM_{146-157}$ for 24 hrs was administered intranasally. Three booster doses were given for the above-mentioned cells or cells exposed to EBV/$gM_{146-157}$ every five days. Besides, to avoid the fungal infection ketoconazole (working concentration; 5mg/kg) was administered from the 10th day of immunosuppression till 15 days. Further mice were maintained and the behavioral assay was recorded for 5 weeks before sacrifice.

4.7.3 Purification of virus particles

The BAC-GFP-EBV has stably transfected HEK 293T cells [76], [77] and were grown in complete DMEM with puromycin selection. EBV particles were obtained by using the following protocol as illustrated previously [5].

4.7.4 qRT-PCR

EBV infections and inflammatory genes profile was analyzed using qRT-PCR. 2.5×10^4 cells were seeded in a 6-well plate followed by $gM_{146-157}$ and EBV exposure for 12, 24 and 48 h. Total RNA extraction, complementary DNA preparation and qRT-PCR were carried out as described earlier [5]. Gene-specific primers were designed from Primer-BLAST and are listed in Table S1. Glyceraldehyde 3-phosphate dehydrogenase (GAPDH) was used as a housekeeping gene and the experiment was performed in three biological and one technical repeat.

4.7.5 Immunofluorescence assay

The assay was used for demonstrating EBV infections and inflammation using APP (CT695, Invitrogen), Apoe4 (4E4, Cell Signaling Technology (CST), Danvers, MA, USA), and MBP (2H9 from CST) antibodies. 2.5×10^4 cells were seeded in a 6-well plate onto the coverslips and exposed with gM and EBV for 12, 24, and 48 h and immunostaining were performed as explained previously [5]. Cells were observed under a fluorescence microscope (CellSens Dimensions 2.3, Shinjuku-ku, Tokyo, Japan). Analysis and quantification of the image were done as mentioned previously [5]. The fluorescence intensity was calculated and plotted compared to the uninfected control of the respective groups.

4.7.6 Western blotting

IMR-32 cells infected with EBV along gM treated samples were harvested, washed with PBS and lysed in radioimmunoprecipitation assay buffer (RIPA) as described earlier [5]. Antibodies against APP, APOE4, MBP, NF-kB (1:1000; D14E12 from CST) and GAPDH (14C10, 1:1000, Cell Signaling Technology, Danvers, MA, USA) were used as per the protocol [78]. An housekeeping gene GAPDH was used and the image analysis and quantification of blots were performed using Image J software (National Institutes of Health, Bethesda, MA, USA).

4.7.7 Ca^{2+} ion detection

Total Ca^{2+} ions were detected using Fura 2/AM (203052; Santa Cruz Biotechnology, Inc.). 1mM stock of Fura 2/AM was prepared and 1μM final concentration was used for the experiment. Cultured IMR-32 cells were incubated with Fura 2/AM for 30 minutes in dark and washed with PBS, visualization was performed with an excitation wavelength of 340 and 380 nm and emission were 505 nm under a fluorescence microscope (IX83, Olympus). The absorbance is also observed at the above-mentioned wavelengths.

4.7.8 Morris-water Maze behavioural assay

The MWM was used to assess hippocampal-dependent spatial memory. The circular maze has a diameter of 100-120 cm and was filled with water with 24-25°C. An escape platform was submerged below the water surface in the centre of the maze. In the acquisition phase, each mouse was given 120 s time for a trial to find the hidden platform and remain seated on the platform for 10 s, followed by mice were returned to their home cage after drying with a towel. Mice were trained for a week before any treatment. Then, the assay was recorded upon administration of immunosuppressives, during EBV/gM$_{146-157}$ exposure and post-exposure.

4.7.9 Brain tissue collection

After 5 weeks of experimentation, mice were sacrificed by using isoflurane inhalation followed by decapitation as per approved protocol of IAEC and CPCSEA. Brains were excised and kept in a formalin solution for further usage. Further, the tissue was weighed and snap-frozen in liquid nitrogen followed by homogenisation in the PBS (9ml of PBS in 1gm of tissue chunk). Subsequently, the protein estimation was done using the Bradford assay and this protein was further used in ELISA and western blotting.

4.7.10 Enzyme-linked immunosorbent assay

Sandwich ELISA was performed as per the kit from "Fine Test" for TNF-α (cat.log# EM0183), IL-6 (cat.log# EM0121), APP (cat.log# EM1924) and MBP (cat.log# EM1202) on serum and brain tissue samples of mice. For the serum sample preparation, the blood of mice was collected during decapitation. The serum was collected and centrifuged at 1000g for 20 min at 4°C and the assay was carried out. Tissue sample preparation is mentioned in the "4.7.9. Brain tissue collection" section.

The standard for all aforementioned proteins was prepared as per the kit. Subsequently, 100 ul of serum samples were loaded onto the well and tissue samples were diluted with sample buffer so that the final concentration of protein in each well was ~0.3 mg/ml. Plates were sealed and incubated for 90 minutes at 37°C. After decanting, the plates were washed twice in the washing buffer. The 100 ul of biotin-labelled antibody was added in each well with the dilution of 1:100 and kept at 37°C. After removing the antibody, the plate was washed thrice in washing buffer. Subsequently, SABC solution (100 ul) was added (1:100) for 30 min at 37°C. The plate was washed 5 times and 90 ul of TMB solution was added in each well for 20 min. Stop solution (50 ul) was added and immediately absorbance was recorded at 450 nm. Further, data were normalised with control and protein concentration (pg/ml, ng/ml) was calculated.

4.7.11 Haematoxylin and eosin staining

This staining was performed on the mice brain tissues (5 mm sections) post paraffinization and 5 mm tissue sectioning with microtome. Deparaffinization and hydration was performed in the coupling jar containing 40 ml of xylene for 5 minutes (min). Then, slides were transferred into xylene:100% ethanol (1:1) for 3 min followed by the incubation in 100% ethanol for 5 min. Subsequently, slides were incubated in 95% of ethanol for 3 min and in 70 % ethanol for next 3 minutes. Further, 50% ethanol was added for 3 min and then gently washed with 1xPBS. Further, nuclear staining was done using haematoxylin for 5 min followed by washing in tap water. Excess dye was removed from the sections by dipping the slide into 1% acid alcohol (1% HCl in 70% ethanol) for 30 sec. Soon after slides were washed in tap water, bluing of sections was done by dipping it into ammonia water. Counterstain 1% eosin was used for 10 min and washed the tissue sections in tap water. Then, dehydration was done using increasing concentrations of alcohol followed by incubation in xylene for clearing the slides. Eventually, sections were mounted in mounting media and observed under bright-field microscope (magnifications; 10x, 20x and 40x).

4.7.12 Immunohistochemistry

The immunohistochemistry (IHC) protocol was taken from abcam-paraffin and performed on the mice brain tissues (5 mm sections) post paraffinization and tissue sectioning with microtome.[79] (i). Deparaffinization and hydration was performed in

the coupling jar containing 40 ml of xylene for 5 minutes (min). Then, slides were transferred into xylene:100% ethanol (1:1) for 3 min followed by the incubation in 100% ethanol for 5 min. Subsequently, slides were incubated in 95% of ethanol for 3 min and in 70 % ethanol for next 3 minutes. Further, 50% ethanol was added for 3 min and then gently washed with 1xPBS. ii). For the retrieval of antigens, we used 10 mM sodium citrate buffer (PH-6.0). Slides were shifted into a coupling jar filled with 10 mM sodium citrate buffer and incubated at 80°C for 2 hrs in the water bath. Coupling jar was then removed from water bath and kept at room temperature for 5 min and washed with 1xPBS once. 4% paraformaldehyde was used to fix the brain sections on the slide for 20-40 minutes followed by gentle wash with 1xPBS. iii). Antigen-antibody interaction: the permeabilization of tissues was done with 0.2% trito1n-X-100 for 20 min which was prepared in 1xPBS. Soon after slides were washed with 1xPBS once. 1% bovine serum albumin (BSA) was used for blocking the non-specific epitopes for 1 hr afterwards 3 washes in 1xPBS. Primary antibody was added for 2 hrs APP (CT695, Invitrogen), Apoe4 (4E4, Cell Signaling Technology (CST), Danvers, MA, USA) and MBP (2H9 from CST), and neurotensin receptor 2 (118006, Abgenex) followed by two 1xPBS washes. Then, secondary antibody was added anti-rabbit (7074, CST) and anti-mouse (7076, CST) with DAPI (1:500; CST) for 45 min in dark. Immediately slides were washed thrice in 1xPBS. Mounting of the slides was done in antifade by covering the section with 18 mm coverslip and stored it at 0°C. iv). Visualization was done by confocal microscopy (OLYMPUS IX). mage analysis and quantification of blots were performed using Image J software (National Institutes of Health, Bethesda, MA, USA).

4.7.13 Statistical analysis

All the *in-vitro* experiments were carried out in three biological replicates. Data were presented as means ± standard error mean (SEM) of three independent experiments. One-way ANOVA followed by post hoc analysis was performed to compare the differences in the mean values of IMR-32 cells with IMR-32 cells exposed to EBV/gM$_{146-157}$. The statistical significance of p-values <0.05, <0.01 and <0.0001 were considered to be */#, **/## and ***/### for upregulation/downregulation respectively.

4.8 References

1. Young LS, Rickinson AB (2004) Epstein–Barr virus: 40 years on. Nat Rev Cancer 4:757–768. https://doi.org/10.1038/nrc1452

2. Handel AE, Williamson AJ, Disanto G, Handunnetthi L, Giovannoni G, Ramagopalan SV (2010) An Updated Meta-Analysis of Risk of Multiple Sclerosis following Infectious Mononucleosis. PLoS ONE 5:e12496. https://doi.org/10.1371/journal.pone.0012496

3. Huang S-Y, Yang Y-X, Kuo K, Li H-Q, Shen X-N, Chen S-D, Cui M, Tan L, Dong Q, Yu J-T (2021) Herpesvirus infections and Alzheimer's disease: a Mendelian randomization study. Alzheimers Res Ther 13:158. https://doi.org/10.1186/s13195-021-00905-5

4. Jha HC, Mehta D, Lu J, El-Naccache D, Shukla SK, Kovacsics C, Kolson D, Robertson ES (2015) Gammaherpesvirus Infection of Human Neuronal Cells. mBio 6:e01844-15. https://doi.org/10.1128/mBio.01844-15

5. Jakhmola S, Jha HC (2021) Glial cell response to Epstein-Barr Virus infection: A plausible contribution to virus-associated inflammatory reactions in the brain. Virology 559:182–195. https://doi.org/10.1016/j.virol.2021.04.005

6. Tiwari D, Singh VK, Baral B, Pathak DK, Jayabalan J, Kumar R, Tapryal S, Jha HC (2021) Indication of Neurodegenerative Cascade Initiation by Amyloid-like Aggregate-Forming EBV Proteins and Peptide in Alzheimer's Disease. ACS Chem Neurosci 12:3957–3967. https://doi.org/10.1021/acschemneuro.1c00584

7. Xu S, Gaskin F (1997) Increased incidence of anti-β-amyloid autoantibodies secreted by Epstein-Barr virus transformed B cell lines from patients with Alzheimer's disease. Mech Ageing Dev 94:213–222. https://doi.org/10.1016/S0047-6374(96)01861-1

8. Lanz TV, Brewer RC, Ho PP, Moon J-S, Jude KM, Fernandez D, Fernandes RA, Gomez AM, Nadj G-S, Bartley CM, Schubert RD, Hawes IA, Vazquez SE, Iyer M, Zuchero JB, Teegen B, Dunn JE, Lock CB, Kipp LB, Cotham VC, Ueberheide BM, Aftab BT, Anderson MS, DeRisi JL, Wilson MR, Bashford-Rogers RJM, Platten M, Garcia KC, Steinman L, Robinson WH (2022) Clonally

expanded B cells in multiple sclerosis bind EBV EBNA1 and GlialCAM. Nature 603:321–327. https://doi.org/10.1038/s41586-022-04432-7

9. Lünemann JD, Jelčić I, Roberts S, Lutterotti A, Tackenberg B, Martin R, Münz C (2008) EBNA1-specific T cells from patients with multiple sclerosis cross react with myelin antigens and co-produce IFN-γ and IL-2. J Exp Med 205:1763–1773. https://doi.org/10.1084/jem.20072397

10. Angelini DF, Serafini B, Piras E, Severa M, Coccia EM, Rosicarelli B, Ruggieri S, Gasperini C, Buttari F, Centonze D, Mechelli R, Salvetti M, Borsellino G, Aloisi F, Battistini L (2013) Increased CD8+ T Cell Response to Epstein-Barr Virus Lytic Antigens in the Active Phase of Multiple Sclerosis. PLoS Pathog 9:e1003220. https://doi.org/10.1371/journal.ppat.1003220

11. Tiwari D, Srivastava G, Indari O, Tripathi V, Siddiqi MI, Jha HC (2023) An *in-silico* insight into the predictive interaction of Apolipoprotein-E with Epstein-Barr virus proteins and their probable role in mediating Alzheimer's disease. J Biomol Struct Dyn 41:8918–8926. https://doi.org/10.1080/07391102.2022.2138978

12. Gate D, Saligrama N, Leventhal O, Yang AC, Unger MS, Middeldorp J, Chen K, Lehallier B, Channappa D, De Los Santos MB, McBride A, Pluvinage J, Elahi F, Tam GK-Y, Kim Y, Greicius M, Wagner AD, Aigner L, Galasko DR, Davis MM, Wyss-Coray T (2020) Clonally expanded CD8 T cells patrol the cerebrospinal fluid in Alzheimer's disease. Nature 577:399–404. https://doi.org/10.1038/s41586-019-1895-7

13. Cheng W (2012) Cross-reactivity of autoreactive T cells with MBP and viral antigens in patients with MS. Front Biosci 17:1648. https://doi.org/10.2741/4010

14. Smith C, Khanna R (2023) Adoptive T-cell therapy targeting Epstein–Barr virus as a treatment for multiple sclerosis. Clin Transl Immunol 12:e1444. https://doi.org/10.1002/cti2.1444

15. Läderach F, Münz C (2022) Altered Immune Response to the Epstein–Barr Virus as a Prerequisite for Multiple Sclerosis. Cells 11:2757. https://doi.org/10.3390/cells11172757

16. Tengvall K, Huang J, Hellström C, Kammer P, Biström M, Ayoglu B, Lima Bomfim I, Stridh P, Butt J, Brenner N, Michel A, Lundberg K, Padyukov L, Lundberg IE, Svenungsson E, Ernberg I, Olafsson S, Dilthey AT, Hillert J, Alfredsson L, Sundström P, Nilsson P, Waterboer T, Olsson T, Kockum I (2019) Molecular mimicry between Anoctamin 2 and Epstein-Barr virus nuclear antigen 1 associates with multiple sclerosis risk. Proc Natl Acad Sci 116:16955–16960. https://doi.org/10.1073/pnas.1902623116

17. Sokal EM, Hoppenbrouwers K, Vandermeulen C, Moutschen M, Léonard P, Moreels A, Haumont M, Bollen A, Smets F, Denis M (2007) Recombinant gp350 Vaccine for Infectious Mononucleosis: A Phase 2, Randomized, Double-Blind, Placebo-Controlled Trial to Evaluate the Safety, Immunogenicity, and Efficacy of an Epstein-Barr Virus Vaccine in Healthy Young Adults. J Infect Dis 196:1749–1753. https://doi.org/10.1086/523813

18. Pender MP, Burrows SR (2014) Epstein–Barr virus and multiple sclerosis: potential opportunities for immunotherapy. Clin Transl Immunol 3:e27. https://doi.org/10.1038/cti.2014.25

19. Jakhmola S, Jonniya NA, Sk MF, Rani A, Kar P, Jha HC (2021) Identification of Potential Inhibitors against Epstein–Barr Virus Nuclear Antigen 1 (EBNA1): An Insight from Docking and Molecular Dynamic Simulations. ACS Chem Neurosci 12:3060–3072. https://doi.org/10.1021/acschemneuro.1c00350

20. Amor S, Puentes F, Baker D, Van Der Valk P (2010) Inflammation in neurodegenerative diseases. Immunology 129:154–169. https://doi.org/10.1111/j.1365-2567.2009.03225.x

21. Enders M, Heider T, Ludwig A, Kuerten S (2020) Strategies for Neuroprotection in Multiple Sclerosis and the Role of Calcium. Int J Mol Sci 21:1663. https://doi.org/10.3390/ijms21051663

22. Tapias V (2019) Editorial: Mitochondrial Dysfunction and Neurodegeneration. Front Neurosci 13:1372. https://doi.org/10.3389/fnins.2019.01372

23. Jakhmola S, Upadhyay A, Jain K, Mishra A, Jha HC (2021) Herpesviruses and the hidden links to Multiple Sclerosis neuropathology. J Neuroimmunol 358:577636. https://doi.org/10.1016/j.jneuroim.2021.577636

24. Marrodan M, Alessandro L, Farez MF, Correale J (2019) The role of infections in multiple sclerosis. Mult Scler J 25:891–901. https://doi.org/10.1177/1352458518823940

25. Gosztyla ML, Brothers HM, Robinson SR (2018) Alzheimer's Amyloid-β is an Antimicrobial Peptide: A Review of the Evidence. J Alzheimers Dis 62:1495–1506. https://doi.org/10.3233/JAD-171133

26. Mancuso R, Delbue S, Borghi E, Pagani E, Calvo MG, Caputo D, Granieri E, Ferrante P (2007) Increased prevalence of varicella zoster virus DNA in cerebrospinal fluid from patients with multiple sclerosis. J Med Virol 79:192–199. https://doi.org/10.1002/jmv.20777

27. Bello-Morales R, Andreu S, Ripa I, López-Guerrero JA (2021) HSV-1 and Endogenous Retroviruses as Risk Factors in Demyelination. Int J Mol Sci 22:5738. https://doi.org/10.3390/ijms22115738

28. Fujiwara S, Imadome K-I, Takei M (2015) Modeling EBV infection and pathogenesis in new-generation humanized mice. Exp Mol Med 47:e135–e135. https://doi.org/10.1038/emm.2014.88

29. Wirtz T, Weber T, Kracker S, Sommermann T, Rajewsky K, Yasuda T (2016) Mouse model for acute Epstein–Barr virus infection. Proc Natl Acad Sci 113:13821–13826. https://doi.org/10.1073/pnas.1616574113

30. Huang S, Yasuda T (2021) Pathologically Relevant Mouse Models for Epstein–Barr Virus–Associated B Cell Lymphoma. Front Immunol 12:639844. https://doi.org/10.3389/fimmu.2021.639844

31. Barton E, Mandal P, Speck SH (2011) Pathogenesis and Host Control of Gammaherpesviruses: Lessons from the Mouse. Annu Rev Immunol 29:351–397. https://doi.org/10.1146/annurev-immunol-072710-081639

32. Efstathiou S, Ho YM, Hall S, Styles CJ, Scott SD, Gompels UA (1990) Murine herpesvirus 68 is genetically related to the gammaherpesviruses Epstein-Barr virus and herpesvirus saimiri. J Gen Virol 71:1365–1372. https://doi.org/10.1099/0022-1317-71-6-1365

33. Marathe BM, Mostafa HH, Vogel P, Pascua PNQ, Jones JC, Russell CJ, Webby RJ, Govorkova EA (2017) A pharmacologically immunosuppressed mouse model for assessing influenza B virus pathogenicity and oseltamivir treatment. Antiviral Res 148:20–31. https://doi.org/10.1016/j.antiviral.2017.10.021

34. Chaturvedi UC, Tandon P, Mathur A (1977) Effect of Immunosuppression on Dengue Virus Infection in Mice. J Gen Virol 36:449–458. https://doi.org/10.1099/0022-1317-36-3-449

35. Torii Y, Kawada J, Murata T, Yoshiyama H, Kimura H, Ito Y (2017) Epstein-Barr virus infection-induced inflammasome activation in human monocytes. PLOS ONE 12:e0175053. https://doi.org/10.1371/journal.pone.0175053

36. Perluigi M, Coccia R, Butterfield DA (2012) 4-Hydroxy-2-Nonenal, a Reactive Product of Lipid Peroxidation, and Neurodegenerative Diseases: A Toxic Combination Illuminated by Redox Proteomics Studies. Antioxid Redox Signal 17:1590–1609. https://doi.org/10.1089/ars.2011.4406

37. Wang Y, Xu E, Musich PR, Lin F (2019) Mitochondrial dysfunction in neurodegenerative diseases and the potential countermeasure. CNS Neurosci Ther 25:816–824. https://doi.org/10.1111/cns.13116

38. Espargaró A, Sabate R, Ventura S (2012) Thioflavin-S staining coupled to flow cytometry. A screening tool to detect in vivo protein aggregation. Mol Biosyst 8:2839. https://doi.org/10.1039/c2mb25214g

39. Cribbs DH, Azizeh BY, Cotman CW, LaFerla FM (2000) Fibril Formation and Neurotoxicity by a Herpes Simplex Virus Glycoprotein B Fragment with

Homology to the Alzheimer's Aβ Peptide. Biochemistry 39:5988–5994. https://doi.org/10.1021/bi000029f

40. Singh VK, Kumar S, Tapryal S (2020) Aggregation Propensities of Herpes Simplex Virus-1 Proteins and Derived Peptides: An *In Silico* and *In Vitro* Analysis. ACS Omega 5:12964–12973. https://doi.org/10.1021/acsomega.0c00730

41. Eimer WA, Vijaya Kumar DK, Navalpur Shanmugam NK, Rodriguez AS, Mitchell T, Washicosky KJ, György B, Breakefield XO, Tanzi RE, Moir RD (2018) Alzheimer's Disease-Associated β-Amyloid Is Rapidly Seeded by Herpesviridae to Protect against Brain Infection. Neuron 99:56-63.e3. https://doi.org/10.1016/j.neuron.2018.06.030

42. Cheng W (2012) Cross-reactivity of autoreactive T cells with MBP and viral antigens in patients with MS. Front Biosci 17:1648. https://doi.org/10.2741/4010

43. Greenfield AL, Hauser SL (2018) B-cell Therapy for Multiple Sclerosis: Entering an era: MS: Entering the Era of B-Cell Therapy. Ann Neurol 83:13–26. https://doi.org/10.1002/ana.25119

44. Lassmann H (2018) Multiple Sclerosis Pathology. Cold Spring Harb Perspect Med 8:a028936. https://doi.org/10.1101/cshperspect.a028936

45. Poitelon Y, Kopec AM, Belin S (2020) Myelin Fat Facts: An Overview of Lipids and Fatty Acid Metabolism. Cells 9:812. https://doi.org/10.3390/cells9040812

46. Voskuhl RR, Itoh N, Tassoni A, Matsukawa MA, Ren E, Tse V, Jang E, Suen TT, Itoh Y (2019) Gene expression in oligodendrocytes during remyelination reveals cholesterol homeostasis as a therapeutic target in multiple sclerosis. Proc Natl Acad Sci 116:10130–10139. https://doi.org/10.1073/pnas.1821306116

47. Levy YS, Gilgun-Sherki Y, Melamed E, Offen D (2005) Therapeutic Potential of Neurotrophic Factors in Neurodegenerative Diseases: BioDrugs 19:97–127. https://doi.org/10.2165/00063030-200519020-00003

48. Deleidi M, Jäggle M, Rubino G (2015) Immune aging, dysmetabolism, and inflammation in neurological diseases. Front Neurosci 9:. https://doi.org/10.3389/fnins.2015.00172

49. Boggs JM (2006) Myelin basic protein: a multifunctional protein. Cell Mol Life Sci 63:1945–1961. https://doi.org/10.1007/s00018-006-6094-7

50. Habibi MA, Nezhad Shamohammadi F, Rajaei T, Namdari H, Pashaei MR, Farajifard H, Ahmadpour S (2023) Immunopathogenesis of viral infections in neurological autoimmune disease. BMC Neurol 23:201. https://doi.org/10.1186/s12883-023-03239-x

51. Lamers KJ, de Reus HP, Jongen PJ (1998) Myelin basic protein in CSF as indicator of disease activity in multiple sclerosis. Mult Scler J 4:124–126. https://doi.org/10.1177/135245859800400306

52. Lomakin Y, Arapidi GP, Chernov A, Ziganshin R, Tcyganov E, Lyadova I, Butenko IO, Osetrova M, Ponomarenko N, Telegin G, Govorun VM, Gabibov A, Belogurov A (2017) Exposure to the Epstein–Barr Viral Antigen Latent Membrane Protein 1 Induces Myelin-Reactive Antibodies In Vivo. Front Immunol 8:777. https://doi.org/10.3389/fimmu.2017.00777

53. Jakhmola S, Jonniya NA, Sk MF, Rani A, Kar P, Jha HC (2021) Identification of Potential Inhibitors against Epstein–Barr Virus Nuclear Antigen 1 (EBNA1): An Insight from Docking and Molecular Dynamic Simulations. ACS Chem Neurosci 12:3060–3072. https://doi.org/10.1021/acschemneuro.1c00350

54. Garvin RA (2015) Elevated Phospholipid Transfer Protein in Subjects with Multiple Sclerosis. J Lipids 2015:1–5. https://doi.org/10.1155/2015/518654

55. Marrie RA, Rudick R, Horwitz R, Cutter G, Tyry T, Campagnolo D, Vollmer T (2010) Vascular comorbidity is associated with more rapid disability progression in multiple sclerosis. Neurology 74:1041–1047. https://doi.org/10.1212/WNL.0b013e3181d6b125

56. Laudiero LB, Aloe L, Levi-Montalcini R, Buttinelli C, Schilter D, Gillessen S, Otten U (1992) Multiple sclerosis patients express increased levels of β-nerve

growth factor in cerebrospinal fluid. Neurosci Lett 147:9–12. https://doi.org/10.1016/0304-3940(92)90762-V

57. Acosta CMR, Cortes C, MacPhee H, Namaka MP (2014) Exploring the Role of Nerve Growth Factor in Multiple Sclerosis: Implications in Myelin Repair. CNS Neurol Disord - Drug Targets 12:1242–1256. https://doi.org/10.2174/18715273113129990087

58. Barnhart CD, Yang D, Lein PJ (2015) Using the Morris Water Maze to Assess Spatial Learning and Memory in Weanling Mice. PLOS ONE 10:e0124521. https://doi.org/10.1371/journal.pone.0124521

59. Jurgens HA, Amancherla K, Johnson RW (2012) Influenza Infection Induces Neuroinflammation, Alters Hippocampal Neuron Morphology, and Impairs Cognition in Adult Mice. J Neurosci 32:3958–3968. https://doi.org/10.1523/JNEUROSCI.6389-11.2012

60. Barnhart CD, Yang D, Lein PJ (2015) Using the Morris Water Maze to Assess Spatial Learning and Memory in Weanling Mice. PLOS ONE 10:e0124521. https://doi.org/10.1371/journal.pone.0124521

61. Armien AG, Hu S, Little MR, Robinson N, Lokensgard JR, Low WC, Cheeran MC (2010) Chronic Cortical and Subcortical Pathology with Associated Neurological Deficits Ensuing Experimental Herpes Encephalitis. Brain Pathol 20:738–750. https://doi.org/10.1111/j.1750-3639.2009.00354.x

62. Liedtke W, Opalka B, Zimmermann CW, Lignitz E (1993) Age distribution of latent herpes simplex virus 1 and varicella-zoster virus genome in human nervous tissue. J Neurol Sci 116:6–11. https://doi.org/10.1016/0022-510X(93)90082-A

63. Li F, Wang Y, Yu L, Cao S, Wang K, Yuan J, Wang C, Wang K, Cui M, Fu ZF (2015) Viral Infection of the Central Nervous System and Neuroinflammation Precede Blood-Brain Barrier Disruption during Japanese Encephalitis Virus Infection. J Virol 89:5602–5614. https://doi.org/10.1128/JVI.00143-15

64. Jurgens HA, Amancherla K, Johnson RW (2012) Influenza Infection Induces Neuroinflammation, Alters Hippocampal Neuron Morphology, and Impairs Cognition in Adult Mice. J Neurosci 32:3958–3968. https://doi.org/10.1523/JNEUROSCI.6389-11.2012

65. Shih R-H, Wang C-Y, Yang C-M (2015) NF-kappaB Signaling Pathways in Neurological Inflammation: A Mini Review. Front Mol Neurosci 8:77. https://doi.org/10.3389/fnmol.2015.00077

66. Kyriatzis G, Bernard A, Bôle A, Pflieger G, Chalas P, Masse M, Lécorché P, Jacquot G, Ferhat L, Khrestchatisky M (2021) Neurotensin receptor 2 is induced in astrocytes and brain endothelial cells in relation to neuroinflammation following pilocarpine-induced seizures in rats. Glia 69:2618–2643. https://doi.org/10.1002/glia.24062

67. De Chiara G, Piacentini R, Fabiani M, Mastrodonato A, Marcocci ME, Limongi D, Napoletani G, Protto V, Coluccio P, Celestino I, Li Puma DD, Grassi C, Palamara AT (2019) Recurrent herpes simplex virus-1 infection induces hallmarks of neurodegeneration and cognitive deficits in mice. PLoS Pathog 15:e1007617. https://doi.org/10.1371/journal.ppat.1007617

68. Itzhaki RF, Wozniak MA (2008) Herpes simplex virus type 1 in Alzheimer's disease: the enemy within. J Alzheimers Dis JAD 13:393–405. https://doi.org/10.3233/jad-2008-13405

69. Assistant Lecturer in Medical Microbiology in Erbil medical technical institute/ Erbil Polytechnic University, Bakir SH, Rasoul AA, Neurology specialist FIBMS (Neurology) lecturer in Kurdistan Board for medical specialties., Hamad MS, Neurology lecturer in College of Medicine/ Hawler Medical University, Hussain SG, Assist. Professor in Immunology in College of Medicine/ Hawler Medical University (2017) Multiple Sclerosis: Possible Role of Epstein-Barr virus in the Etiology and Relapses. Adv Med J 3:26–32. https://doi.org/10.56056/amj.2017.20

70. Tejada-Simon MV, Zang YCQ, Hong J, Rivera VM, Zhang JZ (2003) Cross-reactivity with myelin basic protein and human herpesvirus-6 in multiple sclerosis. Ann Neurol 53:189–197. https://doi.org/10.1002/ana.10425

71. Augutis K, Axelsson M, Portelius E, Brinkmalm G, Andreasson U, Gustavsson MK, Malmeström C, Lycke J, Blennow K, Zetterberg H, Mattsson N (2013) Cerebrospinal fluid biomarkers of β-amyloid metabolism in multiple sclerosis. Mult Scler J 19:543–552. https://doi.org/10.1177/1352458512460603

72. Luczynski P, Laule C, Hsiung G-YR, Moore GRW, Tremlett H (2021) Coexistence of Multiple Sclerosis and Alzheimer Disease Pathology: A Case Series. J Neurol Res 11:60–67. https://doi.org/10.14740/jnr666

73. Londoño DP, Arumaithurai K, Constantopoulos E, Basso MR, Reichard RR, Flanagan EP, Keegan BM (2022) Diagnosis of coexistent neurodegenerative dementias in multiple sclerosis. Brain Commun 4:fcac167. https://doi.org/10.1093/braincomms/fcac167

74. Indari O, Chandramohanadas R, Jha HC (2021) Epstein–Barr virus infection modulates blood–brain barrier cells and its co-infection with *Plasmodium falciparum* induces RBC adhesion. Pathog Dis 79:ftaa080. https://doi.org/10.1093/femspd/ftaa080

75. PLOS ONE Editors (2021) Expression of Concern: Early Events Associated with Infection of Epstein-Barr Virus Infection of Primary B-Cells. PloS One 16:e0256674. https://doi.org/10.1371/journal.pone.0256674

76. Halder S, Murakami M, Verma SC, Kumar P, Yi F, Robertson ES (2009) Early Events Associated with Infection of Epstein-Barr Virus Infection of Primary B-Cells. PLoS ONE 4:e7214. https://doi.org/10.1371/journal.pone.0007214

77. Yuen K-S, Chan C-P, Kok K-H, Jin D-Y (2017) Mutagenesis and Genome Engineering of Epstein–Barr Virus in Cultured Human Cells by CRISPR/Cas9. In: Reeves A (ed) In Vitro Mutagenesis. Springer New York, New York, NY, pp 23–31

78. Kashyap D, Baral B, Jakhmola S, Singh AK, Jha HC (2021) Helicobacter pylori and Epstein-Barr Virus Coinfection Stimulates Aggressiveness in Gastric Cancer through the Regulation of Gankyrin. mSphere 6:e00751-21. https://doi.org/10.1128/mSphere.00751-21

79. Kim S-W, Roh J, Park C-S (2016) Immunohistochemistry for Pathologists: Protocols, Pitfalls, and Tips. J Pathol Transl Med 50:411–418. https://doi.org/10.4132/jptm.2016.08.08

Chapter 5: Demethoxycurcumin and Rosmarinic acid are plausible inhibitors against glycoprotein 350 of Epstein Barr virus in the neuronal milieu

5.1 Graphical abstract
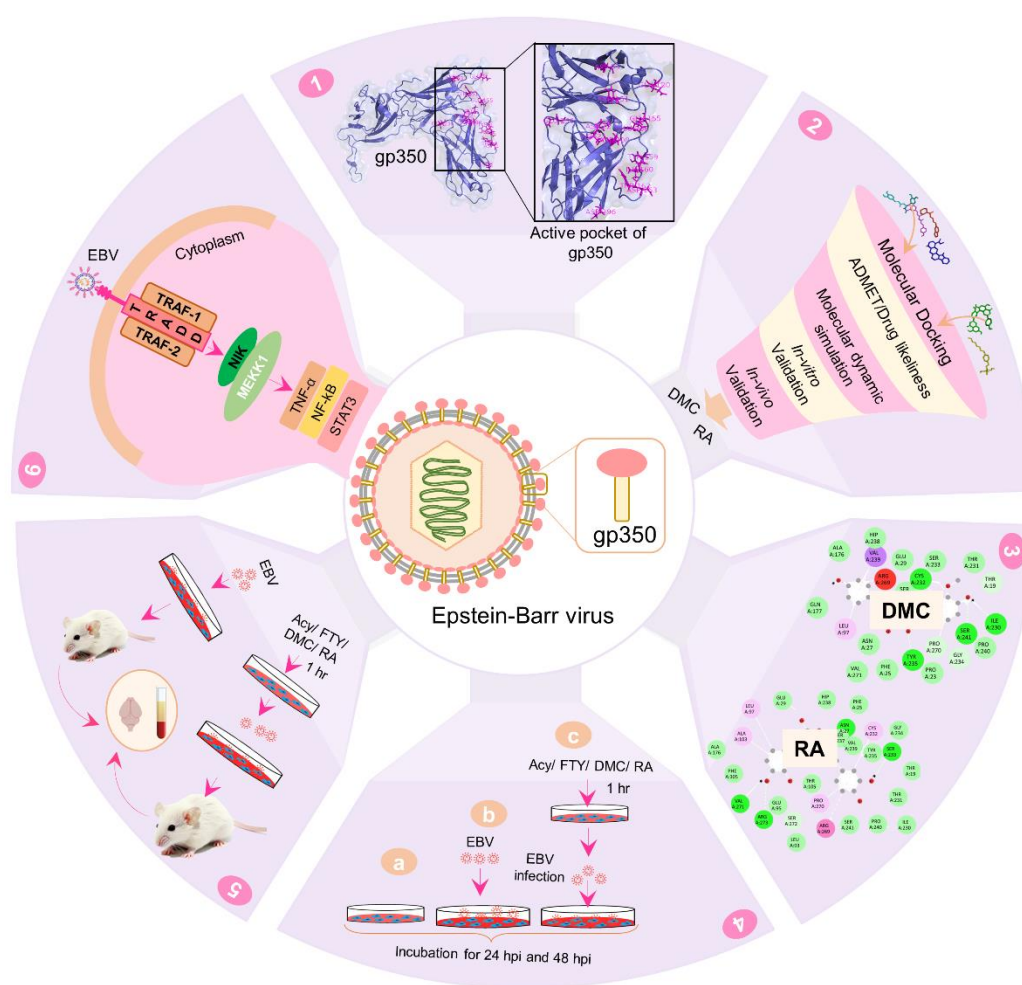
5.2 Abstract

The Epstein-Barr virus (EBV) proteins like EBNA1, LMP1, BZLF1 and gp350 have shown continuous presence in the cerebrospinal fluid of patients suffering from neurological disorders. Earlier reports showed that EBV establishes its infection in brain cells, hence, the limited information is available on its entry mechanisms. EBV proteins like gp350 have a key role in the viral tropism. Thereby, in the present study, the extra virion region of gp350 was targeted *in-silico* with phytocompounds. Further, based on the binding affinity, phytocompounds were subjected to molecular dynamics

simulation for 100 ns. Compounds, namely demthoxycurumin (DMC) and rosmarinic acid (RA) were considered for further validation *in-vitro* and *in-vivo*. Our study indicated a decline of gp350 in DMC+EBV and RA+EBV samples compared to EBV-infected samples. EBV-exposed IMR-32 cells have shown an increase in transcript level of neuro-inflammatory markers like *il-1β, il-6, il-10, il-13* and *tnf-α* while DMC+EBV and RA+EBV exhibited a decrease in these markers. Likewise, the levels of TNF-α, NF-kB and STAT3, which play crucial roles in the inflammatory cascades have shown temporal mitigation. Mice hippocampal cells showed apoptotic restoration in phytocompound exposed groups. Inflammatory factor TNF-α found to be elevated in EBV-exposed samples and indicated decline upon treatment drugs. Therefore, it suggests DMC and RA showed appreciable anti-gp350 effects, and it can be used as therapeutic agents.

Keywords: Glycoprotein 350, Epstein-Barr virus, demethoxycurcumin, rosmarinic acid

5.3 Introduction

Epstein-Barr virus (EBV) infects nearly 90% of the adult human population worldwide and only a few individuals develop EBV-related diseases [1]. This virus is associated with infectious mononucleosis (IM), several cancers and neurological diseases. Numerous studies have reported that EBV proteins like EBNA1, EBNA3A, LMP1, LMP2A, BZLF1, gp350 and BNLF-2a are associated with multiple sclerosis (MS), Alzheimer's disease (AD), Parkinson's disease (PD), meningitis and encephalitis [2]. A meta-analysis revealed that EBV-positive individuals are at a 15 times higher risk of developing MS than EBV-negative individuals [3]. The precise mechanism of EBV's association with neurological diseases is still elusive. This virus maintains its tropism in epithelial and B-cells. Previously, reports have suggested EBV entry into B-cells involves gp350 and gH/gL/gp42 protein complexes. The gp350/220 is a heavily glycosylated protein having 907 residues that express in two spliced forms of 350 and 220 kDa. The N-terminal domain consists of 470 residues of protein and plays an essential role in binding with human cellular complement receptor 2 (CR2/CD21) of B-lymphocytes [4]. Gp350 can also trigger the attachment of EBV with epithelial cells [5]. Blocking of gp350 possibly aids in mitigating EBV entry into epithelial or B-cells and eventually subside the EBV-associated pathologies [5].

Numerous anti-EBV compounds are predicted and proved to target the EBV latent and lytic cycles [6]. Till now, no FDA (Food and Drug Administration) or EMA (European Medicines Agency) approved anti-EBV drug is available [7]. In contrast, a wide range of phytochemicals, namely andrographolide, quercetin, curcumin, sulforaphane, epigallocatechin gallate, moronic acid and glycyrrhizic acid have shown anti-EBV activities through *in-vitro* studies [8]. The often-used antivirals show limited efficacy and severe adverse effects [9]. In comparison, herbal extracts are considered as good options due to their antiviral properties and fewer side effects [10]. The antiviral mechanism of phytochemicals can be explained based on their scavenging capacities, antioxidant activities, inhibition of DNA/RNA synthesis, inhibition of virion production or inhibition of viral entry. For example, curcumin effectively inhibits Kaposi's sarcoma-associated herpesvirus (KSHV) replication by altering the redox reaction of apurinic/apyrimidinic endonuclease 1 (APE1) [11]. Also, rosmarinic acid (RA) is a naturally occurring phenolic ester which has shown antiviral activity against herpes simplex viruses (HSV-1) in kidney epithelial cells [12]. In addition, the infection of EBV exhibits atherogenic lipid changes in IM [13]. It alters the metabolism of lipids and elevates the level of free fatty acids, proinflammatory cytokines and low-density lipoprotein receptors (LDLR) for endocytosis of cholesterol-rich LDL in nasopharyngeal cells [14], [15]. Jakhmola et al. showed EBV infection in the CNS glial cells (i.e., U-87 MG) and observed a significant increase in inflammatory genes profile [16]. Notably, increased levels of neurotrophic factors such as BDNF, NGF, CNTF and VEGF were also detected in patients with EBV-induced meningitis, leading to neuronal inflammation [17]. Thus, EBV has an important undeciphered role in neurological disorders. Furthermore, drugs against EBV may help to subside the EBV-associated pathologies.

This work aimed to find out natural compounds against the EBV's gp350. Hereby, we have screened 79 phytochemicals with anti-viral as well as neuroprotective properties and an FDA-approved drug acyclovir (Acy), fingolimod (FTY) was considered as a positive control. Their binding affinity with gp350 were examined using *in-silico* approaches. Strongly bound ligands such as demethoxycurcumin (DMC) and RA were selected for *in-vitro* and *in-vivo* evaluation. Moreover, the effects of DMC and RA were also assessed on cell inflammatory markers such as *il-1β, il-6, il-10, il-13* and *tnf-α*. A downstream cascade of TNF-α was explored by using protein markers like

NF-kB and STAT3. Subsequently, the effect of phytocompounds were validated at *in-vivo* level. Overall, our results highlighted the anti-gp350 activity of DMC and RA that can further be used against gp350 to combat EBV infection.

5.4 Result

5.4.1 Molecular docking of phytochemicals

To understand the blocking of gp350 by these phytochemicals, we have performed site-specific docking on the extra virion region (CR2 interacting region) of gp350 (Figure 5.1).
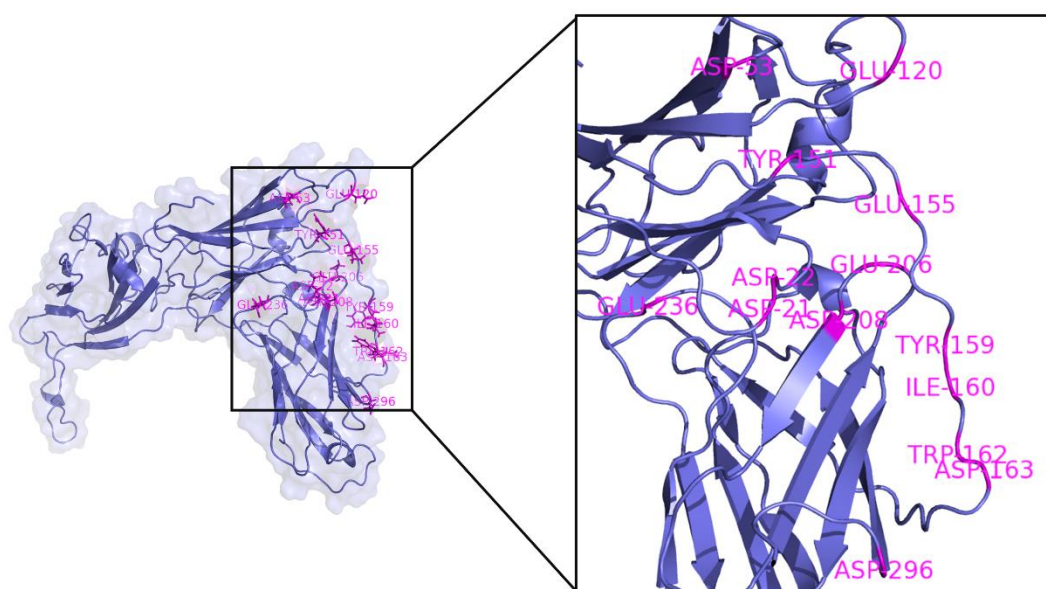
Figure 5.1: Representation of labelled gp350 pocket used for site specific docking in the region around gp350-CR2 and anti-gp350 mAb interaction.
The labelled pocket includes amino acids: E21, D22, D53, E119, Y151, E155, Y159, I160, W162, D163, E201, D208, E210, E214, D215, E236, D296.

Among all the considered ligands, piperin, ajmalicine, amentoflavone, DMC, RA and FTY bound strongly to gp350 with binding affinity -9.2, -9.1, -9.0, -8.9, -8.8 and -8.0 kcal/mol respectively (Table 5.1). All ligands were checked for their drug likeliness and ADMET properties followed by stable binding interaction with gp350 via molecular dynamics simulation.

Table 5.1: Description of active phytocompounds and their respective plants.

S. No	Neuroprotective and anti-viral plants	Neuroprotective and anti-viral bioactive compounds (PubChem ID)	Binding affinity (kcal/mol)
1.	Piper nigrum	Piperin (638024)	-9.2
2.	Rauvolfia serpentina	Ajamalicine (387095918)	-9.1
3.	Ginkgo biloba	Amentoflavone (5281600)	-9
4.	Curcuma longa	Demethoxycurcumin (5469424)	-8.9
5.	Salvia triloba	Rosmarinic acid (5281792)	-8.8
6.	Rauvolfia serpentina	Serpentine (73391)	-8.7
7.	Rauvolfia serpentina	Ajmaline (6100671)	-8.6
8.	Curcuma longa	Curcumin (969516)	-8.6
9.	Withania somnifera	Withanolide D (161671)	-8.5
10.	Tribulus terrestris	Hecogenin (91453)	-8.5
11.	Adhatoda vasica	Luteolin (5280445)	-8.4
12.	Salvia triloba	Proanthocyanidin (108065)	-8.4
13.	Salvia triloba	Quercetin (5280343)	-8.4
14.	Emblica officinalis	Ellagic acid (5281855)	-8.4
15.	Entandrophragma angolense	7α-obacunol (57390140)	-8.3
16.	Nardostachys jatamansi	Oroselol (160600)	-8.3
17.	Corydalis ternate	Protopine (4970)	-8
18.	Terminalia arjuna	Arjunic acid (15385516)	-8
19.	Emblica officinalis	Corilagin (73568)	-7.9
20.	Withania somnifera	Withaferin A (265237)	-7.8
21.	Withania coagulaus	17beta-Hydroxywithanolide K (44562998)	-7.7
22.	Adhatoda vasica	Vasicinolone (158720)	-7.7
23.	Ocimum sanctum	Oleanolic acid (10494)	-7.7

S. No	Neuroprotective and anti-viral plants	Neuroprotective and anti-viral bioactive compounds (PubChem ID)	Binding affinity (kcal/mol)
24.	Peganum harmala	Harmalol (3565)	-7.7
25.	Tabernaemontana divaricata	α-Amyrin (73170)	-7.6
26.	Grapes	Resveratol (445154)	-7.6
27.	Nardostachys jatamansi	β-eudesmol (91457)	-7.6
28.	Withania somnifera	Warfarin (54678486)	-7.5
29.	Rauvolfia serpentina	Yohimbine (8969)	-7.5
30.	Adhatoda vasica	Kaempferol (5280863)	-7.5
31.	Ferula assafoetida	Germacrene B (5281519)	-7.5
32.	Ptychopetalum olacoides	Lupeol (259846)	-7.5
33.	Brassica species	Brassicasterol (5281327)	-7.4
34.	Centella asiatica/gotu kola	Asiatic acid (119034)	-7.4
35.	Adhatoda vasica	Vasicinol (442934)	-7.4
36.	Peganum harmala	Harmine (5280953)	-7.4
37.	Baccopa monnieri/Brahmi	Betulinic acid (64971)	-7.3
38.	Holarrhena antidysenterica/Kutaj	Conessine (441082)	-7.2
39.	Terminalia arjuna	Arjunolic acid (73641)	-7.2
40.	Adhatoda vasica	Vasicine (667496)	-7.2
41.	Nardostachys jatamansi	Nardol (101286216)	-7.2
42.	Nardostachys jatamansi	Angelicin (10658)	-7
43.	Terminalia chebula	Arjungenin (12444386)	-7
44.	Peganum harmala	Norharmane (64961)	-7
45.	Terminalia chebula	Chebulic acid (71308174)	-7
46.	Ganoderma lucidum	Ganoderic acid A (471002)	-6.9
47.	Panax ginseng	Ginsenoside F1 (9809542)	-6.8

S. No	Neuroprotective and anti-viral plants	Neuroprotective and anti-viral bioactive compounds (PubChem ID)	Binding affinity (kcal/mol)
48.	Rauvolfia serpentina	Reserpine (5770)	-6.8
49.	Emblica officinalis	Gallic acid (370)	-6.8
50.	Adhatoda vasica	Vasicol (92470596)	-6.8
51.	Anogeissus leiocarpus	Flavogallonic acid (71308200)	-6.7
52.	Tabernaemontana divaricata	Voafinidine (11121012)	-6.7
53.	Khaya senegalensis	Rel-Khayseneganin D (71658779)	-6.6
54.	Tabernaemontana divaricata	β-sitosterol (222284)	-6.6
55.	Baccopa monnieri/Brahmi	Stigmastanol (241572)	-6.6
56.	Zingiber Officinale	Shogaol (5281794)	-6.6
57.	Withania somnifera	Anaferine (443143)	-6.5
58.	Zingiber Officinale	Gingerol (442793)	-6.5
59.	Brassica species	Sinapic acid (637775)	-6.4
60.	Mucuna pruriens/velvet bean	L-dopa (6047)	-6.4
61.	Salvia triloba	Ferulic acid (445858)	-6.4
62.	Acorus calamus	β-asarone (5281758)	-6.3
63.	Acorus calamus	α-asarone (636822)	-6.1
64.	Zingiber Officinale	Zingerone (31211)	-6
65.	Origanum ehrenbergii	Carvacrol (10364)	-6
66.	Abrus precatorius	Abrine (160511)	-5.9
67.	Syzygium aromaticum	Trans-β-caryophyllene (5281515)	-5.8
68.	Mentha spicata	Carvone (7439)	-5.8
69.	Cymbopogon schoenanthus	Pipertone (92998)	-5.8
70.	Acorus calamus	Methyleugenol (7127)	-5.8
71.	Nardostachys jatamansi	Calarene (28481)	-5.7
72.	Origanum ehrenbergii	Thymol (6989)	-5.7

S. No	Neuroprotective and anti-viral plants	Neuroprotective and anti-viral bioactive compounds (PubChem ID)	Binding affinity (kcal/mol)
73.	Syzygium aromaticum	α-Humulene (5281520)	-5.6
74.	Mentha spicata	Limonene (22311)	-5.6
75.	Syzygium aromaticum	Eugenol (3314)	-5.5
76.	Ptychopetalum olacoides	α-pinene (6654)	-5.3
77.	Ptychopetalum olacoides	β-pinene (14896)	-5.3
78.	Nardostachys jatamansi	Elemol (92138)	-5.3
79.	Brassica species	Sinapine (5280385)	-5
80.	FDA approved	Fingolimod (107970)	-8
81	FDA approved	Acyclovir (135398513)	-6.3

5.4.2 ADMET and drug likeliness of selected phytochemicals

ADMET stands for drug candidates' absorption, distribution, metabolism, excretion, and toxicity (ADMET) properties (Table S2-S6). It plays an essential role in early-stage drug discovery and screening of druggable compounds which further can be investigated *in-vitro* [18]. Here we analysed the ADMET properties of the selected phytochemicals. Notably, all these compounds were recorded to have intestinal permeability of <50%. (Table S2). Considering the lipophilicity of DMC and RA scored 2.458 and -3.347 log p-values respectively which eventually suggests their potential to cross blood-brain barrier (Table S3). Top compounds have not shown any toxicity i.e., all simulated ligands were tested non-mutagenic via AMES test (Table S2E). Moreover, the drug likeability of the natural compounds was predicted using the Lipinski rule of five (Table S7) and suggested favourable drug molecule of all the top ligands [19].

5.4.3 Molecular dynamic simulation

MD simulation was applied to investigate the time-dependent dynamics of protein atoms and the stability of the ligands at the site mapped by the grid for docking. Based on molecular docking results of the phytochemicals, MD simulations were performed to interpret the dynamics of apo-gp350 (as control) and gp350-piperin/ ajamlicine/ amentoflavone/ DMC/ RA/ FTY complexes for 100 ns. As per the observations, the stable interactions between the protein and ligands increased with simulation time. Parameters such as root mean square deviation (RMSD), root mean square fluctuations (RMSF) and the radius of gyration (Rg) were analysed to scrutinize the dynamic behaviour of the system. RMSD is a parameter that provides information about the stability of the simulated system which was analysed for the protein backbone with respect to time as depicted in Figure 5.2. The gp350-fingolimod showed very stable binding throughout the simulation process. The gp350-DMC/ajmalicine complex was also stable till 80 ns with slight fluctuation at 40 and 60 ns. Piperin and amentoflavone showed the lowest binding affinity during molecular docking, yet these were the most oscillating complexes during the simulation. Contrarily, the RA-gp350 complex showed slight fluctuation till 25 ns, and after that, it remained stable till 100 ns (Figure 5.2).

Nonetheless, for depicting the per-residue fluctuation of the protein-ligand bound complex, the RMSF in six complexes and apoprotein was monitored. The RMSF parameters featured the possible protein motions involving all residues of all the systems. Figure 5.2 showed the RMSF plot of gp350 with or without all 6 ligands. Slight fluctuations were observed in the region of Ser190 of gp350 in the case of gp350-amentoflavone. Similarly, a fluctuation was observed in the gp350-fingolimod near residue number Gln300 of gp350 (Figure 5.2). No significant changes were observed for the residues compared to apo-protein. Additionally, the Rg plots provide insight into the compactness of the protein during the simulation. Also, it helps to analyse the structural drifts in the protein complexes. Gp350 in the presence of ligands such as RA and piperin showed major fluctuation. RA showed major inconsistency after 40 ns whereas piperin showed from 20 to 40 ns and at 100 ns. Protein-FTY complex also showed minor variations in the Rg plot from 80 to 100 ns of simulation (Figure 5.2). Hereby, we observed that in the presence of ligands, there are few significant changes in the compactness of gp350 in the complex with RA and piperin.
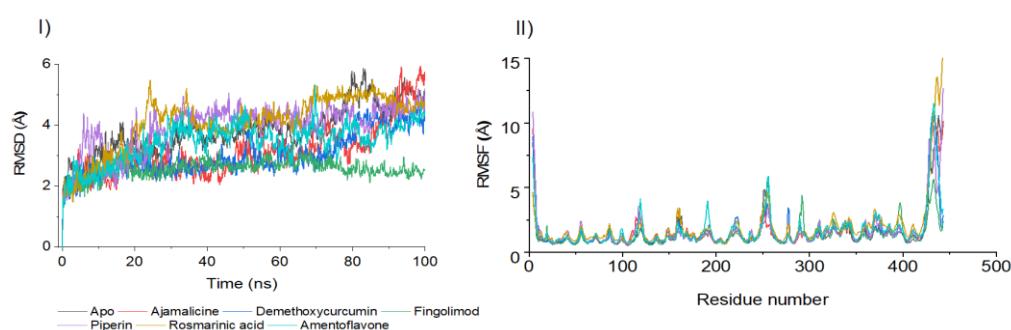
Figure 5.2: Ilustration of RMSD and RMSF plot of apo-gp350 and gp350-piperin/ ajmalicine/ amentoflavone/ demethoxycurcumin/ rosmarinic acid/ fingolimod complexes.
I). RMSD plot in the presence and absence of ligands for 100ns. II) RMSF plot ligands-gp350 complexes have not shown major fluctuations compared to apo-gp350 during simulation. C) Rg of gp350 with and without ligands. gp350-rosmarinic acid showed fluctuation in Rg, while gp350-piperin and gp350-fingolimod showed slight alterations compared to apo-gp350.

Lastly, we investigated the crucial residues involved in the binding of gp350-ligand complexes through 2D structures of all the complexes (Figure 5.3). All ligands interact with gp350 through strong (H-bond) and weak (π−alkyl, π−σ, π−cation, unfavourable donor-donor, and halogen) interactions observed using the discovery studio 2D

visualization tool (Figure 5.3). Piperin interacts with gp350 through several weak interactions and H-bond such as Thr231 and Ser241 (Figure 5.3). Further, Cys232, Glu236 and Ser241 interact with ajmalicine while Arg20, and Asn229 Ile230, Cys232 and Ser241 build H-bond with amentoflavone (Figure 5.3). DMC forms with more H-bonds at position Thr19, Ile230, Cys232, Gly234, Thr235, Ser241 and Pro270 whereas RA links with Asn27, Ser233, Val217, Ser272 and Arg273 (Figure 5.3). In contrast, FTY bridges the H-bond with Glu29 and Ser237 (Figure 5.3).
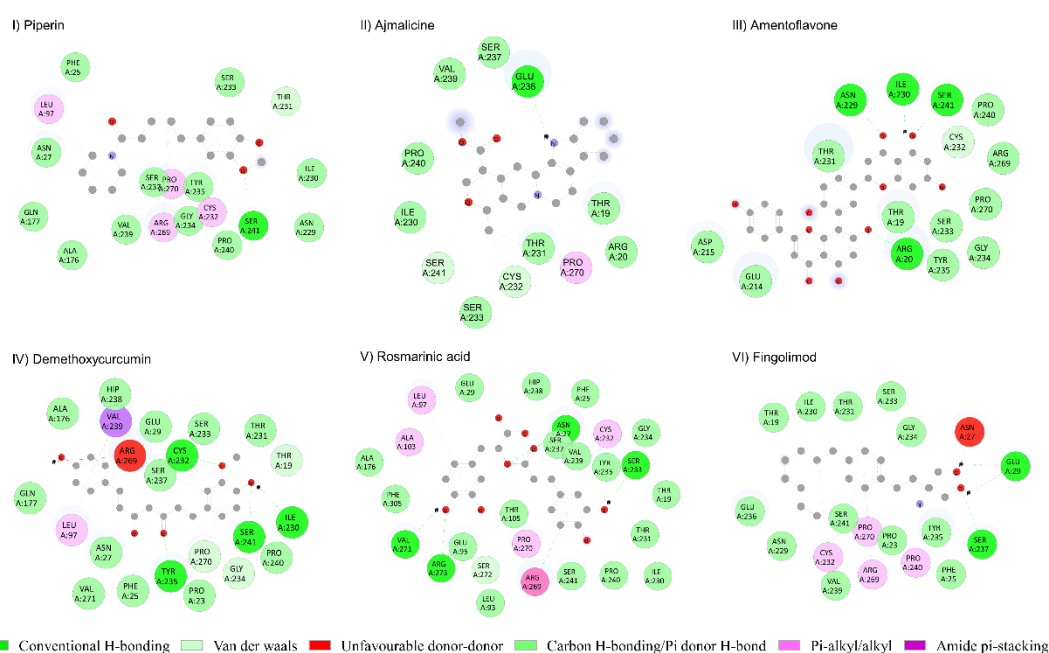
Figure 5.3: 2D visualization of gp350-piperin/ ajmalicine/ amentoflavone/ demethoxycurcumin/ rosmarinic acid/ fingolimod.
These ligands remained bound to gp350 throughout the simulation, establishing stable connections.

5.4.4 Demethoxycurcumin and Rosmarinic acid curtail the level of gp350

DMC and RA have an antiviral effect against several viral infections [11], [12]. For evaluating the anti-gp350 role of DMC and RA, the level of gp350 (transcript and protein) was assessed post-EBV infection to IMR-32. The inhibitory concentration 50 (IC_{50}) value of each phytochemical was evaluated through MTT assay. IC_{50} of Acy, FTY, DMC and RA are 195.8 μM, 12.39 μM, 13.26 μM and 1.70 mM, respectively (Figure 5.4). For further experiments, 70 μM and 5 μM concentration was used for Acy, FTY/DMC, while 250 μM concentration was used for RA because more than 90% of cells were alive at these doses (Figure 5.4). Further, the virus titre was

calculated as mentioned previously [16] on the IMR-32 cells through qRT-PCR and ultimately multiplicity of infection (MOI) 5 was used for the all the further experiments (Figure 5.4).
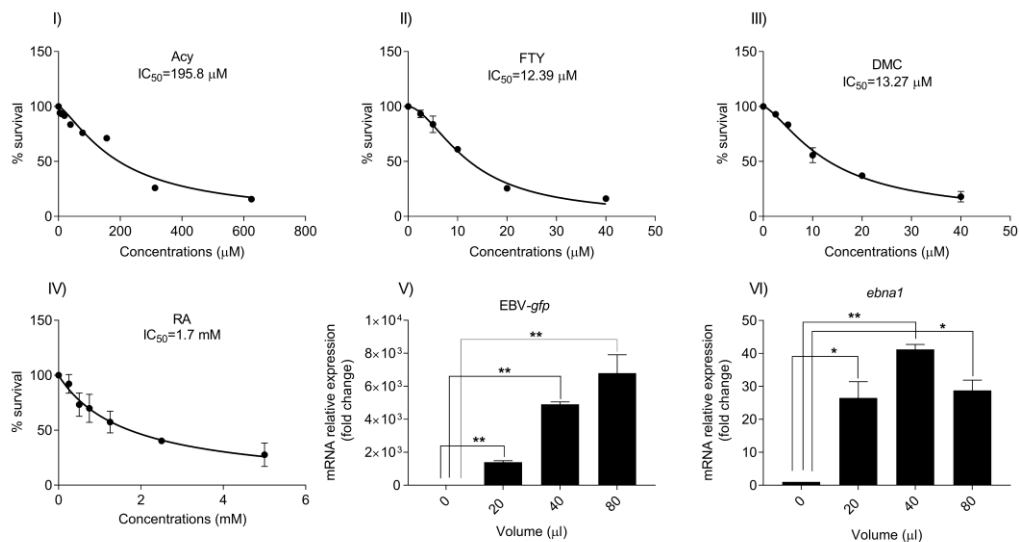
Figure 5.4: Cell viability and EBV titer determination.
Inhibitory concentration 50 (IC_{50}) for Acy, FTY, DMC and RA were 195.8 μM, 12.29 μM, 13.27 μM and 1.70 mM. EBV titer determination on IMR-32 cells through qRT-PCR. MOI 5 was used for the rest of all the experiments and 50 ul of dissolved EBV corresponds to 5 MOI.

The mRNA level of *gp350* in the EBV-infected neurons was significantly upregulated ($p<0.05$) compared to uninfected cells (Figure 5.5). Treatment with FTY, DMC and RA before EBV infection at 48 hrs revealed a significant decrease ($p<0.05$, $p<0.01$ and $p<0.01$) in *gp350* expression (Figure 5.5). Transcript result of gp350 was verified through immunofluorescence (IF) assay (Figure 5.5). IF revealed a significant reduction in the gp350 intensity upon exposure to Acy, FTY, DMC and RA compared to EBV infection at 48 hrs ($p<0.05$ and $p<0.01$) (Figure 5.5).
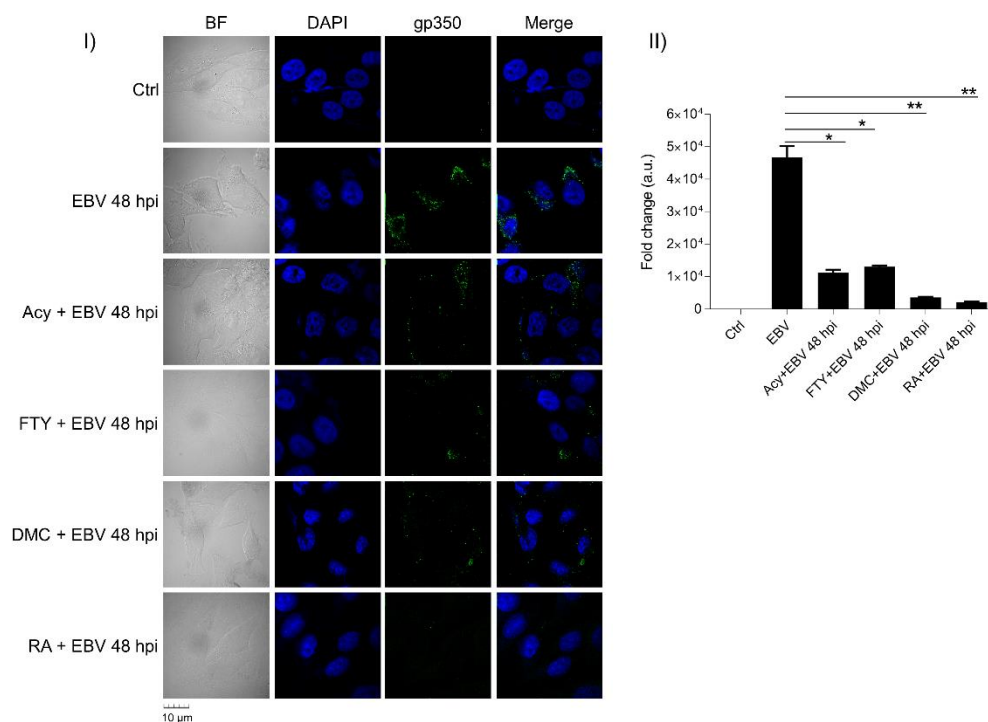
Figure 5.5: Decline in the gp350 levels upon exposure to DMC and RA.
I-II) Representation of gp350 immunofluorescence. A significant reduction in the intensity of gp350 was observed in neuronal cells when subjected to 48 hrs of EBV infection. III) Depiction of the transcript level of gp350 post-EBV infection. At 48 hpi gp350, mRNA level was significantly reduced in phytocompound-treated samples compared to EBV-infected IMR-32 cells. Represented data experiments have been performed on two biologicals and two technical replicates. In the given plots; the *x*-axis, sample types; *y*-axis, and fold change with respect to EBV-infected samples. Two samples t-test was used where *p*-values of <0.05, <0.01 and <0.0001 are considered statistically significant and are represented with #, ## and ### respectively. The increase and decrease are represented by * and # respectively. This experiment was performed on three biological replicates.

5.4.5 Blocking of EBV-gp350 can reduce inflammation in the IMR-32 cells

The infection of EBV is known to initiate several autoimmune and inflammatory cascades in cells like B-lymphocytes and nasopharyngeal epithelial cells [20]. Thus, for evaluating the effect of phytochemicals on EBV-mediated changes in the neuronal cells, the inflammatory (*il-1β, il-6, il-10, il-13, tnf-α*) and neurotrophic (*vegf, ngf, bdnf, and cntf*) factors profile was investigated at mRNA level. Also, virus-specific genes such as *EBV nuclear antigen 1* (*ebna1)* and virus-tagged protein [EBV-*Green fluorescent protein* (*gfp)*] were examined to check for successful EBV infection into IMR-32 cells. Expression of *ebna1* and EBV-*gfp* was found to be significantly high at both 24 (p<0.01) and 48 hrs (p<0.01) compared to the uninfected IMR-32 (Figure

5.6). Pre-treatment with Acy+EBV, FTY+EBV, DMC+EBV and RA+EBV showed a significant decrease (p<0.05) in both the markers at 24 and 48 hrs (Figure 5.6)
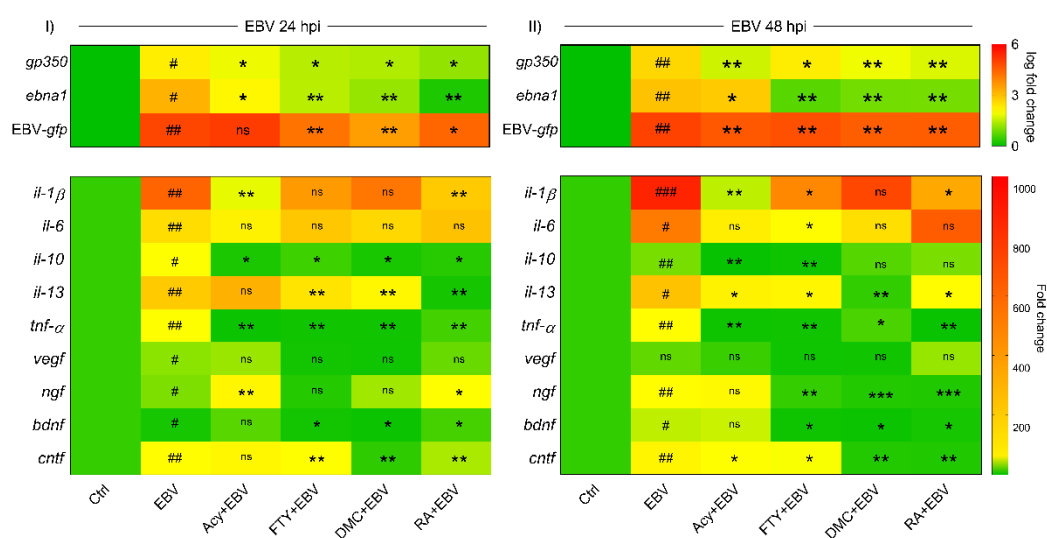
Figure 5.6: Pre-treatment of DMC and RA reduced cell-inflammatory genes at the transcript level in neuronal cells.
I-II) EBV marker genes *ebna1* and *gfp* showed EBV infection in IMR-32 cells at 24 and 48 hrs. Both *ebna1* and *GFP* showed mitigated mRNA levels in DMC and RA treated samples. I-II) Inflammatory genes like *il-1β, il-6, il-10, il-13* and *tnf-α* showed decline in transcript level in DMC+EBV and RA+EBV treated samples. Neurotrophic factors *vegf, ngf, bdnf* and *cntf* also decreased in both treatments. We observed that inflammatory and neurotrophic factor genes were appreciably decreased compared to the FDA-approved drug, fingolimod. In the above graphs; the *x*-axis, sample types; *y*-axis, and fold change with respect to EBV-infected samples. Two samples t-test was used where *p*-values of <0.05, <0.01 and <0.0001 are considered statistically significant and are represented with #, ## and ### respectively. The increase and decrease are represented by * and # respectively.

Further, the assessment of inflammatory markers post-EBV infection showed upregulation at 24 and 48 hrs compared to uninfected cells (Figure 5.6). At 24 hrs, DMC and RA have the highest anti-inflammatory activity and significantly reduced the transcript level of all the studied inflammatory markers (*il-1β, il-10, il-13, tnf-α*; p<0.01, <0.05, <0.01, <0.01) except *il-6* (Figure 5.6). Further at 48 hrs, *il-1β, il-13,* and *tnf-α* showed significant reduction (p<0.05, <0.05, <0.01) after administration with RA+EBV, Acy+EBV and FTY+EBV pre-treated sample (Figure 5.6). While DMC+EBV reduced the transcripts of *il-13* and *tnf-α* significantly (p<0.01 and p<0.05), no change was observed in the level of *il-1β* compared to EBV infection (Figure 5.6). DMC+EBV and RA+EBV treatment showed no effect on the expression

level of *il-6* and *il-10,* whereas FTY+EBV treatment showed significant downregulation ($p<0.05$ and *$p<0.01$*) (Figure 5.6).

EBV infection also triggers the upregulation of specific neurotrophic factors, which play a crucial role in neural inflammation. Neurotrophic factors, *vegf, ngf, bdnf,* and *cntf,* showed overexpression upon EBV infection relative to uninfected neural cells. Pre-treatment of FTY+EBV, DMC+EBV and RA+EBV in 48 hrs samples showed significant downregulation of *ngf* and *bdnf* with $p<0.0001$ and $p<0.05$, respectively (Figure 5.6). In contrast, at 24 hrs, *ngf* showed no statistically significant changes. Additionally, the level of *cntf* was found to be downregulated after exposure to Acy+EBV, FTY+EBV, DMC+EBV and RA+EBV compared to EBV-infected IMR-32 ($p<0.01$) at both time points (Figure 5.6).

5.4.6 NF-kB, STAT3 and TNF-α levels get diminished temporally in the neuronal cells

EBV infection activate the inflammatory cascades e.g., TNF-α in the B- and brain cells. TNF-α is an inflammatory cytokine produced during acute inflammation and is responsible for a diverse range of signalling events within cells, leading to necrosis or apoptosis [21]. It activates STAT3 and NF-kB in the downstream signalling. In continuation to our transcriptome study of *tnf-α*, the protein level of TNF-α was assessed. Similar to the transcript expression upon EBV infection, the TNF-α level exhibited a significant decline ($p<0.05$) at 48 hrs compared to EBV infection (Figure 5.7). The level of TNF-α is further regulated by transcription factor NF-kB. NF-kB have shown mitigation ($p<0.01$) only at 24 hrs in Acy+EBV, FTY+EBV, DMC+EBV and RA+EBV samples while we observed a decrease ($p<0.01$) in STAT3 at both the time points (Figure 5.7). These results suggest a decline in the inflammatory moieties upon exposure to DMC and RA.
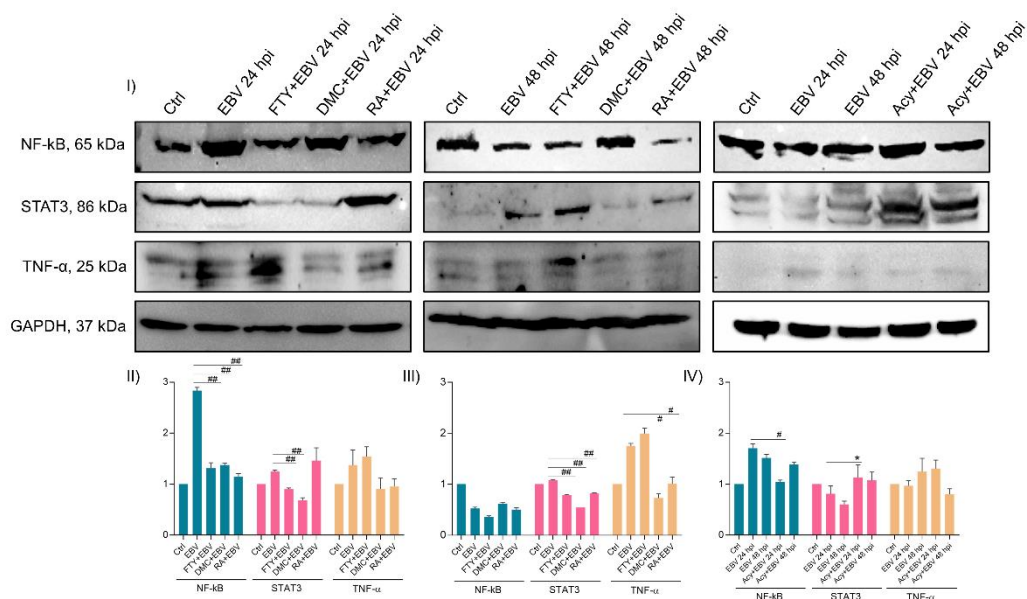
Figure 5.7: Evaluation of TNF-α, NF-kB and STAT3 levels after DMC and RA administration in EBV infection models.
I-IV) Representation of western blot of TNF-α after 24 and 48 hrs of EBV. I-IV) Relative quantification of protein blotting showing downregulation of TNF-α in DMC+EBV and RA+EBV exposed samples. NF-kB showed reduced protein only at 24 hrs whereas STAT3 showed decline at both the time points. Given plots; *x*-axis, sample types; *y*-axis, fold change with respect to EBV infected samples. Two samples t-test was used where *p*-values of <0.05, <0.01 and <0.0001 are considered statistically significant and are represented with #, ## and ### respectively. The increase and decrease are represented by * and # respectively.

5.4.7 Evaluation of Spatial cognition and hippocampal morphology in mice exposed with EBV and phytocompounds

The spatial learning in the rodents depends on the distal cues for navigation from the start point to the perimeter in the open maze to locate the submerged platform of the Morris-water maze (MWM) assay. This assay strongly correlated with the hippocampal synaptic plasticity and NMDA receptor function [22]. Hippocmapus is known to modulate stress and anxiety-like symptoms in mice [23]. Hereby, Group 1 (G1) indicates immunosuppressed control mice, G2 represents only IMR-32 exposed mice, G3 mice were infected with only EBV while G4, G5, G6, G7 mice corresponds to Acy+EBV, FTY+EBV, DMC+EBV and RA+EBV respectively.
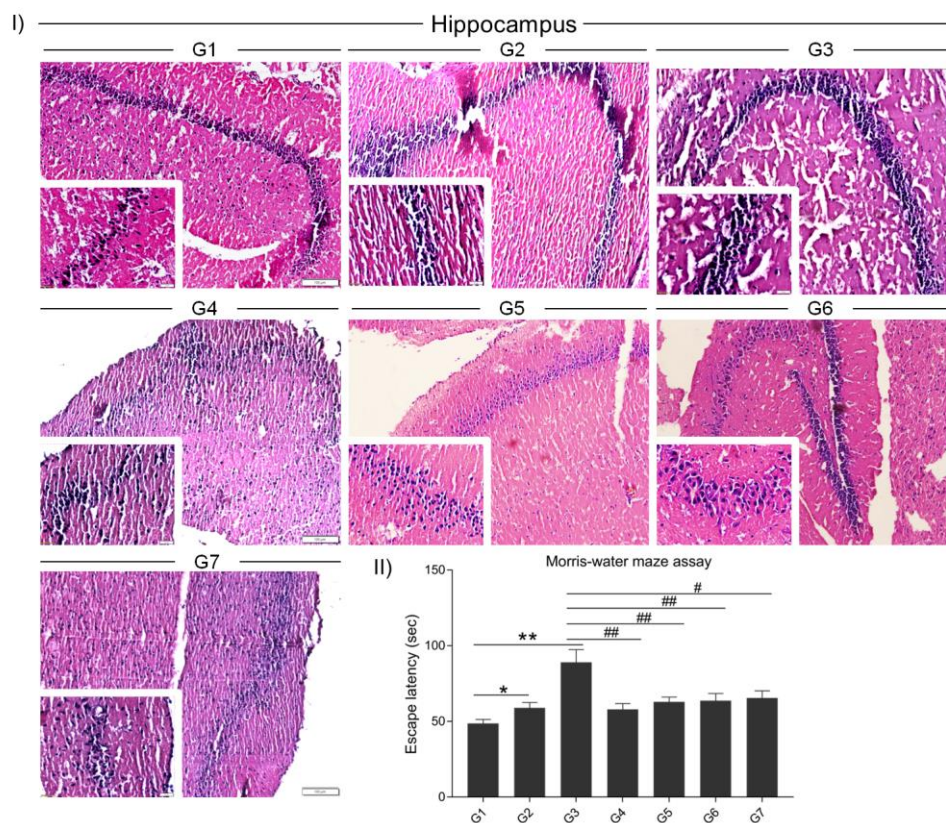
Figure 5.8: Representation of effect of phytocompounds DMC and RA on mice cognition.
I) Haematoxylin and eosin staining on mice hippocampal region. More number of pyknotic cells observed in G3. The restorative effect was observed in groups like G5 and G6. II) Escape latency of Morris-water maze assay upon exposure to Acy, FTY, DMC and RA.

We have observed differences in the morphology of hippocampal neurons. More number of spindle cell morphology observed in the FTY+EBV (G5) and DMC+EBV (G7) compared to EBV (G3) (Figure 5.8I). It suggests phytocompound DMC has a more restorative effect on cognition. We have also performed an MWM assay to assess the mice's cognition upon exposure to Acy+EBV, FTY+EBV, DMC+EBV and RA+EBV (Figure 5.8II). A significant difference was observed in the G4, G5, G6, G7 comprred to the G3 $p<0.01$ and $p<0.05$ respectively (Figure 5.8II).

5.4.8 Demonstration of the mitigation in the inflammation upon exposure to DMC and RA

The infection of several pathogens including viruses is known to trigger inflammation in rodents [24]. TNF-α plays a vital role in inflammatory cytokine bursts, employs the

innate immune response and activates the NF-kB signalling pathway. The blocking of TNF-α exhibited a decline in the inflammatory immune responses, and it provides protection against lethal influenza infection [25]. In the current, we have found a decline in TNF-α levels in mice brain tissue and serum samples of Acy+EBV, FTY+EBV, DMC+EBV and RA+EBV compared to only EBV infection.
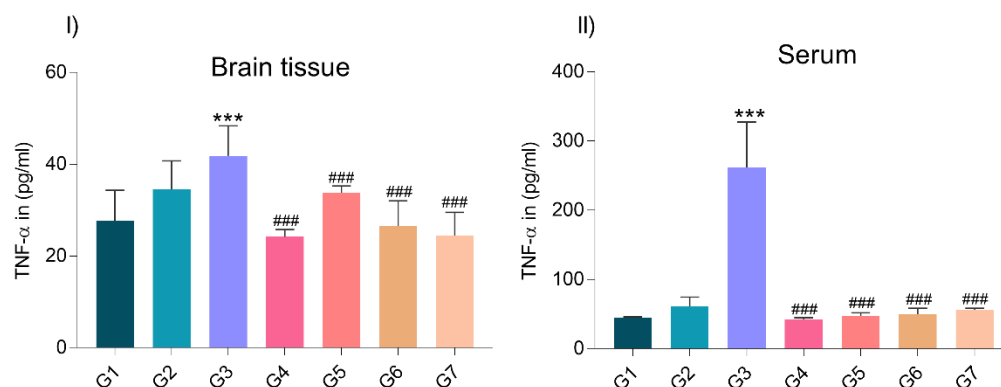
Figure 5.9: Underpinning the decline in the TNF-α in the mice brain and serum samples.
I) In mice brain, TNF-α level was found to be elevated in G3 and in turn a decline was observed in treated samples like G4, G5, G6, and G7. II) In the mice serum, TNF-α level was found to mitigated in all the treated group (G4, G5, G6, G7) compared to G3.

5.5 Discussion

EBV infection in the CNS can disrupt homeostasis, resulting in neurological dysfunction like meningitis, MS, Guillain-Barré syndrome, etc [2]. EBV-gp350 possibly aids its entry into brain cells. Studies have shown that adsorption and infection of EBV gets blocked by soluble gp350, gp220, or even gp220 amino-terminus derivatives [26]. Multiple phytocompounds and their derivatives have shown an anti-EBV potential [10]. Previous studies have shown that DMC and RA possess anti-inflammatory, antiviral [27], [28], and neuroprotective roles [29], [30], *in-vitro* and *in-vivo*. Our study interpreted the possible anti-gp350 activity of these phytocompounds at *in-vitro* and *in-vivo* levels. EBV-gp350 docked with phytoligands proclaimed drug likeliness through the Lipinski rule of five, and the *in-silico* ADMET analysis has not predicted any toxicity for these selected molecules. Further, during molecular dynamic simulation, DMC and RA have shown consistent stable binding with gp350 which suggests its potential inhibitory ability. The binding of the

aforementioned ligands to the same site of gp350 anticipates its potential for hindering similar interactions in neuronal cells. Hence, we further investigated their anti-gp350 activity *in-vitro* on IMR-32 cells and eventually on mice.

IMR-32 is an established cell line of neuronal origin and is commonly used in toxicology and cancer research [31]. DMC+EBV and RA+EBV showed an anti-gp350 effect in transcript and protein levels of neuronal cells at 48 hrs. Likewise, DMC has shown antiviral properties against Zika virus (ZIKV), Chikungunya virus (CHIKV) and H1N1 viral neuraminidase [32]. RA has also been found to show an anti-viral effect by reducing the mortality of mice infected with the Japanese encephalitis virus (JEV) [33]. Notably, in JEV infection, RA reduces the viral replication within the brain or secondary inflammation results from microglial activation [33]. It suggests that RA could be a potential therapeutic agent for treating and mitigating EBV infection by blocking gp350. In addition, EBV genes like ebna*1* and EBV-*gfp* was examined at mRNA level and found to be reduced in DMC+EBV and RA+EBV samples. It suggests decrease in the number of EBV virions in the above-mentioned cells.

Moreover, EBV infection is well known to set off autoimmune responses by activating several inflammatory pathways [20]. EBV infection triggers inflammatory gene expression, such as *il-6* in U-87 MG cells and *il-6* and *il-8* in human gingival fibroblasts [16], [34]. Hence, we have assessed the EBV-mediated expression of several inflammatory genes such as *il-1β, il-6, il-10, il-13* and *tnf-α* in neuronal cells. EBV-infection accelerated the expression of the inflammatory genes, while DMC+EBV and RA+EBV samples showed a reduction in the expression of these genes. An *in-vivo* study conducted on rats also reported similar observations upon DMC treatment [27]. Besides, RA plays a key role against inflammatory and oxidative markers, including NO, COX-2, IL-1β, PGE-2 and MMP2 in sciatic nerve chronic constriction injury (CCI) of rats and IL-1β and TNF-α in zebrafish [28]. Moreover, DMC and RA showed an appreciable decline in the inflammatory profile compared to positive control (FTY). TNF-α exhibited mitigation in DMC+EBV and RA+EBV exposed neuronal cells at protein level at *in-vitro* as well as *in-vivo* level. Proteins involved in the downstream cascade of TNF-α such as NF-kB and STAT3 have shown decline upon treatment with these phytocompounds. EBV proteins like latent membrane protein 1 (LMP1) alter the host TNF-α signalling and eventually trigger

the inflammatory pathways [35]. LMP1 recruits TRADD and activates NF-kB, phosphatidylinositol 3-kinase, JAK/STAT and mitogen-activated protein kinase signalling and subverts TRADD's potentially to induce apoptosis [36].

Along with neuronal inflammation, EBV infection also amends the level of neurotrophic factors. Increased BDNF synthesis during the acute phase of meningitis possibly triggers the proliferation of dentate granule cells and promotes neurogenesis after bacterial meningitis [37]. Hereby, the transient exposure of EBV showed an increase in neurotrophic factors. The elevated expression of NGF triggers the proinflammatory cytokines production, such as IL-1 and TNF-α in cultured airway epithelial cells, *in-vitro* [38]. The ephemeral release of these factors can lead to neuronal healing [29]. Besides, bis-demethoxycurcumin treatment downregulated MMP-9, VEGF, TGF-β, IL-6 and IL-8 and upregulated TIMP-2 levels [39]. RA exhibits a mimetic neurotrophic effect in PC12 cells by activating ERK1/2-mediated cell differentiation and enhancing cholinergic activity [40]. RA can suppress the secretion of VEGF, TGF-β, IL-6, and TNF-α which further can corroborate with the inflammation [41]. Furthermore, the effect of EBV infection on neurotrophic factors' profile is a broad area that further needs investigation. DMC exhibited a restorative effect on the morphology of hippocampal neurons compared to EBV-infected samples. Previously, turmeric demonstrated a positive effect on memory improvement by averting oxidative stress, inhibiting the apoptosis and programmed cell death of neurons [42]. Another study suggested the neuroprotective role of curcumin and demthoxycurcumin on retaining memory in Wister rats [43]. Overall, the current study has shown that DMC and RA could be potential plant-derived inhibitors of EBV-gp350.

Conclusively, phytocompounds plausibly show anti-gp350 properties by omitting the side effects. DMC and RA have shown anti-g350 activity at transcript and protein levels. These compounds also mitigated the virus-mediated changes in the neuronal cells. Further, DMC and RA also showed diminishing effects on inflammatory cell markers such as *il-1β, il-6, il-10*, *il-13* and *tnf-α*. Downstream protein molecules of TNF-α, namely NF-kB and STAT3 showed significant reduction in a time-dependent manner. Likewise, at *in-vivo* level, TNF-α also exhibited a decline in phytocompounds treated samples and the morphology of hippocampal neurons indicated improvement.

Altogether, DMC and RA have a crucial anti-gp350 effect on EBV infection and could be potential drug target molecules.

5.6 Material and methods

5.6.1 Structure retrieval and protein-ligand preparation

A 3.50 Å crystal structure (PDB ID: 2H6O) of EBV gp350 was retrieved from the Protein Data Bank (PDB) [44], [45]. Before docking, the structure was simulated for 100 ns for proper protein folding. After that, molecular docking was performed using AutoDock Vina1.1.2 and protein preparation was carried out by removing water molecules and adding polar hydrogens and Kollman charges. Ligands information was searched in the literature and 79 active phytocompounds with anti-viral and neuroprotective properties were selected (Table 2). Ligand structures in the SDF format were obtained from PubChem and processed into PDB format using pymol. Ligand preparation is accomplished by merging non-polar hydrogens, the addition of Gasteiger charges, and the identification of aromatic carbons and rotatable bonds along with the setting of the torsion tree.

5.6.2 Molecular docking

Following the identification of plausible active sites, the grid dimensions in AutoDock Tool (ADT) 1.5.6. was set as $50 \times 48 \times 58$ for XYZ points with a grid spacing of 0.375 Å, and the grid centre was designated at dimensions (x, y, and z): (-7.017, 11.623 and 15.901) for molecular docking. The grid was set around gp350-CR2 and anti-gp350 mAb interacting region, which mainly possessed the following amino acids: E21, D22, D53, E119, Y151, E155, Y159, I160, W162, D163, E201, D208, E210, E214, D215, E236, D296. AutoDock Vina was used for running the docking program, which employs iterated local search global optimizer. The binding affinities (kcal/mol) values of each ligand are presented in Table 2. Furthermore, the ligands interacting amino acids were checked using Discovery studio.

5.6.3 Molecular dynamic (MD) simulation

MD simulations up to 100 ns timescale were performed to obtain a properly folded and minimized energy structure of gp350 prior to docking. Afterward, MD simulations were performed for apoprotein and protein-ligand complexes using

similar conditions to evaluate their binding potential under physiological mimetic conditions. The Desmond simulation package by D.E. Shaw Research was utilized to carry out these simulations. Desmond package uses Optimized Potential for Liquid Simulations (OPLS) 2005 forcefield to calculate the potential energy and other related parameters for frames at every 2 femtoseconds (fs). The physiological mimetic conditions were set using TIP4P water model, Na and Cl as counterions, and 0.15 M salt concentration in the orthorhombic simulation box with an edge distance of 10 Å. Before running the final production run, the simulation setup was energy minimized using the steepest descent method for 50000 steps. Finally, the 100 ns long simulation was performed using the Noose Hover thermostat and Martina Thomas Klein Barostat for temperature and pressure coupling, respectively. All systems were analysed using Schrodinger's Maestro.

5.6.4 ADMET/Drug-likeness Properties

The pharmacokinetic properties (ADMET) were calculated for the natural ligand molecules by practising the pk-CSM pharmacokinetics web server (Table S2-S6) [46]. The drug-likeness of all-natural compounds was deciphered by implementing Lipinski's rule (Table S7) using SwissADME [47].

5.6.5 Cells and animals

The human neuroblastoma cell line (IMR-32) was procured from the National Centre for Cell Science, Pune, India. For virus purification, HEK 293T cells were used, which contain stably transfected bacterial artificial chromosome (BAC) green fluorescent protein (GFP)-EBV [48]. The cells were cultured in Dulbecco's modified Eagle's medium (DMEM; Himedia Laboratories Pvt. Limited, India) supplemented with 10% fetal bovine serum (FBS; Himedia Laboratories Pvt. Limited, India), 50 U/ml, 100 μg/ml and 2 mM of penicillin, streptomycin and L-Glutamine respectively. The growing cell environment was humidified with 5% CO_2 at 37 °C. FTY, DMC and RA were obtained from Sigma-Aldrich Corp., St. Louis, MO with purity ≥98% (HPLC). Adult Swiss albino female mice weighing ~30 gms, age approximately 2 months were housed in polypropylene cages and acclimated for a week before experimentation in a 14 hrs light: 10 hrs dark in an environment with a temperature of 23 ± 2 °C and humidity under control, with free access to laboratory feed and drinking water.

Animals were maintained as per the guidelines of the Institutional Animal Ethics Committee (IAEC), the Committee for the Purpose of Control and Supervision of Experiments on Animals (CPCSEA), and the Ministry of Environment and Forests, Government of India, New Delhi. The experimental protocol was approved by the IAEC of the School of Biotechnology, Devi Ahilya Vishwavidyalaya, Indore.

5.6.6 Purification of virus particles

The BAC-GFP-EBV was stably transfected HEK 293T cells [48], [49] and were grown in complete DMEM with puromycin selection. EBV particles were obtained using the protocol described in [16].

5.6.7 Cell cytotoxicity through MTT assay

For (3-(4,5-Dimethylthiazol-2-yl)-2,5-Diphenyltetrazolium Bromide) (MTT) assay 10×10^3 IMR-32 cells were seeded in a 96-well culture plate in complete DMEM supplemented with 10% of FBS and maintained for 24 hrs at 37 °C with 5% CO_2. FTY was dissolved in DMSO while DMC and RA were dissolved in milli-Q water and made the final stock of 1 mM. Upon treatment with FTY, DMC and RA the morphological changes in the cells were monitored using bright-field microscopy. After 24 hrs of treatment, media was removed and 100 μL of fresh media containing 0.5 mg/mL MTT was added to each well and incubated for 3 hrs at 37 °C. The MTT reagent was removed and 100 μL of DMSO was added to dissolve formazan crystals by shaking for 2 hrs and absorbance were measured at 570 and 590 nm.

5.6.8 qRT-PCR

EBV infections and inflammatory genes profile were analysed using qRT-PCR. 2.5×10^4 cells were seeded in a 6-well plate and pre-treated with the FTY, DMC and RA followed by EBV infection for 24 and 48 hrs. Total RNA extraction, complementary DNA preparation and qRT-PCR were carried out as described earlier [16], [50] Gene-specific primers were designed from Primer-BLAST and are listed in Table S1. The qPCR was performed on two biological and two technical replicates with glyceraldehyde 3-phosphate dehydrogenase (GAPDH) as a housekeeping gene.

5.6.9 Immunofluorescence

Immunofluorescence assay was used for demonstrating EBV infections and inflammation using gp350 (ab6525, 1:200, Abcam biotechnology) and TNF-α (D1G2, 1:200, Cell Signalling Technology) antibodies. 2.5×10^4 cells were seeded in a 6-well plate onto the coverslips and pre-treated with the FTY, DMC and RA for 1hr before EBV infection for 24 and 48 hrs and immunostaining was performed as explained previously [16]. Cells were observed under a fluorescence microscope (CellSens Dimensions 2.3, Shinjuku-ku, Tokyo, Japan). The image was analysed and quantified as mentioned previously [16]. The fluorescence intensity was calculated and plotted compared to the uninfected control of the respective groups.

5.6.10 Western Blotting

IMR-32 cells exposed with EBV, FTY+EBV, DMC+EBV and RA+EBV were harvested, washed with PBS and lysed in radioimmunoprecipitation assay buffer (RIPA) as described earlier [51]. Antibodies against TNF-α and GAPDH (14C10, 1:1000, Cell Signalling Technology, Danvers, MA, USA) were used as described in [16]. GAPDH was used as a housekeeping gene and the image analysis and quantification of blots were performed using Image J software (National Institutes of Health, Bethesda, MA, USA).

5.6.11 Morris-water Maze behavioural assay

The MWM was used to assess hippocampal-dependent spatial memory. Mice were trained for a week before any treatment. Then, the assay was recorded upon administration of immunosuppressives, during EBV and Acy, FTY, DMC and RA as mentioned previously [52].

5.6.12 Brain tissue collection

After 5 weeks of experimentation, mice were sacrificed by using isoflurane inhalation followed by decapitation as per approved protocol of IAEC and CPCSEA. Brains were excised and kept in a formalin and PBS solution for further ELISA and IHC experimentation.

5.6.13 Enzyme-linked immunosorbent assay

Sandwich ELISA was performed as per the kit from "Fine Test" for TNF-α (cat.log# EM0183) and IL-6 (cat.log# EM0121) on serum and brain tissue samples of mice. The protocol was performed as mentioned previously [52].

5.6.14 Haematoxylin and eosin staining

This staining was performed on the mice brain tissues (5 mm sections) post paraffinization and 5 mm tissue sectioning with microtome. The protocol was followed as discussed previously [52]. Eventually, sections were mounted in mounting media and observed under bright-field microscope (magnifications; 10x, 20x and 40x).

5.6.15 Statistical analysis

The t-test (two-samples) was carried out to compare values of compound-treated samples with EBV infection samples. The t-statistic was significant at the 0.05 critical alpha level, $P < 0.05$ at the 95% confidence interval.

5.7 References

1. Wong Y, Meehan MT, Burrows SR, Doolan DL, Miles JJ (2022) Estimating the global burden of Epstein-Barr virus-related cancers. J Cancer Res Clin Oncol 148:31–46. https://doi.org/10.1007/s00432-021-03824-y

2. Zhang N, Zuo Y, Jiang L, Peng Y, Huang X, Zuo L (2022) Epstein-Barr Virus and Neurological Diseases. Front Mol Biosci 8:816098. https://doi.org/10.3389/fmolb.2021.816098

3. Ahmed SI, Aziz K, Gul A, Samar SS, Bareeqa SB (2019) Risk of Multiple Sclerosis in Epstein-Barr Virus Infection. Cureus 11:e5699. https://doi.org/10.7759/cureus.5699

4. Young KA, Herbert AP, Barlow PN, Holers VM, Hannan JP (2008) Molecular Basis of the Interaction between Complement Receptor Type 2 (CR2/CD21) and Epstein-Barr Virus Glycoprotein gp350. J Virol 82:11217–11227. https://doi.org/10.1128/JVI.01673-08

5. Rani A, Jakhmola S, Karnati S, Parmar HS, Chandra Jha H (2021) Potential entry receptors for human γ-herpesvirus into epithelial cells: A plausible therapeutic target for viral infections. Tumour Virus Res 12:200227. https://doi.org/10.1016/j.tvr.2021.200227

6. Hui KF, Yiu SPT, Tam KP, Chiang AKS (2019) Viral-Targeted Strategies Against EBV-Associated Lymphoproliferative Diseases. Front Oncol 9:81. https://doi.org/10.3389/fonc.2019.00081

7. Kanekiyo M, Bu W, Joyce MG, Meng G, Whittle JRR, Baxa U, Yamamoto T, Narpala S, Todd J-P, Rao SS, McDermott AB, Koup RA, Rossmann MG, Mascola JR, Graham BS, Cohen JI, Nabel GJ (2015) Rational Design of an Epstein-Barr Virus Vaccine Targeting the Receptor-Binding Site. Cell 162:1090–1100. https://doi.org/10.1016/j.cell.2015.07.043

8. Cao Y, Xie L, Shi F, Tang M, Li Y, Hu J, Zhao L, Zhao L, Yu X, Luo X, Liao W, Bode AM (2021) Targeting the signaling in Epstein–Barr virus-associated diseases: mechanism, regulation, and clinical study. Signal Transduct Target Ther 6:15. https://doi.org/10.1038/s41392-020-00376-4

9. Drosu NC, Edelman ER, Housman DE (2020) Tenofovir prodrugs potently inhibit Epstein-Barr virus lytic DNA replication by targeting the viral DNA polymerase. Proc Natl Acad Sci U S A 117:12368–12374. https://doi.org/10.1073/pnas.2002392117

10. Mukherjee PK (2019) Antiviral Evaluation of Herbal Drugs. In: Quality Control and Evaluation of Herbal Drugs. Elsevier, pp 599–628

11. Jennings MR, Parks RJ (2020) Curcumin as an Antiviral Agent. Viruses 12:1242. https://doi.org/10.3390/v12111242

12. Ansari M, Sharififar F, Arabzadeh AM, Mehni F, Mirtadzadini M, Iranmanesh Z, Nikpour N (2014) In vitro evaluation of anti-herpes simplex-1 activity of three standardized medicinal plants from Lamiaceae. Anc Sci Life 34:33–38. https://doi.org/10.4103/0257-7941.150777

13. Gazi IF, Elisaf MS (2010) Effect of infection on lipid profile: focus on Epstein–Barr virus. Clin Lipidol 5:607–610. https://doi.org/10.2217/clp.10.53

14. Huang Y, Liang J, Hu W, Liang Y, Xiao X, Zhao W, Zhong X, Yang Y, Pan X, Zhou X, Zhang Z, Cai Y (2022) Integration Profiling Between Plasma Lipidomics, Epstein-Barr Virus and Clinical Phenomes in Nasopharyngeal Carcinoma Patients. Front Microbiol 13:919496. https://doi.org/10.3389/fmicb.2022.919496

15. Wang LW, Wang Z, Ersing I, Nobre L, Guo R, Jiang S, Trudeau S, Zhao B, Weekes MP, Gewurz BE (2019) Epstein-Barr virus subverts mevalonate and fatty acid pathways to promote infected B-cell proliferation and survival. PLoS Pathog 15:e1008030. https://doi.org/10.1371/journal.ppat.1008030

16. Jakhmola S, Jha HC (2021) Glial cell response to Epstein-Barr Virus infection: A plausible contribution to virus-associated inflammatory reactions in the brain. Virology 559:182–195. https://doi.org/10.1016/j.virol.2021.04.005

17. Friedman EA (1989) Renal failure in diabetes: a substantive problem in provision of health care. Verh - K Acad Voor Geneeskd Van Belg 51:81–149; discussion 149-151

18. Dong J, Wang N-N, Yao Z-J, Zhang L, Cheng Y, Ouyang D, Lu A-P, Cao D-S (2018) ADMETlab: a platform for systematic ADMET evaluation based on a comprehensively collected ADMET database. J Cheminformatics 10:29. https://doi.org/10.1186/s13321-018-0283-x

19. Jakhmola S, Jonniya NA, Sk MF, Rani A, Kar P, Jha HC (2021) Identification of Potential Inhibitors against Epstein-Barr Virus Nuclear Antigen 1 (EBNA1): An Insight from Docking and Molecular Dynamic Simulations. ACS Chem Neurosci 12:3060–3072. https://doi.org/10.1021/acschemneuro.1c00350

20. Draborg AH, Duus K, Houen G (2013) Epstein-Barr virus in systemic autoimmune diseases. Clin Dev Immunol 2013:535738. https://doi.org/10.1155/2013/535738

21. Idriss HT, Naismith JH (2000) TNF alpha and the TNF receptor superfamily: structure-function relationship(s). Microsc Res Tech 50:184–195. https://doi.org/10.1002/1097-0029(20000801)50:3<184::AID-JEMT2>3.0.CO;2-H

22. Vorhees CV, Williams MT (2006) Morris water maze: procedures for assessing spatial and related forms of learning and memory. Nat Protoc 1:848–858. https://doi.org/10.1038/nprot.2006.116

23. Mehta K, Kaur B, Pandey KK, Kaler S, Dhar P (2020) Curcumin supplementation shows modulatory influence on functional and morphological features of hippocampus in mice subjected to arsenic trioxide exposure. Anat Cell Biol 53:355–365. https://doi.org/10.5115/acb.18.169

24. Ma H, Yang Y, Nie T, Yan R, Si Y, Wei J, Li M, Liu H, Ye W, Zhang H, Cheng L, Zhang L, Lv X, Luo L, Xu Z, Zhang X, Lei Y, Zhang F (2024) Disparate macrophage responses are linked to infection outcome of Hantan virus in humans or rodents. Nat Commun 15:438. https://doi.org/10.1038/s41467-024-44687-4

25. Shi X, Zhou W, Huang H, Zhu H, Zhou P, Zhu H, Ju D (2013) Inhibition of the inflammatory cytokine tumor necrosis factor-alpha with etanercept provides protection against lethal H1N1 influenza infection in mice. Crit Care 17:R301. https://doi.org/10.1186/cc13171

26. van Zyl DG, Mautner J, Delecluse H-J (2019) Progress in EBV Vaccines. Front Oncol 9:104. https://doi.org/10.3389/fonc.2019.00104

27. Gullaiya S, Nagar A, Dubey V, Singh V, Kumar A, Tiwari P, Agrawal SS (2013) Modulation of disease related immune events by demethoxycurcumin against autoimmune arthritis in rats. Biomed Aging Pathol 3:7–13. https://doi.org/10.1016/j.biomag.2013.01.005

28. Ghasemzadeh Rahbardar M, Amin B, Mehri S, Mirnajafi-Zadeh SJ, Hosseinzadeh H (2017) Anti-inflammatory effects of ethanolic extract of Rosmarinus officinalis L. and rosmarinic acid in a rat model of neuropathic pain.

Biomed Pharmacother Biomedecine Pharmacother 86:441–449. https://doi.org/10.1016/j.biopha.2016.12.049

29. Rajan P, Symes AJ, Fink JS (1996) STAT proteins are activated by ciliary neurotrophic factor in cells of central nervous system origin. J Neurosci Res 43:403–411. https://doi.org/10.1002/(SICI)1097-4547(19960215)43:4<403::AID-JNR2>3.0.CO;2-J

30. Blanc CA, Rosen H, Lane TE (2014) FTY720 (fingolimod) modulates the severity of viral-induced encephalomyelitis and demyelination. J Neuroinflammation 11:138. https://doi.org/10.1186/s12974-014-0138-y

31. Rao RR, Kisaalita WS (2002) Biochemical and electrophysiological differentiation profile of a human neuroblastoma (IMR-32) cell line. In Vitro Cell Dev Biol Anim 38:450–456. https://doi.org/10.1290/1071-2690(2002)038<0450:BAEDPO>2.0.CO;2

32. Ferreira LLC, Abreu MP, Costa CB, Leda PO, Behrens MD, Dos Santos EP (2022) Curcumin and Its Analogs as a Therapeutic Strategy in Infections Caused by RNA Genome Viruses. Food Environ Virol 14:120–137. https://doi.org/10.1007/s12560-022-09514-3

33. Swarup V, Ghosh J, Ghosh S, Saxena A, Basu A (2007) Antiviral and anti-inflammatory effects of rosmarinic acid in an experimental murine model of Japanese encephalitis. Antimicrob Agents Chemother 51:3367–3370. https://doi.org/10.1128/AAC.00041-07

34. Yokoe S, Hasuike A, Watanabe N, Tanaka H, Karahashi H, Wakuda S, Takeichi O, Kawato T, Takai H, Ogata Y, Sato S, Imai K (2022) Epstein-Barr Virus Promotes the Production of Inflammatory Cytokines in Gingival Fibroblasts and RANKL-Induced Osteoclast Differentiation in RAW264.7 Cells. Int J Mol Sci 23:809. https://doi.org/10.3390/ijms23020809

35. Wang L, Ning S (2021) New Look of EBV LMP1 Signaling Landscape. Cancers 13:5451. https://doi.org/10.3390/cancers13215451

36. Kieser A (2008) Pursuing different 'TRADDes': TRADD signaling induced by TNF-receptor 1 and the Epstein-Barr virus oncoprotein LMP1. bchm 389:1261–1271. https://doi.org/10.1515/BC.2008.144

37. Xu D, Lian D, Wu J, Liu Y, Zhu M, Sun J, He D, Li L (2017) Brain-derived neurotrophic factor reduces inflammation and hippocampal apoptosis in experimental Streptococcus pneumoniae meningitis. J Neuroinflammation 14:156. https://doi.org/10.1186/s12974-017-0930-6

38. Scuri M, Samsell L, Piedimonte G (2010) The Role of Neurotrophins in Inflammation and Allergy. Inflamm Allergy - Drug Targets 9:173–180. https://doi.org/10.2174/187152810792231913

39. Mohankumar K, Francis AP, Pajaniradje S, Rajagopalan R (2021) Synthetic curcumin analog: inhibiting the invasion, angiogenesis, and metastasis in human laryngeal carcinoma cells via NF-kB pathway. Mol Biol Rep 48:6065–6074. https://doi.org/10.1007/s11033-021-06610-8

40. Venkatesan R, Ji E, Kim SY (2015) Phytochemicals That Regulate Neurodegenerative Disease by Targeting Neurotrophins: A Comprehensive Review. BioMed Res Int 2015:1–22. https://doi.org/10.1155/2015/814068

41. Cao W, Hu C, Wu L, Xu L, Jiang W (2016) Rosmarinic acid inhibits inflammation and angiogenesis of hepatocellular carcinoma by suppression of NF-κB signaling in H22 tumor-bearing mice. J Pharmacol Sci 132:131–137. https://doi.org/10.1016/j.jphs.2016.09.003

42. Eliza M, Sarona A, Ples M, Ii R (2018) Neurotrophic effects of turmeric on the memory of the mouse using the Morris water maze test. Natl J Physiol Pharm Pharmacol 1. https://doi.org/10.5455/njppp.2018.8.1039116012018

43. Dairam A, Limson JL, Watkins GM, Antunes E, Daya S (2007) Curcuminoids, Curcumin, and Demethoxycurcumin Reduce Lead-Induced Memory Deficits in Male Wistar Rats. J Agric Food Chem 55:1039–1044. https://doi.org/10.1021/jf063446t

44. Szakonyi G, Klein MG, Hannan JP, Young KA, Ma RZ, Asokan R, Holers VM, Chen XS (2006) Structure of the Epstein-Barr virus major envelope glycoprotein. Nat Struct Mol Biol 13:996–1001. https://doi.org/10.1038/nsmb1161

45. Bank RPD RCSB PDB - 2H6O: Epstein Barr Virus Major Envelope Glycoprotein. https://www.rcsb.org/structure/2H6O. Accessed 6 Mar 2023

46. Pires DEV, Blundell TL, Ascher DB (2015) pkCSM: Predicting Small-Molecule Pharmacokinetic and Toxicity Properties Using Graph-Based Signatures. J Med Chem 58:4066–4072. https://doi.org/10.1021/acs.jmedchem.5b00104

47. Daina A, Michielin O, Zoete V (2017) SwissADME: a free web tool to evaluate pharmacokinetics, drug-likeness and medicinal chemistry friendliness of small molecules. Sci Rep 7:42717. https://doi.org/10.1038/srep42717

48. Halder S, Murakami M, Verma SC, Kumar P, Yi F, Robertson ES (2009) Early Events Associated with Infection of Epstein-Barr Virus Infection of Primary B-Cells. PLoS ONE 4:e7214. https://doi.org/10.1371/journal.pone.0007214

49. Yuen K-S, Chan C-P, Kok K-H, Jin D-Y (2017) Mutagenesis and Genome Engineering of Epstein-Barr Virus in Cultured Human Cells by CRISPR/Cas9. Methods Mol Biol Clifton NJ 1498:23–31. https://doi.org/10.1007/978-1-4939-6472-7_2

50. Indari O, Chandramohanadas R, Jha HC (2021) Epstein-Barr virus infection modulates blood-brain barrier cells and its co-infection with Plasmodium falciparum induces RBC adhesion. Pathog Dis 79:ftaa080. https://doi.org/10.1093/femspd/ftaa080

51. Kashyap D, Baral B, Jakhmola S, Singh AK, Jha HC (2021) Helicobacter pylori and Epstein-Barr Virus Coinfection Stimulates Aggressiveness in Gastric Cancer through the Regulation of Gankyrin. mSphere 6:e00751-21. https://doi.org/10.1128/mSphere.00751-21

52. Rani A, Patra P, Verma TP, Singh A, Jain AK, Jaiswal N, Narang S, Mittal N, Parmar HS, Jha HC (2024) Deciphering the Association of Epstein–Barr Virus

and Its Glycoprotein M Peptide with Neuropathologies in Mice. ACS Chem Neurosci 15:1254–1264. https://doi.org/10.1021/acschemneuro.4c00012

Chapter 6: Conclusion and Future Prospects

EBV shares an enigmatic connection with neurological ailments. Reports have suggested the tropism of EBV towards different brain cells and subsequently the activation of neuroinflammatory cascades. The thesis work discussed the insights about virus entry into brain astrocyte cell lines, i.e., LN-229 and U-87 MG. For the virus entry, receptors are considered a critical moiety for the infection, therefore, receptors like Ephs NRPs and NMHC-IIs were screened in a time-dependent manner. Receptors namely, ephA4, ephA10 and NMHC-IIB (*myh9*) were found to be pertinently regulated, thereby, the knockdown of these receptors will further aid in EBV entry in brain cells (Figure 6.1). Consistent with this, the crucial role of the lipid raft region and dynamin protein suggests EBV undergo an endocytic pathway in the neuronal cells. Ablation of dynamin protein in the brain cells will be an aspect of the future. The significantly augmented presence of EBV in the endosomal markers further affirms the entry of EBV via the endocytic pathway such as EEA1, Rab5, Rab7 and LAMP1 (Figure 6.1). As reported previously in KSHV, EBV also likely to exits the late endosome to establish successful infection in the cells, though it needs further validation. Deciphering the preferred pathway of EBV entry and replication in the brain cells helps design the prophylactic intervention strategies to mitigate the EBV infection.

As EBV entry is facilitated by the membrane cholesterol region of the plasma membrane, we further investigated the downstream pathways as well as the intracellular biomolecular changes occurring in these cells under EBV influence. An EBV latent protein LMP1 localised in the lipid raft region of the plasma membrane and upon depletion of this region, we found amendments in the downstream signalling molecules like RIP, NF-kB, STAT3 and TNF-α (Figure 6.1). Eventually, the biomolecular signature changes were observed at the periphery and nucleus of the cell by utilizing the Raman spectroscopy tool (Figure 6.1). We observed that EBV infection gets differentially regulated in these cells. Viral entry and its induced effects started as soon as 2 hrs post-infection and major biomolecules were found to be altered at the periphery of these cells in a temporal-manner. Briefly, significant modulation is observed in the lipids, cholesterol, CH2 asymmetric stretch, protein, fatty acids, nucleic acid and polysaccharides signals. Notably, cholesterol or lipid moieties

showed significant changes at different time points in the periphery of the cells. These biomolecules ultimately play key roles in the viral usurpation of cells. Besides, some of these factors were previously reported to be associated with EBV infection or neurological disorders.
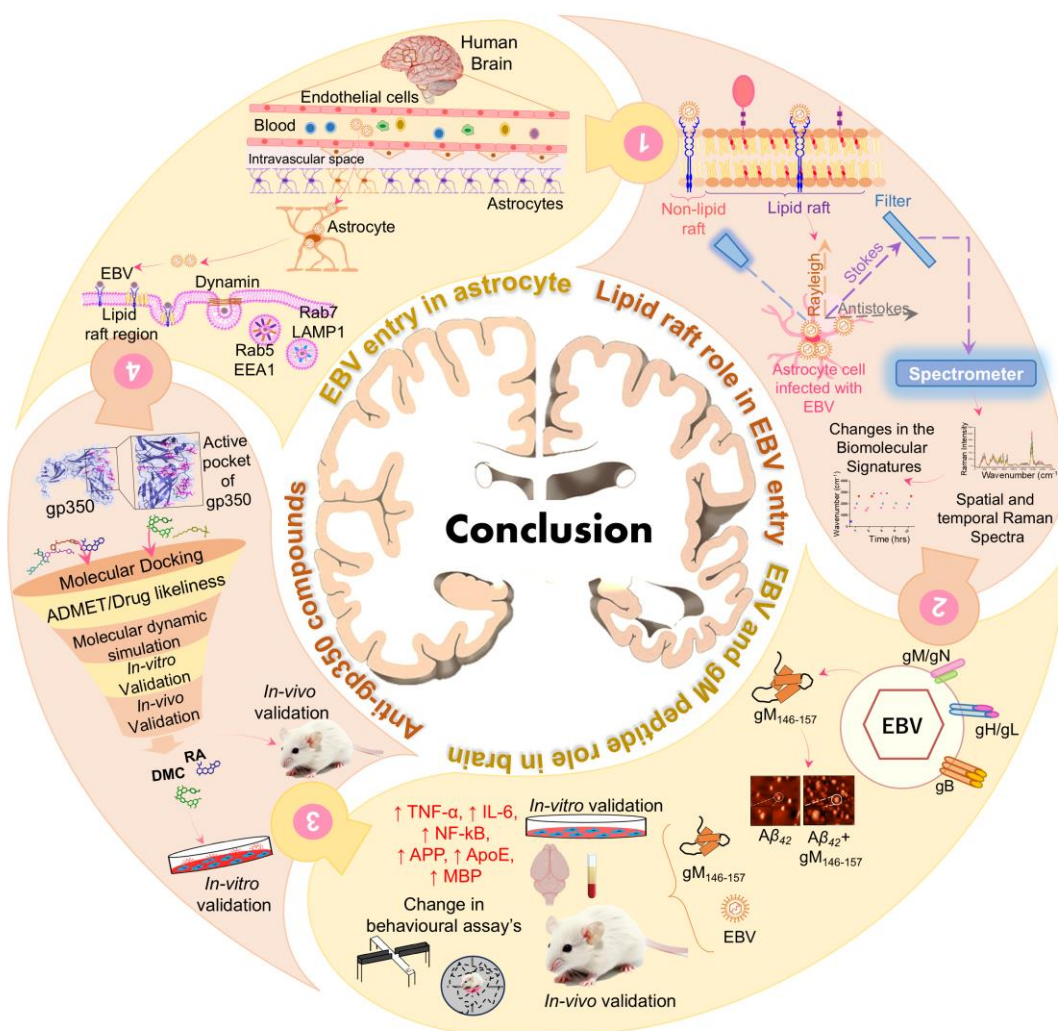
Figure 6.1: Illustration of brief inferences of the thesis work.
Chapter 1, indicates that EBV follows an endocytic mechanism to enter the brain cells where Ephs, NRPs, NMHCs, receptors, lipid raft region, dynamin protein and endosomes play crucial roles. In chapter 2, upon membrane cholesterol depletion the LMP1-downstream signalling suggested perturbations and eventually the biomolecular signature was assessed by Raman spectroscopy. Chapter 3, deals with the association of EBV and its glycoprotein M peptide with the neuropathologies which was checked at *in-vitro* and *in-vivo* levels. Eventually, in the chapter 4, compounds against another EBV entry glycoprotein 350 were screened.

Therefore, the use of Raman spectroscopy could efficiently help to decipher major biomolecular changes in complex systems like cells during altering events such as infections. Indeed, our current investigation may help in laying the foundation stone

for the exploration of the intracellular biochemistry of EBV infection. The study opens the gateways to investigate the importance of the mentioned biomolecules and their associated factors, observed in the provided connectome, in viral infections and related neurological manifestations. EBV entry into epithelial cells is assisted by the gHgL complex followed by the gB interaction which enables the virus to establish infection. Intriguingly, in herpesvirus, gM is known to play a role in directing capsids to the site of envelopment by recruiting capsid-associating tegument protein. The gMgN complex is also involved in the efficient incorporation of gHgL protein in the virion membrane, which in turn helps in herpes simplex virus (HSV) entry, fusion as well as in viral replication. Ablation of gM unravelled the inefficiency in extra virion localisation of gHgL. Notably, upon screening of >100 EBV-associated proteins, a 12 amino acid peptide of gM was found to have self-aggregation properties and showed elevation in the aggregation of $A\beta_{42}$ (Figure 6.1). Hereby, we investigated the direct connection of EBV and $gM_{146-157}$ with neurological manifestation on a cell-line and mice-based models. In the *in-vitro* system, inflammatory species and Ca^{2+} ions suggested neuroinflammation and amendments in the myelin-sheath associated protein and enzymes have also been observed. Likewise, upregulation in the inflammatory moieties, i.e., TNF-α and IL-6 were observed in the brain tissue samples upon exposure to EBV/$gM_{146-157}$. Exposure to EBV/$gM_{146-157}$ also exhibited a decline in spatial memory formation and an increase in anxiety-like symptoms in mice (Figure 6.1). Hippocampal neurons of mice brains showed significant disorganisation as well as cell shrinkage which suggested apoptotic changes. Eventually, the neurological disease markers like APP, ApoE and MBP suggested an increase in a time-dependent manner. Taken together, it provides a direct link between EBV/$gM_{146-157}$ with neurological diseases in the *in-vivo* model system and further raises the need to investigate the detailed mechanism, so, that we can find numerous potent therapeutic targets.

EBV proteins like EBNA1, LMP1, BZLF1 and gp350 have shown continuous presence in the cerebrospinal fluid of patients suffering from neurological disorders. Earlier reports indicated that EBV establishes its infection in brain cells, yet limited information is available on its entry mechanisms. EBV proteins like gp350 have a vital role in the viral tropism. Vaccination development attempts against EBV-gp350 have previously exhibited a declined severity of infectious mononucleosis but were unable

to subside the viral infection. Further, the lack of anti-EBV drugs is probably because of the difficulty in diagnosis of EBV-induced infectious mononucleosis and also due to the inability of the drugs to achieve high concentrations in the oropharynx where EBV is released in high titres. Several other herpesvirus drugs are being used to mitigate the EBV infection. We have screened phytocompounds against the extra-virion region of gp350 through an *in-silico* study and validated it further at the *in-vitro* and *in-vivo* levels. Phytocompounds like DMC and RA exhibited stable interaction with gp350 through RMSD, RMSF and Rg analysis. Subsequently, DMC and RA have shown anti-g350 activity at transcript and protein levels compared to positive control Acy and FTY (Figure 6.1). These compounds also showed diminishing effects on inflammatory cell markers such as *il-1β, il-6, il-10, il-13* and *tnf-α*. Downstream protein molecules of TNF-α, namely NF-kB and STAT3 showed significant reduction in a time-dependent manner. On mice, these phytocompounds exhibited rescue in the cognition. Hippocampal cells organisation and morphology indicated improvement upon exposure to DMC and RA. TNF-α level was also found decline in the mice's brain tissues, suggesting effective mitigation in the inflammation. Overall, DMC and RA have a crucial anti-gp350 effect on EBV infection and could be potential drug target molecules.

Appendix-A

Supplementary Tables:

Table S 1: List of primers used for the qRT-PCR.

S. No.	Gene name	Primer Sequence
1	Glyceraldehyde-3-Phosphate Dehydrogenase (GAPDH)	F: TGCACCACCAACTGCTTAG
		R: GATGCAGGGATGATGTTC
2	Green fluorescent protein (GFP)	F: ACGTAAACGGCCACAAGTTC
		R: AAGTCGTGCTGCTTCATGTG
3	EBV nuclear antigen 1 (EBNA1)	F: CACCATTGAGTCGTCTCCCC
		R: TCAAAGCTGCACACAGTCAC
4	Ephrin receptor A1 (EPHA1)	F: GTGGACACTGTCATAGGAGAAGG
		R: GGTCTTAATGGCCACAGTCTTG
5	EPHA2	F: CCCGATGAGATCACCGTCAG
		R: GGCACCGATATCCTGGAAGG
6	EPHA3	F: ATTTTGGCAATGGGCATTTA
		R: ATGTATGTGGGTCAACATAAGTCC
7	EPHA4	F: GGAAGGCGTGGTCACTAAAT
		R: TCTGCCATCATTTTTCCTGA
8	EPHA5	F: GCCCGGCAGTATGTGTCTGTAA
		R: TCCATTGGGACGATCTGGTTC
9	EPHA6	F: TGATCCAGACACCTATGAAGAC
		R: CAAATTCACCTGCTCCAATCAC
10	EPHA7	F: TCCAGGCACCAAAACCTACAT
		R: GCTCCTTGGCGAATTGATGG
11	EPHA8	F: CTCACGTATCCGGCTCA
		R: TCATGACGTTGCAAACCTG
12	EPHA10	F: CTTTGGCTGAACATCGAGAGG
		R: GGAGTCCTGCCTTGGAAGAAT
13	EPHB1	F: GCCCAATGGCATCATCCTG
		R: ATCAATCCTTGCTGTGTTGGTCTG

Appendix-A

S. No.	Gene name	Primer Sequence
14	EPHB2	F: GAAGGAGCTCAGTGAGTACAACG
		R: GCACCTGGAAGACATAGATGG
15	EPHB3	F: GGCCATAGCCTATCGGAAGT
		R: TCCCAGTAGGGTCGCTCTC
16	EPHB4	F: CGCGCGGAGTATCGG
		R: CGGGTAGGATCCGAACTGA
17	EPHB6	F: GACCAATGGGAACATCCTGGAC
		R: CCCGCACCTGGAAACCATAG
18	Neuropilin 1 (NRP1)	F: GGGACCCATTCAGGATCACA
		R: ATAAACCACAGGGCTCACCA
19	NRP2	F: TGTTCGAGGGAGTGATAGGG
		R: AAAATTCTCACCTGCAAAAGCC
20	Non-muscle myosin heavy chain-IIA (NMHC-IIA)	F: GAAGCAGAAACGGGACCTTG
		R: CTCCTGCTCACGTTTTGACC
21	NMHC-IIB	F: CGACGCGTGCCAACGCATC
		R: GACACAGTTGATCTTTCAGGAAGG
22	NMHC-IIC	F: CTCTGAATGACAACGTCGCAG
		R: AAGAGAACTGCTGGAAGCCC
23	EBV nuclear antigen 2 (EBNA2)	F: GAACTTCAACCCACACCATC
		R: CGTGGTTCTGGACTATCTGG
24	EBV nuclear antigen 3A (EBNA3A)	F: GGTGAAACGCGAGAAGAAAG
		R: TTTAGCAGTTCCTCCGCACT
25	EBV nuclear antigen 3B (EBNA3B)	F: AGAAGAGGCCCTTGTGTCTT
		R: GGATTTCAAGAGGGTCAGGT
26	EBV nuclear antigen 3C (EBNA3C)	F: AGAAGGGGAGCGTGTGTTGT
		R: GGCTGGTTTTTGACGTCGGC
27	EBV nuclear antigen LP (EBNALP)	F: TCCCCTCGGACAGCTCCTA
		R: CCACTTACCACCTCCCCTTCT
28	Latent membrane protein 1 (LMP1)	F: CCCGCACCCTCAACAAGCTACCGAT

156

S. No.	Gene name	Primer Sequence
		R: TTGTCAGGACCACCTCCAGGTGCGC
29	Latent membrane protein 2A (LMP2A)	F: CTACTCTCCACGGGATGACTCAT
		R: GGCGGTCACAACGGTACTAACT
30	Latent membrane protein 2B (LMP2B)	F: CGGGAGGCCGTGCTTTAG
		R: GGCGGTCACAACGGTACTAACT
31	Glycoprotein 350 (gp350)	F: AGGTGCTGCAGCCCTCGAGGAAGTC
		R: GGCTAGCGAGAATCCATCACCGACT
32	Interleukin 1 beta (IL1β)	F: GGGCCTCAAGGAAAAGAATC
		R: TTCTGCTTGAGAGGTGCTGA
33	Interleukin 6 (IL6)	F: TACCCCCAGGAGAAGATTCC
		R: TTTTCTGCCAGTGCCTCTTT
34	Interleukin 10 (IL10)	F: TGCCTTCAGCAGAGTGAAGA
		R: GGTCTTGGTTCTCAGCTTGG
35	Interleukin 4 (IL 4)	F: GCCACCATGAGAAGGACACT
		R: ACTCTGGTTGGCTTCCTTCA
36	Interleukin 13 (IL13)	F: TGGGTGACTGCAGTCCTGGCT
		R: GTTGCTTTGTGTAGCTGAGCA
37	Tumour necrosis factor alpha (TNFα)	F: CAGAGGGCCTGTACCTCATC
		R: GGAAGACCCCTCCCAGATAG
38	Transforming growth factor beta (TGFβ)	F: GGGACTATCCACCTGCAAGA
		R: CCTCCTTGGCGTAGTAGTCG
39	Nerve growth factor (NGF)	F: TCAGCATTCCCTTGACACTG
		R: TGCTCCTGTGAGTCCTGTTG
40	Brain derived neurotropic factor (BDNF)	F: AAACATCCGAGGACAAGGTG
		R: AGAAGAGGAGGCTCCAAAGG
41	Cholesteryl ester transfer protein (CETP1)	F: ACCTGGAGTCCCATCACAAG
		R: TTGGAAGATTTCCTGGTTGG
42	Farnesyl Diphosphate Synthase (FDPS)	F: CAAGGAGGTCCTGGAGTACAA
		R: GGAGACTATCAGCATCCTGTTTC

Appendix-A

S. No.	Gene name	Primer Sequence
43	Hydroxymethylglutaryl-CoA synthase (HMGCS)	F: CAAAAAGATCCATGCCCAGT
		R: AAAGGCTTCCAGGCCACTAT
44	Isopentenyl diphosphate (IDI1)	F: TCTCATTGGGCATGAAGGTC
		R: CATAAAACCTCGGGCTCCTT
45	Thiolase	F: GATGCCTTCTTACCCCAACA
		R: CCCAACCACTGCATAAGACC

Table S 2: Absorption of the phytochemicals.

Ligand Name	Water solubility (Log Mol/L)	Caco2 permeability (log Papp in 10-6 cm/s)	Intestinal absorption (human) (% Absorbed)	Skin Permeability (log Kp)	P-glycoprotein substrate	P-glycoprotein I inhibitor	P-glycoprotein II inhibitor
Piperin	-3.464	1.596	94.444	-3.131	Yes	Yes	No
Ajamalicine	-3.824	1.126	94.29	-3.303	Yes	Yes	No
Amentoflavone	-2.892	0.145	84.356	-2.735	Yes	Yes	Yes
Demethoxycurcumin	-3.566	1.023	91.393	-2.768	Yes	Yes	Yes
Rosmarinic acid	-3.059	-0.937	32.516	-2.735	Yes	Yes	No
Serpentine	-3.715	0.999	97.736	-2.799	Yes	No	Yes
Ajmaline	-2.851	1.23	98.073	-2.841	Yes	Yes	No
Curcumin	-4.01	-0.093	82.19	-2.764	Yes	Yes	Yes
Withanolide D	-5.127	0.831	99.2	-3.267	Yes	Yes	Yes
Hecogenin	-5.028	1.432	96.696	-3.506	No	Yes	Yes
Luteolin	-3.094	0.096	81.13	-2.735	Yes	No	No
Proanthocyanidin	-2.892	0.188	71.723	-2.735	Yes	Yes	Yes
Quercetin	-2.925	-0.229	77.207	-2.735	Yes	No	No
Ellagic acid	-3.181	0.335	86.684	-2.735	Yes	No	No
7α-obacunol	-4.735	0.837	98.427	-3.024	No	No	No
Oroselol	-3.655	1.006	95.157	-2.714	Yes	No	No
Protopine	-3.825	1.065	97.593	-3.064	Yes	Yes	No
Arjunic acid	-3.057	0.583	62.88	-2.735	No	No	No
Corilagin	-2.892	-1.337	58.509	-2.735	Yes	Yes	Yes

Appendix-A

Ligand Name	Water solubility (Log Mol/L)	Caco2 permeability (log Papp in 10-6 cm/s)	Intestinal absorption (human) (% Absorbed)	Skin Permeability (log Kp)	P-glycoprotein substrate	P-glycoprotein I inhibitor	P-glycoprotein II inhibitor
Withaferin A	-5.063	0.829	85.345	-3.202	Yes	Yes	Yes
17beta-Hydroxywithanolide K	-5.384	0.76	95.535	-3.585	Yes	No	No
Vasicinolone	-2.577	0.083	98.31	-2.788	Yes	No	No
Oleanolic acid	-3.074	1.17	99.931	-2.735	No	No	No
Harmalol	-3.221	1.221	92.396	-2.846	Yes	No	No
α-Amyrin	-6.499	1.227	94.062	-2.814	No	Yes	Yes
Reseveratol	-3.178	1.17	90.935	-2.737	Yes	No	No
β-eudesmol	-4.9	1.508	94.296	-1.967	No	No	No
Warfarin	-4.513	0.928	96.161	-2.754	Yes	No	No
Yohimbine	-3.106	0.975	94.708	-2.767	Yes	No	No
Kaempferol	-3.04	0.032	74.29	-2.735	Yes	No	No
Germacrene B	-5.465	1.426	94.629	-1.636	No	No	No
Lupeol	-5.861	1.226	95.782	-2.744	No	Yes	Yes
Brassicasterol	-6.974	1.235	95.05	-2.862	No	Yes	Yes
Asiatic acid	-3.008	0.479	62.855	-2.735	No	No	No
Vasicinol	-2.537	1.137	80.398	-3.091	No	No	No
Harmine	-3.148	1.496	93.499	-2.774	No	No	No
Betulinic acid	-3.122	1.175	99.763	-2.735	No	No	No
Conessine	-2.978	1.197	87.78	-2.841	No	Yes	No
Arjunolic acid	-3.01	0.472	63.497	-2.735	No	No	No
Vasicine	-2.433	1.595	86.22	-2.827	No	No	No

Ligand Name	Water solubility (Log Mol/L)	Caco2 permeability (log Papp in 10-6 cm/s)	Intestinal absorption (human) (% Absorbed)	Skin Permeability (log Kp)	P-glycoprotein substrate	P-glycoprotein I inhibitor	P-glycoprotein II inhibitor
Nardol	-4.171	1.524	94.138	-2.003	No	No	No
Angelicin	-2.556	1.358	97.593	-2.214	No	No	No
Arjungenin	-3.012	0.421	48.918	-2.735	Yes	No	No
Norharmane	-3.117	1.662	93.985	-2.275	No	No	No
Chebulic acid	-2.891	-1.258	0.957	-2.735	Yes	No	No
Ganoderic acid A	-3.984	0.608	64.393	-2.737	Yes	No	Yes
Ginsenoside F1	-4.263	0.34	43.644	-2.755	Yes	Yes	No
Reserpine	-5.345	1.017	100	-2.762	Yes	Yes	Yes
Gallic acid	-2.56	-0.081	43.374	-2.735	No	No	No
Vasicol	-2.002	0.077	65.276	-3.126	No	No	No
Flavogallonic acid	-2.892	-1.693	71.447	-2.735	Yes	No	No
Voafinidine	-3.264	1.259	96.203	-3.306	Yes	No	No
Rel-Khayseneganin D	-4.928	0.864	100	-3.128	No	Yes	No
β-sitosterol	-6.773	1.201	94.464	-2.783	No	Yes	Yes
Stigmastanol	-6.063	1.2	94.938	-2.737	No	Yes	Yes
Shogoal	-3.941	1.391	92.686	-2.584	No	Yes	No
Anaferine	-1.204	1.336	93.738	-3.337	No	No	No
Gingerol	-3.164	0.94	92.416	-2.817	Yes	No	No
Sinapic acid	-2.869	0.272	93.064	-2.725	Yes	No	No
L-dopa	-2.89	-0.289	47.741	-2.735	Yes	No	No
Ferulic acid	-2.817	0.176	93.685	-2.72	No	No	No

Ligand Name	Water solubility (Log Mol/L)	Caco2 permeability (log Papp in 10-6 cm/s)	Intestinal absorption (human) (% Absorbed)	Skin Permeability (log Kp)	P-glycoprotein substrate	P-glycoprotein I inhibitor	P-glycoprotein II inhibitor
β-asarone	-2.536	1.914	95.49	-1.885	No	No	No
α-asarone	-2.536	1.914	95.49	-1.885	No	No	No
Zingerone	-1.7	1.233	94.103	-2.653	No	No	No
Carvacrol	-2.789	1.606	90.843	-1.62	No	No	No
Abrine	-2.171	0.664	100	-2.735	Yes	No	No
Trans-β-caryophyllene	-5.212	1.42	95.234	-1.564	No	No	No
Carvone	-2.324	1.413	97.702	-2.145	No	No	No
Pipertone	-2.076	1.611	97.354	-3.243	No	No	No
Methyleugenol	-2.671	1.528	94.532	-1.916	No	No	No
Calarene	-5.644	1.406	95.748	-1.733	No	No	No
Thymol	-2.789	1.606	90.843	-1.62	No	No	No
α-Humulene	-5.191	1.421	94.682	-1.739	Yes	No	No
Limonene	-3.568	1.401	95.898	-1.721	Yes	No	No
Eugenol	-2.25	1.559	92.041	-2.207	No	No	No
α-pinene	-3.733	1.38	96.041	-1.827	No	No	No
β-pinene	-4.191	1.385	95.525	-1.653	No	No	No
Elemol	-4.649	1.517	93.486	-1.58	No	No	No
Sinapine	-2.431	0.466	95.901	-3.036	No	No	No

Table S 3: Distribution of the phytochemicals.

Ligand Name	VDss (human) (Log L/kg)	Fraction unbound (human) (mean) (Fu)	BBB permeability (log BB)	CNS permeability (log PS)
Piperin	0.158	0.134	-0.102	-1.879
Ajamalicine	1.261	0.228	0.51	-1.989
Amentoflavone	-1.066	0.268	-1.653	-3.2
Demethoxycurcumin	-0.075	0	-0.337	-2.458
Rosmarinic acid	0.393	0.348	-1.378	-3.347
Serpentine	1.442	0.235	0.692	-2.123
Ajmaline	0.728	0.403	0.122	-1.623
Curcumin	-0.215	0	-0.562	-2.99
Withanolide D	-0.048	0.093	-0.315	-0.315
Hecogenin	0.221	0.012	-0.043	-1.443
Luteolin	1.153	0.168	-0.907	-2.251
Proanthocyanidin	-0.307	0.272	-1.682	-3.989
Quercetin	1.559	0.206	-1.098	-3.065
Ellagic acid	0.375	0.083	-1.272	-3.533
7α-obacunol	0.193	0.132	-0.54	-3.004
Oroselol	0.214	0.303	0.418	-2.736
Protopine	0.696	0.134	-0.226	-1.977
Arjunic acid	-1.476	0.114	-0.63	-1.775
Corilagin	0.462	0.31	-2.828	-5.044

Appendix-A

Ligand Name	VDss (human) (Log L/kg)	Fraction unbound (human) (mean) (Fu)	BBB permeability (log BB)	CNS permeability (log PS)
Withaferin A	-0.131	0.105	-0.03	-2.72
17beta-Hydroxywithanolide K	0.067	0.224	-0.88	-3
Vasicinolone	0.879	0.462	0.212	-2.94
Oleanolic acid	-1.085	0	-0.14	-1.157
Harmalol	0.337	0.341	0.312	-2.102
α-Amyrin	0.266	0	0.674	-1.773
Reseveratol	0.296	0.166	-0.048	-2.067
β-eudesmol	0.459	0.164	0.634	-1.858
Warfarin	-0.266	0.023	-0.17	-2.045
Yohimbine	1.335	0.509	0.137	-2.17
Kaempferol	1.274	0.178	-0.939	-2.228
Germacrene B	0.518	0.311	0.658	-2.392
Lupeol	0	0	0.726	-1.714
Brassicasterol	0.407	0	0.764	-1.705
Asiatic acid	-1.6	0.119	-0.646	-1.984
Vasicinol	0.075	0.51	-0.294	-2.411
Harmine	0.358	0.218	0.417	-1.466
Betulinic acid	-1.18	0.018	-0.322	-1.343
Conessine	0.256	0.398	0.908	-2.53
Arjunolic acid	-1.6	0.115	-0.666	-1.954
Vasicine	0.08	0.4	-0.127	-2.159

Ligand Name	VDss (human) (Log L/kg)	Fraction unbound (human) (mean) (Fu)	BBB permeability (log BB)	CNS permeability (log PS)
Nardol	0.455	0.313	0.589	-2.339
Angelicin	-0.276	0.311	0.462	-1.699
Arjungenin	-1.787	0.206	-0.803	-2.967
Norharmane	0.151	0.292	0.203	-1.875
Chebulic acid	-0.353	0.481	-1.786	-3.824
Ganoderic acid A	-0.599	0.182	-0.911	-3
Ginsenoside F1	-0.833	0.253	-1.144	-3.597
Reserpine	0.356	0.019	-0.788	-3.364
Gallic acid	-1.855	0.617	-1.102	-3.74
Vasicol	-0.058	0.497	0.497	-2.735
Flavogallonic acid	-0.667	0.113	-2.085	-4.263
Voafinidine	0.779	0.38	0.387	-1.805
Rel-Khayseneganin D	-0.312	0.121	-0.964	-3.123
β-sitosterol	0.193	0	0.781	-1.705
Stigmastanol	-0.108	0	0.813	-1.435
Shogoal	0.501	0.147	-0.197	-1.777
Anaferine	0.908	0.754	0.112	0.112
Gingerol	0.524	0.258	-0.727	-2.788
Sinapic acid	-1.11	0.45	-0.247	-2.663
L-dopa	-0.105	0.604	-0.843	-3.032
Ferulic acid	-1.367	0.343	-0.239	-2.612

Appendix-A

Ligand Name	VDss (human) (Log L/kg)	Fraction unbound (human) (mean) (Fu)	BBB permeability (log BB)	CNS permeability (log PS)
β-asarone	0.087	0.263	0.229	-1.993
α-asarone	0.087	0.263	0.229	-1.993
Zingerone	0.177	0.407	0.006	-2.175
Carvacrol	0.512	0.203	0.407	-1.664
Abrine	-1.782	0.413	-0.23	-2.55
Trans-β-caryophyllene	0.626	0.293	0.744	-2.126
Carvone	0.179	0.53	0.588	-2.478
Pipertone	0.189	0.532	0.558	-2.461
Methyleugenol	0.265	0.208	0.422	-1.922
Calarene	0.779	0.192	0.801	-1.959
Thymol	0.512	0.203	0.407	0.407
α-Humulene	0.505	0.347	0.663	-2.555
Limonene	0.396	0.48	0.732	-2.37
Eugenol	0.24	0.251	0.374	-2.007
α-pinene	0.667	0.425	0.791	-2.201
β-pinene	0.685	0.35	0.818	-1.857
Elemol	0.407	0.245	0.625	-2.151
Sinapine	0.311	0.422	-0.288	-2.88

Table S 4: Metabolism of the phytochemicals.

Ligand Name	CYP2D6 substrate	CYP3A4 substrate	CYP1A2 inhibitor	CYP2C19 inhibitor	CYP2C9 inhibitor	CYP2D6 inhibitor	CYP3A4 inhibitor
Piperin	No	Yes	No	Yes	No	No	No
Ajamalicine	No	Yes	No	No	No	Yes	No
Amentoflavone	No	Yes	No	No	No	No	No
Demethoxycurcumin	No	Yes	Yes	Yes	Yes	Yes	Yes
Rosmarinic acid	No	No	No	No	No	No	No
Serpentine	No	Yes	Yes	No	No	Yes	No
Ajmaline	Yes	Yes	No	No	No	No	No
Curcumin	No	Yes	Yes	Yes	Yes	No	Yes
Withanolide D	No	Yes	Yes	Yes	Yes	Yes	Yes
Hecogenin	No	Yes	No	No	No	No	No
Luteolin	No	No	Yes	No	Yes	No	No
Proanthocyanidin	No	No	No	No	No	No	No
Quercetin	No	No	Yes	No	No	No	No
Ellagic acid	No	No	Yes	No	No	No	No
7α-obacunol	No	Yes	No	No	No	No	No
Oroselol	No	No	Yes	No	No	No	No
Protopine	No	Yes	Yes	Yes	No	No	No
Arjunic acid	No	Yes	No	No	No	No	No
Corilagin	No	No	No	No	No	No	No
Withaferin A	No	Yes	No	No	No	No	No
17beta-Hydroxywithanolide K	No	Yes	No	No	No	No	No
Vasicinolone	No	No	Yes	No	No	No	No
Oleanolic acid	No	Yes	No	No	No	No	No
Harmalol	Yes	No	Yes	No	No	No	No

Ligand Name	CYP2D6 substrate	CYP3A4 substrate	CYP1A2 inhibitor	CYP2C19 inhibitor	CYP2C9 inhibitor	CYP2D6 inhibitor	CYP3A4 inhibitor
α-Amyrin	No	Yes	No	No	No	No	No
Reseveratol	No	Yes	Yes	Yes	No	No	No
β-eudesmol	No	Yes	No	No	No	No	No
Warfarin	No	Yes	Yes	Yes	Yes	No	Yes
Yohimbine	No	Yes	No	No	No	Yes	No
Kaempferol	No	No	Yes	No	No	No	No
Germacrene B	No	No	No	No	No	No	No
Lupeol	No	Yes	No	No	No	No	No
Brassicasterol	No	Yes	No	No	No	No	No
Asiatic acid	No	Yes	No	No	No	No	No
Vasicinol	No	No	No	No	No	No	No
Harmine	No	No	Yes	No	No	No	No
Betulinic acid	No	Yes	No	No	No	No	No
Conessine	No	Yes	No	No	No	No	No
Arjunolic acid	No	Yes	No	No	No	No	No
Vasicine	No	Yes	No	No	No	No	No
Nardol	No	No	No	Yes	No	No	No
Angelicin	No	No	Yes	Yes	No	No	No
Arjungenin	No	Yes	No	No	No	No	No
Norharmane	No	No	Yes	No	No	No	No
Chebulic acid	No	No	No	No	No	No	No
Ganoderic acid A	No	Yes	No	No	No	No	No
Ginsenoside F1	No	Yes	No	No	No	No	No
Reserpine	No	Yes	No	No	No	No	Yes
Gallic acid	No	No	No	No	No	No	No

Ligand Name	CYP2D6 substrate	CYP3A4 substrate	CYP1A2 inhibitor	CYP2C19 inhibitor	CYP2C9 inhibitor	CYP2D6 inhibitor	CYP3A4 inhibitor
Vasicol	No	No	No	No	No	No	No
Flavogallonic acid	No	No	No	No	No	No	No
Voafinidine	No	Yes	No	No	No	Yes	No
Rel-Khayseneganin D	No	Yes	No	No	No	No	Yes
β-sitosterol	No	Yes	No	No	No	No	No
Stigmastanol	No	Yes	No	No	No	No	No
Shogoal	No	Yes	Yes	Yes	Yes	No	No
Anaferine	No	No	No	No	No	No	No
Gingerol	No	No	Yes	Yes	Yes	No	No
Sinapic acid	No	No	No	No	No	No	No
L-dopa	No	No	No	No	No	No	No
Ferulic acid	No	No	No	No	No	No	No
β-asarone	No	No	Yes	No	No	No	No
α-asarone	No	No	Yes	No	No	No	No
Zingerone	No	No	No	No	No	No	No
Carvacrol	No	No	Yes	No	No	No	No
Abrine	No	No	No	No	No	No	No
Trans-β-caryophyllene	No	No	No	No	No	No	No
Carvone	No	No	No	No	No	No	No
Pipertone	No	No	No	No	No	No	No
Methyleugenol	No	No	Yes	No	No	No	No
Calarene	No	Yes	No	No	No	No	No
Thymol	No	No	Yes	No	No	No	No
α-Humulene	No	No	No	No	No	No	No
Limonene	No	No	No	No	No	No	No

Ligand Name	CYP2D6 substrate	CYP3A4 substrate	CYP1A2 inhibitor	CYP2C19 inhibitor	CYP2C9 inhibitor	CYP2D6 inhibitor	CYP3A4 inhibitor
Eugenol	No	No	Yes	No	No	No	No
α-pinene	No	No	No	No	No	No	No
β-pinene	No	No	No	No	No	No	No
Elemol	No	No	No	No	No	No	No
Sinapine	No	No	No	No	No	No	No

Table S 5: Excretion of the phytochemicals.

Ligand Name	Total clearance (log ml/min/kg)	Renal OCT2 substrate
Piperin	0.232	Yes
Ajamalicine	0.962	No
Amentoflavone	0.484	No
Demethoxycurcumin	0.026	No
Rosmarinic acid	0.25	No
Serpentine	1.153	Yes
Ajmaline	0.893	No
Curcumin	-0.002	No
Withanolide D	0.347	No
Hecogenin	0.315	Yes
Luteolin	0.495	No
Proanthocyanidin	0.054	No
Quercetin	0.407	No
Ellagic acid	0.537	No
7α-obacunol	0.198	No
Oroselol	0.679	No
Protopine	0.936	Yes
Arjunic acid	0.007	No
Corilagin	0.229	No
Withaferin A	0.435	Yes
17beta-Hydroxywithanolide K	0.486	No
Vasicinolone	0.482	No
Oleanolic acid	-0.081	No
Harmalol	0.522	Yes
α-Amyrin	0.119	No

Ligand Name	Total clearance (log ml/min/kg)	Renal OCT2 substrate
Reseveratol	0.076	No
β-eudesmol	1.032	No
Warfarin	0.719	No
Yohimbine	0.829	No
Kaempferol	0.477	No
Germacrene B	1.405	No
Lupeol	0.153	No
Brassicasterol	0.57	No
Asiatic acid	0.202	No
Vasicinol	0.379	No
Harmine	0.65	No
Betulinic acid	0.116	No
Conessine	0.205	No
Arjunolic acid	0.038	No
Vasicine	0.58	No
Nardol	1.106	No
Angelicin	0.718	No
Arjungenin	0.116	No
Norharmane	0.419	No
Chebulic acid	0.548	No
Ganoderic acid A	0.242	No
Ginsenoside F1	0.465	No
Reserpine	0.522	No
Gallic acid	0.518	No
Vasicol	0.361	No
Flavogallonic acid	0.461	No

Ligand Name	Total clearance (log ml/min/kg)	Renal OCT2 substrate
Voafinidine	0.825	No
Rel-Khayseneganin D	0.329	No
β-sitosterol	0.628	No
Stigmastanol	0.621	No
Shogoal	1.44	No
Anaferine	1.272	No
Gingerol	1.339	No
Sinapic acid	0.718	No
L-dopa	0.43	No
Ferulic acid	0.623	No
β-asarone	0.441	No
α-asarone	0.441	No
Zingerone	0.307	No
Carvacrol	0.207	No
Abrine	0.781	No
Trans-β-caryophyllene	1.216	No
Carvone	0.225	No
Pipertone	1.09	No
Methyleugenol	0.338	No
Calarene	0.923	No
Thymol	0.211	No
α-Humulene	1.282	No
Limonene	0.213	No
Eugenol	0.282	No
α-pinene	0.043	No
β-pinene	0.03	No

Ligand Name	Total clearance (log ml/min/kg)	Renal OCT2 substrate
Elemol	1.311	No
Sinapine	0.857	Yes

Table S 6: Toxicity of the phytochemicals.

Ligand Name	AMES toxicity	Max. tolerated dose (human) (log mg/kg/day)	hERGI inhibitor	hERGII inhibitor	Oral rat acute toxicity (LD50) (Mol/kg)	Oral rat chronic toxicity (LOAEL) (logmg/kg_bw/day)	Hepatotoxicity	Skin Sensitisation	T.Pyriformis toxicity	Minnow toxicity
Piperin	No	-0.38	No	No	2.811	1.51	Yes	No	1.879	1.732
Ajamalicine	No	-0.519	No	Yes	2.974	0.431	Yes	No	0.672	-0.641
Amentoflavone	No	0.438	No	Yes	2.527	3.572	No	No	0.285	2.685
Demethoxycurcumin	No	-0.12	No	Yes	1.973	2.236	No	No	0.593	-0.426
Rosmarinic acid	No	0.152	No	No	2.811	2.907	No	No	0.302	2.698
Serpentine	No	-0.594	No	Yes	2.924	1.642	Yes	No	0.569	-2.181
Ajmaline	No	0.032	No	Yes	3.016	2.258	No	Yes	0.289	1.196
Curcumin	No	0.081	No	No	1.833	2.228	No	No	0.494	-0.081
Withanolide D	No	-0.867	No	No	2.831	1.776	No	No	0.305	1.178
Hecogenin	No	-0.615	No	No	2.028	1.133	No	No	0.339	1.192
Luteolin	No	0.499	No	No	2.455	2.409	No	No	0.326	3.169
Proanthocyanidin	No	0.438	No	Yes	2.483	3.845	No	No	0.285	8.303
Quercetin	No	0.499	No	No	2.471	2.612	No	No	0.288	3.721
Ellagic acid	No	0.476	No	No	2.399	2.698	No	No	0.295	2.11
7α-obacunol	No	-0.806	No	No	3.193	1.448	Yes	No	0.296	0.223
Oroselol	Yes	-0.223	No	No	2.479	0.955	No	No	0.646	1.222
Protopine	Yes	-0.446	No	No	2.993	1.93	No	No	0.64	1.237

Appendix-A

Ligand Name	AMES toxicity	Max. tolerated dose (human) (log mg/kg/day)	hERGI inhibitor	hERGII inhibitor	Oral rat acute toxicity (LD50) (Mol/kg)	Oral rat chronic toxicity (LOAEL) (logmg/kg_bw/day)	Hepatotoxicity	Skin Sensitisation	T.Pyriformis toxicity	Minnow toxicity
Arjunic acid	No	0.129	No	No	2.388	-0.082	No	No	0.285	1.17
Corilagin	No	0.438	No	Yes	2.482	6.333	No	No	0.285	11.281
Withaferin A	No	-0.695	No	No	2.779	0.918	No	No	0.299	0.738
17beta-Hydroxywithanolide K	No	-0.701	No	No	2.3	2.158	No	No	0.291	1.687
Vasicinolone	No	-0.244	No	No	2.012	2.016	No	No	0.431	1.648
Oleanolic acid	No	0.203	No	No	2.349	2.085	Yes	No	0.285	-0.823
Harmalol	No	-0.616	No	No	2.42	1.786	No	No	0.854	0.921
α-Amyrin	No	-0.571	No	Yes	2.467	0.856	No	No	0.384	-1.309
Reseveratol	Yes	0.331	No	No	2.529	1.533	No	No	0.746	1.522
β-eudesmol	No	-0.22	No	No	1.727	1.304	No	Yes	1.805	0.412
Warfarin	No	0.294	No	No	1.773	1.081	No	No	0.591	0.034
Yohimbine	No	-1.355	No	Yes	2.942	0.687	No	No	0.339	-0.165
Kaempferol	No	0.531	No	No	2.449	2.505	No	No	0.312	2.885
Germacrene B	No	0.494	No	No	1.73	1.416	No	Yes	1.478	0.511
Lupeol	No	-0.502	No	Yes	2.563	0.89	No	No	0.316	-1.696
Brassicasterol	No	-0.506	No	Yes	2.057	0.909	No	No	0.636	-1.813
Asiatic acid	No	0.078	No	No	2.592	0.575	No	No	0.285	1.106

Ligand Name	AMES toxicity	Max. tolerated dose (human) (log mg/kg/day)	hERGI inhibitor	hERGII inhibitor	Oral rat acute toxicity (LD50) (Mol/kg)	Oral rat chronic toxicity (LOAEL) (logmg/kg_bw/day	Hepatotoxicity	Skin Sensitisation	T.Pyriformis toxicity	Minnow toxicity
Vasicinol	No	-0.391	No	No	2.436	0.98	No	No	0.441	2.303
Harmine	Yes	0.062	No	No	2.477	1.499	No	No	0.672	-0.137
Betulinic acid	No	0.144	No	No	2.256	2.206	Yes	No	0.285	-1.174
Conessine	No	0.247	No	Yes	2.682	0.512	Yes	No	0.287	0.322
Arjunolic acid	No	0.081	No	No	2.594	0.553	No	No	0.285	1.07
Vasicine	Yes	0.204	No	No	2.697	1.427	No	No	0.736	1.86
Nardol	No	0.4	No	No	1.655	1.343	No	Yes	1.452	0.689
Angelicin	Yes	-0.476	No	No	2.669	1.173	No	No	0.538	1.546
Arjungenin	No	0.078	No	No	2.427	2.309	No	No	0.285	1.977
Norharmane	Yes	-0.204	No	No	3.346	2.089	No	No	0.438	1.295
Chebulic acid	No	0.44	No	No	2.482	3.931	No	No	0.285	6.774
Ganoderic acid A	No	0.147	No	No	2.622	1.85	No	No	0.285	1.645
Ginsenoside F1	No	-1.105	No	Yes	2.672	2.786	No	No	0.285	2.772
Reserpine	No	-0.133	No	Yes	2.958	1.158	No	No	0.286	0.303
Gallic acid	No	0.7	No	No	2.218	3.06	No	No	0.285	3.188
Vasicol	No	0.039	No	No	2.273	1.466	No	No	0.045	2.036
Flavogallonic acid	No	0.442	No	No	2.488	3.669	No	No	0.285	6.499
Voafinidine	No	-0.213	No	Yes	2.891	1.091	Yes	No	0.66	1.504

Appendix-A

Ligand Name	AMES toxicity	Max. tolerated dose (human) (log mg/kg/day)	hERGI inhibitor	hERGII inhibitor	Oral rat acute toxicity (LD50) (Mol/kg)	Oral rat chronic toxicity (LOAEL) (logmg/kg_bw/day)	Hepatotoxicity	Skin Sensitisation	T.Pyriformis toxicity	Minnow toxicity
Rel-Khayseneganin D	No	-0.718	No	No	3.415	1.807	No	No	0.294	1.961
β-sitosterol	No	-0.621	No	Yes	2.552	0.855	No	No	0.43	-1.802
Stigmastanol	No	No	No	Yes	2.783	0.847	No	No	0.323	-1.919
Shogoal	No	0.759	No	Yes	2.081	2.159	No	Yes	2.475	0.15
Anaferine	No	0.132	No	No	2.483	0.833	No	Yes	0.14	2.062
Gingerol	No	0.635	No	No	1.958	1.631	No	Yes	1.487	0.966
Sinapic acid	No	1.193	No	No	2.24	2.324	No	No	0.262	2.18
L-dopa	No	0.922	No	No	2.234	2.699	Yes	No	0.281	3.143
Ferulic acid	No	1.082	No	No	2.282	2.065	No	No	0.271	1.825
β-asarone	No	0.792	No	No	1.939	2.114	No	Yes	1.48	0.786
α-asarone	No	0.792	No	No	1.939	2.114	No	Yes	1.48	0.786
Zingerone	No	0.544	No	No	2.129	1.953	Yes	No	0.634	1.645
Carvacrol	No	1.007	No	No	2.074	2.212	Yes	Yes	0.387	1.213
Abrine	No	0.694	No	No	1.838	1.573	No	No	0.285	1.059
Trans-β-caryophyllene	No	0.408	No	No	1.625	1.457	No	Yes	1.257	0.622
Carvone	No	0.775	No	No	1.86	1.972	No	Yes	0.41	1.445
Pipertone	Yes	0.597	No	No	1.9	2.342	No	Yes	-0.093	1.42
Methyleugenol	Yes	0.959	No	No	1.973	2.119	No	Yes	0.742	1.449

Ligand Name	AMES toxicity	Max. tolerated dose (human) (log mg/kg/day)	hERGI inhibitor	hERGII inhibitor	Oral rat acute toxicity (LD50) (Mol/kg)	Oral rat chronic toxicity (LOAEL) (logmg/kg_bw/day)	Hepatotoxicity	Skin Sensitisation	T.Pyriformis toxicity	Minnow toxicity
Calarene	No	0.07	No	No	1.567	1.385	No	No	1.36	0.373
Thymol	No	1.007	No	No	2.074	2.212	Yes	Yes	0.387	1.213
α-Humulene	No	0.551	No	No	1.766	1.336	No	Yes	1.451	0.716
Limonene	No	0.777	No	No	1.88	2.336	No	Yes	0.579	1.203
Eugenol	Yes	1.024	No	No	2.118	2.049	No	Yes	0.3	1.702
α-pinene	No	0.48	No	No	1.77	2.262	No	No	0.45	1.159
β-pinene	No	0.371	No	No	1.673	2.28	No	No	0.628	1.012
Elemol	No	0.283	No	No	1.686	1.229	No	Yes	1.921	0.543
Sinapine	No	0.683	No	No	2.31	1.491	No	No	0.871	1.662

Table S 7: Drug-likeness of natural compounds by Lipinski rule.

Ligand Name	MW ≤500 g/mol	Hbond Donor ≤5 (OH and NHs)	H-bond acceptor ≤10 (Ns and Os)	Octanol water partition coefficient Log P ≤4.15 (MLOGP)	Topological polar surface area (TPSA) ≤140 Å²	Lipinski rule violation	Drug likeness
Piperin	285.34	0	3	2.39	38.77	0	YES
Ajamalicine	352.43	1	4	2.13	54.56	0	YES
Amentoflavone	538.46	6	10	0.25	181.80	2	NO
Demethoxycurcumin	338.35	2	5	1.80	83.83	0	YES
Rosmarinic acid	360.31	5	8	0.90	144.52	0	YES
Serpentine	349.40	1	3	2.21	55.20	0	YES
Ajmaline	326.43	2	3	2.67	46.94	0	YES
Curcumin	368.38	2	6	1.47	93.06	0	YES
Withanolide D	470.60	2	6	2.75	96.36	0	YES
Hecogenin	430.62	1	4	4.09	55.76	0	YES
Luteolin	286.24	4	6	-0.03	111.13	0	YES
Proanthocyanidin	592.55	9	12	-0.07	209.76	3	NO
Quercetin	302.24	5	7	-0.56	131.36	0	YES
Ellagic acid	286.19	3	7	0.66	121.11	0	YES
7α-obacunol	456.53	1	7	2.24	98.50	0	YES
Oroselol	244.24	1	4	1.44	63.58	0	YES
Protopine	353.37	0	6	1.90	57.23	0	YES
Arjunic acid	488.70	4	5	4.14	97.99	0	YES
Corilagin	634.45	11	18	-2.42	310.66	3	NO

Ligand Name	MW ≤500 g/mol	Hbond Donor ≤5 (OH and NHs)	H-bond acceptor ≤10 (Ns and Os)	Octanol water partition coefficient Log P ≤4.15 (MLOGP)	Topological polar surface area (TPSA) ≤140 Å²	Lipinski rule violation	Drug likeness
Withaferin A	470.60	2	6	2.75	96.36	0	YES
17beta-Hydroxywithanolide K	470.60	3	6	2.67	104.06	0	YES
Vasicinolone	218.21	2	4	0.22	75.35	0	YES
Oleanolic acid	456.70	2	3	5.82	57.53	1	YES
Harmalol	200.24	2	2	1.14	48.38	0	YES
α-Amyrin	426.72	1	1	6.92	20.23	1	YES
Reseveratol	228.24	2	1	2.26	60.69	0	YES
β-eudesmol	222.37	1	1	3.67	20.23	0	YES
Warfarin	308.33	1	4	2.51	67.51	0	YES
Yohimbine	354.44	2	4	2.21	65.56	0	YES
Kaempferol	286.24	4	6	-0.03	111.13	0	YES
Germacrene B	204.35	0	0	4.53	0.00	1	YES
Lupeol	426.72	1	1	6.92	20.23	1	YES
Brassicasterol	398.66	1	1	6.43	20.23	1	YES
Asiatic acid	488.70	4	5	4.14	97.99	0	YES
Vasicinol	204.23	2	3	0.99	56.06	0	YES
Harmine	212.25	1	2	1.56	37.91	0	YES
Betulinic acid	456.7	2	3	5.82	57.53	1	YES
Conessine	356.59	0	2	4.80	6.48	1	YES

Appendix-A

Ligand Name	MW ≤500 g/mol	Hbond Donor ≤5 (OH and NHs)	H-bond acceptor ≤10 (Ns and Os)	Octanol water partition coefficient Log P ≤4.15 (MLOGP)	Topological polar surface area (TPSA) ≤140 Å^2	Lipinski rule violation	Drug likeness
Arjunolic acid	488.70	4	5	4.14	97.99	0	YES
Vasicine	188.23	1	2	1.57	35.83	0	YES
Nardol	222.37	1	1	3.67	20.23	0	YES
Angelicin	186.16	0	3	1.48	43.35	0	YES
Arjungenin	504.70	5	6	3.33	118.22	1	YES
Norharmane	168.19	1	1	1.62	28.68	0	YES
Chebulic acid	356.24	6	11	-1.01	198.89	2	NO
Ganoderic acid A	516.67	3	7	2.26	128.97	1	YES
Ginsenoside F1	638.87	7	9	1.77	160.07	2	NO
Reserpine	608.68	1	10	1.75	117.78	2	NO
Gallic acid	170.12	4	5	-0.16	97.99	0	YES
Vasicol	206.24	2	2	0.32	66.56	0	YES
Flavogallonic acid	454.30	7	12	-0.18	219.10	2	NO
Voafinidine	328.45	2	3	2.09	48.63	0	YES
Rel-Khayseneganin D	502.55	1	9	1.60	121.50	1	YES
β-sitosterol	414.71	1	1	6.73	20.23	1	YES
Stigmastanol	416.72	1	1	6.88	20.23	1	YES
Shogoal	276.37	1	3	2.90	46.53	0	YES
Anaferine	224.34	2	2	1.34	41.13	0	YES
Gingerol	294.39	2	4	2.14	66.76	0	YES

Ligand Name	MW ≤500 g/mol	Hbond Donor ≤5 (OH and NHs)	H-bond acceptor ≤10 (Ns and Os)	Octanol water partition coefficient Log P ≤4.15 (MLOGP)	Topological polar surface area (TPSA) ≤140 Å²	Lipinski rule violation	Drug likeness
Sinapic acid	224.21	2	5	0.73	75.99	0	YES
L-dopa	197.19	7	8	-2.26	103.78	0	YES
Ferulic acid	194.18	2	4	1.00	66.76	0	YES
β-asarone	208.25	0	3	1.97	27.69	0	YES
α-asarone	208.25	0	3	1.97	27.69	0	YES
Zingerone	194.23	1	3	1.42	46.53	0	YES
Carvacrol	150.22	1	1	2.76	20.23	0	YES
Abrine	218.25	3	3	-1.38	65.12	0	YES
Trans-β-caryophyllene	204.35	0	0	4.63	0.00	1	YES
Carvone	150.22	0	1	2.10	17.07	0	YES
Pipertone	152.23	0	1	2.20	17.07	0	YES
Methyleugenol	178.23	0	2	2.30	18.46	0	YES
Calarene	204.35	0	0	5.65	0.00	1	YES
Thymol	150.22	1	1	2.76	20.23	0	YES
α-Humulene	204.35	0	0	4.53	0.00	1	YES
Limonene	136.23	0	0	3.27	0.00	0	YES
Eugenol	164.20	1	2	2.01	29.46	0	YES
α-pinene	136.23	0	0	4.29	0.00	1	YES
β-pinene	136.23	0	0	4.29	0.00	1	YES
Elemol	222.37	1	1	3.56	20.23	0	YES

Appendix-A

Ligand Name	MW ≤500 g/mol	Hbond Donor ≤5 (OH and NHs)	H-bond acceptor ≤10 (Ns and Os)	Octanol water partition coefficient Log P ≤4.15 (MLOGP)	Topological polar surface area (TPSA) ≤140 Å²	Lipinski rule violation	Drug likeness
Sinapine	310.37	1	5	-2.44	64.99	0	YES

Appendix-A